



UNIVERSITY
OF
JOHANNESBURG

COPYRIGHT AND CITATION CONSIDERATIONS FOR THIS THESIS/ DISSERTATION



- Attribution — You must give appropriate credit, provide a link to the license, and indicate if changes were made. You may do so in any reasonable manner, but not in any way that suggests the licensor endorses you or your use.
- NonCommercial — You may not use the material for commercial purposes.
- ShareAlike — If you remix, transform, or build upon the material, you must distribute your contributions under the same license as the original.

How to cite this thesis

Surname, Initial(s). (2012) Title of the thesis or dissertation. PhD. (Chemistry)/ M.Sc. (Physics)/ M.A. (Philosophy)/M.Com. (Finance) etc. [Unpublished]: [University of Johannesburg](https://ujdigispace.uj.ac.za). Retrieved from: <https://ujdigispace.uj.ac.za> (Accessed: Date).

**THE EVALUATION OF DENDRIMER ENCAPSULATED RUTHENIUM
NANOPARTICLES, IMMOBILISED ON SILICA, AS CATALYSTS IN VARIOUS
CATALYTIC REACTIONS AND THE EFFECT OF IONIC LIQUIDS ON THE
CATALYTIC ACTIVITY**

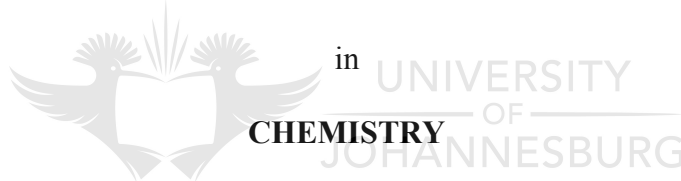
By

NATHAN CHARLES ANTONELS

THESIS

Submitted in fulfillment of the requirements for the degree

PHILOSOPHIAE DOCTOR



at the

UNIVERSITY OF JOHANNESBURG

JUNE 2014

SUPERVISOR: PROF R MEIJBOOM

CO-SUPERVISOR: PROF A MULLER



**AFFIDAVIT: MASTER AND DOCTORAL STUDENTS
TO WHOM IT MAY CONCERN**

This serves to confirm that _____
Full Name(s) and Surname

ID Number/
Passport _____

Student number _____ enrolled for the Qualification _____

_____ in the Faculty of Science

Herewith declare that my academic work is in line with the Plagiarism Policy of the University of Johannesburg with which I am familiar.

I further declare that the work presented in the _____ (minor dissertation/dissertation/thesis) is authentic and original unless clearly indicated otherwise and in such instances full reference to the source is acknowledged and I do not pretend to receive any credit for such acknowledged quotations, and that there is no copyright infringement in my work. I declare that no unethical research practices were used or material gained through dishonesty. I understand that plagiarism is a serious offence and that should I contravene the Plagiarism Policy notwithstanding signing this affidavit, I may be found guilty of a serious criminal offence (perjury) that would amongst other consequences compel the University of Johannesburg to inform all other tertiary institutions of the offence and to issue a corresponding certificate of reprehensible academic conduct to whomever requests such a certificate from the institution.

Signed at Johannesburg _____ on this _____ of _____ 2015

Signature _____ Print name _____

STAMP: COMMISSIONER OF OATHS

Affidavit certified by a Commissioner of Oaths

This affidavit conforms with the requirements of the JUSTICES OF THE PEACE AND COMMISSIONERS OF OATHS ACT 16 OF 1963 and the applicable Regulations published in the GG GNR 1258 of 21 July 1972; GN 903 of 10 July 1998; GN 109 of 2 February 2001 as amended.

Dedication

*I dedicate this thesis to my Lord for his ceaseless grace continuously
blessing me and my mother for always supporting me.*



Acknowledgements

I would like to thank:

God for blessing me through all the years. I have been blessed with many opportunities during my studies whether it be funding or opportunities for growth. His Spirit has provided me with all the strength and endurance I needed to face my challenges.

My supervisors, Assoc Prof Reinout Meijboom and Assoc Prof Alfred Muller. Their help in my understanding of this research project has benefitted me in ways I could not have imagined before. During this time I have been given opportunities to not only experience new research but new cultures as well. Thank you for always challenging me to expand the boundaries of my understanding.

The chemistry department and Meta-catalysis research group. Thank you for all your support during my studies. You guys are like my second family. A special thanks to my friends, Kariska, Frikkie, Sizwe, Pam and Rebekah, you guys always put a smile on my face especially in the times I need it most. The two ladies who I always bother, Eureka and Nelmarie, thank you for always being helpful even in the times when things are stressful you always help me.

The Lehrstuhl für Chemische Reaktionstechnik (CRT). Thank you especially to Dr Peter Wasserscheid, Dr Marco Haumann, Andreas Schönweiz and Willi Peters. Their expertise and access to lab resources, have helped with the batch and continuous flow toluene hydrogenation reactions.

The University of Johannesburg and the National Research Foundation for funding. You made my studies possible.

My extended family here in Johannesburg, of which there are too many to name, you have welcomed me into your homes and made this city a little more homely. Last but not least, my family in Cape Town. Thank you to my best friends, Rehana and Juliet. I really do appreciate how special you are. My mom, there are no words that express my thanks well enough. You are the reason I am able to be here and you have been there through everything and sacrificed so much for me to develop myself.

Thank you.

Publications and presentations

Portions of this thesis that resulted in publications:

N.C. Antonels and R. Meijboom. Preparation of Well-Defined Dendrimer Encapsulated Ruthenium Nanoparticles and Their Evaluation in the Reduction of 4-Nitrophenol According to the Langmuir–Hinshelwood Approach, *Langmuir*, 2013, 29(44), 13433–13442

Conference presentations:

N.C. Antonels and R. Meijboom (2013). The preparation of dendrimer encapsulated ruthenium nanoparticles and their evaluation in the reduction of 4-nitrophenol according to the Langmuir-Hinshelwood kinetic model. Catalysis Society of South Africa (CATSA). Oral presentation delivered, Wild Coast Sun, South Africa.

N.C. Antonels, A. Schönweiz and R. Meijboom (2012). The catalytic evaluation of immobilised ruthenium nanoparticles: Effects of nanoparticle size and reaction media. Catalysis Society of South Africa (CATSA). Poster presentation delivered, Langebaan, South Africa.

N.C. Antonels, A. Schönweiz and R. Meijboom (2011). Templated preparation of ruthenium nanoparticles and its evaluation as nano-SILP catalyst in hydrogenation. Catalysis Society of South Africa (CATSA). Poster presentation delivered, Johannesburg, South Africa.

N.C. Antonels, R. Meijboom and A. Muller (2010). The use of Cu and Ru dendrimer encapsulated nanoparticles (DEN) as catalysts for the reduction of *p*-nitrophenol to *p*-aminophenol. Catalysis Society of South Africa (CATSA). Poster presentation delivered, Bloemfontein, South Africa.

Abbreviations

[(TESP)MIm]	-	<i>N</i> -3-(3-tri-ethoxysilylpropyl)-3-methylimidazolium
[BMIM][BF₄]	-	1-butyl-3-methylimidazolium tetrafluoroborate
	-	1-butyl-3-methylimidazolium
[BMIM][NTf₂]		bis(trifluoromethanesulfonyl)amide
[BMIM][NTf₂]	-	1-butyl-3-methylimidazolium
		bis(trifluoromethanesulfonyl)imide
[BMIM][OcS]	-	1-butyl-3-methylimidazolium octylsulfate
[BMIM][PF₆]	-	1-butyl-3-methylimidazolium hexafluorophosphate
[EMIM][EtS]	-	1-ethyl-3-methylimidazolium ethylsulfate
[EMIM][OcS]	-	1-ethyl-3-methylimidazolium ethylsulfate
[HMIM][NTf₂]	-	1-hexyl-3-methylimidazolium
		bis(trifluoromethanesulfonyl)amide
[NB4MPy][BF₄]	-	<i>N</i> -butyl-4-methylpyridinium tetrafluoroborate
[OMIM][NTf₂]	-	1-octyl-3-methyl-imidazolium trifluoromethanesulfonate
4AP	-	4-aminophenol
4NP	-	4-nitrophenol
acac	-	acetylacetonate
AOT	-	dioctyl sodium sulfosuccinate
BML.PF₄	-	1- <i>n</i> -butylimidazolium tetrafluoroborate
BML.PF₆	-	1- <i>n</i> -butyl-3-methylimidazolium hexafluoroborate
CAL	-	cinnamaldehyde
CNF	-	carbon nanofiber
COD	-	1,5-cyclooctadiene
COL	-	cinnamyl alcohol
COT	-	1,5,7-cyclooctatriene
CTAB	-	hexadecyltrimethylammonium bromide
DCM	-	dichloromethane
DEN	-	dendrimer encapsulated nanoparticle
DMF	-	<i>N,N</i> -dimethylformamide
DMN	-	dendrimer-metal nanocomposites

DOS	-	density of states
EpB	-	3,4-epoxy-1-butene
FTIR	-	fourier transform infrared
HCAL	-	hydrocinnamaldehyde
HCOL	-	hydrocinnamyl alcohol
HRTEM	-	high resolution transmission electron microscopy
HSAG	-	high surface area commercial graphite
ICP-OES	-	inductively coupled plasma optical emissions spectroscopy
MWCNT	-	multi-walled carbon nanotubes
NP	-	nanoparticle
o/w	-	oil in water
OAc	-	acetate
PAMAM	-	poly(amidoamine)
PS-<i>b</i>-P4VP	-	polystyrene-block-poly-4-vinylpyridine
PVP	-	poly(N-vinyl-2-pyrrolidone)
PXRD	-	powder X-ray diffractometry
QSE	-	quantum size effects
RuDEN	-	dendrimer encapsulated ruthenium nanoparticle
RuSil	-	silica supported RuDEN
sc-CO₂	-	supercritical CO ₂
SCILL	-	solid catalysts with ionic liquid layer
SEM	-	scanning electron microscopy
SIL	-	supported ionic liquid
SILP	-	supported ionic liquid phase
SMIT	-	size induced metal-insulator transition
TBAB	-	tetra- <i>n</i> -butylammonium bromide
TBHP	-	<i>t</i> -butyl hydroperoxide
TEAB	-	tetraethylammonium bromide
TGA	-	thermogravimetric analysis
TOA	-	trioctylamine
TOAF	-	tetraoctylammonium formate
TOF	-	turnover frequency
TON	-	turnover number

- UV/Vis** - ultraviolet and visible spectrophotometry
- w/o** - water in oil
- w/sc-CO₂** - water-in-supercritical-CO₂



Abstract

This study discusses the preparation of various sized dendrimer encapsulated ruthenium nanoparticles (RuDEN) with the use of the generation 4 (G4), generation 5 (G5) and generation 6 (G6) hydroxyl-terminated poly(amidoamine) (PAMAM-OH) dendrimers as templating agents. The size of the nanoparticles ranges from 1.1-2.2 nm. The RuDENs were used as nanoparticle solutions in catalytic reactions or immobilised on amorphous silica 60 and silica 100 and subsequently referred to as RuSil catalysts. These catalysts were evaluated in the reduction of 4-nitrophenol, toluene hydrogenation, citral hydrogenation, cinnamaldehyde hydrogenation and styrene oxidation. The effect of ionic liquids as a catalyst coating or additive in the hydrogenation and oxidation reactions were investigated using the ionic liquids, 1-butyl-3-methylimidazolium bis(trifluoromethanesulfonyl)imide [BMIM][NTf₂], 1-octyl-3-methylimidazolium bis(trifluoromethanesulfonyl)imide [OMIM][NTf₂], 1-butyl-3-methylimidazolium tetrafluoroborate [BMIM][BF₄], 1-butyl-3-methylimidazolium hexafluorophosphate [BMIM][PF₆], 1-ethyl-3-methylimidazolium octylsulfate [EMIM][OcS], 1-ethyl-3-methylimidazolium ethylsulfate [EMIM][EtS], and 1-butyl-3-imidazolium octylsulfate [BMIM][OcS]. The prepared nanoparticles were characterised using Transmission Electron Microscopy (TEM), UV/Vis spectrophotometry, Infrared spectroscopy (IR) and Nuclear Magnetic Resonance (NMR). Supported nanoparticles were characterised using Thermogravimetric Analysis (TGA) and *Brunauer-Emmett-Teller* (BET). Catalytic reactions were analysed using Gas Chromatography (GC).

The 4-nitrophenol reduction kinetic data was modelled using the Langmuir-Hinshelwood mechanistic model. The model allows the relation of the apparent rate constant to the total surface area S of the nanoparticle, to the kinetic constant k which is related to the rate-determining step and the adsorption constants K_{ANP} and K_{BH_4} for 4-nitrophenol and borohydride respectively.

An increase in selectivity towards methylcyclohexenes was observed during the toluene hydrogenation reactions when coating the RuSil catalysts with an ionic liquid. The highest methylcyclohexene selectivity was observed when using [BMIM][NTf₂] as a coating.

The hydrogenation of α,β -unsaturated compounds were investigated for the compounds, citral and cinnamaldehyde. The RuSil catalysts were evaluated as well as select ionic liquid coated catalysts based on the use of G5-RuSil60 as the uncoated catalyst. An increase in activity was observed when using [BMIM][NTf₂] and [EMIM][OCS] as catalyst coatings for the hydrogenation of citral and cinnamaldehyde respectively.

The oxidation of styrene was investigated for the catalysts G5-RuDEN and G6-RuDEN given the higher stability of these particles due to the larger dendritic stabilisation. The RuDENS showed good activity as oxidation catalysts and showed an enhanced catalytic activity over the minimal autocatalysis normally observed when using *t*-butyl hydroperoxide as an oxidant in styrene oxidation. The ionic liquids [BMIM][NTf₂], [BMIM][BF₄], [BMIM][PF₆], [EMIM][EtS] and [EMIM][OCS] were used as additives in the catalytic reaction and in general increased the selectivity towards benzaldehyde. Enhanced activity was observed when using [EMIM][OCS] as an additive.



Table of contents

Affidavit	i
Dedication	ii
Acknowledgements	iii
Publications and presentations	iv
Abbreviations	v
Abstract	viii
Chapter 1 – Review on the scope of nanoparticle preparation and utilisation of ruthenium nanoparticles	1
1.1 Introduction	1
1.2 Properties of nanoparticles	1
1.3 The mechanism of nanoparticle formation	4
1.4 Model reactions as a means to study surface characteristics and reaction kinetics	7
1.5 Synthetic approaches to preparing nanoparticles	8
1.5.1 <i>Electrochemical synthesis of metal nanoparticles</i>	8
1.5.2 <i>Radiolysis and photolysis</i>	9
1.5.3 <i>Thermal decomposition of complexes for nanoparticle preparation</i>	9
1.5.4 <i>Organometallic synthesis of metal nanoparticles including ligand displacement and ligand reduction</i>	10

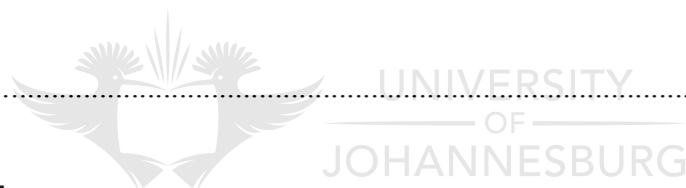
1.5.5	<i>Chemical reduction of transition metal complex precursors</i>	10
1.6	Stabilisation of metal nanoparticles	12
1.6.1	<i>Stabilisation of nanoparticles using surfactants, micelles and microemulsions</i>	12
1.6.2	<i>Ligand stabilised nanoparticles</i>	14
1.6.3	<i>Nanoparticles stabilised by ionic liquids</i>	15
1.6.4	<i>Nanoparticles stabilised by macromolecules</i>	15
1.6.4.1	<i>Polymers</i>	16
1.6.4.2	<i>Dendrimers</i>	16
1.7	Nanoparticles supported on solid supports	19
1.8	The best of both worlds: ionic liquid coated solid catalysts	20
1.9	Application of ruthenium nanoparticles in catalysis	21
1.9.1	<i>Catalytic evaluation of ruthenium colloidal suspensions</i>	21
1.9.2	<i>Catalytic evaluation of supported ruthenium nanoparticles</i>	25
1.9.3	<i>Catalytic evaluation of supported ruthenium nanoparticles coated in ionic liquid</i>	26
1.10	Aims, objectives and overview	27
1.11	Conclusion	29
1.12	References	29
Chapter 2	– The preparation of RuDEN, RuSil and RuSCILL catalysts	36
2.1	Introduction	36
2.2	Experimental	38

2.2.1	<i>Preparation of RuDENs for evaluation in 4-nitrophenol reduction</i>	39
2.2.2	<i>General preparation of RuDENs for extraction of Ru nanoparticles</i>	40
2.2.2.1	<i>Extraction of Ru NPs from the RuDENs using [BMIM][PF₆]</i>	40
2.2.2.2	<i>Extraction of Ru NPs from the RuDENs using [BMIM][BF₄]</i>	40
2.2.2.3	<i>Extraction of Ru NPs from the RuDENs using octylamine</i>	41
2.2.2.4	<i>Extraction of Ru NPs from the RuDENs using oleylamine</i>	41
2.2.3	<i>Preparation of silica supported RuDEN catalysts, RuSil</i>	41
2.2.4	<i>Preparation of RuSCILL catalysts</i>	42
2.2.4.1	<i>Preparation of the [BMIM][NTf₂] coated G5-RuSCILL catalyst with a 10 % and 20 % pore filling</i>	43
2.2.4.2	<i>Preparation of the [BMIM][BF₄] coated G5-RuSCILL catalyst with a 10 % pore filling</i>	43
2.2.4.3	<i>Preparation of the [BMIM][PF₆] coated G5-RuSCILL catalyst with a 10 % pore filling</i>	43
2.2.4.4	<i>Preparation of the [EMIM][EtS] coated G5-RuSCILL catalyst with a 10 % pore filling</i>	43
2.2.4.5	<i>Preparation of the [EMIM][OcS] coated G5-RuSCILL catalyst with a 10 % pore filling</i>	44
2.2.4.6	<i>Preparation of the [BMIM][NTf₂] coated G6-RuSCILL catalyst with a 10 % and 20 % pore filling</i>	44
2.2.4.7	<i>Preparation of the [BMIM][BF₄] coated G6-RuSCILL catalyst with a 10 % and 20 % pore filling</i>	44
2.2.4.8	<i>Preparation of the [BMIM][PF₆] coated G6-RuSCILL catalyst with a 10 % and 20 % pore filling</i>	44
2.2.4.9	<i>Preparation of the [OMIM][NTf₂] coated G6-RuSCILL catalyst with a 10, 20% and 30% pore filling</i>	45
2.2.4.10	<i>Preparation of the [BMIM][OcS] coated G6-RuSCILL catalyst with a 10% pore filling</i>	45
2.3	Results and discussion	45
2.3.1	<i>Preparation of dendrimer encapsulated Ru nanoparticles</i>	45
2.3.1.1	<i>UV/Vis analysis for the preparation of RuDENs</i>	46
2.3.1.2	<i>FTIR analysis for the preparation of RuDENs</i>	47
2.3.1.3	<i>HRTEM analysis of the RuDENs</i>	48

2.3.2	<i>Extraction of Ru nanoparticles using ionic liquids and alkylamines as extractants and phase transfer agents</i>	51
2.3.2.1	<i>UV/Vis study of the extraction of Ru nanoparticles using ionic liquids</i>	52
2.3.2.2	<i>UV/Vis study of the extraction of Ru nanoparticles using alkylamines</i>	54
2.3.2.3	<i>HRTEM analysis of the Ru nanoparticles extracted using octylamine</i>	55
2.3.3	<i>The immobilisation of RuDENSs on silica 60 and silica 100</i>	58
2.3.3.1	<i>TGA analysis of the RuSil catalysts</i>	59
2.3.3.2	<i>HRTEM analysis of the RuSil catalysts</i>	61
2.3.4	<i>Preparation of solid catalysts with ionic liquid layer (SCILL)</i>	65
2.3.4.1	<i>TGA analysis of the RuSCILL catalysts</i>	65
2.3.4.2	<i>BET analysis of the RuSCILL catalysts</i>	68
2.4	Conclusion	69
2.5	References	69
Chapter 3	Catalytic reduction of 4-nitrophenol using ruthenium dendrimer encapsulated nanoparticles	71
3.1	Introduction	71
3.2	Experimental	74
3.2.1	<i>Catalytic reduction of 4NP using RuDENSs</i>	75
3.3	Results and Discussion	75
3.3.1	<i>Kinetic Analysis</i>	77
3.3.1.1	<i>Investigation into the effects of surface area changes</i>	77
3.3.1.2	<i>Calculation of Langmuir-Hinshelwood parameters</i>	79
3.3.2	<i>Calculation of thermodynamic parameters</i>	85
3.4	Conclusion	87
3.5	References	87

Chapter 4 – Catalytic hydrogenation of toluene and the influence of various ionic liquids as catalyst coatings	90
4.1 Introduction	90
4.2 Experimental	92
4.2.1 <i>Catalytic hydrogenation of toluene in a 100 cm³ autoclave</i>	92
4.2.2 <i>Catalytic hydrogenation of toluene in a 300 cm³ autoclave</i>	93
4.2.3 <i>Continuous flow catalytic hydrogenation of toluene</i>	93
4.3 Results and discussion	95
4.3.1 <i>The catalytic evaluation of the silica 60 supported RuDENSs, RuSil60</i>	95
4.3.2 <i>Evaluation of the Ru-SCILL catalysts, based on RuSil60, in the hydrogenation of toluene and the influence of various ionic liquids on activity and selectivity</i>	99
4.3.3 <i>The catalytic evaluation of the silica 60 supported RuDENSs, RuSil100</i>	109
4.3.4 <i>Evaluation of the RuSil100-based RuSCILL catalysts in the hydrogenation of toluene and the influence of various ionic liquids on activity and selectivity</i>	112
4.3.5 <i>Continuous flow hydrogenation of toluene utilising RuSil100 and RuSCILL catalysts</i>	114
4.4 Conclusion	118
4.5 References	119
Chapter 5 – Hydrogenation of α,β -unsaturates	121
5.1 Introduction	121
5.2 Experimental	125
5.2.1 <i>Hydrogenation of citral</i>	125

5.2.2	<i>Hydrogenation of cinnamaldehyde</i>	126
5.3	Results and discussion	126
5.3.1	<i>Evaluation of RuSil60 catalaysts in the hydrogenation of citral</i>	126
5.3.2	<i>Evaluation of RuSCILL catalysts in the hydrogenation of citral</i>	129
5.3.3	<i>Evaluation of RuSil60 catalyts in the hydrogenation of CAL</i>	132
5.3.4	<i>Evaluation of RuSCILL catalysts in the hydrogenation of CAL</i>	135
5.4	Conclusion	137
5.5	References	138
Chapter 6 – The oxidation of styrene using RuDENs and silica-supported		
RuDENs as catalysts with <i>t</i> -butyl hydroperoxide as oxidant		
and the effect of ionic liquids as additives		
		141
6.1	Introduction	141
6.2	Experimental	144
6.2.1	<i>Catalytic oxidation of styrene</i>	144
6.3	Results and Discussions	144
6.3.1	<i>Evaluation of RuDEN catalysts</i>	145
6.3.1.1	<i>The effects of overall concentration of catalyst, substrate and oxidant on catalytic activity</i>	145
6.3.1.2	<i>Effects of oxidant loading</i>	146
6.3.1.3	<i>Effects of catalyst loadings</i>	148
6.3.1.4	<i>Temperature effects</i>	151
6.3.1.5	<i>Solvent effects</i>	153
6.3.1.6	<i>The effects of catalyst choice</i>	155
6.3.1.7	<i>Effects of ionic liquids and amounts of ionic liquids used</i>	158
6.3.2	<i>Evaluation of RuSil60 catalyts</i>	160
6.3.2.1	<i>Effects of catalyst loadings</i>	160



6.3.2.2	<i>Solvent effects</i>	163
6.3.2.3	<i>The effects of catalyst choice</i>	165
6.3.2.4	<i>Effects of ionic liquids and amounts of ionic liquids used</i>	167
6.4	Conclusion	169
6.5	References	170
Chapter 7	– Conclusion and recommendations	172
7.1	Conclusion	172
7.2	Recommendations	175



Chapter 1 – Review on the scope of nanoparticle preparation and utilisation of ruthenium nanoparticles

1.1 Introduction

The term nanoparticle loosely refers to a series of ultrafine particles, more specifically, falling within a defined size range of 1-100 nm. Nanoparticles belong between the realms of the molecular species and that of bulk systems, somewhat tethering the properties of both. This makes them attractive in both applications and fundamental studies, given the possibility to exploit their interesting properties. Transition metal nanoparticles consist of tens to thousands of transition metal atoms clustered together to form nanoparticles of various sizes. These nanoparticles are stabilised by additives such as ligands, surfactants, polymers or dendrimers to help protect their surface and prevent agglomeration of the smaller nanoparticles to form larger nanoparticles. Nanoparticles are soluble in most organic solvents and can be used in homogeneous systems* or deposited on supports and thus heterogenised. Therefore, nanoparticles are incorporated into both the fields of homogeneous and heterogeneous catalysis and are sometimes referred to as semi-heterogeneous catalysts.¹⁻⁸ This review will provide a brief overview of nanoparticles in general, how they are synthesised and further elaboration on the catalytic evaluation of Ru nanoparticles on which this study is based.

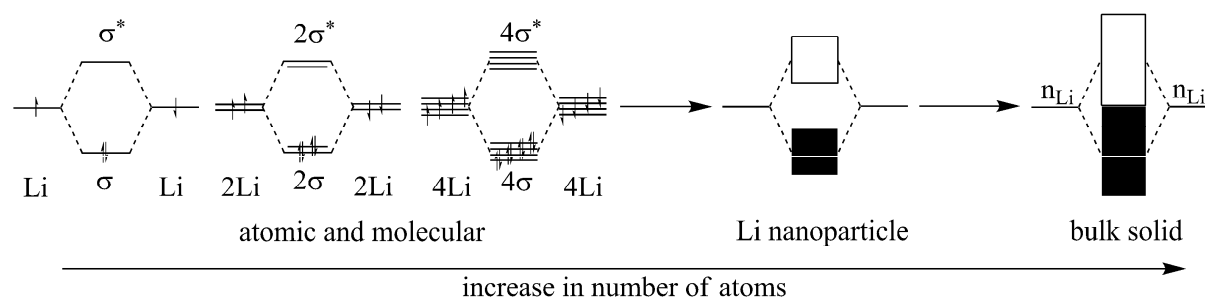
1.2 Properties of nanoparticles.

Nanoparticles are characterised by their large surface to total atom ratio. Gram for gram, compared to the bulk metals, nanoparticles have a higher surface area. To help understand why nanoparticles have gained much interest, from a fundamental perspective, we note changes in the electronic and chemical nature for nano-sized materials. Size reduction down to the regime of the De Broglie wavelength leads to a loss in the mobility of the electrons when compared to the bulk material. This results in the formation of discrete energy levels that the electron may occupy, a phenomenon referred to as the quantum size effects (QSE).

* Here the term homogeneous is used with the definition of using filtration to separate a solid/ligand system. When using the idea that there is a “bilayer” separating the bulk solution from the external surface, a case can be made that nanoparticles are heterogeneous systems.

The difference between molecules, nano-sized particles and bulk material derives from understanding of the molecular orbital theory and the extended form thereof, the band theory of metals. Essentially, the overlap of atomic orbitals leads to molecular orbitals consisting of bonding orbitals, non-bonding orbitals and anti-bonding orbitals. Increased overlap of orbitals leads to an increase in the energy gap observed between the bonding and anti-bonding orbitals. Additionally, an increase in the number of overlapping orbitals with increase in the amount of bonding atoms causes the orbital energies of the valence electrons to approach a continuum. For simplicity, and given that hydrogen does not bond beyond its diatomic form, consider lithium which provides a simplistic model for the transition from a molecule to the bulk state of an element. The available valence electrons in the 2s-orbitals of two Li atoms bond upon orbital overlap as shown in Scheme 1.1. This leads to the formation of σ and σ^* , bonding and anti-bonding orbitals respectively. The energy gap between the bonding and anti-bonding orbitals is a function of this overlap. An increase in the amount of bonding atoms causes an increase in the amount of σ and σ^* orbitals occupying the energy gap and describing a particular orbital energy. Eventually, this forms a continuum of orbital energies referred to as an energy band.

This simplistic view is true for the combination of s-orbitals to form molecular orbitals and becomes more complex for higher molecular weight metals. The characteristic of the bands are similar to those of molecular orbitals where less orbital overlap results in a weaker interaction and a narrow energy band. The d-orbitals show this behaviour given their specific shapes and orientation that is retained in the metal. In contrast, bonding s-electrons are highly delocalised forming what is referred to as a “sea” of electrons. The s-electron wave functions observe a great overlap leading to a variety of energy levels being occupied in the energy continuum and hence a broader energy band. Each of these occupied energy levels is referred to as a “state”. In contrast to the broad energy band observed for s-electrons, d-electrons occupy a narrow portion of the entire energy continuum. This collection of states occupying the portion of the energy continuum is referred to as the density of states (DOS). This is observed for the bulk material.⁹⁻¹⁰



Scheme 1.1. Change in valence level bands upon transition from a molecule to the bulk metal using lithium as a model.

Consider, bulk metal consisting of a lattice framework of metal atoms. The lattice orbitals consisting of the collection of atomic orbitals in the lattice, are filled with electrons. Essentially, the electronic structure of the crystalline solid is described by periodic combinations of atomic orbitals. Given the translational symmetry of a crystal lattice, the electrons are described by the superposition of plane waves through the entire structure. This is characteristic of the broad energy bands earlier mentioned. For smaller crystals typically in the nanometer range, the system can no longer be described by the same model as bulk solids where translational symmetry of the crystal lattice is assumed to an infinite boundary. Considering nanocrystals, these have neither the translational symmetry nor assumed infinite size of the bulk material. The electronic properties of a nanocrystal should therefore be intermediate between the discrete energy levels of a molecule and the broad energy bands of a bulk material. Essentially, as you decrease the dimensions of the bulk system to that of a nanocrystal, the band gap increases. This leads to the formation of discrete closely spaced orbital energy levels that no longer resemble the continuum of the energy band. This results in different quantum size effects most noticeable in changes in electronic, optical and importantly, catalytic properties.¹¹

The previous rationalisation started from the molecular level using molecular orbital theory and band theory to help account for some of the properties of the nanoparticle. Alternatively, the concept of quantum confinement in a solid can be used to describe the changes occurring when reducing an object to the smaller dimensions of a nanoparticle. The mobile electrons are limited in their movement, for materials, typically when the De Broglie wavelength of the valence electrons is equal to the thickness of the particle. Consider the reduction of a three-dimensional material to a zero dimensional quantum dot as illustrated in Figure 1.1. Reducing the size of a three dimensional object to a two dimensional object, typical of a monolayer of

atoms, significantly restricts the motion of the electrons within a quantum wall. Conceptually, further decreasing the dimension of the material leads to a quantum wire construct that has only one dimension for the electron to move in.

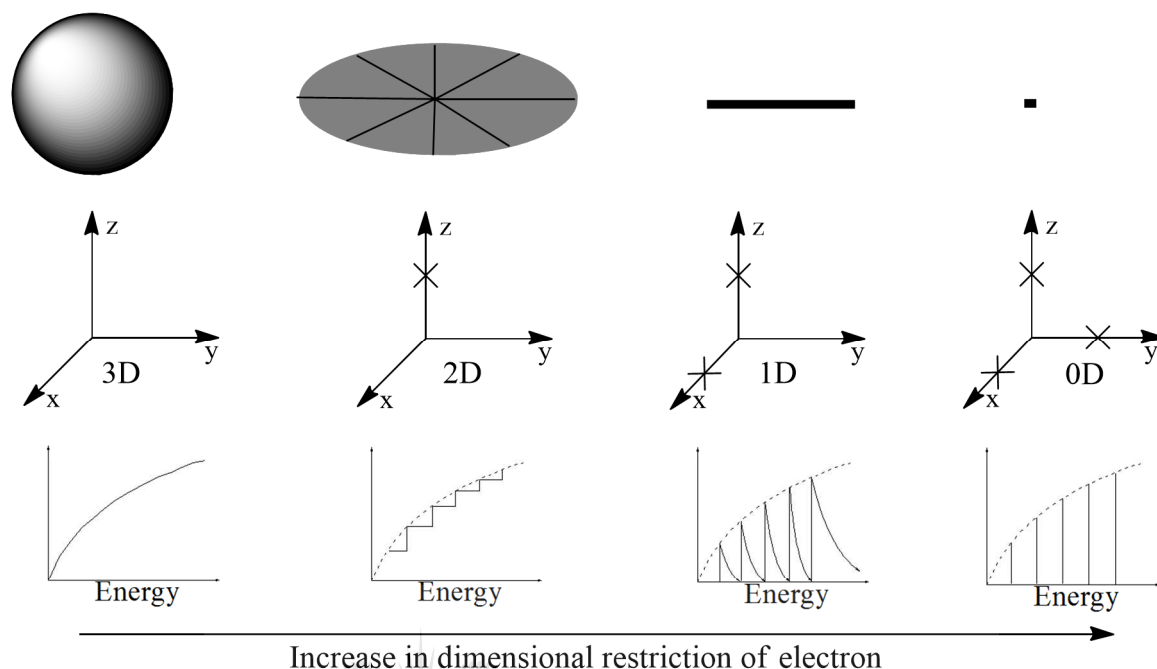


Figure 1.1. The effects of reducing the dimensions of a material on the physical and electronic properties. Nanoparticles fall within the zero-dimensional category, with distinct and restricted energy states.

Finally, reducing the dimensions of the material to a zero dimensional construct, the characteristic mobility of the electrons in a bulk metal is lost. Essentially, the electron is fenced within this geometrically confined system. The systematic decrease in size, affects the physical and chemical characteristics of the nanoparticle - especially those in the range of 1-10 nm. This effect that causes a change in the properties of the material is referred to as the Size Induced Metal-Insulator Transition (SMIT).¹¹

1.3 The mechanism of nanoparticle formation.

Gold nanoparticles were first used about 2000 years ago as pigments.¹²⁻¹³ Today, syntheses are inspired by the method Faraday developed about 150 years ago.¹²⁻¹³ The research involved synthesising Au nanoparticles by reducing $[\text{AuCl}_4]^-$ using phosphorus as a reducing agent.¹³ Numerous reviews have been written on the synthesis of nanoparticles.¹⁴⁻¹⁸ There are two

approaches to synthesising metal nanoparticles, also commonly referred to as metal colloids namely the “top-down” and “bottom-up” synthetic method. The top-down approach entails the formation of metal nanoparticles by mechanical means. These include the mechanical grinding of bulk metals to form metal nanoparticles and stabilisation of these by use of colloidal protecting agents¹⁹⁻²⁰ and methods such as size reduction lithography.²¹ The bottom up approach involves the synthesis of metal nanoparticles starting with metal complex precursors that are reduced using a reducing agent and subsequently stabilised by a variety of chemical stabilisers.²²⁻²³ The bottom-up approach is most commonly applied to nanoparticle synthesis as it gives better control of particle size when compared to the top-down approach, therefore more research advances were made using this methodology.

With specific focus on the bottom-up approach, the formation of nanoparticles relies on the processes of nucleation, growth and stabilisation of the nanoparticle. Similar to the process of crystallisation, for any particular crystal to form, the concentration of the solute in the solvent should exceed its equilibrium solubility or the reaction conditions should facilitate this process. The latter can be facilitated by decreasing the temperature. In the case of nanoparticles, the metal atoms are the atoms involved in the formation of the seed particles. These seed particles are the result of the nucleation process.²⁴⁻²⁶ As illustrated in Figure 1.2 the initial step in nanoparticle formation is the nucleation process.

This can occur via heterogeneous or homogeneous nucleation, but more likely a combination of both. The homogeneous nucleation consists of the spontaneous condensation of metal atoms to form the seed particle prior to growth. Heterogeneous nucleation is facilitated by the presence of impurities in the reaction mixture. The growth of nanoparticles depends on the remaining concentration of metal atoms in solution once the concentration of the metal decreases below the critical equilibrium solubility.²⁴⁻²⁶ Additionally, existing seed particles can coalesce to form larger nanoparticles, a process facilitated by Brownian movement of the particles in solution. The process of growth leads to the formation of larger nanoparticles and if uncontrolled, leads to eventual precipitation of the bulk metal.

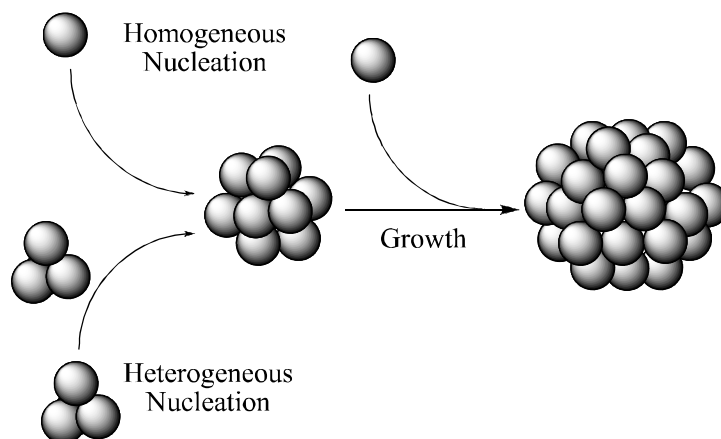


Figure 1.2. Nucleation and growth process of nanoparticles where the spheres represent the metal atoms.

One drawback of the preparation of nanoparticles in solution is the possible dissolution of the atoms comprising the nanoparticle.²⁷ These atoms can contribute to the growth of existing nanoparticles and increase the size distribution while decreasing the amount of nanoparticles. This process is referred to as Ostwald ripening. The stabilisation of metal nanoparticles during their preparation is therefore important as a means to control the nanoparticle size and minimise Ostwald ripening. The smallest nanoparticle that can form comprises of one central atom and twelve surrounding atoms giving a completely shelled polyhedron.²⁸ Stable nanoparticles defined as completely shelled polyhedrons are nanoparticles with 13, 55, 147, 309, 561 or 1415 atoms. These are referred to as magic numbers and are defined by the equation:

$$N = 1 + \sum_{i=1}^n (10i^2 + 2)$$

where N is the magic number and n is the number of atom layers or, as earlier referred to, shells. Due to the small size of nanoparticles, a high percentage of the atoms are surface atoms. This makes most of the atoms available for catalysis and can lead to an increase in catalytic activity.²⁹

1.4 Model reactions as a means to study surface characteristics and reaction kinetics.

The catalytic application of nanoparticles is usually driven by eventual commercial application but essentially the catalytic behaviour of NPs can be used to infer some information about the surface nature of the NP. Model reactions are used to evaluate a catalyst and compare it to other existing catalysts given its wide use.³⁰ These reactions can be readily conducted. One commonly explored reaction is the aqueous reduction of 4-nitrophenol (4NP) to 4-aminophenol (4AP). The reaction is readily monitored by observing a decrease in the concentration of the 4-nitrophenolate anion in the presence of the catalyst and sodium borohydride as reducing agent. The model allows for a complete kinetic evaluation of the catalyst. This reaction has been the subject of review with specific focus on modelling kinetic data according to the Langmuir-Hinshelwood model.³⁰ This model assumes the adsorption of at least two reactive species on a catalyst surface before any reaction occurs. This differs from the Eley-Rideal mechanism where only one reactant adsorbs to the catalyst surface. The other reactant moves within the system and reacts with the surface adsorbed species upon which desorption of the product occurs. This is the rate determining step.³¹ In the Langmuir-Hinshelwood mechanism, both reactants compete for surface sites on the catalyst surface. The Langmuir isotherm used to model surface coverage of the catalyst surface by a particular adsorbate, assumes that adsorption is not dependant on the degree of surface coverage. This is, however, only applicable to ideal situations and to account for the change, the Langmuir isotherm is combined with the Freundlich isotherm. The Freundlich isotherm takes into account that for higher surface coverage, the adsorption rate decreases and full surface coverage is never attained. The combination of the two isotherms allows for a model that better describes “non-ideal” systems and will be further discussed in a later chapter.³¹ With regards to studies evaluating ruthenium nanoparticles using this approach, the study does not extend beyond the benchmarking of the catalytic system. A study on the facile preparation of bimetallic Ru/Ni DENs utilised the model catalytic reduction of 4-nitrophenol to benchmark the activity of their catalyst. An increase in reaction rate was observed for the inclusion of Ni when compared to the RuDEN catalyst.³² In this case, the reduction of 4-nitrophenol was only used to benchmark the catalytic activity and not used to study the characteristics of the surface reactions. This reaction serves as a potential avenue for investigating the catalysts prepared in this study and will be demonstrated in a later chapter.

1.5 Synthetic approaches to preparing nanoparticles.

Various methods exist for the preparation of colloidal solutions of nanoparticles. As earlier mentioned there are two main approaches for the preparation of nanoparticles. These are the “top-down” approach and “bottom-up” approach. A few of the preparation methods are highlighted in this section to give an idea of the various options available for preparing the elemental metal namely:

- Electrochemical synthesis of metal nanoparticles.
- Radiolysis and photolysis.
- Thermal decomposition of complexes for nanoparticle preparation.
- Organometallic synthesis of metal nanoparticles including ligand displacement and ligand reduction.
- Chemical reduction of transition metal complex precursors.

1.5.1 Electrochemical synthesis of metal nanoparticles.

The method was developed by Reetz and co-workers in the 1990's.³³⁻³⁴ It consists of a five step process shown in Figure 1.3.

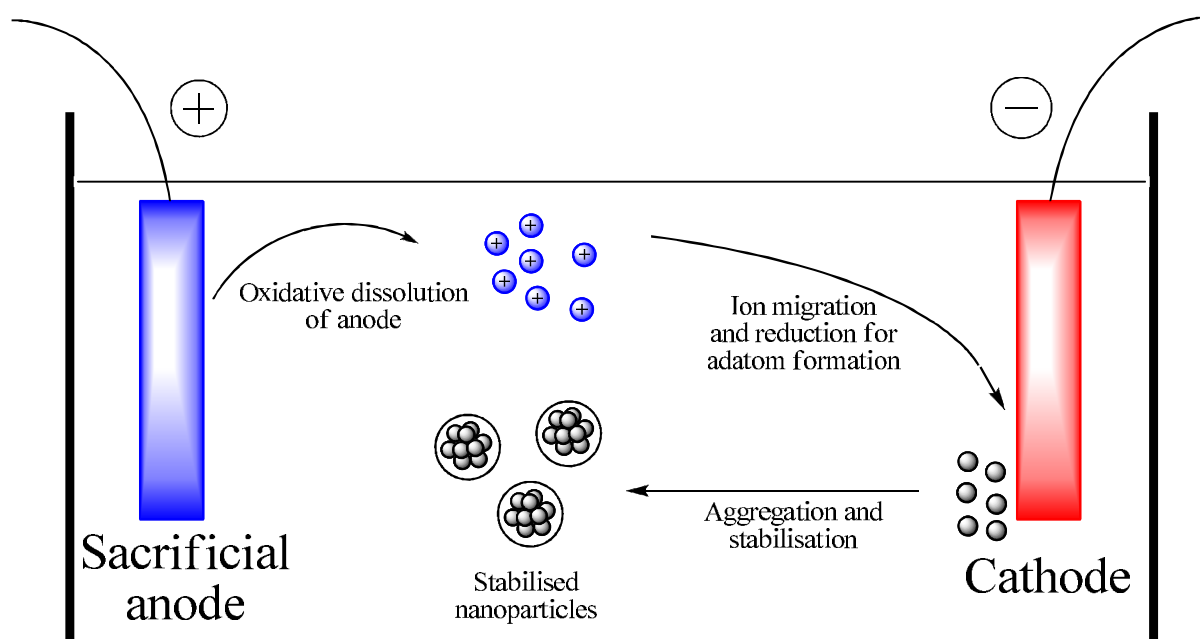
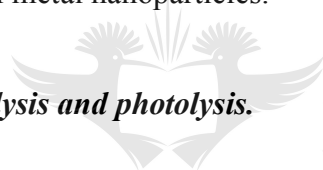


Figure 1.3. Preparation of metal NP's by electrochemical synthesis.

- Step 1: The bulk anode is oxidised and dissolution of the metal occurs.
- Step 2: The metal ions migrate to the bulk cathode.
- Step 3: These oxidised metal particles are then reduced to zerovalent metal atoms.
- Step 4: The atoms agglomerate to form particles via a process of nucleation and growth.
- Step 5: These particles can be stabilised as metal nanoparticles using a stabiliser e.g. trialkylammonium ions.

There are advantages to using this method over the conventional wet reduction. There is no need for reducing agents whose by-products could contaminate the nanoparticles formed. Nanoparticle size can be controlled by altering experimental parameters such as distance between electrodes, reaction time and temperature and solvent polarity. High current density, for instance, leads to the formation of smaller nanoparticles and vice versa. The versatility of this method lends to the formation of bimetallic alloys by use of two sacrificial metal anodes.³⁵ This method can be used in tandem with wet chemical methods to prepare bimetallic core/shell metal nanoparticles.³⁶

1.5.2 Radiolysis and photolysis.



UNIVERSITY
OF
JOHANNESBURG

Nanoparticles prepared by the photochemical reduction methods can arise either by reduction of the metal complex by radiolytically produced reducing agents such as free radicals and electrons or photolysis of photolabile metal complexes. Essentially, the methodology differs according to the reducing species generated which in turn depends on the solvent and added solute. The advantage of this method is the instantaneous and homogeneous production of metal nuclei prepared for the formation of nanoparticles.¹¹

1.5.3 Thermal decomposition of complexes for nanoparticle preparation.

Thermolysis refers to the thermal decomposition of a compound. Certain metal complexes can decompose thermally to produce their respective metal nuclei and can be achieved under mild conditions. These can include the thermal decomposition of metal carbonyls for the metals palladium, platinum, rhodium and ruthenium amongst others.¹¹ Polymer stabilised nanoparticles prepared utilising this method have particle sizes ranging from 1-10 nm. The nanoparticles can be synthesised in the absence of a stabiliser as was witnessed for the

preparation of palladium nanoparticles from palladium acetate and palladium acetylacetonate.¹¹ The stability of acetylacetonate complexes can necessitate the use of higher temperatures to ensure thermolysis. In this case, higher boiling solvents are used as reaction media. The absence of stabiliser consequently, allows for the preparation of nanoparticles with a broad size distribution. Addition of polymeric stabilisers such as poly(N-vinyl-2-pyrrolidone), (PVP), allowed for the preparation of copper-palladium nanoparticles with diameters of 1-4 nm as reported by Toshima *et al.*³⁷

1.5.4 Organometallic synthesis of metal nanoparticles including ligand displacement and ligand reduction.

The reduction of metals prior to the preparation of nanoparticles provides a source of the zero-valent metal available for nucleation. Organometallic precursors such as metal carbonyls can be synthesised and subjected to thermolysis. An extension of this is the replacement of existing ligands using an excess of weakly bound ligands and subsequent reduction of the ligand. This allows the generation of metal nanoparticles at low temperatures. Various examples utilising this technique exists in literature with a review recently published by Chaudret *et al.*³⁸ The review focused on the application of [Ru(COD)(COT)], (COD = 1,5-cyclooctadiene, COT = 1,5,7-cyclooctatriene), as a metal precursor in the preparation of Ru NPs. The [Ru(COD)(COT)] is easily reduced under a hydrogen atmosphere and at relatively low temperature. Nanoparticles of various sizes were prepared using various stabilisers including polymers, ionic liquids, organic ligands and alcohols.

This approach is not limited to Ru. Studies dated as early as the 1970s demonstrated the use of dibenzylideneacetone complexes of Pt and Pd as useful metal precursors in the preparation of their respective nanoparticles. Nanoparticles were easily obtained by reacting these complexes under mild conditions with hydrogen or carbon monoxide.³⁹

1.5.5 Chemical reduction of transition metal complex precursors.

Chemical reduction of transition metal complexes is one of the most commonly used routes to metal nanoparticle synthesis. This encompasses the use of different methodologies sharing the common theme of being reduction reactions. There are various reducing agents used in the preparation of metal nanoparticles and a few of those most commonly utilised, will be

highlighted here. The classical Faraday-route of preparing gold nanoparticles produces gold nanoparticles of approximately 20 nm using sodium citrate as a reducing agent. Citrate therefore functions as both the reducing agent and the stabilising agent. Reproducibility utilising this synthesis was demonstrated by Turkevich *et al.*⁴⁰⁻⁴¹ Equation 1.1 illustrates the general reactants required for the preparation of metal nanoparticles.



Equation 1.1. General equation for the reduction of a metal salt to eventually form the metal nanoparticle.

Metal nanoparticles are therefore prepared from a transition metal salt, an appropriate reducing agent, and a stabilizing agent to help prevent excessive agglomeration of metal atoms and control the size and size distribution of the metal nanoparticles formed.⁴² Similarly, hydrazine hydrate is a reducing agent utilised in the preparation of aqueous suspensions of metal nanoparticles. It is a versatile reducing agent used for the preparation of Pt,⁴³ Au⁴⁴ and Cu⁴⁵ nanoparticles amongst others.

In some cases the solvent can serve a two-fold purpose, increasing the efficiency of nanoparticle preparation. Alcohols are an example of reducing agents that serve a dual purpose. Given the ease of oxidation at certain reaction conditions, these easily oxidized solvents serve in the reduction of the metal complex as well as a diluent for the nanoparticles formed. Most commonly, the resulting NPs are stabilised by polymers such as PVP, and poly(vinylalcohol).⁴⁶⁻⁴⁸ Typically, alcohols utilised in these reactions have an α -hydrogen present, therefore, alcohols such as tertiary-butanol are not suitable. For instance, Pd organosols are prepared by heating palladium acetate in methanol under reflux. To help stabilise the NPs that form, PVP is used as stabiliser. Where higher reactions temperatures are required for NP preparation, higher boiling alcohols such as 2-ethoxy-ethanol can be used. On average, these reactions yield Pd NPs with a diameter of 6.5 nm.

The scope for nanoparticle preparation techniques is ever increasing. One of the most commonly used reducing agents for the preparation of metal NPs is sodium borohydride. First introduced by Brust *et al.*, as a method to reduce gold salts in the presence of alkanethiols, NPs with an average diameter of 1-3 nm were prepared.⁴⁹ Despite the efficacy of these

reducing agents, stabilisation of the forming nanoparticles is of great importance. The various stabilisation models will be discussed in the following section to provide insight into their usefulness.

1.6 Stabilisation of metal nanoparticles.

There are many routes utilised for the preparation of nanoparticles. Of importance is the control of the nucleation and growth process. Nanoparticles therefore need to be stabilised upon preparation because in their naked state they are kinetically unstable. These stabilising agents adsorb onto the surface of the nanoparticles thus preventing further nucleation and growth and controlling the dimensions of the nanoparticle.

There are three types of nanoparticle stabilisation techniques used. Electrochemical stabilisation of nanoparticles occurs when the cations and anions in solution associate with the nanoparticles. This forms an electrical double layer that surrounds the metal nanoparticle causing coulombic repulsion and preventing further agglomeration. Steric stabilisation relies on the adsorption of large molecules on the nanoparticle surface. The third stabilisation is referred to as electrosteric stabilisation and is a combination of electrochemical and steric stabilisation. The following section provides an overview of the practical methods used in nanoparticle stabilisation.

1.6.1 Stabilisation of nanoparticles using surfactants, micelles and microemulsions.

Surfactant stabilised nanoparticles were reported as early as the 1970s.⁵⁰ Upon reduction of metal salt precursors to zero-valent metal centres, the surfactant helps to prevent excessive agglomeration of metal atoms by forming a protective monolayer around the core of the nanoparticle.

Tetraalkylammonium halides $[R_4N^+X^-]$ are a common type of lipophilic surfactant used in producing stable nanoparticle organosols. Pd nanoparticles were prepared using these tetraalkylammonium salts by reduction of Pd salt precursors.⁵¹⁻⁵² The nanoparticles had a size distribution of 1-5 nm. Reducing agents are not always necessary as demonstrated by Reetz and Maase in 1999.⁵³ They prepared nanoparticles by gentle heating of a Pd precursor in an organic solvent containing an excess of tetraalkylammonium carboxylates. These long chain

alkyl groups provided a protective monolayer around the NPs maintaining a size distribution of 1-10 nm.⁵¹

Wet chemical methods allow for the preparation of NPs containing one or more metals. Bimetallic Cu-Pd NPs were synthesised using the same method as Singla *et al.*⁵⁴ This involves the synthesis of monodisperse Ni NPs in water using, hexadecyltrimethylammonium bromide (CTAB) in a tetraethylammonium bromide (TEAB) and tetra-*n*-butylammonium bromide (TBAB) mixture. This may lead to a synergistic effect between the two metals and when applied to catalysis may lead to an enhanced catalytic rate and selectivity. From an economic viewpoint, this can be useful when working with more expensive metal salt precursors. In the case of core/shell bimetallic NPs, the core could consist of a cheaper metal coated in the more expensive and catalytically active metal, an example being Ni/Pd core/shell nanoparticles.

Nanoparticles stabilised by micelles were investigated in the 1990s for their applications in catalysis.⁵⁵⁻⁵⁷ Micelles are an ordered aggregation of amphiphilic surfactant molecules consisting of a hydrophilic tail and hydrophobic head. A micelle solution consists of the hydrophilic head being in contact with the aqueous solution surrounding a core of hydrophobic tails. This behaviour allows for the immersion of hydrophobic molecules by encapsulation into the hydrophobic core of the micelle. A microemulsion consists of micelles or inverse micelles in solution. This mixture is a thermodynamically stable mixture of two immiscible fluids like oil and water stabilised by surfactant molecules (Fig 1.4). The various microemulsions used are water in oil (w/o), oil in water (o/w) and water-in-supercritical-CO₂ (w/sc-CO₂) microemulsion. Water containing inverse micelles provides a useful method for preparing monodispersed NPs.

Seregina *et al.* prepared monometallic and bimetallic NPs.⁵⁸ These were stabilised in a micellar core consisting of polystyrene-block-poly-4-vinylpyridine (PS-*b*-P4VP) in toluene and used for hydrogenation. A problem with this method is the difficulty in separation of reaction products from the catalyst system. Ultrafiltration or the use of sc-CO₂ as solvent is one way to overcome this.

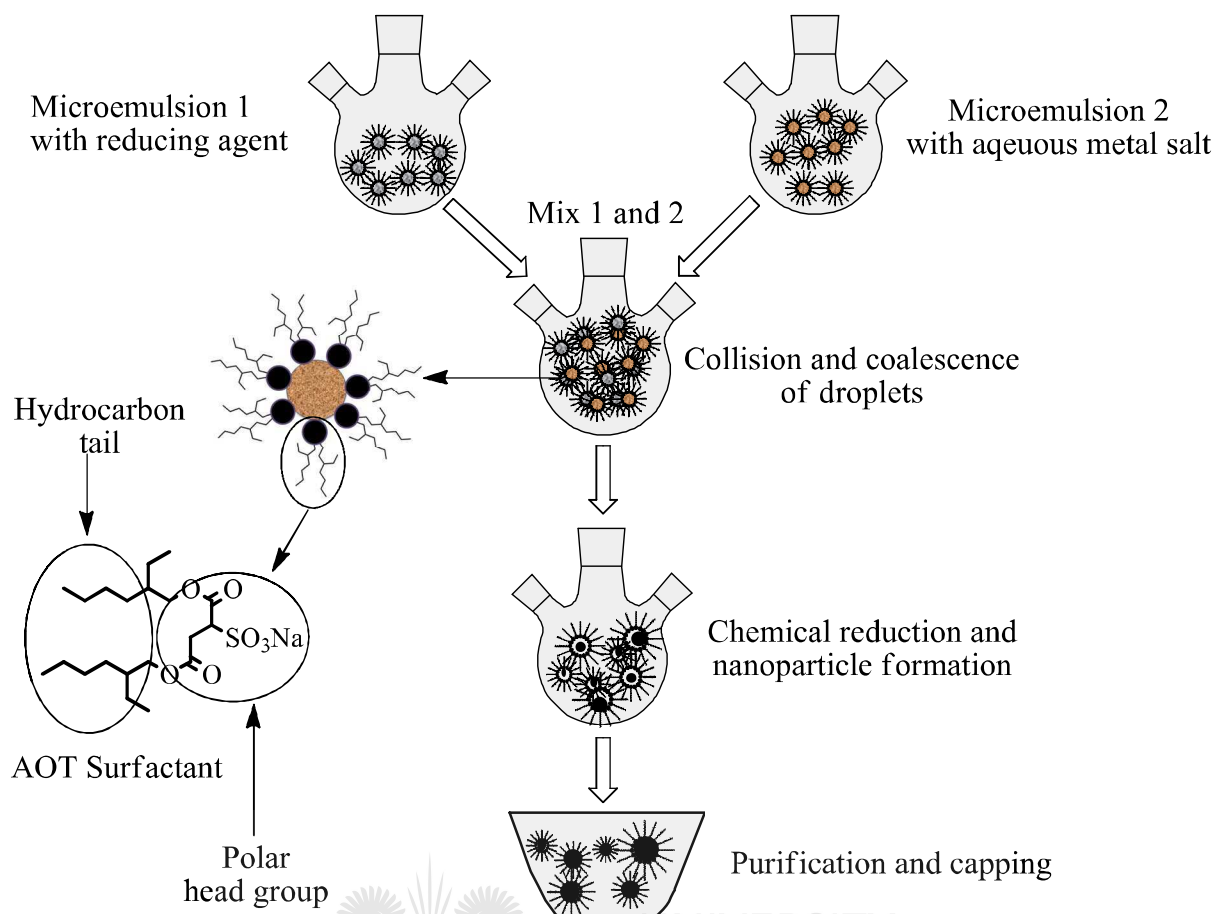


Figure 1.4. Synthesis of nanoparticles using the reverse-micelle methodology where the nanoparticles are capped with the capping agent dioctyl sodium sulfosuccinate (AOT).

Water containing inverse micelles were used by Boutonnet *et al.* to synthesise Au, Pd, Pt and Rh NPs by reduction of the relevant metal salt precursors using N_2H_4 and H_2 .⁵⁹ Metal NP size can be controlled by changing the water-to-surfactant ratio. The method is, however, limited by the types of reducing agents, N_2H_4 and $NaBH_4$ being commonly used.

1.6.2 Ligand stabilised nanoparticles.

Ligands as nanoparticle stabilisers are of particular interest due to the potential of creating an asymmetric environment around the nanoparticle. This is important when trying to achieve enantioselective conversion of a particular substrate. One of the first examples entailed research by Nasar *et al.*, who observed that the Rh NP catalysed hydrogenation of disubstituted aromatic rings formed the chiral amine, R-dioctylcyclohexyl-1-ethylamine.⁶⁰ Preparation of these ligand stabilised nanoparticles is similar to that of microemulsions. Silanes (RSiH) such as *t*-butyldimethylsilane are also being used as stabilising agents for

PdX_2 ($\text{X} = \text{Cl}^-, \text{OAc}^-$) in *N,N*-dimethylacetamide. The NP solution formed was used to catalyse, amongst others, the coupling of silane with phenyl and vinyl thioethers giving thiosilanes and silthianes.⁶¹

Similar to core/shell nanoparticles that are stabilised in microemulsions, those stabilised by ligands have also been prepared. Bimetallic NPs were synthesised by thermal decomposition (135 °C) with Ni as the core and Pd as the shell from the precursors $[\text{Ni}(\text{acac})_2]$ and $[\text{Pd}(\text{acac})_2]$ (acac = acetylacetonato) respectively. Trioctylphosphine was utilised as stabilising ligand. Ni decomposed before Pd and these NPs were employed as catalysts in the Sonogashira coupling of *p*-bromoacetophenone with phenylacetylene.⁶²

1.6.3 *Nanoparticles stabilised by ionic liquids.*

Ionic liquids are used in the preparation of NPs since they can function as both stabilisers and solvent. Bulky cations are known to favour electrostatic stabilisation of NPs. When employed in catalytic reactions that are usually multiphase, the nanoparticles remain in the ionic solution. The catalyst can therefore be easily recovered by decanting the catalytic ionic solution and then subsequently reused.⁶³ Stability of nanoparticles can be further increased by addition of a co-stabilizer. Ionic co-polymer⁶⁴ and PVP⁶⁵ were shown to increase NP stability and activity. Placing ligands on the nanoparticle surface may lead to the formation of more stable NPs. The addition of phenanthroline to Pd NPs in an ionic liquid showed a decrease in Pd agglomeration when compared to NPs in the ionic liquid alone. This system was utilised as a catalyst for alkene hydrogenation and the system could be recycled and reused several times without significant loss of activity.

1.6.4 *Nanoparticles stabilised by macromolecules.*

Macromolecules are characterised by their large molecular weights and the steric constraint they may provide. The latter is particularly useful in steric stabilisation of nanoparticles. The macromolecule, PVP is a versatile polymer for these purposes as it fulfils both steric and ligand requirements.

1.6.4.1 *Polymers*

The methodology for preparation of polymer stabilised nanoparticles is similar to that for surfactants as stabilising agents. Due to their large size they provide steric stabilisation for the most part where stabilisation efficiency is measured by a protection value. To illustrate this, PVP, poly(vinyl alcohol) and polyacrylamide have protection values of 50.0, 5.0 and 1.3 respectively.⁶⁶ The polymer, PVP, is commonly used because of its solubility in most polar solvents and its low environmental toxicity.⁶⁷ Polymers can act as reducing agents as well. The use of PVP in aqueous media for the preparation of Au and Ag nanoparticles was investigated where PVP functioned as both stabilising and reducing agent.⁶⁸⁻⁶⁹

1.6.4.2 *Dendrimers*

Another type of macromolecule used to stabilise metal nanoparticles are dendrimers. Dendrimers are characterised by their well-defined three-dimensional architecture and, in contrast to conventional polymers, have a polydispersity of 1.0.⁷⁰⁻⁷¹ Dendrimers have a characteristic tree-like structure for the lower generations and a more globular shape for the higher generations. This definite shape allows them to be monodispersed when in solution. The architectural versatility of dendrimers allows the introduction of functional groups within dendritic branches. Dendrimers therefore have the ability to accommodate nanoparticles within their branches and hence act as molecular boxes.

The first dendrimer was synthesised in 1978 by Buhleier *et al.*,⁷² a poly(propyleneimine) dendrimer. Other dendritic scaffolds utilised include poly(amidoamine) (PAMAM),⁷³⁻⁷⁴ as illustrated in Figure 1.5, arborol dendrimers by Newkome *et al.*⁷⁵⁻⁷⁷ and polyether dendrimers by Fréchet *et al.*⁷⁸⁻⁸⁰ The heteroatoms within dendrimer branches help stabilize the nanoparticles in conjunction with the steric stabilisation provided by the dendritic scaffold. Dendrimers as stabilising agents for nanoparticles are attractive for various reasons. They allow for the control of nanoparticle composition and solubility.⁸¹ The dendritic scaffold helps prevent excessive aggregation of metal surface that could obstruct catalytic sites on the nanoparticles surface.⁸²⁻⁸³ The potential use of dendrimer stabilised nanoparticles was first investigated in 1998 by the research groups of Crooks,⁸⁴⁻⁸⁶ Tomalia⁸⁷⁻⁸⁸ and Esumi.⁸⁹⁻⁹⁰

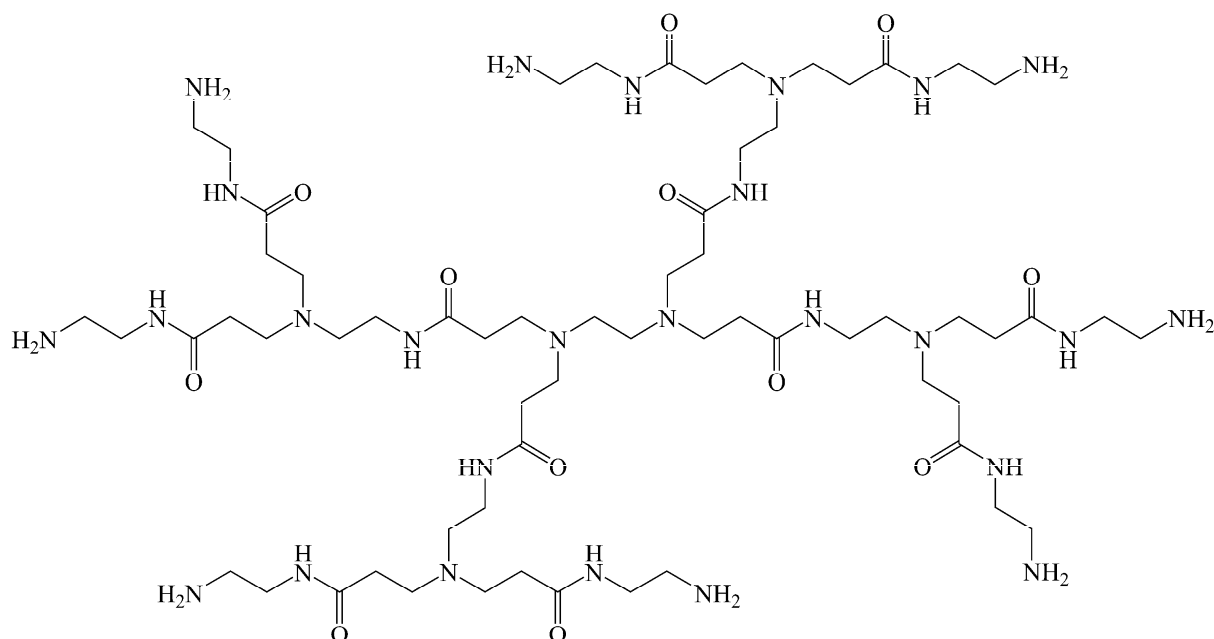


Figure 1.5. First generation amine terminated PAMAM dendrimer.

Therefore, dendrimers are well-suited for stabilisation of metal NPs for the following reasons:

1. Their template structure is uniform in structure yielding well defined nanoparticles.
2. NPs are encapsulated by the dendrimer preventing excessive agglomeration.
3. Stabilisation is sterically driven therefore there is minimal passivation of the nanoparticle by coordinating functional groups.
4. Dendrimer branches can act as access gates allowing size selective entry of certain substrates.
5. Terminal groups on the dendrimer can be altered to control the solubility of the dendrimer-nanoparticle hybrid.

Crooks and co-workers used the PAMAM dendrimers and complexed various metal ions (Cu^{2+} , Au^{3+} , Pd^{2+} , Ru^{3+})⁸⁴⁻⁸⁶ to the inner tertiary nitrogens of these dendrimers. The coordinated metal complexes were then reduced to form metal nanoparticles with the dendrimer entrapping the nanoparticles (Fig. 1.6).

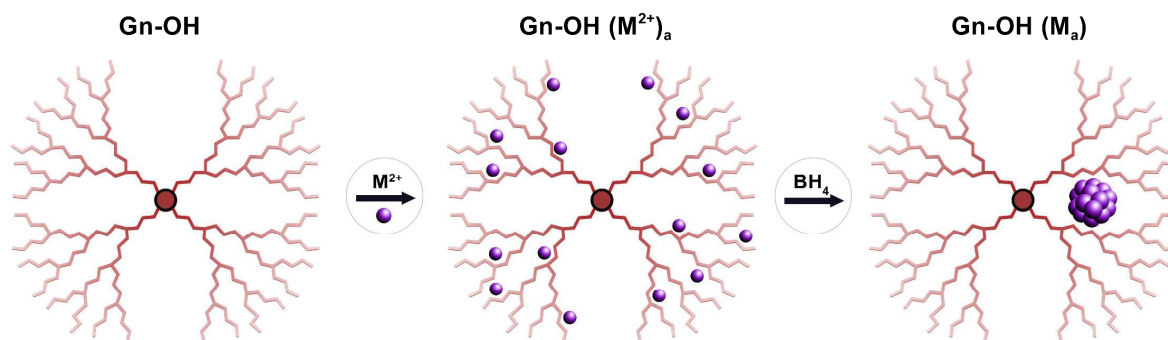


Figure 1.6. General synthetic methodology for the preparation of DENs where the metal complex is first coordinated to the dendrimer and then reduced to form the DEN.

Similar to nanoparticles stabilised by surfactants and other stabilising agents, bimetallic nanoparticles can be synthesised using dendrimers. Figure 1.7 shows three general strategies for preparing bimetallic dendrimer stabilised nanoparticles.

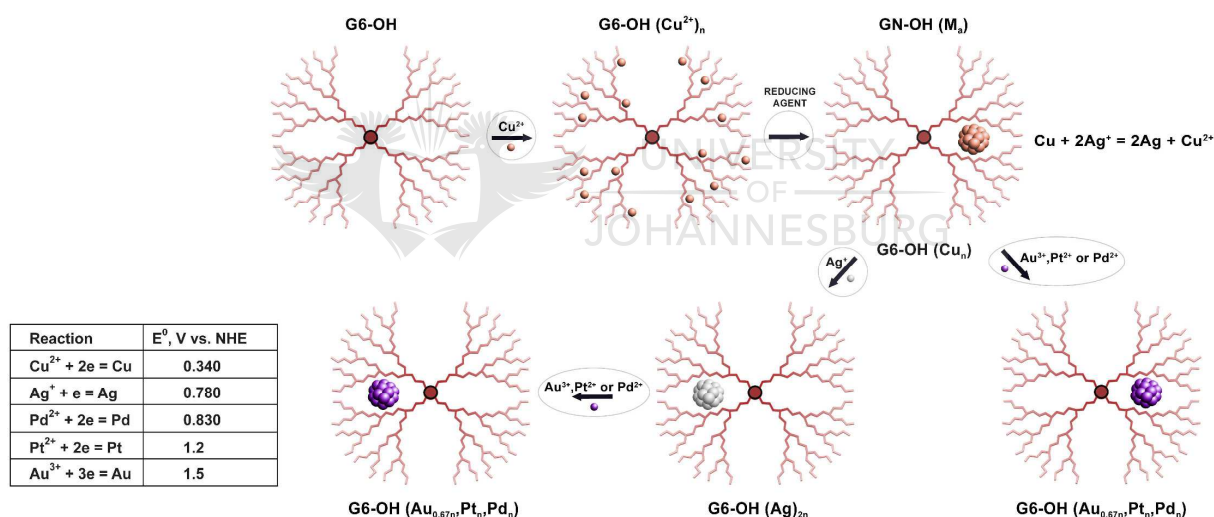


Figure 1.7. Various general strategies utilised in the preparation of bimetallic DENs.⁹¹⁻⁹²

Co-complexation allows for the preparation of alloys while sequential and partial displacement methods form alloys or core/shell materials. An example being Pd/Pt alloys prepared via the co-complexation routes. The Pd/Pt DENs show considerable stability for over a year in solution while maintaining a nearly monodispersed average NP diameter of 1.9 nm.⁹³

1.7 Nanoparticles supported on solid supports.

A problem in the use of nanoparticles is the issue of atom/ion leaching. One way to overcome this problem is by supporting nanoparticles on a solid support. There are many metal oxide support materials utilised, some which are based on Si,⁹⁴ Ti,⁹⁵ Zr,⁹⁶ Ca,⁹⁷ Mg,⁹⁸ and Zn.⁹⁹ Silica based supports are most commonly used in its various forms including SiO₂ sol-gels,¹⁰⁰ silica spheres,¹⁰¹ silica microemulsions,¹⁰² molecular sieves¹⁰³ and zeolites.¹⁰⁴

Immobilising nanoparticles on a solid support provides the catalytic system with the advantages of a heterogeneous catalyst. Due to the high surface area of the supports, the nanoparticles are dispersed. This helps maintain the high catalytic rates due to the dispersal of active nanoparticles and may even enhance them. Should the latter occur, this could indicate a definite synergistic effect between the nanoparticles and the support.

Nanoparticle supports must be stable at high temperatures, which is why silica- and titania-based supports are ideal. There are two ways to prepare supported nanoparticles that have been templated on dendrimers. Firstly, DENs may be used as a template for the support itself during sol-gel synthesis, in which case the dual-purpose dendritic template is removed by calcination.¹⁰⁵ Secondly, the support may be modified by grafting dendritic scaffolds onto the support and preparing the DENs on these supported dendrimers. Alper and co-workers were one of the first groups to dendronise solid supports.^{68, 69} They dendronised silica with PAMAM dendrimers and used it as a support for rhodium-based hydroformylation catalysts. This was further extended to the dendronisation of polystyrene.¹⁰⁶⁻¹⁰⁹

Preparation of the supported nanoparticles involves adsorption of the nanoparticle and stabiliser on the support and subsequent calcination to remove the stabiliser. This process of calcination is referred to as thermal activation. Su *et al.* conducted research on the preparation of Ru nanoparticles supported on SBA silica.¹¹⁰ The Ru nanoparticles were immobilised on the support by simple thermal reduction. The Ru NPs showed good dispersion and resistance against oxidation with lack of aggregation and pore blocking and less leaching. Higher catalytic rates were experienced for benzene hydrogenation compared to the traditionally prepared catalysts.

1.8 The best of both worlds: ionic liquid coated solid catalysts.

As earlier discussed, ionic liquids can be used as reaction media for the preparation of nanoparticles. Additionally, it has a stabilising effect on the nanoparticles due to interaction of the ionic liquid with the nanoparticle surface. When utilised in catalysis, ionic liquids form a bulk phase in biphasic reactions serving as a solvent and stabiliser for the nanoparticles. This has been demonstrated for hydrogenation reactions¹¹¹⁻¹¹³ amongst others. Catalytic reactions conducted in biphasic ionic liquid based reactions, usually observe a lower activity compared to those conducted in the absence of the ionic liquid.¹¹⁴⁻¹¹⁵ The biphasic nature of the reaction is characterised by a considerable amount of ionic liquid present for the bulk ionic liquid phase. Due to a generally lower solubility of gases in ionic liquids, this leads to mass transfer limitations. To help minimise mass transfer limitation, and hence increase gas diffusion, the ionic liquid can be dispersed as a thin layer across a high surface area material. Essentially, the utilisation of ionic liquid coatings have the following potential advantages:¹¹⁶

- the ability to utilise ionic liquids for their inherent properties,
- possibly change catalytic performance with either improvement in activity or selectivity and
- possible improved recovery of catalyst from the reaction mixture and reusability.

Various heterogeneous catalytic systems utilising ionic liquids as coatings exist. The supported ionic liquid (SIL) can serve to host a homogeneous catalyst and once dispersed on a solid support effectively heterogenises the system. This common form of a SIL catalyst is referred to as supported ionic liquid phase (SILP) catalysts. This section will not focus on differentiating the various SIL systems but rather focus on introducing a variant thereof, the solid catalysts with ionic liquid layer (SCILL), catalyst. The concept was initially investigated by Kernchen *et al.*¹¹⁷ The presence of the ionic liquid can influence the catalytic activity either by acting as a catalyst surface modifier through its interaction with the surface atoms of the nanoparticle or change the concentration of substrates and intermediates based on their solubility in the ionic liquid. Hypothetically, in the latter, if the SCILL catalyst was evaluated for arene hydrogenation and the partially hydrogenated intermediate was less soluble in the ionic liquid, the intermediate would partition into the bulk solvent.¹¹⁷ If previously, the uncoated catalyst was selective to the fully hydrogenated product, selectivity would have been enhanced for the partially hydrogenated product. This is but a fraction of the possible efficacy

of these systems and more detailed studies underpin the performance of such systems. The advantages of previously discussed supported NP catalysts and the enhancing properties of ionic liquids are now combined with the possibility to study novel catalytic systems and achieve enhanced catalytic activity. The various ways of utilising NPs as either a colloid solution, supported catalyst or even in SIL systems, creates the potential for a variety of applications. The current study focuses on the use of Ru NPs in various systems and in the following section specific attention is given to its evaluation as a catalyst.

1.9 Application of ruthenium nanoparticles in catalysis.

Nanoparticles have been utilised as catalysts for decades. Due to their nanometer dimension and high surface to volume ratio, they may approximate the catalytic performance experienced when using mononuclear complexes. The most studied metal nanoparticles utilised as catalysts are based on Ru, Rh, Pt, Pd and Au.¹² The Pd and Au NPs have received the most attention amongst these metals with Pd being known as an excellent catalyst for hydrogenation and C-C bond formations.¹² Increased catalytic rates seen when using NPs arise from the size dependent properties of these catalysts. The following section focuses on the use of Ru NPs as catalysts. The Ru NP catalysts are commonly used in hydrogenation reactions with the substrate being mainly alkenes and alkynes.

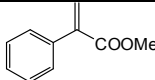
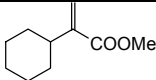
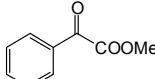
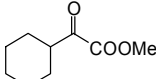
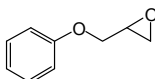
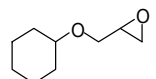
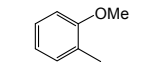
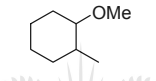
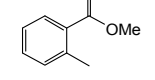
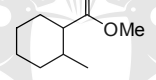
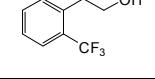
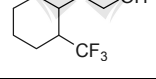
1.9.1 Catalytic evaluation of ruthenium colloidal suspensions.

Structure sensitivity of substrates can have an influence on the activity when evaluating a catalyst for the same catalytic reaction. Ruthenium colloidal systems comprise of reduced RuCl_3 under H_2 and in the presence of trioctylamine (TOA) reduced various aromatic substrates. The reactions were conducted in a water-methanol system with 50 bar H_2 and at room temperature.¹¹⁸ Table 1.1 shows some results obtained for the time taken to reach 100% conversion. The time taken to reach complete conversion is dependent on steric and electronic properties of the substituents on the aromatic ring. The results demonstrate the effect of molecular structure where electron rich substrates favoured a faster reaction.

Ligands as stabilising agents provide a means of tuning the surface state of the nanoparticles by chemical influence of the ligand. The use of asymmetric ligands creates potential applications in enantioselective catalysis by NPs. Studies of Ru ligand stabilised NPs are

minimal and most only focus on their use as hydrogenation catalysts for aromatic substrates. Finke and Süß-Fink proved nano-heterogeneous $\text{Ru}(0)_n$ particles to catalyse the hydrogenation of benzene. Their results show that $\text{Ru}(0)_n$ is responsible for >99% of the observed catalysis.¹¹⁹

Table 1.1. Hydrogenation of various aromatics by Ru/TOA colloids in MeOH/H₂O medium, room temperature, 50 bar H₂.¹¹⁸

Substrates	Products	Reaction time for 100% conversion (hrs)	cis/trans
		9	-
		34	-
		1	-
		1	20
		1	15
		100	17

Chaudret *et al.* conducted research on the preparation of Ru nanoparticles from organometallic precursors and used them in the hydrogenation of benzene and quinoline.¹²⁰⁻¹²¹ The $[\text{Ru}(\text{COD})(\text{COT})]$ was decomposed in MeOH/THF without the presence of added stabiliser. The particles varied in size according to the composition of the solvent mixture with the mean size being 20 nm. An 88% conversion of benzene to cyclohexane was observed after 14 hours at H₂ pressure of 20 bar and temperature of 80 °C. Ionic liquids are useful reaction media since they can act as stabilisers for NPs and help facilitate separation of the catalytic products. Dupont *et al.* prepared Ru NPs by decomposition of $[\text{Ru}(\text{COD})(\text{COT})]$ under 4 bar H₂ and at 75 °C using 1-*n*-butyl-3-methylimidazolium hexafluoroborate (BMI.PF₆) or 1-*n*-butylimidazolium tetrafluoroborate (BMI.PF₄).¹¹⁵ Hydrogenation of various substrates was achieved under mild conditions as shown in Table 1.2.

Table 1.2. Hydrogenation of alkenes by Ru(0) nanoparticles under multiphase and neat conditions (75 °C and 4 bar H₂, substrate/Ru = 500).¹²²

Medium	Substrate	T (h)	Conversion (%)	TON ^a	TOF (h ⁻¹) ^b
neat conditions	1-hexene	0.7	>99	500	714
BMI.BF ₄	1-hexene	0.6	>99	500	833
BMI.BF ₆	1-hexene	0.5	>99	500	1000
neat conditions	cyclohexene	5.0	>99	500	1000
BMI.BF ₄	cyclohexene	8.0	>99	500	100
BMI.BF ₆	cyclohexene	1.2	76	500	62

^a Turnover number TON = mol of hydrogenated product/mol of Ru.

^b Turnover frequency TOF = TON/h.

Gómez *et al.* investigated the hydrogenation of arenes using Ru and Rh nanoparticles.¹²³ They aimed to increase the solubility of these nanoparticles in supercritical CO₂ by using phosphine stabilising agents containing fluorinated groups. The ruthenium nanoparticles showed higher catalytic rates and conversion percentages for the hydrogenation reactions. This could be due to a lower level of agglomeration experienced for the Ru nanoparticles than that of Rh during catalysis.

Catalytic Ru NPs have also been utilised in coupling reactions. Chang *et al.* investigated the use of Cu and Cu-based NPs as a more economic and eco-friendly alternative to using the noble metals alone.¹²⁴ The NPs were prepared by reduction of the metal salts with tetraoctylammonium formate (TOAF) in DMF. The average nanoparticle size ranged from 1.6 nm to 2.1 nm. These were evaluated in the coupling of phenylboronic acid and iodobenzene (Fig 1.8).

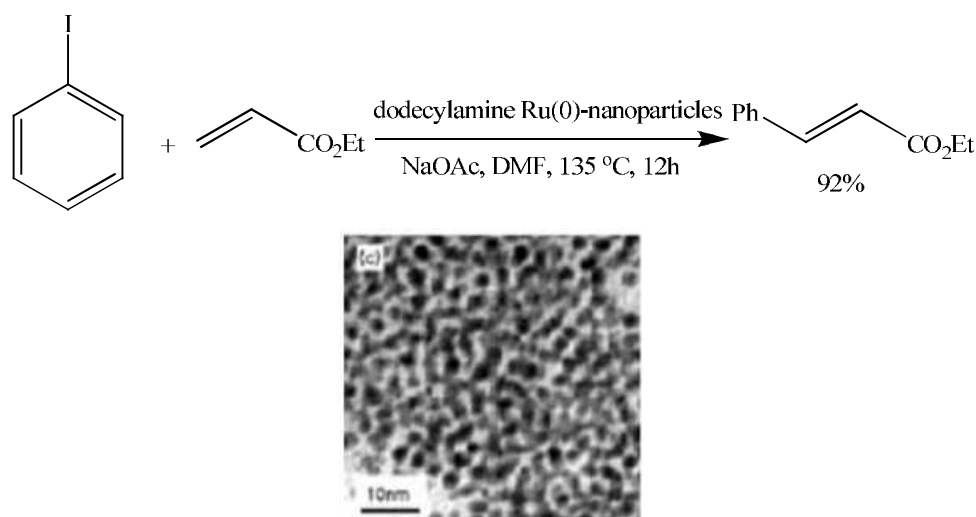


Figure 1.8. Coupling of phenylboronic acid and iodobenzene using dodecylamine capped Ru NPs.¹²⁴

Table 1.3 illustrates results obtained for the various mono-, bi- and multimetallic composite nanoparticles. The multimetallic nanoparticles show a definite advantage over the monometallic counterparts.

Table 1.3. Cross coupling reaction using various nanocolloid catalysts.^{a 124}

Entry	Catalyst (composition)	Yield (%) ^b	k_{obs} (L.mol ⁻¹ .min ⁻¹) ^c
1	Cu	62	3.2×10^{-3}
2	Pd	100	5.9×10^{-2} ^[d]
3	Ru	40	2.0×10^{-3}
4	Pd/Ru	100	2.9×10^{-2}
5	Cu/Pd/Ru	100	3.8×10^{-2} ^[d]

^a Standard reaction conditions: 0.5 mmol iodobenzene, 0.75 mmol phenylboronic acid, 1.5 mmol K₂CO₃, 0.01 mmol catalyst, 12.5 mL DMF, 110 °C.

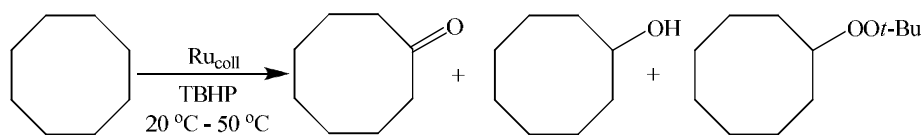
^b GC yield after 6 h, corrected for the presence of internal standard.

^c k_{obs} : Second order reaction rate constant.

^d Value is the average of two repeated experiments.

Oxidation reactions have particular importance in industry. Despite the vast applications of Ru nanoparticles in other catalytic reactions there are few examples reported on their use in oxidation reactions. One example is the oxidation of cyclooctane by *t*-butyl hydroperoxide (TBHP). This was achieved using Ru colloids in a biphasic water/cyclooctane mixture leading

to formation of cyclooctanol and cyclooctanone (Scheme 1.2).¹²⁵⁻¹²⁶ The catalyst is robust enough to be recycled without significant loss of activity for subsequent catalytic runs.



Scheme 1.2. Oxidation of cyclooctene in the presence of a Ru colloid and TBHP.¹²⁵⁻¹²⁶

1.9.2 Catalytic evaluation of supported ruthenium nanoparticles.

The immobilisation of NPs on a solid support allows for ease of recycling post catalytic run and could help minimize leaching. The merits of this study rely on the use of the dendrimer template technique to produce nanoparticles with a narrow size distribution. The presence of the dendrimer can help minimize sintering during immobilisation of the catalyst. This was observed when preparing and immobilising RuDENS on γ -alumina.¹²⁷⁻¹²⁸ Williams *et al.* prepared silica-supported monometallic Pt and Ru and bimetallic Pt-Ru NPs using dendrimer-metal supported complexes as precursors.¹²⁹ Conventional silica-supported catalysts were prepared by incipient wetness for comparison purposes. The catalysts were evaluated in the liquid-phase selective hydrogenation of 3,4-epoxy-1-butene (EpB). The Ru catalysts were less active than Pt-based catalysts. This is likely due to ruthenium's inability to actively dissociate H₂ at low temperatures. They showed that the dendrimer derived bimetallic catalysts were more active in the hydrogenation reaction than the conventionally prepared counterparts. The catalyst showed selectivity for the formation of crotonaldehyde instead of 3-buten-1-ol as seen for the other catalysts. The dendrimer-metal nanocomposites (DMN) methodology utilized, therefore creates a good measure of control on the preparation of bimetallic catalysts for a Pt-Ru bimetallic system. Various other examples of Ru immobilised on solid supports such as hectorite,¹³⁰ mesopolymers,¹³¹ SBA-15¹³² and montmorillonite¹³³ exist detailing their use as hydrogenation catalysts.

In some cases the support can play an integral role in the activity of the catalyst. The effect of support was studied for Ru NPs immobilised on a high surface area commercial graphite (HSAG), zirconia and KL zeolite.¹³⁴ The immobilised catalysts were evaluated in the selective hydrogenation of citral. The observed electronic effects of the support on the Ru NP when immobilising on the supports HSAG and zirconia was highlighted. The hydrogenation

of the C=O double bond was favoured due to the electron-rich nature of the Ru NPs on the electron donating HSAG support. Similarly, activation of the C=O bond was observed when evaluating the Ru-ZrO₂ catalyst with the main products being geraniol and nerol. The results obtained when evaluating KL zeolite as the support demonstrated a higher selectivity towards the unsaturated alcohols at a higher conversion. Unlike the results obtained using HSAG and zirconia, the selectivity towards C=O hydrogenation was driven by steric factors. Smaller metal nanoparticles stuck within the narrow pores of the zeolites demonstrate lower sensitivity towards catalysts poisoning by the decarbonylation side reactions. Additionally, the confined space only allows the end-on adsorption of the aldehyde on the catalyst surface. Despite the selectivity towards the alcohol being low at lower conversions, this steadily increases at high conversions. There is no doubt that the choice of support can influence and even benefit the performance of metal NP catalysts in various ways. The selectivity of catalysts and quite possible the activity can be tuned in other ways as well.

An elegant concept is the use of ionic liquid coatings to influence the catalytic performance of the supported catalyst. Here, the merits of both a heterogenised system and the stabilising effects of an ionic liquid are combined. The combination of these traits, however, reveal more interesting behaviour for these types of systems, the SCILL catalysts.

1.9.3 Catalytic evaluation of supported ruthenium nanoparticles coated in ionic liquid.

The concept of the SCILL catalyst was first described by Kernchen *et al.*¹¹⁷ They evaluated a commercial Ni catalyst and that with a coating of the ionic liquid, butylmethylimidazolium-octylsulfate. The presence of the ionic liquid caused a decrease in the catalytic activity when compared to the uncoated Ni catalyst. The selectivity for the uncoated nickel catalyst is to the fully hydrogenated product, cyclooctane. Despite the decrease in activity observed when evaluating the coated Ni catalyst, there was a marked increase in the selectivity towards the partially hydrogenated product, cyclooctene. As earlier mentioned, the use of ionic liquids is advantageous in their stabilising effects on the nanoparticles but for these biphasic reactions, mass transfer limitations and poor gas solubility are an issue. The dispersion of the ionic liquid across the high surface area support helps minimise the mass transfer limitation albeit does not eliminate it as observed by Kernchen *et al.*¹¹⁷

Chemoselective catalytic reactions give insight into the selectivity profile for catalysts. In the case of the hydrogenation of α,β -unsaturated compounds, there is the possibility of hydrogenating the C=C double bond, a C=O double bond or both. Arras *et al.* evaluated a Ru/Al₂O₃ catalyst in the hydrogenation of citral and the influence of an ionic liquid coating on the catalytic performance.¹³⁵ The ionic liquids 1-butyl-3-methylimidazolium bis(trifluoromethanesulfonyl)amide, [BMIM][NTf₂], and 1-hexyl-3-methylimidazolium bis(trifluoromethanesulfonyl)amide, [HMIM][NTf₂]. The uncoated catalyst demonstrated selectivity towards citronellal, the product of the C=C double bond hydrogenation. An expected decrease in the catalytic activity was observed upon coating the catalyst in ionic liquid. The selectivity, however, increased towards the formation of the alcohols geraniol and nerol with a decrease in the amount of side products formed. The presence of the [NTf₂]⁻ based ionic liquids therefore influences the selectivity of the reaction towards hydrogenation of the C=O double bond. This subject is revisited in a later chapter for the evaluation of various other ionic liquids.

Outside the realms of particle size and reaction conditions, not many other ways to control results for supported nanoparticles exist. Ionic liquid coatings can provide new means to modify catalyst activity. Despite ruthenium being quite versatile as a catalyst used in oxidation and hydrogenation reactions, investigation into its utilisation as nanoparticles in SCILL systems is lacking. The potential to expand the performance profile of supported Ru NP catalysts is therefore high when considering the relatively unexplored use of ionic liquids in these systems.

1.10 Aims, objectives and overview.

This study focuses on the preparation of dendrimer encapsulated ruthenium nanoparticles of various sizes using the hydroxyl terminated poly(amidoamine) dendrimer as a template. The scarcity of examples of their application in literature is the motivation behind the study. The literature examples provided, proves ruthenium to be a versatile metal given the ability to catalyse a variety of reactions. The envisaged stability provided by dendrimers could help in the stabilisation of nanoparticles prepared by the dendrimer templated methodology and hence possibly increase catalytic lifetime. The inherent catalytic activity of ruthenium nanoparticles described in the literature discussed may also be altered by the use of additives. The SCILL concept earlier discussed has not had much application in ruthenium nanoparticle catalysed

reactions when compared to other metals. Given the scope for studies into the application of not only RuDENs but also the application of ionic liquids as additives in the form of catalyst coatings for supported Ru catalysts, the following chapters address these topics as follows:

In Chapter 2, the preparation of dendrimer encapsulated ruthenium nanoparticles is described using various generations of poly(amidoamine) dendrimers as templating agents. Various dendrimer:ruthenium molar ratios are utilised to obtain dendrimer encapsulated ruthenium nanoparticles of different sizes. A preliminary study into the extraction of the nanoparticles will be described with the purpose of trying to recycle the dendrimer template. The nanoparticles will then be immobilised on either silica 60 or silica 100. These solid supported ruthenium catalysts will then be coated in an ionic liquid. These will all be tested as potential catalysts in the forthcoming chapters.

Chapter 3 focuses on the evaluation of the various dendrimer encapsulated ruthenium nanoparticles in the reduction of 4-nitrophenol using sodium borohydride as the reducing agent. The extensive kinetic data obtained from these evaluations will be modelled according to the Langmuir-Hinshelwood model which assumes the adsorption of both substrate and reactant to the catalyst surface for reaction to occur.

Chapter 4 details the evaluation of the silica-supported dendrimer encapsulated ruthenium nanoparticles in the hydrogenation of toluene. These catalysts will be coated in various ionic liquids to evaluate the effect of the ionic liquid on the activity and selectivity of the catalyst. Preliminary results of the evaluation of these catalysts in the continuous flow gas phase hydrogenation of toluene will be presented.

In Chapter 5, the hydrogenation reactions are extended to the chemoselective hydrogenation of the α,β -unsaturated compounds citral and cinnamaldehyde. Similar to Chapter 4, the effects of ionic liquids on the catalyst activity and selectivity will be discussed.

Chapter 6 demonstrates the ability of the dendrimer encapsulated ruthenium nanoparticles and the silica-supported dendrimer encapsulated ruthenium nanoparticles to be utilised as catalysts in the oxidation of styrene in the presence of TBHP as an oxidant. The use of ionic liquids as additives in these reactions has not been the focus of many studies. This study therefore

utilises this approach to investigate the effect on the catalytic activity of the investigated ruthenium catalysts.

Chapter 7 concludes this study and provides recommendations for future studies into the utilisation of dendrimer encapsulated ruthenium nanoparticles and ionic liquids as additives.

1.11 Conclusion

The preparation of nanoparticles is well established with many studies conducted in past decades. However, there is still a great need to prepare nanoparticles with an even narrower size distribution than those obtained currently. This is particularly important in the investigation of structure-sensitive studies and investigations of any synergistic effects between nanoparticles and solid supports. With regard to ruthenium nanoparticles, there is still a lot of work that can be done when compared to metals such as palladium and gold that have been extensively studied. Of particular interest is the preparation of dendrimer encapsulated ruthenium nanoparticles. These nanoparticles then remain to be evaluated as potential catalysts in hydrogenation and oxidation reactions.

1.12 References

- [1] D. Astruc, *Inorg. Chem.* **2007**, *46*, 1884.
- [2] D. Astruc, F. Lu and J. R. Aranzas, *Angew. Chem., Int. Ed.* **2005**, *44*, 7399.
- [3] L. N. Lewis, *Chem. Rev.* **1993**, *93*, 2693.
- [4] G. Schmid, *Chem. Rev.* **1992**, *92*, 1709.
- [5] Y. Shiraishi and N. Toshima, *J. Mol. Catal. A: Chem.* **1999**, *141*, 187.
- [6] Y. Shiraishi and N. Toshima, *Colloid Surf. A* **2000**, *169*, 59.
- [7] N. Toshima and T. Yonezawa, *New J. Chem.* **1998**, 1179.
- [8] J. G. D. Vries, *Dalton Trans.* **2006**, 421.
- [9] J. W. Niemantsverdriet, *Spectroscopy in Catalysis An Introduction*, 3 ed. (Ed.: J. W. Niemantsverdriet), WILEY-VCH Verlag GmbH & Co. KGaA, Weinheim, **2007**, pp. 305-307.
- [10] W. J. Parak, L. Manna, F. C. Simmel, D. Gerion and P. Alivisatos, *Nanoparticles From Theory to Application* (Ed.: G. Schmid), WILEY-VCH Verlag GmbH & Co. KGaA, Weinheim, **2004**, pp. 6-20.

- [11] J. S. Bradley and G. Schmid, *Nanoparticles From Theory to Application* (Ed.: G. Schmid), WILEY-VCH Verlag GmbH & Co. KGaA, Weinheim, **2004**, pp. 186-199.
- [12] D. Astruc, *Nanoparticles and Catalysis*, WILEY-VCH Verlag GmbH & Co. KGaA, Weinheim, **2008**.
- [13] M.-C. Daniel and D. Astruc, *Chem. Rev.* **2004**, *104*, 293.
- [14] H. Bönemann and R. M. Richards, *Eur. J. Inorg. Chem.* **2001**, 2455.
- [15] B. L. Cushing, V. L. Kolesnichenko and C. J. O'Connor, *Chem. Rev.* **2004**, *104*, 3893.
- [16] K. Philippot and B. Chaudret, *C. R. Chim.* **2003**, *6*, 1019.
- [17] G. Schmid and L. F. Chi, *Adv.Mater.* **1998**, *10*, 515.
- [18] J. P. Wilcoxon and B. L. Abrams, *Chem. Soc. Rev.* **2006**, *35*, 1162.
- [19] A. Amulyavichus, A. Daugvila, R. Davidonis and C. Sipavichus, *Fiz. Met. Metalloved.* **1998**, *85*, 111.
- [20] E. Gaffet, M. Tachikart, O. E. Kedim and R. Rahouadj, *Mater. Charact.* **1996**, *36*, 185.
- [21] J. Grunes, J. Zhu and G. A. Somorjai, *Chem. Commun.* **2003**, 2257.
- [22] M. C. Daniel and D. Astruc, *Chem. Rev.* **2004**, *104*, 293.
- [23] M. Faraday, *Philos. Trans.* **1857**, *151*, 183.
- [24] N. Toshima, *Nanoscale Materials* (Eds.: L. M. Liz-Marzán, P. V. Kamat), Springer US, **2004**, pp. 79-84.
- [25] J. Turkevich, *Gold Bull.* **1985**, *18*, 86.
- [26] K. Na, Q. Zhang and G. A. Somorjai, *J. Clust. Sci.* **2014**, *25*, 83.
- [27] P. Atkins, T. Overton, J. Rourke, M. Weller, F. Armstrong and M. Hagerman, *Shriver & Atkins' Inorganic Chemistry*, 5 ed. (Eds.: P. Atkins, T. Overton, J. Rourke, M. Weller, F. Armstrong, M. Hagerman), Oxford University Press, Great Britain, **2010**, p. 659.
- [28] K. An and G. A. Somorjai, *ChemCatChem* **2012**, *4*, 1512.
- [29] R. Pool, *Science* **1990**, *248*, 1186.
- [30] P. Hervés, M. Pérez-Lorenzo, L. M. Liz-Marzán, J. Dzubiella, Y. Lu and M. Ballauff, *Chem. Soc. Rev.* **2012**, *41*, 5577.
- [31] M. A. Vannice, *Kinetics of Catalytic Reactions*, Springer Science + Business Media, Inc, New York, **2005**.
- [32] K. A. Marvin, N. N. Thadani, C. A. Atkinson, E. L. Keller and K. J. Stevenson, *Chem. Commun.* **2012**, 48.
- [33] M. T. Reetz and W. Helbig, *J. Am. Chem. Soc.* **1994**, *116*, 7401.

- [34] M. T. Reetz, W. Helbig and S. A. Quaiser, *Active metals*, A. Fürstner ed., VCH: Weinheim, **1996**.
- [35] M. T. Reetz, W. Helbig and S. A. Quaiser, *Chem. Mater.* **1995**, *7*, 2227.
- [36] L. D. Pachón, M. B. Thathagar, F. Hartl and G. Rothenberg, *Phys. Chem. Chem. Phys.* **2006**, *8*, 151.
- [37] N. Toshima and Y. Wang, *Chem. Lett.* **1993**, *22*, 1611.
- [38] P. Lara, K. Philippot and B. Chaudret, *ChemCatChem* **2013**, *5*, 28.
- [39] Y. Takahashi, T. Ito, S. Sakai and Y. Ishii, *J. Chem. Soc. D* **1970**, 1065.
- [40] J. Turkevich and G. Kim, *Science* **1970**, *169*, 873.
- [41] J. Turkevich, P. C. Stevenson and J. Hillier, *Faraday Discuss. Chem. Soc.* **1951**, *11*, 55.
- [42] L. D. Pachón and G. Rothenberg, *Appl. Organometal. Chem.* **2008**, *22*, 288.
- [43] P. R. V. Rheenen, M. J. McKelvy and W. S. Glaunsinger, *J. Solid State Chem.* **1987**, *67*.
- [44] H. Ishizuka, T. Tano, K. Torigoe, K. Esumi and K. Meguro, *Colloids Surf.* **1992**, *63*, 337.
- [45] A. C. Curtis, D. G. Duff, P. P. Edwards, D. A. Jefferson, B. F. G. Johnson, A. I. Kirkland and A. S. Wallace, *J. Phys. Chem.* **1988**, *92*, 2270.
- [46] N. Toshima and T. Yonezawa, *New J. Chem.* **1998**, *22*, 1179.
- [47] P. Lu, T. Teranishi, K. Asakura, M. Miyake and N. Toshima, *J. Phys. Chem. B.* **1999**, *103*, 9673.
- [48] T. Miyashita, J. Chen, M. Yuasa and M. Mitsuishi, *Polymer J.* **1999**, *31*, 1121.
- [49] M. Brust, A. Walker, D. Bethell, D. J. Schiffrin and R. Whyman, *J. Chem. Soc., Chem. Commun.* **1994**, 801.
- [50] J. Kiwi and M. Grätzel, *Angew. Chem. Int. Ed.* **1979**, *18*, 624.
- [51] M. T. Reetz, W. Helbig, S. A. Quaiser, U. Stimming, N. Breuer and R. Vogel, *Science* **1995**, *267*, 367.
- [52] T. Thurn-Albrecht and W. Vogel, *Chem. Eur. J.* **2001**, *7*, 1084.
- [53] M. T. Reetz and M. Maase, *Adv. Mater.* **1999**, *11*, 773.
- [54] M. L. Singla, A. Negi, V. Mahajan, K. C. Singh and D. V. S. Jain, *Appl. Catal. A Gen.* **2007**, *323*, 51.
- [55] T. Dwars, J. Haberland, I. Grassert, G. Oehme and U. Kragl, *J. Mol. Catal. A: Chem.* **2001**, *168*, 81.

- [56] H. G. Niessen, A. Eichhorn, K. Woelk and J. Bargon, *J. Mol. Catal. A: Chem.* **2002**, 182-183, 463.
- [57] G. Oehme, I. Grassert, E. Paetzold, R. Meisel, K. Drexler and H. Fuhrmann, *Coord. Chem. Rev.* **1999**, 185-186, 585.
- [58] M. V. Seregina, L. M. Bronstein, O. A. Platonova, D. M. Chernyshov, P. M. Valetsky, J. Hartmann, E. Wenz and M. Antonietti, *Chem. Mater.* **1997**, 9, 923.
- [59] M. Boutonnet, J. Kizling and P. Stenius, *Colloids Surf.* **1982**, 5, 209.
- [60] K. Nasar, F. Fache, M. Lemaire, M. Draye, J.C.Béziat, M. Besson and P. Galezot, *J. Mol. Catal.* **1994**, 87, 107.
- [61] M.-K. Chung and M. Schlaf, *J. Am. Chem. Soc.* **2004**, 126, 7386.
- [62] S. U. Son, Y. Jang, J. Park, H. B. Na, H.M. Park, H. J. Yun, J. Lee and T. Hyeon, *J. Am. Chem. Soc.* **2004**, 126, 5026.
- [63] J. Dupont, R. F. d. Souza and P. A. Z. Suarez, *Chem. Rev.* **2002**, 102, 3667.
- [64] X.-d. Mu, J.-q. Meng, Z. C. Li and Y. Kou, *J. Am. Chem. Soc.* **2005**, 127, 9694.
- [65] X. Mu, D. G. Evans and Y. Kou, *Catal. Lett.* **2004**, 97, 151.
- [66] H. Hirai and N. Yakura, *Polym. Adv. Tech.* **2001**, 12, 724.
- [67] B. He, Y. Ha, H. Liu, K. Wang and K. Y. Liew, *J. Coll. Inter. Sci.* **2007**, 307, 105.
- [68] C. E. Hoppe, M. Lazzari, I. Pardiñas-Blanco and M. A. López-Quintela, *Langmuir* **2006**, 22, 7027.
- [69] I. Washio, Y. Xiong, Y. Yin and Y. Xia, *Adv. Mater.* **2006**, 18, 1745.
- [70] D. Astruc, *Dendrimers and nanoscience*, Elsevier, Paris, **2003**.
- [71] G. R. Newkome, C. N. Moorefield and F. Vögtle, *Dendrimers and Dendrons: Concepts, Synthesis, Applications*, Wiley-VCH, Weinheim, **2001**.
- [72] E. Buhleier, W. Wehner and F. Vögtle, *Synthesis* **1978**, 1978, 155.
- [73] D. A. Tomalia, H. Baker, J. Dewald, M. Hall, G. Kallos, S. Martin, J. Roeck, J. Ryder and P. Smith, *Polym. J.* **1985**, 17, 117.
- [74] D. A. Tomalia, A. M. Naylor and W. A. G. III, *Angew. Chem. Int. Ed.* **1990**, 29, 138.
- [75] G. R. Newkome, *Pure Appl. Chem.* **1998**, 70, 2337.
- [76] G. R. Newkome, C. N. Moorefield and G. R. Baker, *Aldrichim. Acta* **1992**, 25, 31.
- [77] G. R. Newkome, Z.-q. Yao, G. R. Baker, V. K. Gupta, P. S. Russo and M. J. Saunders, *J. Am. Chem. Soc.* **1986**, 108, 849.
- [78] C. Hawker and J. M. J. Fréchet, *J. Chem. Soc., Chem. Commun.* **1990**, 1010.
- [79] C. J. Hawker and J. M. J. Fréchet, *J. Am. Chem. Soc.* **1990**, 112, 7638.
- [80] J. M. J. Fréchet, *Science* **1994**, 263, 1710.

- [81] H. Ye, R. W. J. Scott and R. M. Crooks, *Langmuir* **2004**, *20*, 2915.
- [82] R. W. J. Scott, H. Ye, R. R. Henriquez and R. M. Crooks, *Chem. Mater.* **2003**, *15*, 3873.
- [83] L. K. Yeung and R. M. Crooks, *Nano Lett.* **2001**, *1*, 14.
- [84] V. Chechik, M. Zhao and R. M. Crooks, *J. Am. Chem. Soc.* **1999**, *121*, 4910.
- [85] M. Zhao and R. M. Crooks, *Angew. Chem.* **1999**, *111*, 375.
- [86] M. Zhao, L. Sun and R. M. Crooks, *J. Am. Chem. Soc.* **1998**, *120*, 4877.
- [87] L. Balogh, D. R. Swanson, D. A. Tomalia, G. L. Hagnauer and A. T. McManus, *Nano Lett.* **2001**, *1*, 18.
- [88] L. Balogh and D. A. Tomalia, *J. Am. Chem. Soc.* **1998**, *120*, 7355.
- [89] K. Esumi, R. Isono and T. Yoshimura, *Langmuir* **2004**, *20*, 237.
- [90] K. Esumi, A. Susuki, N. Aihara, K. Usui and K. Torigoe, *Langmuir* **1998**, *14*, 3157.
- [91] D. Astruc, E. Boisselier and C. Ornelas, *Chem. Rev.* **2010**, *110*, 1857.
- [92] Y.-M. Chung and H.-K. Rhee, *J. Mol. Catal. A: Chem.* **2003**, *206*, 291.
- [93] R. W. J. Scott, A. K. Datye and R. M. Crooks, *J. Am. Chem. Soc.* **2003**, *125*, 3674.
- [94] H.-F. Lang, R. A. May, B. L. Iversen and B. D. Chandler, *J. Am. Chem. Soc.* **2003**, *125*, 14832.
- [95] L. Guzzi, A. Beck, A. Horvath, Z. Koppany, G. Stefler, K. Frey, I. Sajo, O. Geszti, D. Bazin and J. Lynch, *J. Mol. Catal. A: Chem.* **2004**, *204*, 545.
- [96] S. Pröckl, W. Kleist, M. A. Gruber and K. Köhler, *Angew. Chem. Int. Edn* **2004**, *43*, 1881.
- [97] K. Mori, T. Hara, T. Mizugaki, K. Ebitani and K. Kaneda, *J. Am. Chem. Soc.* **2004**, *126*, 10657.
- [98] P. Pfeifer, K. Schubert, M. A. Liauw and G. Emig, *App. Catal. A Gen.* **2004**, *270*, 165.
- [99] S. Bertarione, D. Scarano, A. Zecchina, V. Johanek, J. Hoffmann, S. Schauer mann, J. Libuda, G. Rupprechter and H.-J. Freund, *J. Catal.* **2004**, *124*, 64.
- [100] K. H. Park, S. U. Son and Y. K. Chung, *Org. Lett.* **2002**, *4*, 4361.
- [101] S.-W. Kim, M. Kim, W. Y. Lee and T. Hyeon, *J. Am. Chem. Soc.* **2002**, *124*, 7642.
- [102] K. Hori, H. Matsune, S. Takenaka and K. M. Kishida, *Adv. Mater.* **2006**, *7*, 678.
- [103] J. Huang, T. Jiang, H.-X. Gao, B.-X. Han, Z.-M. Liu, W.-Z. Wu, Y.-H. Chang and G.-Y. Zhao, *Angew. Chem. Int. Edn* **2004**, *43*, 1397.
- [104] G. Riahi, D. Guillemot, M. Polisset-Tfoin, A. A. Khodadadi and J. Fraissard, *Catal. Today* **2002**, *72*, 115.
- [105] M. R. Knecht and D. W. Wright, *Chem. Mater.* **2004**, *16*, 4890.

- [106] P. Arya, G. Panda, N. V. Rao, H. Alper, S. C. Bourque and L. E. Manzer, *J. Am. Chem. Soc.* **2001**, *123*, 2889.
- [107] P. Arya, N. V. Rao, J. Singkhonrat, H. Alper, S. C. Bourque and L. E. Manzer, *J. Org. Chem.* **2000**, *65*, 1881.
- [108] S.-M. Lu and H. Alper, *J. Am. Chem. Soc.* **2003**, *125*, 13126.
- [109] S.-M. Lu and H. Alper, *J. Org. Chem.* **2004**, *69*, 3558.
- [110] F. Su, L. Lv, F. Y. Lee, T. Liu, A. I. Cooper and X. S. Zhao, *J. Am. Chem. Soc.* **2007**, *129*, 14213.
- [111] M. H. G. Prechtel, M. Scariot, J. D. Scholten, G. Machado, S. R. Teixeira and J. Dupont, *Inorg. Chem.* **2008**, *47*, 8995.
- [112] L. M. Rossi and G. Machado, *J. Mol. Catal. A: Chem.* **2009**, *298*, 69.
- [113] E. T. Silveira, A. P. Umpierre, L. M. Rossi, G. Machado, J. Morais, G. V. Soares, I. L. R. Baumvol, S. R. Teixeira, P. F. P. Fichtner and J. Dupont, *Chem. Eur. J.* **2004**, *10*, 3734.
- [114] S. S. Divekar, B. M. Bhanage, R. M. Deshpande, R. V. Gholap and R. V. Chaudhari, *J. Mol. Catal.* **1994**, *91*, L1.
- [115] E. T. Silveira, A. P. Umpierre, L. M. Rossi, G. Machado, J. Morais, G. V. Soares, I. J. R. Baumvol, S. R. Teixeira, P. F. P. Fichtner and J. Dupont, *Chem. Eur. J.* **2004**, *10*, 3734.
- [116] T. Selvam, A. Machoke and W. Schwieger, *Appl. Catal. A Gen.* **2012**, *445-446*, 92.
- [117] U. Kernchen, B. Etzold, W. Korth and A. Jess, *Chem. Eng. Technol.* **2007**, *30*, 985.
- [118] F. Fache, S. Lehuède and M. Lemaire, *Tetrahedron Lett.* **1995**, *36*, 885.
- [119] C. M. Hagen, L. Vieille-Petit, G. Laurency, G. Süss-Fink and R. G. Finke, *Organometallics* **2005**, *24*, 1819.
- [120] K. Pelzer, K. Philippot and B. Chaudret, *Z. Phys. Chem.* **2003**, *217*, 1.
- [121] K. Pelzer, O. Vidoni, K. Philippot, B. Chaudret and V. Collière, *Adv. Funct. Mater.* **2003**, *13*, 118.
- [122] E. T. Silveira, A. P. Umpierre, L. M. Rossi, G. Machado, J. Morais, G. V. Soares, I. J. R. Baumvol, S. R. Teixeira, P. F. P. Fichtner and J. Dupont, *Chem. Eur. J.* **2004**, *10*, 3734.
- [123] M. V. Escárcega-Bobadilla, C. Tortosa, E. Teuma, C. Pradel, A. Orejón, M. Gómez and A. M. Masdeu-Bultó, *Catal. Today* **2009**, *148*, 398.
- [124] M. B. Thathagar, J. Beckers and G. Rothenberg, *J. Am. Chem. Soc.* **2002**, *124*, 11858.
- [125] F. Launay and H. Patin, *New J. Chem.* **1997**, *21*, 247.

- [126] F. Launay, A. Roucoux and H. Patin, *Tetrahedron Lett.* **1998**, *39*, 1353.
- [127] G. Lafaye, A. Siani, P. Marécot, M. D. Amiridis and C. T. Williams, *J. Phys. Chem. B* **2006**, *110*, 7725.
- [128] G. Lafaye, C. T. Williams and M. D. Amiridis, *Catal. Lett.* **2004**, *96*, 43.
- [129] D. Liu, Y. M. L.-D. Jesús, J. R. Monnier and C. T. Williams, *J. Catal.* **2010**, *269*, 376.
- [130] G. Süss-Fink, B. Mollwitz, B. Therrien, M. Dadras, G. Laurency, A. Meister and G. Meister, *J. Clust. Sci.* **2007**, *18*, 87.
- [131] L. Song, X. Li, H. Wang, H. Wu and P. Wu, *Catal. Lett.* **2009**, *133*, 63.
- [132] J. Huang, T. Jiang, B. Han, W. Wu, Z. Liu, Z. Xie and J. Zhang, *Catal. Lett.* **2005**, *103*, 59.
- [133] S. Miao, Z. Liu, B. Han, J. Huang, Z. Sun, J. Zhang and T. Jiang, *Angew. Chem. Int. Ed.* **2006**, *45*, 266.
- [134] J. Álvarez-Rodríguez, I. Rodríguez-Ramos, A. Guerrero-Ruiz, E. Gallegos-Suarez and A. Arcoya, *Chem. Eng. J.* **2012**, *204-206*, 169.
- [135] J. Arras, D. Ruppert and P. Claus, *Appl. Catal. A Gen.* **2009**, *371*, 73.



Chapter 2 – The preparation of RuDEN, RuSil and RuSCILL catalysts

2.1 Introduction

The dendrimer templated preparation of nanoparticles is an efficient method for preparing a series of size controlled mono- and bimetallic transition metal nanoparticles. Dendrimers are hyperbranched polymeric structures that resemble a globular shape for the higher generation dendrimers. Various groups utilising a variety of metals have explored the uses of dendrimers as templating agents for the preparation of nanoparticles.¹⁻⁴ The maximum size of the encapsulated nanoparticle is constrained by the metal loading capacity of the dendrimer. However, there is flexibility where nanoparticle size control is concerned as the particle size can be controlled by the transition metal:dendrimer ratio.

One of the most widely used dendrimers in the synthesis of nanoparticles is the poly(amidoamine) (PAMAM) dendrimer. These dendrimers contain a number of tertiary amine sites that chelate metal ions. The preparation involves the coordination of a suitable transition metal salt to the dendritic framework and then subsequent reduction to form the atomic metal. The defined number of coordination sites serves as a control for the amount of metal each dendrimer can accommodate, whilst the globular macroenvironment serves an encapsulating role. This microenvironment within each discrete dendrimer helps direct the aggregation of metal atoms present formed by the reduction of the coordinated metal atoms, forming nanoparticles with a narrow size distribution upon reduction. These nanoparticles are referred to as dendrimer encapsulated nanoparticles (DENs). These nanoparticles can show significant stability whilst in solution.²

The use of supported catalysts plays an important role in industrial catalytic processes. Of great importance is the preparation of catalysts with a well-defined average particle size and narrow size distribution especially with regard to catalyst activity and selectivity. Deposition of DENs on a solid support can be achieved by wetness impregnation. This could require concentrated DENs solutions and likely cause agglomeration. The DENs prepared from hydroxyl terminated PAMAM dendrimers can be immobilised on oxide supports using a slow

adsorption technique. Here it is envisaged that the nanoparticle interacts with the oxide. The process can, however, be quite slow as reactions are allowed to progress for approximately 24 hours at a controlled pH.⁵ Another method of immobilisation requires the incorporation of the DENs into a sol-gel mixture.⁶⁻⁸

Conventionally the dendrimer template is removed subsequent to immobilisation on the solid support by calcination.⁹ The thermal instability of the PAMAM dendrimer lends itself to initial decomposition at temperatures as low as 75 °C.⁹ This is expected since the PAMAM dendrimer undergoes retro-Michael addition at about 100 °C.¹⁰ Therefore, any thermal treatment of the dendrimer will cause degradation in the macromolecular scaffold. The removal by calcination does cause some sintering of the nanoparticles, however, the narrow size distribution obtained when using dendrimers as stabilisers is maintained. To help maintain some of the benefit of the dendrimer, milder activation conditions can be utilised to minimise decomposition of the dendrimer. In the case of inhibition of the catalyst, full dendrimer removal is necessary. Later chapters reveal that catalytic activity is still present without full removal of the dendrimer stabiliser.

Particles of different sizes can thus be immobilised on a solid support and stability maintained to some degree by the presence of the dendrimer. The various particle sizes can have an influence on the catalytic performance.¹¹ Stability of the particles is of great importance when preparing a heterogeneous catalyst. The use of ionic liquids in the preparation of catalysts allows for the stabilisation of particles during the catalytic reaction. Usually, catalytic reactions conducted in bulk ionic liquids suffer from diffusion problems due to the low gas permeability and bulk phase nature of the biphasic reactions. One way to minimise the diffusion barrier and maintain the advantageous properties of the ionic liquid is to disperse it over a large surface area support. The focus will be on the preparation of SCILL catalysts where the coating of the solid catalyst is expressed as a pore volume filling, which in most cases, correlates with the mass percentage of the ionic liquid on the catalyst. In this system, a supported catalyst is first prepared and then coated with a certain amount of ionic liquid. The effects of the type and amount of ionic liquid on the catalyst performance (selectivity and activity) will be investigated in later chapters for different catalytic reactions.

The objective of this work is to prepare ruthenium nanoparticles with an average diameter below 3 nm and with a narrow size distribution. This is to maintain the good catalytic activity

seen for smaller nanoparticles especially in hydrogenations. The dendrimer template nanoparticle synthesis methodology is incorporated into this study since it is known to be effective in preparing size controlled nanoparticles with a narrow size distribution. The preparation of the RuDENs was monitored using Ultraviolet and Visible Spectrophotometry (UV/Vis) and Fourier Transform Infrared (FTIR) spectroscopy. The size of the RuDENs was analysed using high resolution transmission electron microscopy (HRTEM). Scanning electron microscopy (SEM) of the RuDENs deposited on etched silicon wafers was attempted but proved unsuccessful due to technical limitations. These RuDENs were then immobilised on silica 60 and silica 100 amorphous silica to prepare a supported catalyst referred to as RuSil. The Ru metal loadings for each of the RuSil catalysts were determined using Inductively Coupled Plasma Optical Emissions Spectroscopy (ICP-OES) and the size of the immobilised nanoparticles analysed using HRTEM. The use of powder X-ray diffractometry (PXRD) was not beneficial since the low metal loading did not allow for suitable analysis. SEM analysis was conducted with EDS mapping but due to the low loading of the metal and size of the particle, the analysis proved insufficient for confirming the presence of the RuDENs. Thermogravimetric analysis (TGA) was used to confirm the presence of the remaining dendritic scaffold post catalyst treatment and activation.

2.2 Experimental

The hydroxyl terminated fourth- (G4OH), fifth- (G5OH) and sixth-generation (G6OH) poly(amidoamine) (PAMAM) dendrimers were purchased as methanol solutions (Sigma-Aldrich). The methanol was removed from these solutions prior to use under high vacuum at ambient temperature for 3 hours. The RuCl₃ hydrate (99.98%) and sodium borohydride were purchased from Sigma-Aldrich and used as is. The Milli-Q (18 MΩ.cm) deionised water was used in all experiments and degassed for 30 minutes prior to use. The amorphous silica 60 and silica 100 were purchased from Merck and used as received. The ionic liquids 1-butyl-3-methylimidazolium bis(trifluoromethanesulfonyl)imide, [BMIM][NTf₂], 1-butyl-3-methylimidazolium tetrafluoroborate, [BMIM][BF₄], 1-butyl-3-methylimidazolium hexafluorophosphate, [BMIM][PF₆], and 1-butyl-3-methylimidazolium octylsulfate, [BMIM][Ocs], were purchased from Sigma-Aldrich and used as received. The ionic liquids 1-ethyl-3-methylimidazolium octylsulfate, [EMIM][Ocs], and 1-ethyl-3-methylimidazolium ethylsulfate, [EMIM][EtS], were purchased from Solvent Innovation and used as received.

The ionic liquid 1-octyl-3-methyl-imidazolium trifluoromethanesulfonate, [OMIM][NTf₂] was purchased from Solvionic and used as received.

UV/Vis spectrophotometry spectra were obtained on a Shimadzu UV1800 UV/Vis spectrophotometer. Fourier Transform Infrared (FTIR) spectra of the compounds were obtained as KBr pellets on a Bruker Tensor 27 FTIR spectrometer. Transmission electron microscopy (HRTEM) images were obtained on a JEOL JEM-2100F with an accelerating voltage of 200 kV equipped with a FEG source. HRTEM samples were prepared by a combination of drop deposition, onto a holey carbon covered HRTEM copper grid, and wicking utilised to remove any excess sample. The average nanoparticle size was calculated by analysing 250 nanoparticles for the RuDENSs and RuDEN extracts and 150 for supported catalysts from the obtained HRTEM images using ImageJ software.¹² Brunauer–Emmett–Teller (BET) analyses were conducted on the Micromeritics Tristar 3000 to calculate surface area, pore volume and pore diameter of the silica supported catalysts with samples degassed with flowing N₂ gas at 100 °C for 8 hours prior to analysis. The metal loadings were determined using inductively coupled plasma optical emission spectrometry (ICP-OES) using the Spectro-Arcos (ICP-OES).

2.2.1 *Preparation of RuDENSs for evaluation in 4-nitrophenol reduction.*

The Ru DENSs were synthesised according to an adapted method previously described by Lafaye *et al.*¹³⁻¹⁴ Similarly, RuDENSs were synthesised by reacting G4-PAMAM-OH, G5-PAMAM-OH and G6-PAMAM-OH with 40, 80 and 160 molar excesses of RuCl₃.nH₂O. A 167 µL aliquot of 600 µM aqueous G4-PAMAM-OH (0.1 µmol) stock solution was transferred into a 50 cm³ Schlenk tube. The reaction was diluted with 5475 µL of Milli-Q water added into the Schlenk tube while stirring. The solution was charged with an aqueous RuCl₃ (4 µmol) solution by pipetting 358 µL of a 11.18 mM RuCl₃ aqueous stock solution. This brings the total volume of the solution to 6 mL. The G4-PAMAM-OH/Ru mixture was stirred under nitrogen atmosphere for 72 hours to allow complete complexation to occur. Thereafter, the ruthenium metallodendrimer was reduced by adding 4 x 1000 µL of freshly prepared 10 mM NaBH₄ (40 µmol) every 10 minutes over a 40 minute period. The reaction was stirred under N₂ gas for 3 hours to allow for complete reduction of ruthenium and formation of the RuDENSs. Similarly, G5-RuDEN was prepared by reacting G5-PAMAM-OH (0.1 µmol) with aqueous RuCl₃ (8 µmol) and reducing with 0.2 M aqueous NaBH₄ (80 µmol)

and in the case of G6-RuDEN reacting G6-PAMAM-OH (0.1 μmol) with aqueous RuCl_3 (16 μmol) and reducing with 0.4 M aqueous NaBH_4 (160 μmol) in a total volume of 10 mL. These give effective dendrimer concentrations of 10 μM .

2.2.2 General preparation of RuDENs for extraction of Ru nanoparticles.

The method for RuDEN preparation is similar to that described in Chapter 2.2.1. The G4-PAMAM-OH/Ru, G5-PAMAM-OH/Ru or G6-PAMAM-OH/Ru was prepared by reacting aqueous solutions RuCl_3 (48 μmol) with either G4-PAMAM-OH (1.20 μmol), G5-PAMAM-OH (0.60 μmol) or G6-PAMAM-OH (0.30 μmol) respectively. An aqueous solution of NaBH_4 (480 μmol) was added to the stirring dendrimer-metal composite and the reactions stirred for 3 hours. Another aliquot of aqueous NaBH_4 (480 μmol) was added to the stirring mixture, prior to extraction, to give a total volume of 15 cm^3 . Either DCM solutions of $[\text{BMIM}][\text{PF}_6]$, $[\text{BMIM}][\text{BF}_4]$, octylamine or a pentane solution of oleylamine were used for extraction of the Ru NPs as described in the following sections 2.2.2.1-2.2.2.4.

2.2.2.1 Extraction of Ru NPs from the RuDENs using $[\text{BMIM}][\text{PF}_6]$.

A solution of $[\text{BMIM}][\text{PF}_6]$ (0.1364 g, 480 μmol) in DCM (20 cm^3) was added to the stirring nanoparticle mixture and the reaction stirred for 1 hour. The organic layer containing the nanoparticles was collected and the trace Ru NPs further extracted from the aqueous solution with DCM (10 cm^3). The organic fraction was washed with degassed deionised water (3 x 20 cm^3). The volume of the extract was reduced to about 15 cm^3 on the rotary evaporator at 30 $^\circ\text{C}$. UV/Vis spectra were taken of the post extraction aqueous fraction, DCM, the DCM and ionic liquid mixture and the DCM-ionic liquid extract.

2.2.2.2 Extraction of Ru NPs from the RuDENs using $[\text{BMIM}][\text{BF}_4]$.

A solution of $[\text{BMIM}][\text{BF}_4]$ (0.1084 g, 480 μmol) in DCM (20 cm^3) was added to the stirring nanoparticle mixture and the reaction stirred for 1 hour. The organic layer containing the nanoparticles was collected and the trace Ru NPs further extracted from the aqueous solution with DCM (10 cm^3). The organic fraction was washed with degassed deionised water (3 x 20 cm^3). The volume of the extract was reduced to about 15 cm^3 on the rotary evaporator at

30 °C. UV/Vis spectra were taken of the post extraction aqueous fraction, DCM, the DCM and ionic liquid mixture and the extract.

2.2.2.3 *Extraction of Ru NPs from the RuDENs using octylamine.*

Octylamine (79.3 μL , 480 μmol) was added to the stirring nanoparticle mixture and the reaction stirred for 1 hour during which the nanoparticles precipitate out of the aqueous mixture. Dichloromethane (10 cm^3) was then added to the mixture to extract the nanoparticle precipitate. The organic layer containing the nanoparticles was collected and further nanoparticles extracted from the aqueous mixture using dichloromethane (2 x 10 cm^3). The organic fractions were collected and washed with degassed deionised water (3 x 20 cm^3). The volume of the extract is reduced to about 15 cm^3 on the rotary evaporator at 30 °C. UV/Vis spectra were taken of the post extraction aqueous fraction, DCM, the DCM and octylamine mixture and the extract.

2.2.2.4 *Extraction of Ru NPs from the RuDENs using oleylamine.*

A solution of oleylamine (158 μL , 480 μmol) in pentane (20 cm^3) was added to the stirring nanoparticle mixture and the reaction stirred for 1 hour. The organic layer containing the nanoparticles was collected and the trace Ru NPs further extracted from the aqueous solution with pentane (10 cm^3). The organic fraction was washed with degassed deionised water (3 x 20 cm^3). The volume of the extract was reduced to about 15 cm^3 on the rotary evaporator at 30 °C. UV/Vis spectra were taken of the post extraction aqueous fraction, pentane, the pentane and oleylamine mixture and the extract.

2.2.3 *Preparation of silica supported RuDEN catalysts, RuSil.*

The RuDENs were prepared from aqueous solutions of G4-PAMAM-OH, G5-PAMAM-OH, G6-PAMAM-OH and RuCl_3 in a dendrimer:Ru ratio of 1:40, 1:80 and 1:160 respectively. Aqueous solutions of G4-PAMAM-OH (2.47 μmol) and RuCl_3 (98.94 μmol) were transferred to a N_2 purged 50 cm^3 Schlenk tube. Milli-Q water was added into the Schlenk tube to a total volume of 24 cm^3 . The G4-PAMAM-OH/Ru mixture was stirred under nitrogen atmosphere for 72 hours at ambient temperature. Thereafter, the ruthenium metallodendrimer was reduced by adding 6 x 1000 μL of freshly prepared 330 mM NaBH_4 (1979 μmol) every 10 minutes

over a 60 minute period and stirred for a further 3 hours. The reaction mixture was transferred to a sealed 20 cm dialysis tube and dialysed against Milli-Q water ($3 \times 1000 \text{ cm}^3$) in an Erlenmeyer flask for 3 hours each with stirring at ambient temperature. Similarly, the G5-RuDEN or G6-RuDEN were prepared by reacting aqueous solutions of either G5-PAMAM-OH ($1.23 \mu\text{mol}$) and G6-PAMAM-OH ($0.62 \mu\text{mol}$) with RuCl_3 ($98.94 \mu\text{mol}$). The G5-RuDENSs and G6-RuDENSs were dialysed against Milli-Q water ($3 \times 1000 \text{ cm}^3$) in an Erlenmeyer flask for 3 hours each with stirring at ambient temperature. The RuDENSs were deposited on either amorphous silica 60 (4 g) or amorphous silica 100 (4 g) by agitation of a mixture of the RuDENSs and amorphous silica on a reciprocating shaker for 6 hours. Higher loading catalysts were prepared using silica 60 (1 g) instead. The mixture was filtered under vacuum suction on a sintered glass frit funnel till dryness. The grey powder was washed with an aqueous ammonia (300 cm^3 , 0.11 M, 0.03 mol) solution by agitation on a vortex shaker and thereafter decanting excess supernatant. The mixture was washed with warm Milli-Q water (200 cm^3) and filtered using vacuum suction on a sintered glass frit funnel till dryness. The physisorbed water was removed on a rotary evaporator at $80 \text{ }^\circ\text{C}$ to give a free-flowing grey powder. The dried catalyst was exposed to a 10 bar hydrogen atmosphere at $150 \text{ }^\circ\text{C}$ to reduce the ruthenium surface atoms and the catalyst stored in a desiccator. Metal loadings were determined using ICP-OES analysis. Prior to analysis, samples were digested with 80% HF/HNO_3 and evaporated to dryness. The Ru was dissolved in *aqua regia*, and a 25 cm^3 solution prepared in Milli-Q water for analysis.

2.2.4 Preparation of RuSCILL catalysts.

The RuSCILL catalysts were prepared from either G5-RuSil60 or G6-RuSil60. The required amount of ionic liquid was weighed into a round bottom flask (50 cm^3). A methanolic solution of the ionic liquid was prepared by transferring methanol (10 cm^3) to the ionic liquid. The RuSil catalyst was transferred to the methanolic solution of the ionic liquid and allowed to agitate of a rotary evaporator without vacuum for 15 minutes and at ambient temperature. The solvent was then removed at $60 \text{ }^\circ\text{C}$ on the rotary evaporator to yield a free-flowing grey powder. The catalyst was further dried under high vacuum for 6 hours at ambient temperature.

2.2.4.1 Preparation of the [BMIM][NTf₂] coated G5-RuSCILL catalyst with a 10% and 20% pore filling.

The [BMIM][NTf₂] coated G5-RuSCILL catalyst with a 10% pore filling, corresponding to an α -value of 0.1, was prepared according to the method described in section 2.2.4 using [BMIM][NTf₂] (0.0364 g) and 0.3051 g of G5-RuSil60 catalyst. Similarly, the G5-RuSCILL catalyst with a 20% pore filling corresponding to an α -value of 0.2, was prepared using [BMIM][NTf₂] (0.0742 g) and 0.3037 g of G5-RuSil60 catalyst

2.2.4.2 Preparation of the [BMIM][BF₄] coated G5-RuSCILL catalyst with a 10% pore filling.

The G5-RuSCILL catalyst with [BMIM][BF₄] ionic liquid coating was prepared according to the method described in section 2.2.4 using [BMIM][BF₄] (0.0344 g) and 0.3044 g of G5-RuSil60 catalyst. The SCILL catalyst obtained has an ionic liquid coating equivalent to a 10% pore filling ($\alpha = 0.1$).

2.2.4.3 Preparation of the [BMIM][PF₆] coated G5-RuSCILL catalyst with a 10% pore filling.

The G5-RuSCILL catalyst with [BMIM][PF₆] ionic liquid coating was prepared according to the method described in section 2.2.4 using [BMIM][PF₆] (0.0335 g) and 0.3049 g of G5-RuSil60 catalyst. The SCILL catalyst obtained has an ionic liquid coating equivalent to a 10% pore filling ($\alpha = 0.1$).

2.2.4.4 Preparation of the [EMIM][EtS] coated G5-RuSCILL catalyst with a 10% pore filling.

The G5-RuSCILL catalyst with [EMIM][EtS] ionic liquid coating was prepared according to the method described in section 2.2.4 using [EMIM][EtS] (0.0294 g) and 0.3039 g of G5-RuSil60 catalyst. The SCILL catalyst obtained has an ionic liquid coating equivalent to a 10% pore filling ($\alpha = 0.1$).

2.2.4.5 Preparation of the [EMIM][Ocs] coated G5-RuSCILL catalyst with a 10% pore filling.

The G5-RuSCILL catalyst with [EMIM][Ocs] ionic liquid coating was prepared according to the method described in section 2.2.4 using [EMIM][Ocs] (0.0259 g) and 0.3044 g of G5-RuSil60 catalyst. The SCILL catalyst obtained has an ionic liquid coating equivalent to a 10% pore filling ($\alpha = 0.1$).

2.2.4.6 Preparation of the [BMIM][NTf₂] coated G6-RuSCILL catalyst with a 10% and 20% pore filling.

The [BMIM][NTf₂] coated G6-RuSCILL catalyst with a 10% pore filling, corresponding to an α -value of 0.1, was prepared according to the method described in section 2.2.4 using [BMIM][NTf₂] (0.0460 g) and 0.4004 g of G6-RuSil60 catalyst. Similarly, the G6-RuSCILL catalyst with a 20% pore filling corresponding to an α -value of 0.2 was prepared using [BMIM][NTf₂] (0.0968 g) and 0.4008 g of G6-RuSil60 catalyst.

2.2.4.7 Preparation of the [BMIM][BF₄] coated G6-RuSCILL catalyst with a 10% and 20% pore filling.

The [BMIM][BF₄] coated G6-RuSCILL catalyst with a 10% pore filling, corresponding to an α -value of 0.1, was prepared according to the method described in section 2.2.4 using [BMIM][BF₄] (0.0293 g) and 0.3016 g of G6-RuSil60 catalyst. Similarly, the G6-RuSCILL catalyst with a 20% pore filling corresponding to an α -value of 0.2 was prepared using [BMIM][BF₄] (0.0795 g) and 0.4034 g of G6-RuSil60 catalyst.

2.2.4.8 Preparation of the [BMIM][PF₆] coated G6-RuSCILL catalyst with a 10% and 20% pore filling.

The [BMIM][PF₆] coated G6-RuSCILL catalyst with a 10% pore filling, corresponding to an α -value of 0.1, was prepared according to the method described in section 2.2.4 using [BMIM][PF₆] (0.0393 g) and 0.3505 g of G6-RuSil60 catalyst. Similarly, the G6-RuSCILL catalyst with an 20% pore filling corresponding to an α -value of 0.2 was prepared using [BMIM][PF₆] (0.0922 g) and 0.4081 g of G6-RuSil60 catalyst.

2.2.4.9 Preparation of the [OMIM][NTf₂] coated G6-RuSCILL catalyst with a 10, 20% and 30% pore filling.

The [OMIM][NTf₂] coated G6-RuSCILL catalyst with a 10% pore filling, corresponding to an α -value of 0.1, was prepared according to the method described in section 2.2.4 using [OMIM][NTf₂] (0.1307 g) and 1.030 g of G6-RuSil100 catalyst. Similarly, the G6-RuSCILL catalyst with an 20% pore filling corresponding to an α -value of 0.2 was prepared using [OMIM][NTf₂] (0.2550 g) and 1.0050 g of G6-RuSil100 catalyst and the G6-RuSCILL catalyst with an 30% pore filling corresponding to an α -value of 0.3 was prepared using [OMIM][NTf₂] (0.4186 g) and 1.1000 g of G6-RuSil100 catalyst.

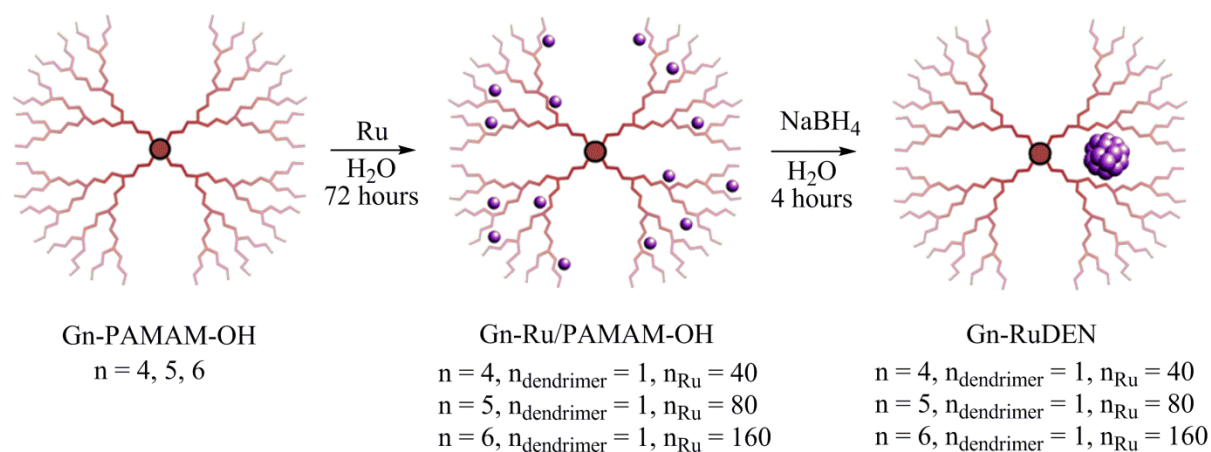
2.2.4.10 Preparation of the [BMIM][Ocs] coated G6-RuSCILL catalyst with a 10% pore filling.

The [BMIM][Ocs] coated G6-RuSCILL catalyst with a 10% pore filling, corresponding to an α -value of 0.1, was prepared according to the method described in section 2.2.4 using [BMIM][Ocs] (0.1063 g) and 1.0200 g of G6-RuSil100 catalyst.

2.3 Results and discussion

2.3.1 Preparation of dendrimer encapsulated Ru nanoparticles.

To obtain Ru NPs with a narrow size distribution the dendrimer templated nanoparticle preparation methodology was adapted from Lafaye *et al.*¹⁴ The preparation of various RuDENSs was achieved using the G4-, G5- and G6-PAMAM-OH dendrimers as templating agents. In each case, the differing loading capacities of the dendrimer for a potential coordinating transition metal was exploited. The increase in dendrimer generation correlates to an increase in the amount of tertiary amines available for coordination of a suitable transition metal. Therefore, higher generation PAMAM-OH dendrimers were utilised for the preparation of larger DENs. The general methodology for the preparation of the RuDENSs is illustrated in Scheme 2.1. The RuDENSs were prepared under an inert atmosphere, in this case N₂ gas, to help minimise any possible oxidation of ruthenium during complexation with the tertiary amines of the dendrimer.



Scheme 2.1. Scheme for the preparation of the various RuDENSs. Reactions were conducted in deionised water at ambient temperature and under N₂ atmosphere. In each case the n-value, “n”, denotes the generation of the dendrimer therefore, the dendrimers G4-, G5- and G6-PAMAM-OH were used in the preparation of G4-, G5- and G6-RuDEN respectively.

The procedure entails the preparation of a dilute aqueous solution of the G4-, G5-, or the G6-PAMAM-OH dendrimer to which the RuCl₃ solution was slowly added with stirring. The Ru of the metallodendrimer is then reduced in the presence of an aqueous solution of NaBH₄ to form the RuDENSs. The reactions occur over a period of three days, a process that was monitored for parts of the reaction using UV/Vis and FTIR spectroscopies.¹³⁻¹⁴

2.3.1.1 UV/Vis analysis for the preparation of RuDENSs.

The characteristic absorbances of the UV/Vis spectra for the aqueous dendrimer, RuCl₃, reaction mixtures thereof and the RuDENSs were recorded to monitor the reaction as illustrated in Figure 2.1. When considering the UV/Vis results obtained for the reactions concerning G4-PAMAM-OH, the UV/Vis spectrum displays an absorbance peak at λ 290 nm and λ 410 nm associated with the dendrimer-metal complex prior to reduction. These absorbance peaks differ considerably from the peaks seen for the aqueous RuCl₃. The RuCl₃ solution displays absorbance peaks at λ 391 nm and λ 548 nm. Upon reduction, these two peaks disappear, the graph flattens and a new peak at λ 282 nm appears which is associated with the formation of RuDENSs.¹⁵ The absorbance peak for the RuDENSs at λ 282 nm is consistent with that observed by Marvin *et al.*¹⁶ and is most likely associated with a Ru-amine type interaction occurring on the surface of the nanoparticle.¹⁴

Similarly, these characteristic peaks were observed at approximately the same wavelengths for the reactions using G5-PAMAM-OH and G6-PAMAM-OH as stabilisers in the preparation of RuDENs.

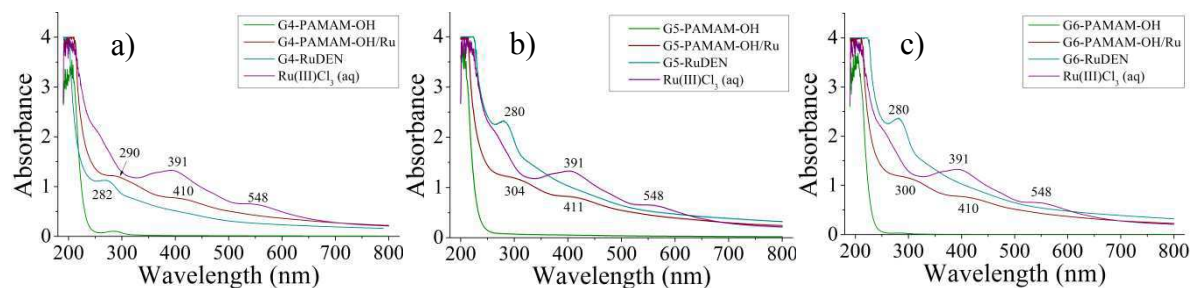


Figure 2.1. UV/Vis spectra for: a) G4-PAMAM-OH dendrimer, G4-PAMAM-OH/Ru metallodendrimer, G4-RuDEN and aqueous RuCl_3 , b) G5-PAMAM-OH dendrimer, G5-PAMAM-OH/Ru metallodendrimer, G5-RuDEN and aqueous RuCl_3 and c) G6-PAMAM-OH dendrimer, G6-PAMAM-OH/Ru metallodendrimer, G6-RuDEN and aqueous RuCl_3 .

2.3.1.2 FTIR analysis for the preparation of RuDENs.

Fourier transform infrared (FTIR) analysis was conducted on the dendrimer and dendrimer-metal complexes prior to reduction, to further ascertain the coordination of ruthenium to the tertiary amines. In each case, the absorption bands for the vibrational stretches are within a similar range for each of the dendrimers as illustrated in Table 2.1. Absorption bands at ν 1064-1066 cm^{-1} and ν 1290-1294 cm^{-1} correspond to C-N stretching vibrations for the tertiary amine groups while absorption bands seen at ν 1550-1553 cm^{-1} correspond to the C-N stretching/C-N-H bending (amide II) vibrations.¹⁷⁻¹⁸ The vibrational stretch observed at ν 1650-1652 cm^{-1} is assigned to the C=O stretching vibration (amide I).¹⁹ Upon coordination of Ru(III) to the dendrimer, there is a significant shift in the absorption bands at ν 1290-1294 cm^{-1} to wavenumbers of 1260-1262 cm^{-1} , further confirming coordination of Ru to the dendrimer. The remaining stretching frequencies, however, do not show such a significant change upon coordination.

Table 2.1. FTIR stretching frequencies for the various dendrimers G4-, G5- and G6-PAMAM-OH and that of their corresponding Ru metallodendrimer complexes.

Compound	FTIR stretches and bends (cm ⁻¹)				
	C-N Stretch	N-H Bend	C=O stretch	N-H stretch	O-H Stretch
G4-PAMAM-OH	1065.14 1262.21	1552.40	1650.61	3127.22	-
G4-PAMAM-OH/Ru	1059.95 1261.47	1553.87	1651.52	3125.37	-
G5-PAMAM-OH	1064.74 1293.10	1555.43	1648.82	-	3406.03
G5-PAMAM-OH/Ru	1059.91 1261.41	1551.31	1652.87	3198.83	3368.66
G6-PAMAM-OH	1065.02 1294.33	1555.60	1647.96	3259.85	3386.51
G6-PAMAM-OH/Ru	1059.03 1260.01	1550.80	1650.31	3131.86	3385.18

The results for the UV/Vis and FTIR gave some insight into the coordination of Ru to the tertiary amines of the PAMAM-OH dendrimers and possible interaction between the encapsulated nanoparticle and the dendrimer. A resulting aspect in the choice of dendrimer and the dendrimer:transition metal ratio is the control of the size of the resulting DEN.

2.3.1.3 HRTEM analysis of the RuDENs.

To investigate whether using the different dendrimer:transition metal ratios for the different generations of PAMAM-OH dendrimers had any effect on the size of the particle, HRTEM micrographs were taken for the various RuDENs. HRTEM micrographs obtained for each of the RuDEN samples were analysed to calculate the average particle diameter and a size distribution histogram of each of the samples generated as detailed in Figure 2.2. A survey of 250 particles was conducted to obtain an average particle size for each of the RuDENs. The average sizes of the nanoparticles for the various DENs were 1.2 ± 0.1 nm, 1.4 ± 0.1 nm and 2.2 ± 0.3 nm for G4-RuDEN, G5-RuDEN and G6-RuDEN respectively.

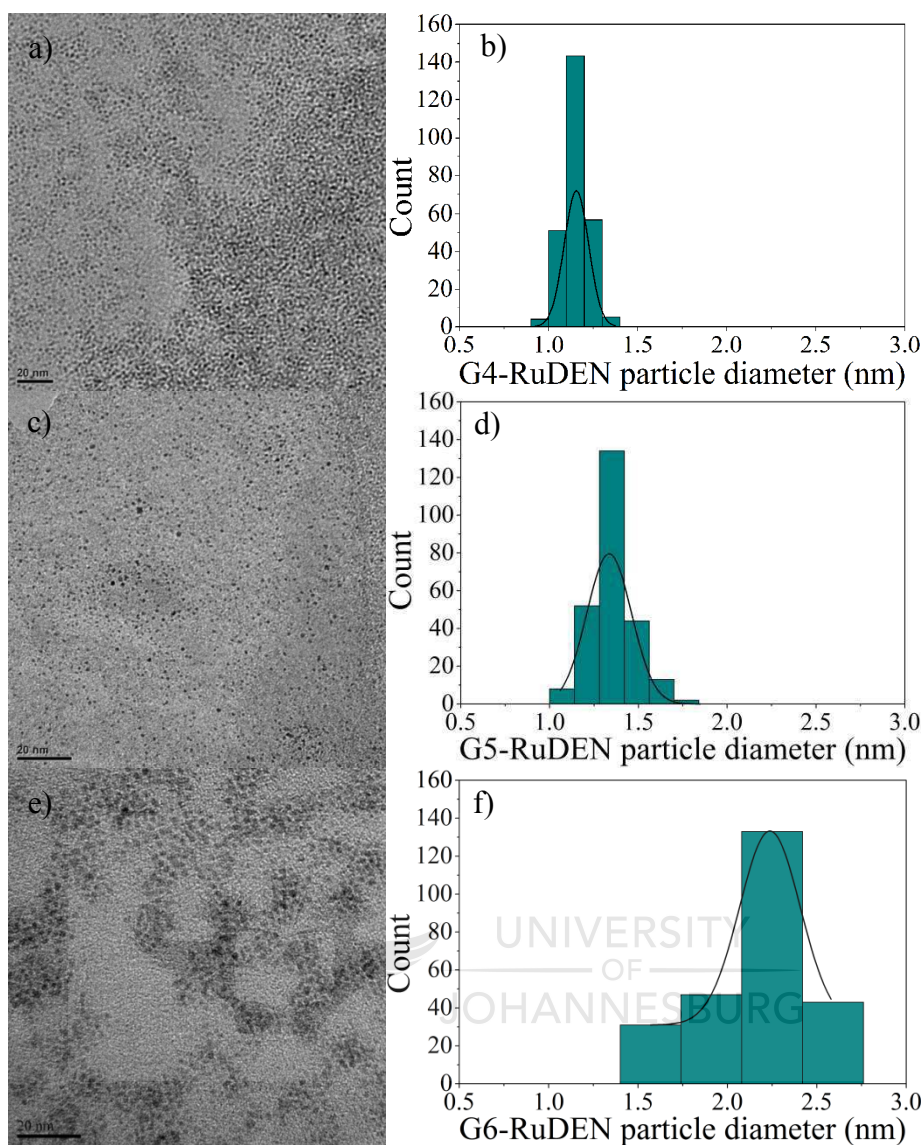


Figure 2.2. a) HRTEM image of G4-RuDEN b) Histogram for the size distribution of G4-RuDEN. c) HRTEM image of G5-RuDEN d) Histogram for the size distribution of G5-RuDEN. e) HRTEM image of G6-RuDEN f) Histogram for the size distribution of G6-RuDEN.

In each case the nanoparticle size distribution was quite narrow, as expected for nanoparticles prepared using dendrimers as templating agents and stabilisers. The HRTEM results revealed a roughly spherical morphology in most cases, similar to the results observed by Lafaye *et al.* Table 2.2 lists the previously discussed nanoparticle diameters for the various RuDENs. The dependence of the size of particle with the dendrimer:transition metal ratio is reflected in the increase in size with increase in ratio. This effect was reported for other research conducted using metals such as Cu, Au, Pt and Pd.^{3-4, 20-22} Insight into the effectiveness of using

dendrimer templates as stabilisers and a means to control the particle size, is gained when comparing the calculated diameter of the nanoparticles to the experimental diameter.

Table 2.2. Comparison of the experimental average RuDEN diameter and the theoretical Ru nanoparticle diameter

RuDEN	Experimental mean diameter ^a (nm)	Theoretical diameter (nm)
G4-RuDEN	1.2	1.02
G5-RuDEN	1.4	1.28
G6-RuDEN	2.2	1.61

^a Particle diameters obtained from average particle diameter calculations represented by the histograms in Figure 2.2

For the purposes of this study, the theoretical diameter of the Ru nanoparticles was calculated for a given number of Ru atoms. The model assumes the Ru nanoparticles to have a close-packed hexagonal single crystal structure. Considering the smallest sphere circumscribing the number of atoms defining the crystal lattice of the nanoparticle, an estimate of the nanoparticle size can be calculated.¹³ The calculations were executed using equations 1-3:

$$D = 2 \cdot \sqrt[3]{\frac{\rho \cdot n \cdot 3}{4 \cdot \pi}} \quad (1)$$

$$V = \frac{\sqrt{3}}{2} a^2 c \quad (2)$$

$$\rho = V/N \quad (3)$$

where V , is the volume of the hexagonal unit cell, N , is the number of atoms per unit cell, ρ , is the volume of the unit cell per atom and n , the number of Ru atoms in the particle. The variables a and c describe part of the unit cell parameters where the Ru unit cell parameters for a close-packed hexagonal single crystal structure are $a = b = 0.27059$ nm, $c = 0.42815$ nm, $\alpha = \beta = 90^\circ$ and $\gamma = 120^\circ$. The calculated theoretical values for the diameter of the nanoparticles are detailed in Table 2.2. The theoretical values that were calculated for the diameter of the G4-, G5- and G6-RuDEN were 1.02 nm, 1.28 nm and 1.61 nm respectively. The percentage difference in the experimental RuDEN size and the theoretical RuDEN size indicates a 18%, 9% and 37% increase from the theoretical size for the G4-, G5- and G6-

RuDENs respectively. The percentage increase in particle size observed was least for the G5-RuDENs and increasingly higher for the G4-RuDEN and G6-RuDEN. In the case of G4-RuDEN, the average experimental particle diameter corresponds to that observed by Lafaye *et al.*¹³

When comparing the results obtained for G5-RuDEN to those obtained by Lafaye *et al.*, the observed particle diameter corresponds to their observed particle diameter of 1.4 nm.¹³ Interestingly, the average particle diameter of 1.4 nm remained constant upon increasing the dendrimer:Ru ratio from 1:60 to 1:100. The authors do not provide any insight into the observation other than the obvious percentage increase. However, in light of the results obtained for the present study and the results obtained by Lafaye *et al.*,¹³ the deviation of experimental mean diameter from theoretical mean diameter decreases, the higher the dendrimer:Ru ratio. This could suggest that for metal loadings approaching the maximum coordinating metal capacity, the average particle diameter tends towards the formation of larger particles up to a maximum threshold. Loading beyond this maximum threshold can lead to the formation of inter-dendrimer stabilised particles. In principle, this equates to results observed for typical dendrimer titration with transition metal complex experiments where the loading capacity of the dendrimer is determined. The highest deviation of particle size from theoretical size was observed for the G6-RuDEN. This suggests that for the higher generation G6-PAMAM-OH dendrimer, the particular loading of metal within the dendrimer is skewing the size distributions towards a larger nanoparticle diameter. This is evident in the particle size histogram for the G6-RuDENs discussed earlier. Further studies into the effect of dendrimer:transition metal ratio, when using G6-PAMAM-OH, will be required to conclusively substantiate this but was not the focus of the study.

2.3.2 Extraction of Ru nanoparticles using ionic liquids and alkylamines as extractants and phase transfer agents.

The dendrimer templated preparation methodology allows for the preparation of metal nanoparticles with a narrow size distribution. The steric stabilisation it provides results from its macromolecular structure. Further stabilisation is ensured by coordination of the tertiary amines of the dendrimer to the nanoparticle surface atoms. Given the expense of PAMAM-OH dendrimers, it is wise to explore methods of possibly extracting the nanoparticle from the dendrimer and recycling the dendrimer for further nanoparticle preparation. The process

needs to be efficient enough to ensure that what remains post extraction is largely the dendrimer. Crooks *et al.* conducted one of the earliest works on the extraction of metal nanoparticles from within a dendrimer template.²³ A toluene solution containing an appropriate *n*-alkanethiol was used to extract the Au nanoparticles from the aqueous Au DENs. Complete ligand exchange between the dendrimer and the *n*-alkanethiol facilitated the phase transfer and extraction of the nanoparticle to the organic toluene phase. The extraction of Ru NPs from the RuDENs was preliminarily investigated using the ionic liquids [BMIM][BF₄] and [BMIM][PF₆] and the alkylamines, octylamine and oleylamine. The extraction was monitored using UV/Vis and in the case of the more efficient extraction, HRTEM micrographs were obtained to investigate any changes in particle size and size distribution upon extraction.

2.3.2.1 *UV/Vis study of the extraction of Ru nanoparticles using ionic liquids.*

The extraction of Ru nanoparticles was investigated for the ionic liquids [BMIM][BF₄] and [BMIM][PF₆] and monitored by UV/Vis as illustrated in Figure 2.3. The objective was to extract nanoparticles into an ionic liquid for use in a supported ionic liquid catalyst (SILCA) system. Alternatively, alkylamines could be used to attempt extraction given that the efficient alkylthiols serve as a catalyst poison towards the catalytic activity of the Ru nanoparticle. Dichloromethane was used as the organic phase given its miscibility with the ionic liquids. As earlier detailed in Figure 2.1, the RuDENs have a characteristic absorbance at a wavelength of approximately λ 280 nm. This absorbance corresponds to the coordination of the tertiary amines with the nanoparticle surface. For the investigation into the extraction and phase transfer, the UV/Vis spectrum of the aqueous layer will be evaluated for the presence of this absorbance as well as any changes in the spectra of the organic phase and extractant mixture. Each of the spectra for the mixture of the extractant and solvent is relatively featureless and changes after extraction. This change indicates the phase transfer of the extracted nanoparticle. When considering the results illustrated in Figure 2.3(a), there is a definite change in the spectrum of the [BMIM][BF₄] in DCM solution. A strong absorbance peak appears at λ 274 nm which could be possible interaction between the imidazolium nitrogens and the surface of the nanoparticle during the extraction. The same absorbance peak was observed when conducting the extraction using [BMIM][PF₆] to extract the Ru NPs as illustrated in Figure 2.3(b).

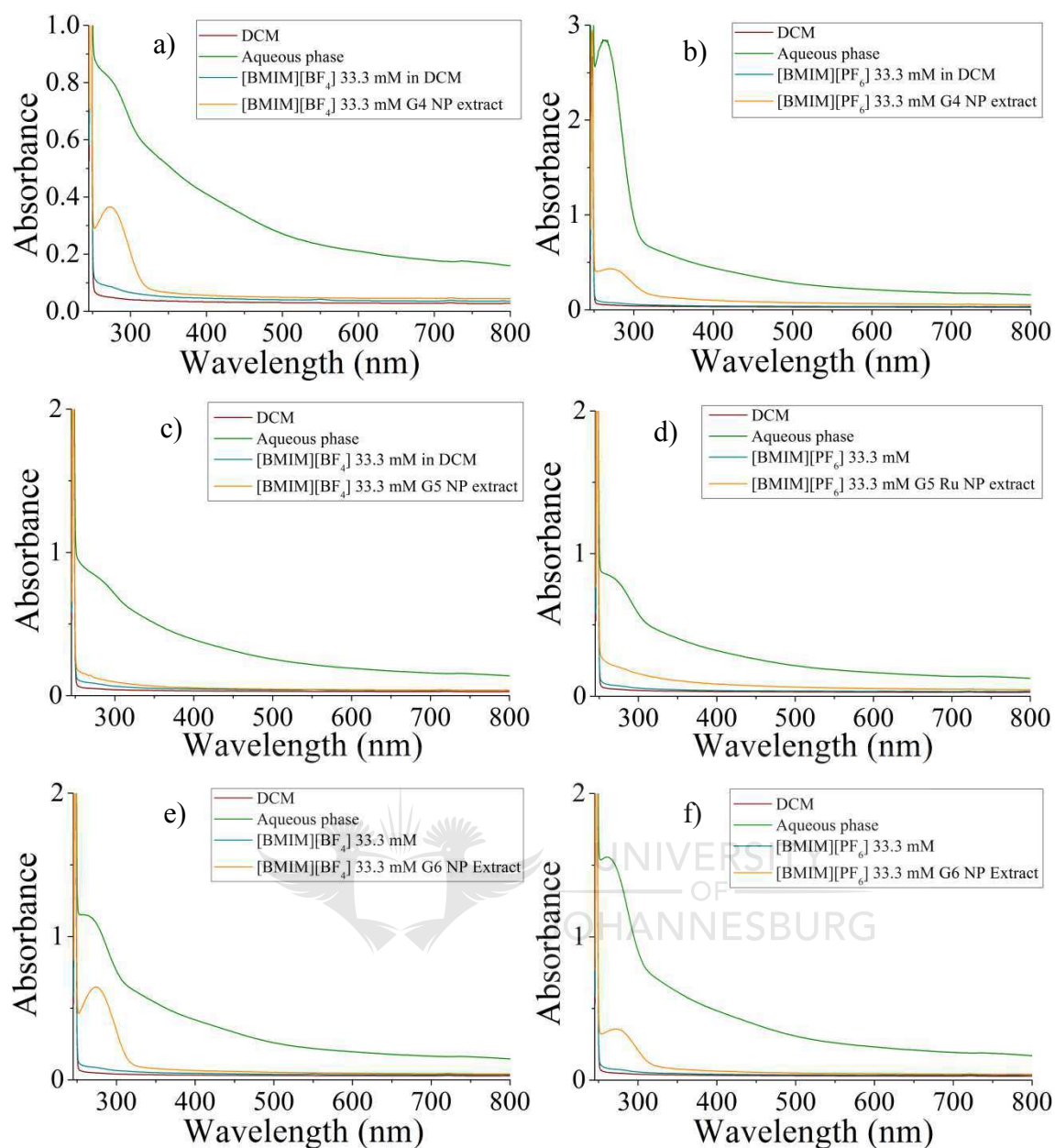


Figure 2.3. UV/Vis/ spectra monitoring the extraction of Ru NPs from the G4-RuDEN and phase transfer into a DCM organic phase for G4-RuDEN using, a) [BMIM][BF₄] and b) [BMIM][PF₆], for G5-RuDEN using c) [BMIM][BF₄] as extractants and d) [BMIM][PF₆] as extractants, and for G6-RuDEN using e) [BMIM][BF₄] and f) [BMIM][PF₆] as extractants.

The extraction using [BMIM][PF₆] in dichloromethane showed a minimal improvement in extraction efficiency when compared to the results obtained using [BMIM][BF₄] in dichloromethane as extractant. There is an increase in the absorbances across the wavelength range when comparing the spectra of [BMIM][PF₆] in dichloromethane and [BMIM][PF₆] in dichloromethane after extraction. Comparing the overall intensity of the aqueous phase spectra in each of these cases, the spectrum from the post extraction organic phases are

significantly lower. Strong absorbances were observed across the wavelength range indicating that a large percentage of the RuDENSs remained in the aqueous phase. Extraction of Ru NPs from the G6-RuDENSs show similar UV/Vis spectra to that obtained when extracting Ru NPs from the G4-RuDENSs, while a decrease in the extraction efficiency was observed when extracting Ru NPs from the G5-RuDENSs.

2.3.2.2 *UV/Vis study of the extraction of Ru nanoparticles using alkylamines.*

A dichloromethane solution of octylamine was used as a phase transfer agent. The effects of using the alkylamines, octylamine and oleylamine as extractants are illustrated in the UV/Vis spectra in Figure 2.4. Comparison of the UV/Vis spectrum of the DCM solution of octylamine before and after extraction shows a significant increase in the absorbances across the measured wavelength range. This is consistent with the phase transfer of the ruthenium nanoparticles from the aqueous phase to the hydrophobic organic phase. Compared to the ionic liquids, the extraction efficiency observed when using a dichloromethane solution of octylamine is higher. Similar behaviour was observed for the extractions of G5- and G6-RuDENSs as seen in Figures 2.4(c) and 2.4(e) respectively. Similar to octylamine, an oleylamine in pentane solution showed an improvement in extraction and phase transfer efficiency when compared to the ionic liquids. This is illustrated in Figure 2.4 by the increase in absorbances for the oleylamine in the pentane spectrum after extraction. The extraction of the Ru NPs from the G5- and G6-RuDENSs was less efficient than extraction attempts conducted on the G4-RuDENSs. This could be due to steric reasons since the G5-PAMAM-OH, G6-PAMAM-OH and oleylamine are bulky molecules. As earlier mentioned, the purpose of extracting the nanoparticles was to disperse them in an ionic liquid and coat the catalyst mixture on a suitable solid support. Ideally, if the ionic liquid could efficiently extract the Ru NPs, there would be no need to investigate the use of the alkylamines. However, the weaker coordination of nitrogen in the alkylamines when compared to alkylthiols, could allow for their removal during the catalyst pre-treatment. When considering the results obtained for the alkylamines, oleylamine has a higher boiling point compared to octylamine and removing any excess oleylamine could prove difficult. Octylamine would therefore be more suited as an extractant. To gain more insight into the effects of the extraction and phase-transfer on the size of the Ru NPs extracted, HRTEM micrographs of each of the extracts were taken and the particle size analysed.

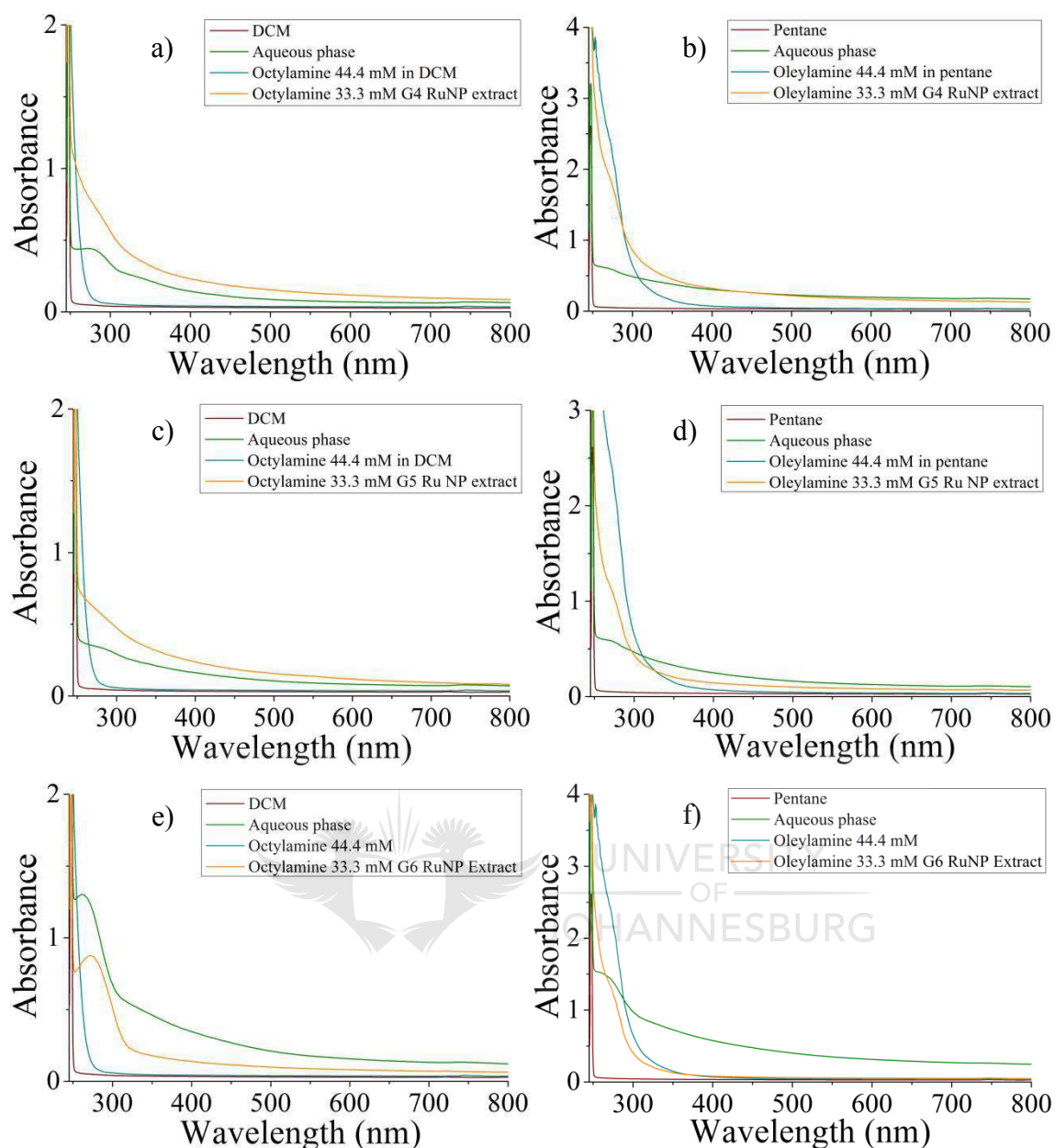


Figure 2.4. UV/Vis/ spectra monitoring the extraction of Ru NPs from the RuDENs and phase transfer into either DCM or pentane for G4-RuDEN using, a) octylamine and b) oleylamine extractants, for G5-RuDEN using c) octylamine and d) oleylamine as extractants, and for G6-RuDEN using e) octylamine and f) oleylamine as extractants.

2.3.2.3 HRTEM analysis of the Ru nanoparticles extracted using octylamine.

The HRTEM images and size distribution histograms for the nanoparticles extracted using octylamine are detailed in Figure 2.5. The narrow size distribution observed for the RuDENs is maintained. This is an indication of the ability of the octylamine to act as an extractant and stabiliser for the nanoparticles.

Despite the effectiveness of octylamine as a stabiliser, changes in the particle size upon extraction were observed when comparing the Ru NP size before and after extraction.

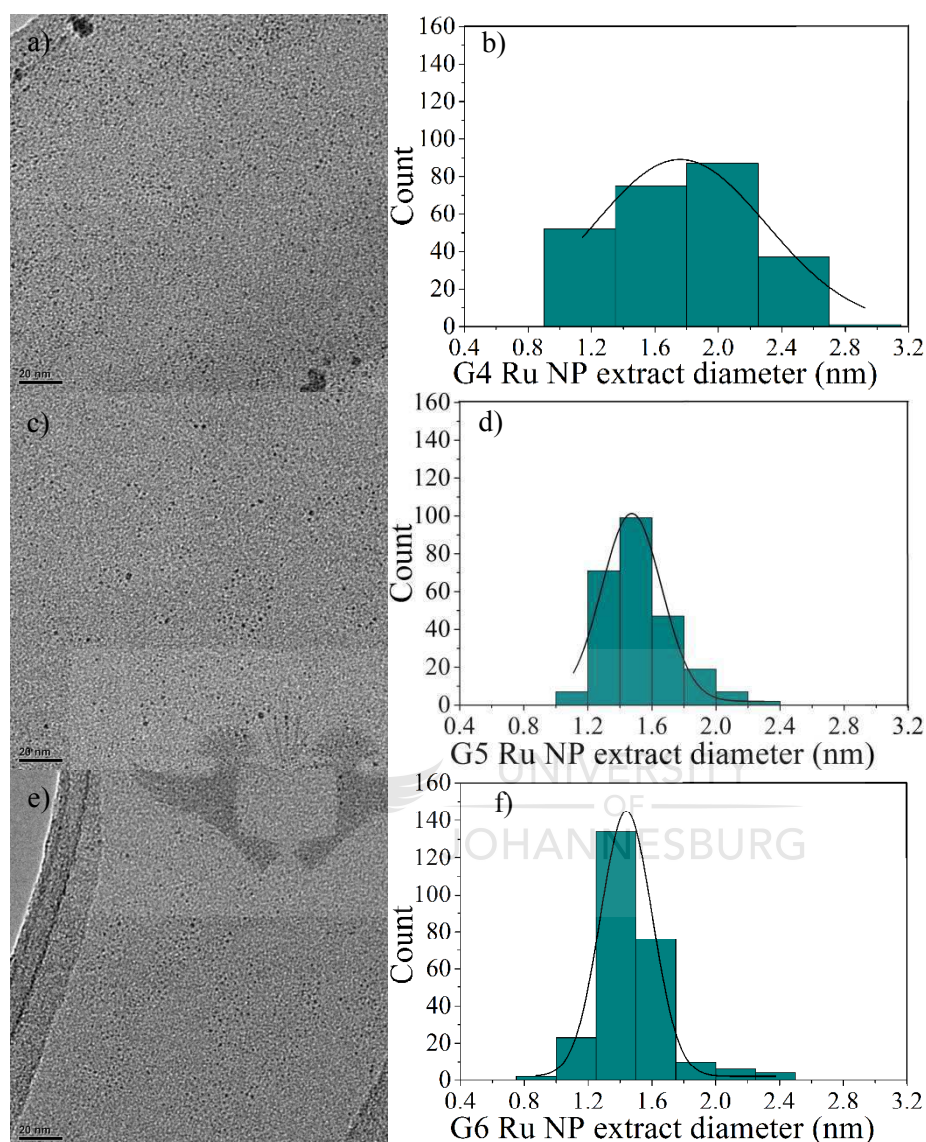


Figure 2.5. Analysis of HRTEM results for the extraction of Ru NPs from the RuDENs using octylamine: a) HRTEM image of G4-RuDEN Ru NP extraction, b) Histogram for the size distribution of G4-RuDEN Ru NP extraction, c) HRTEM image of G5-RuDEN Ru NP extraction, d) Histogram for the size distribution of G5-RuDEN Ru NP extraction, e) HRTEM image of G6-RuDEN Ru NP extraction, f) Histogram for the size distribution of G6-RuDEN Ru NP extraction.

Table 2.3 compares the results for average diameter of the Ru NPs obtained prior to extraction and post extraction. The extraction caused an increase in the particle size when extracting the Ru NPs from the G4-RuDEN and G5-RuDEN of 50% and 7% respectively. The increase in

nanoparticle size indicates possible agglomeration during the particle extraction. Similar to the stabilisation provided by the dendritic macroenvironment, the coordination of octylamine to the nanoparticle surface provides steric stabilisation to the Ru NP. Increase in the amount of octylamine coordinated to the Ru NP surface leads to an increase in the hydrophobicity of the particle. During this gradual surface coverage of the nanoparticle by octylamine, it is possible that even with partial coverage the particles can migrate to the organic phase. During this migration, and given the partial coverage, there is the possibility of nanoparticles to coalesce and form larger particles. This is likely the explanation for the increase in particle size observed upon extraction of the Ru NP from the G4-RuDEN. A 32 % decrease in the average NP diameter was observed when extracting the Ru NPs from the G6-RuDENs.

Table 2.3. Comparison of the average RuDEN diameter and the Ru NP obtained using octylamine as extractant

RuDEN	Average particle diameter prior to extraction (nm)	Average particle diameter after extraction (nm)
G4-RuDEN	1.2 ± 0.1	1.8 ± 0.4
G5-RuDEN	1.4 ± 0.1	1.5 ± 0.2
G6-RuDEN	2.2 ± 0.3	1.5 ± 0.2

The extraction is most likely selective for the extraction of nanoparticles of a certain size. To help justify this observation, consideration should be given to the lower efficiency of the extraction of the Ru NPs from the G6-RuDEN when compared to the other RuDENs as discussed for the UV/Vis spectra. This implication likely originates from selective extraction of certain sized particles from the G6-RuDEN. Here, steric inhibition is likely to play a role since removal of the Ru NP from the more bulky G5-PAMAM-OH and G6-PAMAM-OH proves less facile. For smaller nanoparticles, however, the removal is favoured from the sterically hindered higher generation dendrimer. In this sense, for the G5-RuDENs and G6-RuDENs, extraction of particles with an average diameter of 1.5 nm is favoured. Concerning the G4-RuDEN, there seems to be possible agglomeration during the extraction of the Ru NPs. The complexity and overall inefficiency of extraction of Ru NPs from the PAMAM-OH dendrimers resulted in the choice to immobilise the RuDENs directly on the solid support and use of ionic liquids then as a coating instead of dispersion media.

2.3.3 *The immobilisation of RuDENs on silica 60 and silica 100.*

The G4-, G5- and G6-RuDEN catalysts were prepared as discussed earlier. The Ru precursor used to prepare the RuDENs was RuCl_3 and resulted in an excess of chloride present that could act as a catalyst poison by passivation of the nanoparticle surface. The prepared RuDENs were purified by dialysing against $3 \times 1000 \text{ cm}^3$ of water where the first two dialysis runs were conducted for 3 hours each and the final one for 12 hours. Once the excess chloride was removed, as determined by using silver nitrate as test solution for the formation of silver chloride to confirm chloride, the RuDENs were deposited on a silica support via wetness impregnation. Both silica 60 and silica 100 were used without further calcination for the study. This was to ensure the presence of surface silanols to help increase interaction of the Ru NP surface with the surface of the support. The dialysed RuDEN solutions were shaken on a reciprocating shaker with the silica to allow interaction between the RuDENs and the support. This was to help minimise any mechanical attrition of the support observed when stirring the mixture with a magnetic stirrer bar. It is important to maintain the structural integrity of the silica support during catalyst preparation. This plays an important role in further preparation of the catalysts with an ionic liquid layer to be discussed later. The silica supported RuDEN catalysts will be referred to as $\text{G}_n\text{-RuSil60}$ or $\text{G}_n\text{-RuSil100}$ where “n” denotes the generation of dendrimer, 4, 5 or 6 and “Sil” denotes the silica support. The suffix “60” or “100” denotes the use of silica 60 or silica 100 respectively. The metal loading of the catalyst was confirmed by using ICP-OES. The samples were digested prior to analysis using a hydrofluoric acid and nitric acid mixture to dissolve the silica support. The samples were then dried by evaporation and the remaining Ru dissolved in *aqua regia*. Collectively, the RuSil catalysts had an average Ru metal loading ranging from 0.08%-0.15% Ru when prepared for use in the hydrogenation reactions to be discussed later. Additionally, a series of RuSil catalysts with a higher metal loading of 0.20%-0.40%, as confirmed by ICP-OES, was prepared for evaluation in the oxidation of styrene in the presence of TBHP.

Various attempts to analyse the RuSil catalysts were made including the use of analytical techniques such as PXRD and H_2 chemisorption to study the characteristics of the nanoparticle. Additionally, SEM analysis was conducted on the RuSil catalysts but given the limitations of the equipment, such small nanoparticles were not visible, however, the lack of aggregation to large particles, possibly missed with HRTEM, was confirmed. In the case of the PXRD analysis, an estimate of the average particle size can be calculated. Similarly, an

average particle size can be calculated from chemisorption analysis as well as the amount of surface-active Ru atoms available for catalysis. In the case of the PXRD analysis, no reflection registered for the presence of Ru in the RuSil catalyst and the bulk amorphous silica phase was seen as a broad peak. This also confirmed the SEM data reinforcing that no significant aggregation of the Ru particles occurred. The chemisorption results obtained gave a gross overestimation of the size of the Ru nanoparticles on the RuSil catalysts which did not correlate with the more reliable HRTEM analysis to be discussed later. In addition, the chemisorption results did not correlate to the SEM/PXRD results.

2.3.3.1 TGA analysis of the RuSil catalysts.

The dendrimer template functions as a stabiliser in the preparation of Ru NPs as RuDENSs. The dendrimer template is usually removed, after immobilisation of RuDENSs on a solid support material, by calcination.¹³⁻¹⁴ This is done to help prevent any passivation of the nanoparticle surface in preparation for catalytic evaluation. Consequently, sintering of the nanoparticle is not avoidable during the calcination process. The RuSil catalysts in this study were not calcined to preserve the stabilising effect of the dendrimer and to investigate whether a significant change in particle size was observed and whether the narrow size distribution of the RuDEN is maintained. Firstly, the presence of the dendrimer on the RuSil catalysts needs to be confirmed. The RuSil60 catalysts were used as a model system for investigating the presence of the dendrimer when using amorphous silica to support RuDENSs.

Figure 2.6 illustrates the TGA data obtained for the various RuSil60 catalysts up to a temperature of 500 °C. An initial mass loss for temperatures below 100 °C was observed in all cases and corresponds to the evaporation of physisorbed water on the RuSil60 catalyst surface. A further 1-2% mass loss occurs at 150-350 °C associated with the decomposition of the dendrimer template. This supports the presence of the dendrimer on the RuSil type catalysts and could possibly help stabilise the Ru nanoparticles during immobilisation. The stabilisation of the RuDENSs upon immobilisation is dealt with in more detail by analysis of HRTEM images discussed in the section that follows.

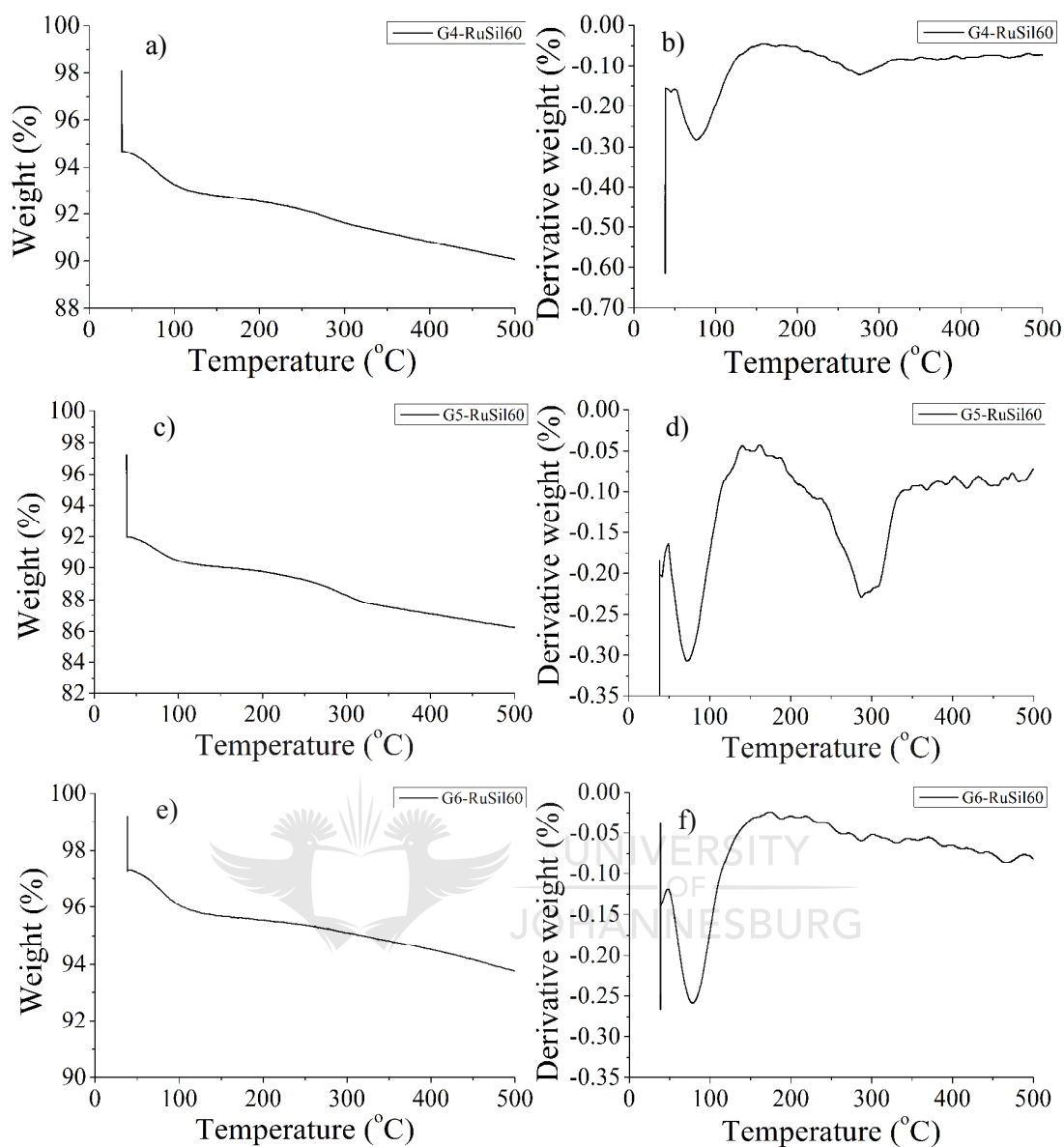


Figure 2.6. TGA data for the RuSil60 catalysts. The results show the a) percentage weight loss and b) derivative of the percentage weight loss for the G4-RuSil60 catalyst, the c) percentage weight loss and d) derivative of the percentage weight loss for the G5-RuSil60 catalyst and the e) percentage weight loss and f) derivative of the percentage weight loss for the G6-RuSil60 catalyst.

2.3.3.2 HRTEM analysis of the RuSil catalysts.

The HRTEM analysis was utilised in the study of the Ru NP size for the RuSil catalysts to investigate whether the size of the particle was conserved upon immobilisation on the silica support. Figure 2.7 shows the characteristic HRTEM images and the respective size distribution histograms for the lower metal loading RuSil60 catalysts to be evaluated as hydrogenation catalysts.

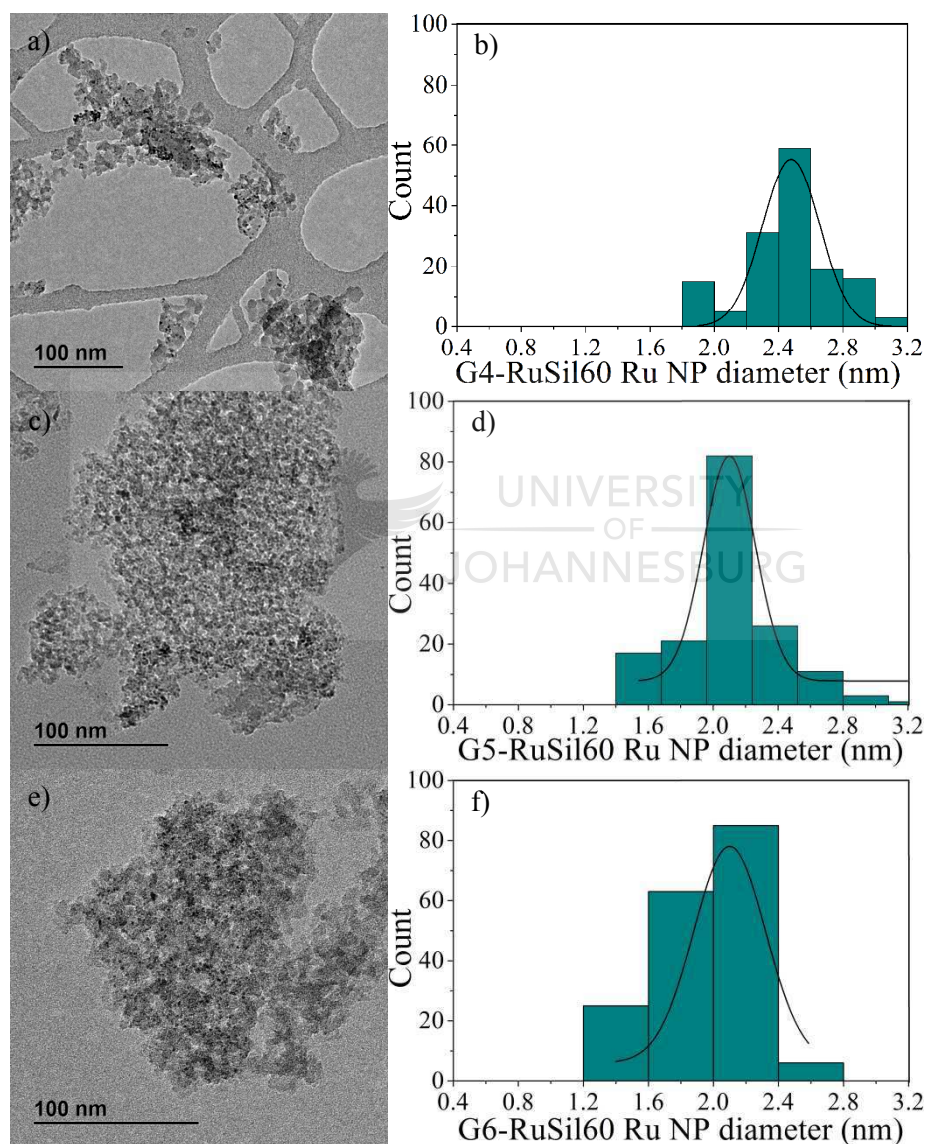


Figure 2.7. a) HRTEM image of G4-RuSil60 b) Histogram for the size distribution of G4-RuSil60. c) HRTEM image of G5-RuSil60 d) Histogram for the size distribution of G5-RuSil60. e) HRTEM image of G6-RuSil60 f) Histogram for the size distribution of G6-RuSil60.

As presented in Table 2.4, the average sizes of the nanoparticles for the various RuDENs on the silica support were 2.4 ± 0.3 , 2.1 ± 0.3 and 2.1 ± 0.3 nm for G4-RuSil60, G5-RuSil60 and G6-RuSil60 respectively. When compared to the RuDENs, there is a size increase upon immobilisation on the silica support. This indicates sintering that occurred during the immobilisation and treatment processes utilised. A 100% and 50% Ru NP size increase was observed for the G4-RuDEN and the G5-RuDEN respectively upon immobilisation. Essentially, the larger the dendrimer, the less sintering occurs. The increased dendrimer generation is beneficial to the stabilisation of the Ru NP especially during the immobilisation on silica. Immobilisation of the G6-RuDEN catalysts on silica 60 observed a 5% decrease in size but given the standard deviation, the size distribution falls within range of the original G6-RuDEN particle size. For the most part, the Ru nanoparticle size and narrow size distribution is maintained upon immobilisation of the G6-RuDEN on the silica 60 support.

Table 2.4. The average Ru NP size for each of the RuDEN catalysts supported on silica 60 and silica 100 and the percentage change in size upon immobilisation.

Entry	Catalyst	Ru NP diameter (nm)	Change in Ru NP diameter (%) ^a
1	G4-RuSil60	2.4 ± 0.3	100 ^b
2	G5-RuSil60	2.1 ± 0.3	50 ^b
3	G6-RuSil60	2.1 ± 0.3	5 ^c
4	G4-RuSil60S	2.3 ± 0.3	92 ^b
5	G5-RuSil60S	1.7 ± 0.3	21 ^b
6	G6-RuSil60S	2.3 ± 0.2	5 ^b
7	G4-RuSil100	1.4 ± 0.2	17 ^b
8	G5-RuSil100	1.5 ± 0.2	7 ^b
9	G6-RuSil100	2.2 ± 0.2	—

^a Change upon immobilisation, ^b Percentage increase upon immobilisation on silica, ^c Percentage decrease upon immobilisation on silica

The second set of RuSil60 catalysts, referred to as RuSil60S catalysts, have a higher Ru metal loading and was prepared for evaluation as catalysts in oxidation reactions. The higher loading catalysts were prepared to help minimise any contribution of the catalyst support to

the activity of the catalyst, a topic that will be addressed in a later chapter. The average Ru NP diameters observed for the RuSil60S catalysts are detailed in Table 2.4 for entries 4-6. An increase in the particle diameter was observed upon immobilisation of the RuDENs on the silica 60 support for each of the RuSil60S catalysts. The percentage increase in size of the Ru NPs upon immobilisation was 92%, 21% and 5% for the G4-RuSil60S, G5-RuSil60S and G6-RuSil60S catalysts respectively.

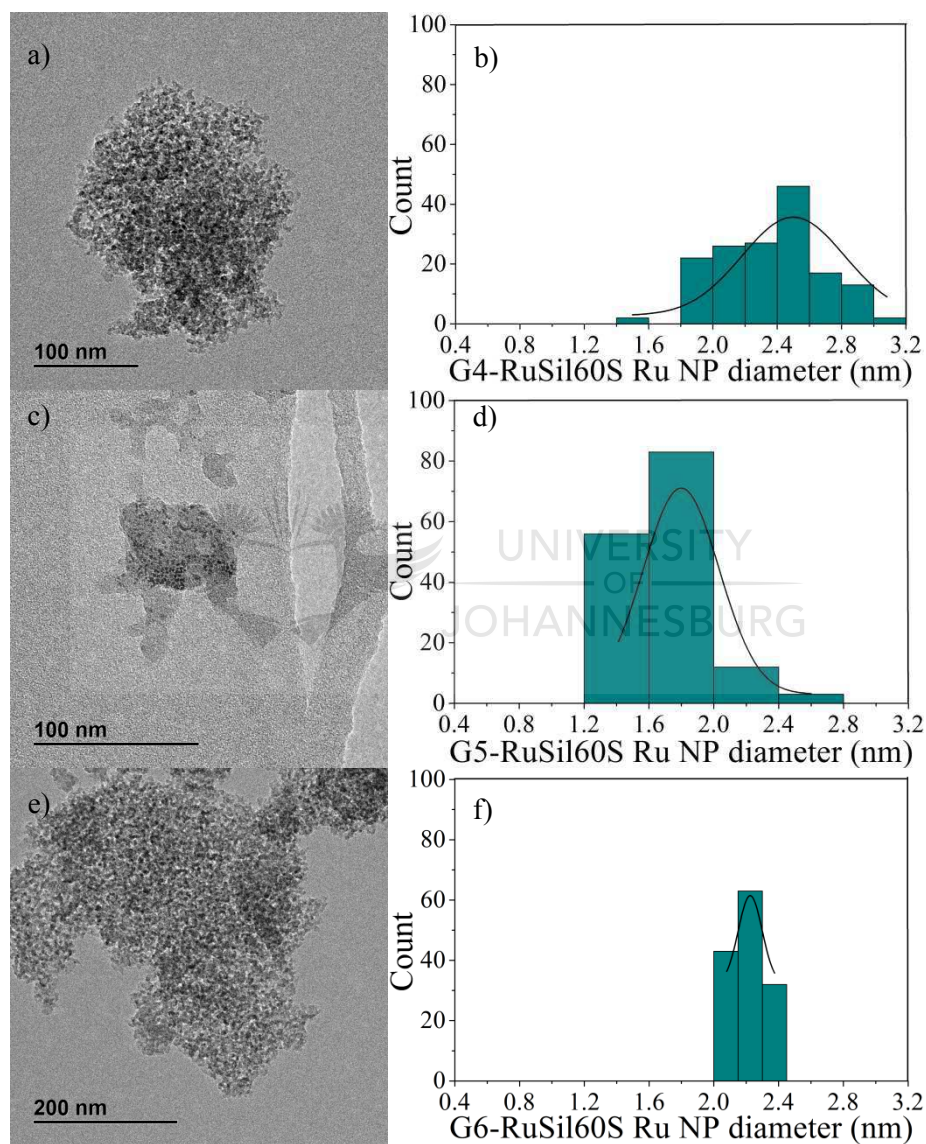


Figure 2.8. a) HRTEM image of G4-RuSil60S b) Histogram for the size distribution of G4-RuSil60S. c) HRTEM image of G5-RuSil60S d) Histogram for the size distribution of G5-RuSil60S. e) HRTEM image of G6-RuSil60S f) Histogram for the size distribution of G6-RuSil60S.

This trend in particle size change is similar to that observed when preparing the RuSil60 catalysts except that an increase in Ru NP particle size is seen upon immobilisation for the G6-RuSil60S instead of a decrease as observed for the G6-RuSil60 catalyst. Despite the change in the size of the RuNP upon immobilisation, the narrow size distribution observed when using dendrimers as templating agents and stabilisers was maintained as illustrated by the Ru NP diameter histograms in Figure 2.8.

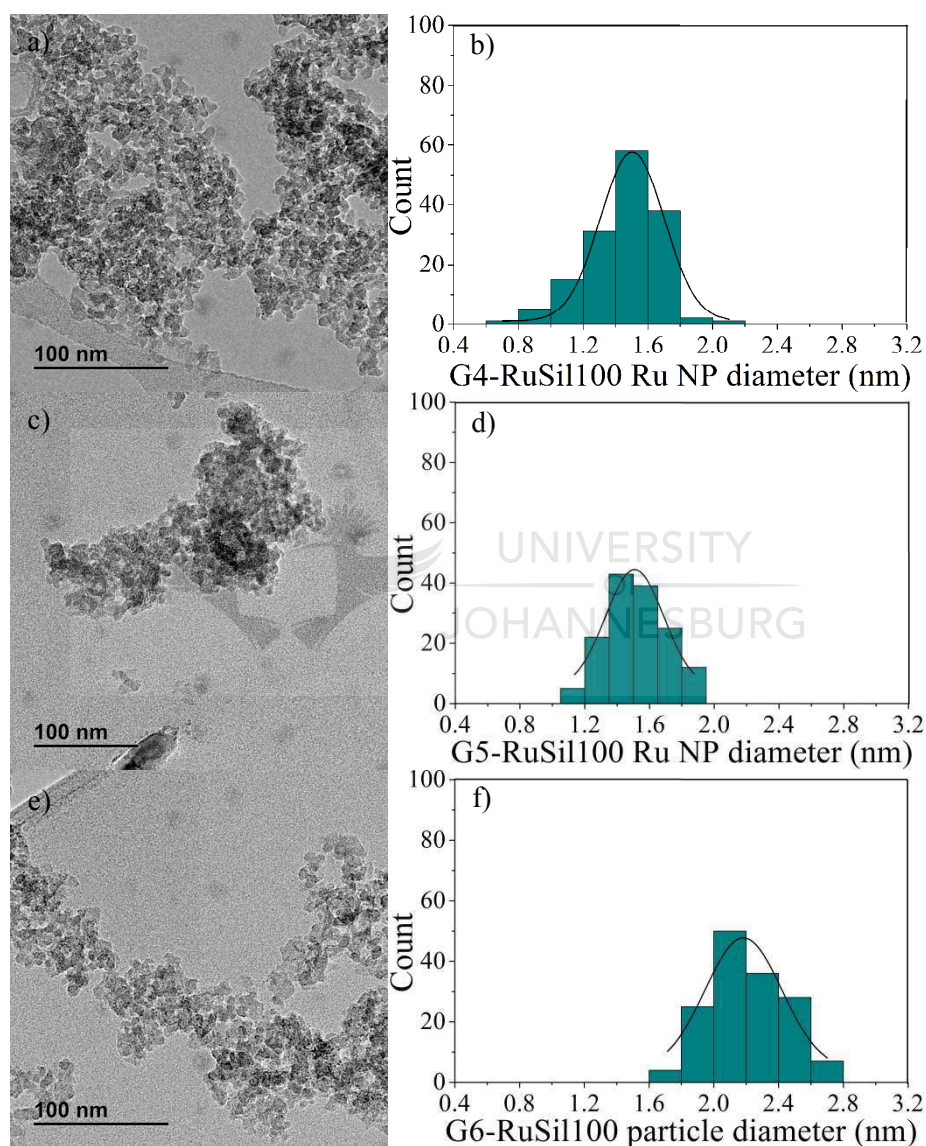


Figure 2.9. a) HRTEM image of G4-RuSil100 b) Histogram for the size distribution of G4-RuSil100. c) HRTEM image of G5-RuSil100 d) Histogram for the size distribution of G5-RuSil100. e) HRTEM image of G6-RuSil100 f) Histogram for the size distribution of G6-RuSil100.

For the purposes of later preliminary studies into the utilisation of the RuSil catalysts in the continuous flow hydrogenation of toluene, the RuDENs were immobilised on silica 100. The larger pore size of silica 100 compared to silica 60 could help with gaseous toluene permeability. The TEM micrograph images and RuNP size histograms of the RuSil100 catalysts are shown in Figure 2.9. The narrow Ru NP size distribution is maintained and more interestingly, the sintering of the G4-RuDEN is minimised upon immobilisation on the silica 100 support when compared to results obtained for G4-RuSil60 and G4-RuSil60S. The decrease in sintering was observed when preparing the G5-RuSil100 as well with only a 7% increase in the particle size upon immobilisation. The immobilisation of G6-RuDEN on silica 100 has no significant effect on the Ru NP diameter, which maintained an average diameter of 2.2 nm.

2.3.4 Preparation of solid catalysts with ionic liquid layer (SCILL).

The series of RuSil catalysts were coated with numerous ionic liquids as a means to screen the effects of the ionic liquid on the catalytic activity of the RuSil catalysts. The [OMIM][NTf₂] and [BMIM][OcS] coated catalysts were not fully characterised and later catalytic evaluations to be discussed later are preliminary. This section focuses on the change in the physical characteristics of some of the RuSil catalysts upon coating with an ionic liquid. The Ru SCILL catalysts will be referred to as RuSCILL catalysts and were prepared from a select RuSil catalyst. Usually, the RuSil catalyst chosen was that for which the highest catalytic activity was observed. The presence of the ionic liquid was confirmed using a combination of TGA and BET data. Important to note, the focus of this section is not on detailed interaction studies of the ionic liquid with the nanoparticle surface but change in physical properties of the RuSil upon coating with ionic liquid.

2.3.4.1 TGA analysis of the RuSCILL catalysts.

The TGA data obtained for the RuSCILL catalysts indicate the amount of ionic liquid present for each RuSCILL catalyst as a function of mass loss over a temperature range. Two types of ionic liquids were used distinguished by the cation namely, the BMIM and EMIM ionic liquids. The following section discusses the TGA results obtained for the RuSCILL catalysts grouped according to their cations. Figure 2.10 illustrates the TGA data obtained for the BMIM RuSCILL catalysts. A significant weight loss occurs from 150-400 °C which is

consistent with the loss of the dendrimer and the ionic liquid. The total mass loss ranged from 10-12% over this temperature range. This is much higher than the dendrimer mass loss of approximately 1-2% as earlier discussed. The observed mass loss of ionic liquid correlates well with the approximately 10 wt% ionic liquid used when preparing the RuSCILL catalyst for catalysts with an α -value of 0.1.

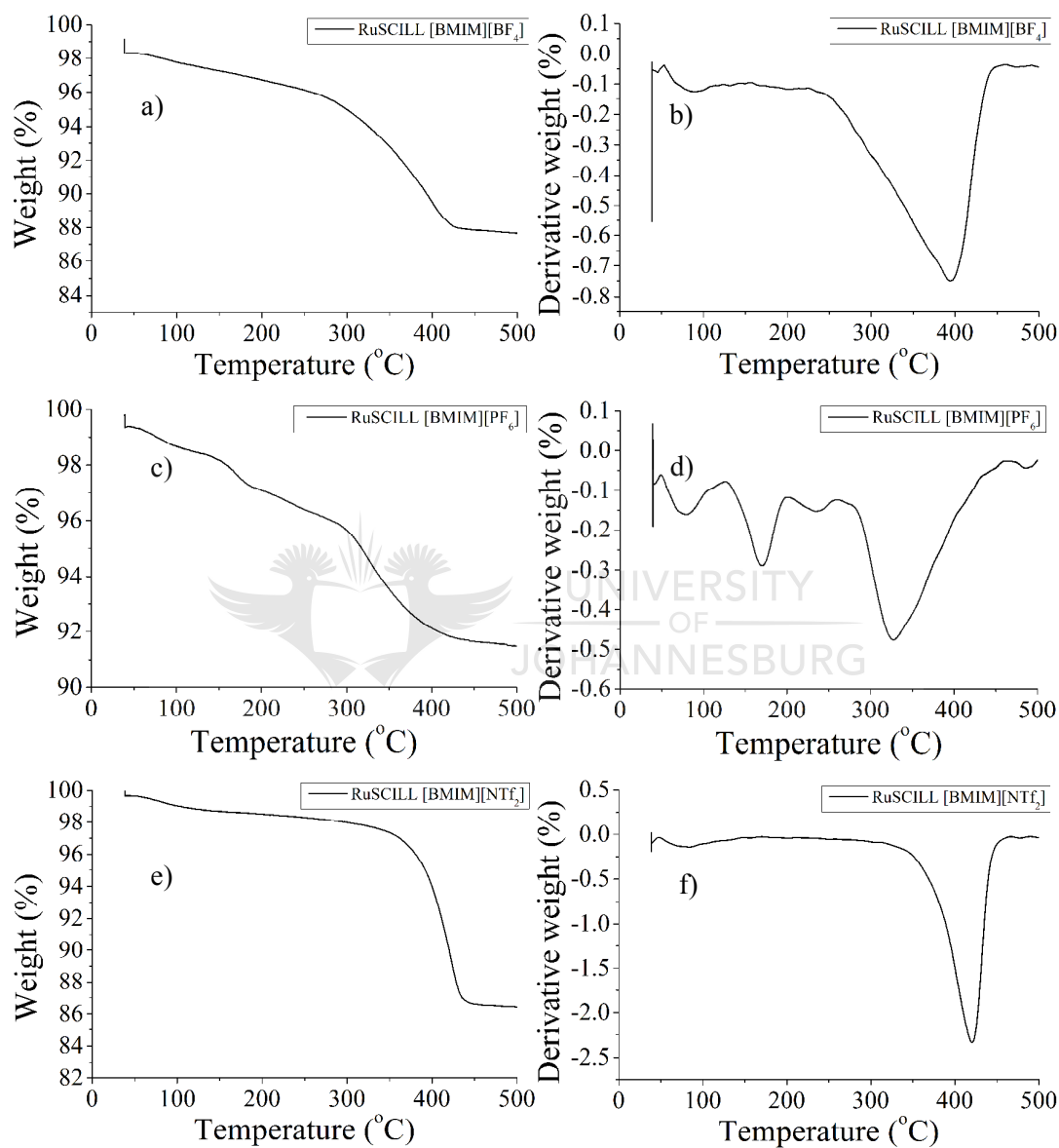


Figure 2.10. TGA data for the RuSCILL catalysts prepared with [BMIM][BF₄], [BMIM][PF₆] and [BMIM][NTf₂]. The results show the a) percentage weight loss and b) derivative of the percentage weight loss for the [BMIM][BF₄] coated RuSCILL, the c) percentage weight loss and d) derivative of the percentage weight loss for the [BMIM][PF₆] coated RuSCILL and the e) percentage weight loss and f) derivative of the percentage weight loss for the [BMIM][NTf₂] coated RuSCILL.

The TGA results obtained when using the EMIM cation based catalysts (Figure 2.11), show similar results to that obtained when analysing the BMIM catalysts. The percentage weight loss for the EMIM based ionic liquids seem to be somewhat lower than that of the BMIM. This could suggest that during the preparation of the EMIM based RuSCILL catalysts, the more hydrophilic EMIM ionic liquid interact to some extent with the glass of the round bottom flask.

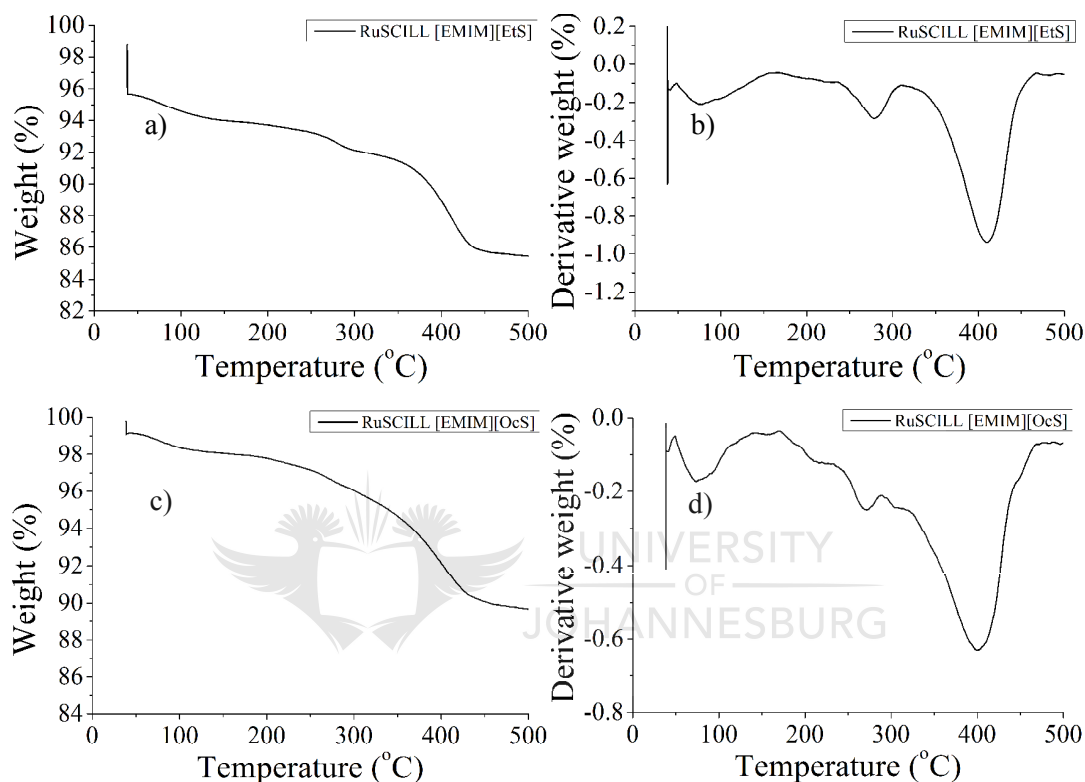


Figure 2.11. TGA data for the RuSCILL catalysts prepared with [EMIM][EtS] and [EMIM][OcS]. The results show the a) percentage weight loss and b) derivative of the percentage weight loss for the [EMIM][EtS] coated RuSCILL and the c) percentage weight loss and d) derivative of the percentage weight loss for the [EMIM][OcS] coated RuSCILL.

This would result in a fraction of the ionic liquid not immobilising on the RuSil catalyst. The average percentage ionic liquid of the EMIM RuSCILL catalysts ranges from 8-10%. The ionic liquid therefore shows good interaction with the support material and has sufficient thermal stability for the reaction conditions of the catalytic reactions to be discussed in later chapters.

2.3.4.2 BET analysis of the RuSCILL catalysts.

The BET data for the RuSCILL catalysts helps confirm the presence of the ionic liquid by monitoring any changes in the physical characteristics of the catalyst. Specific focus is placed on changes in the surface area and pore volume upon coating of the RuSil catalysts with the ionic liquid. The BET results in Table 2.5 show typical changes in the physical characteristics of the RuSil catalysts upon coating with an ionic liquid.

A surface area and pore volume of $462.1 \text{ m}^2\text{g}^{-1}$ and $0.82 \text{ cm}^3\text{g}^{-1}$ was observed for the uncoated G5-RuSil60 catalyst respectively. The RuSCILL catalysts presented in Table 2.5 represents a series of SCILL catalysts for a 10 % pore filling with ionic liquid represented by an α -value of 0.1.

Table 2.5. Typical surface area, average pore volume and average pore diameter changes for the uncoated and coated G5-RuSil60 catalysts

Catalyst	Surface area, $S_{\text{BET}} (\text{m}^2\cdot\text{g}^{-1})^{\text{a}}$	Total pore volume, $V_{\text{T}} (\text{cm}^3\cdot\text{g}^{-1})^{\text{b}}$	Average pore diameter, D_{p} (Å) ^b
Uncoated G5-RuSil60	462.1	0.82	56.2
10% [BMIM][BF ₄] G5-RuSCILL	323.5	0.66	58.4
10% [BMIM][PF ₆] G5-RuSCILL	344.9	0.65	55.7
10% [BMIM][NTf ₂] G5-RuSCILL	357.5	0.65	53.6
10% [EMIM][EtS] G5-RuSCILL	342.1	0.63	55
10% [EMIM][OcS] G5-RuSCILL	347.8	0.67	56.7

^a Determined by BET analysis, ^b Determined by BJH analysis

An expected decrease in surface area and pore volume to 323-358 m^2g^{-1} and 0.63-0.67 cm^3g^{-1} was observed respectively when compared to the results obtained for the uncoated catalyst. This not only confirms the presence of the ionic liquid but the expected behaviour of the ionic liquid upon coating the RuSil catalyst surface.

2.4 Conclusion

The dendrimer templated preparation of Ru NPs allows for the preparation of nanoparticles with a narrow size distribution. The extraction of Ru NPs from RuDENs is an area of research that requires some attention to assist in developing methodologies of recycling the dendrimer. This is especially important considering the cost of the dendrimer. Despite this, the control of particle size obtained using this template is beneficial. The use of ionic liquids in catalysis has seen numerous catalytic applications as an alternative to conventional solvents allowing for recyclability, especially in biphasic reactions. The issue of low gas diffusion in bulk ionic liquids is minimised when using a SCILL catalyst. The preparation of the SCILL catalysts discussed in this study is straightforward. The effects of the ionic liquid on the catalytic performance of the prepared RuSil catalysts are of great importance and will be discussed in the chapters to follow.

2.5 References

- [1] Y. M. Chung and H. K. Rhee, *Catal. Lett.* **2003**, *85*, 159.
- [2] R. M. Crooks, B. I. L. III, L. Sun, L. K. Yeung and M. Zhao, *Top. Curr. Chem.* **2001**, *21*, 81.
- [3] R. M. Crooks, M. Zhao, L. Sun, V. Chechik and L. K. Yeung, *Acc. Chem. Res.* **2001**, *34*.
- [4] R. W. J. Scott, A. K. Datye and R. M. Crooks, *J. Am. Chem. Soc.* **2003**, *123*, 3708.
- [5] N. N. Hoover, B. J. Auten and B. D. Chandler, *J. Phys. Chem. B* **2006**, *110*, 8606.
- [6] L. W. Beakley, S. E. Yost, R. Cheng and B. D. Chandler, *Appl. Catal. A: Gen.* **2005**, *292*, 124.
- [7] R. W. J. Scott, C. Sivadinarayana, O. M. Wilson, Z. Yan, D. W. Goodman and R. M. Crooks, *J. Am. Chem. Soc.* **2005**, *127*, 1380.
- [8] R. W. J. Scott, O. M. Wilson and R. M. Crooks, *Chem. Mater.* **2004**, *16*, 5682.
- [9] *Nanoparticles and Catalysis*, WILEY-VCH Verlag GmbH & Co. KGaA, Weinheim, **2008**.
- [10] R. W. J. Scott, O. M. Wilson and R. M. Crooks, *J. Phys. Chem. B* **2005**, *109*, 692.
- [11] K. An and G. A. Somorjai, *ChemCatChem* **2012**, *4*, 1512.
- [12] W. Rasband, 1.47v ed., National Institute of Health, USA, **2013**.

- [13] G. Lafaye, A. Siani, P. Marécot, M. D. Amiridis and C. T. Williams, *J. Phys. Chem. B* **2006**, *110*, 7725.
- [14] G. Lafaye, C. T. Williams and M. D. Amiridis, *Catal. Lett.* **2004**, *96*, 43.
- [15] N. C. Antonels and R. Meijboom, *Langmuir* **2013**, *29*, 13433.
- [16] K. A. Marvin, N. N. Thadani, C. A. Atkinson, E. L. Keller and K. J. Stevenson, *Chem. Commun.* **2012**, 48.
- [17] G. Socrates, *Infrared and Raman Characteristic Group Frequencies: Tables and Charts*, 3rd ed., Wiley, Chichester, **2001**.
- [18] D. Lin-Vien, N. B. Colthup, W. G. Fateley and J. G. Grasselli, *Infrared and Raman Characteristic Frequencies of Organic Molecules*, Academic Press, **1991**.
- [19] K. P. Ishida and P. R. Griffiths, *Appl. Spectrosc.* **1993**, *47*, 584.
- [20] Y.-G. Kim, S.-K. Oh and R. M. Crooks, *Chem. Mater.* **2004**, *16*, 167.
- [21] H. Lang, R. A. May, B. L. Iversen and B. D. Chandler, *J. Am. Chem. Soc.* **2003**, *125*, 14832.
- [22] M. Zhao, L. Sun and R. M. Crooks, *J. Am. Chem. Soc.* **1998**, *120*, 4877.
- [23] J. C. Garcia-Martinez and R. M. Crooks, *J. Am. Chem. Soc.* **2004**, *126*, 16170.



Chapter 3 – Catalytic reduction of 4-nitrophenol using ruthenium dendrimer encapsulated nanoparticles.

3.1 Introduction

The use of transition metal nanoparticles has gained widespread application in the field of catalysis.¹ Due to the high ratio of surface to total atoms in transition metal nanoparticles, they closely approximate the behaviour of conventional mononuclear transition metal catalysts. This property places transition metal nanoparticles on the border between homogeneous and heterogeneous catalysis, as they are able to operate as both.² Of great importance in the preparation of nanoparticles is the stabilisation of metal nanoparticles and control of their size. The preparation of nanoparticles with a narrow size distribution is highly desirable. Aggregation of nanoparticles during synthesis results in the formation of thermodynamically favoured larger sized nanoparticles, with a concomitant decrease in catalytic activity. There are various methods of stabilising metal nanoparticles including the use of ionic liquids,³ polymers,⁴ low molecular weight⁵ and macromolecular organic ligands⁶ to name a few. There are various modes of stabilisation, including electrostatic stabilisation and steric stabilisation.⁷ Electrostatic stabilisation occurs when anions and cations associate with the nanoparticle surface creating an electrical double layer with Coulombic repulsion preventing agglomeration. Steric stabilisation occurs when large macromolecules associate with the nanoparticle surface. The combination of both these stabilisation modes is referred to as electrosteric stabilisation. The stabilisation and size of nanoparticles obtained is, however, dependant on the amount of these stabilisers, and a fine balance between amount of metal and stabiliser is needed.

The use of dendrimers as stabilisers allows for the templated preparation of nanoparticles in solution and their stabilisation is ensured by internal functional groups on the dendrimer that can coordinate to the nanoparticle surface with minimal passivation.^{6, 8-9} Dendrimers are discrete, well-defined hyperbranched macromolecular polymers where their size is denoted by their generation.¹⁰ In the synthetic methodology for the dendrimer templated preparation of transition metal nanoparticles, the size of the nanoparticle is controlled by the overall loading capacity of the dendrimer for a particular transition metal complex and, more importantly, by

the metal ion:dendrimer ratio. One of the most commonly used dendrimers in the preparation of transition metal nanoparticles are the commercially available poly(amidoamine) (PAMAM) dendrimers.⁶ This class of dendrimers have tertiary amines present within its branches that provide sites for the coordination of transition metal complexes. Different sized nanoparticles can therefore be prepared by using different sized dendrimers where higher generation dendrimers are able to partition a larger amount of transition metal complexes into its interior.⁶

Ruthenium nanoparticles are known for their activity in hydrogenation reactions¹¹⁻¹⁵ and have been reviewed for various catalytic systems, comprising ruthenium nanoparticles stabilised by polymers, alcohols, ionic ligands, various organic ligands and solid supports.¹⁶⁻¹⁷ Despite the progress in the preparation of dendrimer encapsulated transition metal nanoparticles, there are few articles cited for the preparation and utilisation of monometallic dendrimer encapsulated ruthenium metal nanoparticles (RuDEN) and their evaluation as catalysts. One of the first preparations of ruthenium dendrimer encapsulated nanoparticles was conducted by Lafaye *et al.* who prepared ruthenium DENs and immobilised the nanoparticles on an alumina support.¹⁸⁻¹⁹ Superior control of the nanoparticle size was achieved compared to Ru/Al₂O₃ prepared by wetness impregnation using an aqueous solution of RuCl₃. The preparation of these ruthenium DENs suffer from the lengthy 48-72 hour period it takes for full coordination of the ruthenium to the tertiary amines; a procedure that was improved upon by Stevenson *et al.*²⁰ Their study utilised the partial galvanic displacement of nickel by ruthenium from a PAMAM-OH/Ni complex, and then the subsequent reduction of this complex by sodium borohydride to yield bimetallic Ru/Ni DENs. Galvanic displacement reactions have been utilised by Crooks *et al.* and proves a facile method in the preparation of bimetallic dendrimer encapsulated nanoparticles.^{8, 21-22} In the case of the research conducted by Stevenson *et al.*, they never mentioned this galvanic displacement used for the complete displacement of nickel to form monometallic RuDENs. The Ru/Ni DENs were briefly evaluated in the catalytic reduction of 4-nitrophenol (4NP) where the catalytic activity was enhanced by the presence of nickel when compared to monometallic RuDENs.²⁰

The catalytic reduction of 4NP has been used as a benchmark reaction by many research groups for the evaluation of the catalytic activity of metal nanoparticles, owing to its ease of execution.²³⁻²⁷ The reaction is conducted in aqueous media and can easily be followed using UV/Vis spectrophotometry by observing the disappearance of the phenolate absorbance peak

at λ 400 nm upon reduction of 4NP to 4-aminophenol (4AP). Despite the widespread use of this reaction, there have been relatively few investigations into the mechanism involved in this reaction.

Esumi *et al.* investigated the effect of various generations of poly(propyleneimine) (PPI) and PAMAM dendrimers used to prepare Pt, Pd and Ag DENs on the rate 4NP reduction and found the reaction to be diffusion controlled.²⁸ Saha *et al.* investigated the effects of varying the concentration of 4NP in the evaluation of the catalytic activity of their catalytic system.²⁴ The study provided a few key insights into the mechanism of the reaction as depicted in Figure 3.1.

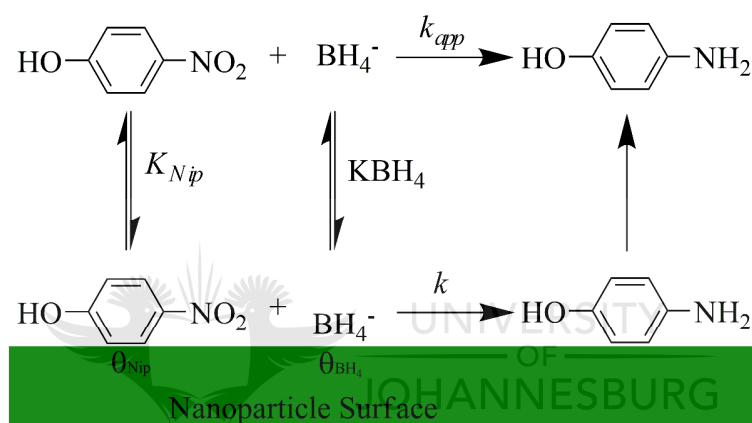


Figure 3.1. A simple mechanistic depiction of the 4NP reduction. The green shaded area represents the RuDEN surface where the reaction occurs. A BH_4^- and 4NP molecule adsorbs on the catalyst surface in which case the adsorption and desorption of both are fast processes and can be modelled by the Langmuir-Hinshelwood mechanism and quantitatively described by the adsorption constants K_{BH_4} and $K_{4\text{NP}}$ respectively. The rate-determining step is the reduction of 4NP to 4AP and is described by the surface rate constant k .

They concluded that the mechanism relies on adsorption of the reactant on the surface then, diffusion of the 4NP and BH_4^- molecule to the active site to form a surface complex, reaction of the surface complex to form the product and finally desorption of the product.²⁴ Zhang *et al.* further dealt with the mechanistic aspect of this surface reaction by evaluating Ag nanoclusters deposited on TiO_2 .²⁹ They surmised the initial adsorption of BH_4^- for transferral of a surface hydrogen and subsequent adsorption of 4NP to the surface to react and form 4AP. This would suggest a Langmuir-Hinshelwood mechanistic model that requires both substrate

and reactant to adsorb on the catalyst surface before reaction occurs. Wunder *et al.* conducted a more comprehensive kinetic evaluation of their platinum and gold nanoparticles supported in polyelectrolyte brushes for the reduction of 4NP.³⁰ The authors investigated both the effects of variation in 4NP concentration and BH_4^- concentration on the rate of the reaction. They confirmed that the catalytic reduction of 4NP in the presence of BH_4^- and metallic nanoparticles can be modelled according to Langmuir-Hinshelwood kinetics. Three constants were identified to describe the catalytic system, a kinetic constant, k , that describes the surface reactivity of the species and two thermodynamic adsorption constants, K_{4NP} for 4NP and K_{BH_4} for BH_4^- .

Given the aforementioned merits of ruthenium nanoparticle catalysts in hydrogenation reactions and the necessity for further insights into the kinetic mechanism of 4NP reduction, this study aims at providing a kinetic analysis of the RuDEN type catalysts in the evaluation of 4NP reduction with the use of the Langmuir-Hinshelwood mechanism, the works of which has been published.³¹ This mechanism requires the adsorption of both substrate and reactant to the nanoparticle surface with the rate-determining step being the reaction of the adsorbed species to form the product. The dendrimer structure does not provide a significant diffusion barrier as will be discussed later, therefore the process is not expected to be diffusion controlled.

3.2 Experimental

The sodium borohydride and 4-nitrophenol were purchased from Sigma-Aldrich and used as received. The sodium hydroxide was purchased from Associated Chemical Enterprises (ACE) and used as received. The Milli-Q (18 M Ω .cm) deionised water was used in all experiments. The 4-nitrophenol reduction reactions were conducted in PLASTIBRAND PMMA standard disposable cuvettes purchased from Sigma-Aldrich. The specific surface area was calculated from the average radius obtained and the total nanoparticle concentration based on the concentration of the dendrimer.

3.2.1 Catalytic reduction of 4NP using RuDENs

The catalyst was prepared by transferring 2500 μL of the RuDEN (10 μM) solution to a N_2 purged round bottom flask with degassed Milli-Q water (7500 μL) resulting in a 2.5 μM catalyst solution based on the dendrimer concentration. Each of the six cuvettes were charged with a set amount of the RuDEN catalyst solution that has a dendrimer encapsulated nanoparticle concentration of 2.5 μM . The required amount of NaBH_4 (0.1 M or 0.2 M) solution was pipetted into each cuvette followed by degassed Milli-Q water. The cuvettes were placed in the cuvette compartments of the UV/Vis spectrophotometer and the temperature allowed to equilibrate at 298 K for 15 minutes. In the temperature dependant studies, temperatures of 308 K, 318 K and 328 K were used as well. The required amount of aqueous 4-nitrophenol (600 μM) solution was pipetted into each cuvette to start the reduction reaction. The UV/Vis spectrophotometer was programmed to record absorbance readings at λ 400 nm and λ 550 nm every few seconds. The catalytic reactions were conducted in triplicate to obtain the relevant kinetic data. Catalytic data was processed using Kinetic Studio software³² and all kinetic modelling was conducted using the Origin Pro 8.5 graphing and modelling software.³³



UNIVERSITY
OF
JOHANNESBURG

3.3 Results and Discussion

The reduction of 4NP can be followed by monitoring changes in the absorbance peak at about λ 400 nm for the nitrophenolate anion upon reduction to 4AP. The latter is accompanied by the growth in an absorbance peak at about λ 300 nm. The presence of isosbestic points prove that no side reactions occur allowing for accuracy in interpretation of catalytic results.³⁴⁻³⁶ Of importance is realising the evolution of hydrogen gas during the reaction. This can cause shifts in the entire spectrum and can be corrected by applying a baseline correction of the absorbance value at λ 400 nm with that of the absorbance at λ 550 nm. An induction period, classified as t_0 , can be seen for catalytic runs during which no catalysis takes place and the reaction usually proceeds after this. In the case of the catalytic runs conducted in this study, the induction period is not always seen as the BH_4^- and catalyst interact during the 15-minute period allowed for temperature equilibration prior to the addition of 4NP.

The kinetic analysis was conducted by collecting k_{app} data while keeping the BH_4^- constant and varying the 4NP concentration at the same temperature. A second set of measurements was conducted while keeping the 4NP concentration constant and varying the BH_4^- concentration. Two noteworthy observations are the usual increase in k_{app} with increasing BH_4^- concentration and the decrease in k_{app} with increase in 4NP concentration as reported by Saha *et al.* and Wunder *et al.*^{24, 30} It makes sense that this reaction is not diffusion restricted as opposite behavioural trends would be observed, as was reported for the reduction of ferrocyanate(III) by borohydride with the use of gold nanoparticles as catalysts.³⁷

One important factor in the kinetic studies is the consideration for possible diffusion barriers in the catalytic carrier. The RuDENs consist of a nanoparticle surface where the reaction occurs. Diffusion limitation occurs when the rate of catalytic turnover at the surface of the catalyst is considerably faster than the diffusion of the reactants. These two processes can be related to each other by use of the second Damköhler equation (*DaII*):

$$DaII = \frac{k_{app}c^{n-1}}{\beta a} \quad (1)$$

Here k_{app} is the apparent rate constant, c the concentration of the reactant, n is the order of the reaction, β is the mass transport coefficient and a is the area of the interface which in this case is the volume normalised area of the nanoparticle. The β parameter is further defined as diffusion coefficient divided by the characteristic length scale, δ , a distance over which the mass transfer takes place. The diffusion coefficient previously calculated is $6.92 \times 10^{-10} \text{ m}^2 \cdot \text{s}^{-1}$.³⁸ The values for the remaining parameters of the three catalytic systems are detailed in Table 3.1.

Table 3.1. *DaII* parameter values for the RuDEN catalysts disqualifying diffusion limitations.

Catalyst	k_{app} ($\times 10^{-4} \text{ s}^{-1}$) ^a	δ ($\times 10^{-9} \text{ m}$)	β ($\text{m} \cdot \text{s}^{-1}$)	a (m^{-1})	<i>DaII</i> ($\times 10^{-5}$)
G4-RuDEN	3.96	4.5	0.154	125.56	2.05
G5-RuDEN	6.40	5.4	0.128	84.47	5.77
G6-RuDEN	2.90	6.7	0.103	218.65	1.28

^a k_{app} at 0.1 mM 4NP and 5 mM NaBH_4

In the evaluation of the $DaII$ value, diffusion control is negligible since $DaII \ll 1$. The three catalytic systems evaluated all give calculated $DaII$ values of orders 10^{-5} . Given the low $DaII$ value, the reduction of 4NP in the presence of the various PAMAM-OH carriers is not diffusion controlled.

3.3.1 Kinetic Analysis

3.3.1.1 Investigation into the effects of surface area changes.

The rate of any reaction is directly proportional to the concentration of the catalyst available. In the case of homogeneous catalysts, catalytic activity is easily correlated with the total amount of catalyst present where each catalyst molecule represents a discrete active site. Heterogeneous nanoparticle catalysts requires that catalytic activity be correlated to the amount of potential active sites based on the total surface atoms in the particular batch of nanoparticle catalyst. This value may be calculated with some degree of certainty from the average diameter of the particle based on the assumption that the particle is spherical.

In the case of RuDENS, each dendrimer is likened to a discrete macromolecular container for a ruthenium nanoparticle. The nanoparticle concentration of any RuDEN solution in this study was therefore based on the concentration of the dendrimer for that particular solution and correlates with the total surface area of the DENS. The catalytic reactions were conducted under *pseudo* first-order reaction conditions by ensuring a large excess of BH_4^- , relative to the amount of 4NP, present for each reaction. The apparent rate constant for the reduction of 4NP was calculated for the various DENS to quantitatively compare the catalytic activities. The rate constant is proportional to the total surface area as shown in equation 2:

$$-\frac{d[4NP]}{dt} = k_{app}[4NP] = k_1 S [4NP] \quad (2)$$

where $[4NP]$ refers to the 4NP concentration at time t and k_1 is the apparent rate constant normalised to the surface area, S , of the Ru nanoparticle, which is normalised to the unit volume of the catalytic reaction system. The surface normalised rate constant was calculated by finding the slope of the plot k_{app} against the volume normalised surface area S as given in the derived equation 3:

$$k_1 = \frac{k_{app}}{S} \quad (3)$$

Figures 3.2(a)-3.2(c) and illustrates the k_{app} values plotted against the surface area, S , for generations 4, 5 and 6 RuDENs at a constant 4NP and BH_4^- concentration respectively.

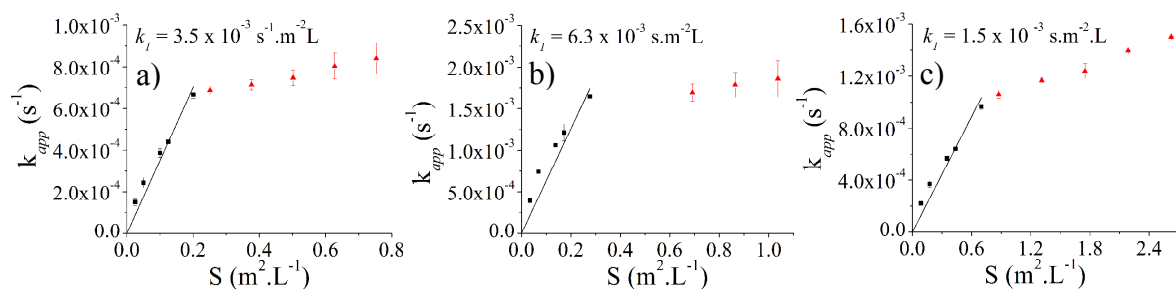


Figure 3.2. Apparent rate constant correlated with volume normalised surface area with the slope being the surface normalised rate constant k_l and the red triangles indicating the volume normalised surface area where diffusion control occurs for: a) G4-RuDEN, b) G5-RuDEN and c) G6-RuDEN.

As previously mentioned, the BH_4^- concentration was kept in large excess of the 4NP concentration to ensure *pseudo* first-order reaction conditions. The apparent rate constant shows a linear relationship with the surface area. This was expected since the reaction rate should increase with an increase in catalytic surface area. In each case, the surface normalised rate constant is the calculated slope of the line.

The surface area normalised rate constant k_l was calculated for each of the RuDEN catalysts where G4-RuDEN, G5-RuDEN and G6-RuDEN showed values of $(3.5 \pm 0.22) \times 10^{-3} \text{ s} \cdot \text{m}^2 \cdot \text{L}^{-1}$, $(6.3 \pm 0.35) \times 10^{-3} \text{ s} \cdot \text{m}^2 \cdot \text{L}^{-1}$ and $(1.5 \pm 0.10) \times 10^{-3} \text{ s} \cdot \text{m}^2 \cdot \text{L}^{-1}$ respectively. The red triangular data points correspond to the apparent rate constants where diffusion control occurs and therefore were not included in the calculation of the surface area normalised rate constant k_l . The surface normalised rate constants show an increase in value from G4-RuDEN to the G5-RuDEN and then a decrease going to G6-RuDEN from G5-RuDEN. The observed trend in surface rate constant values is possibly linked to the morphology as well the size of the nanoparticle surface for any given particle. One could argue that another possibility could be the difference in size of the dendrimer relative to the nanoparticle for each of the RuDEN catalysts and that a steric effect is in operation. The effect of dendrimer concentration on the rate constant was investigated by Esumi *et al.* who reported the effect of the PAMAM

dendrimer generation for the preparation of silver, platinum and palladium nanoparticles and its evaluation in the catalytic reduction of 4NP.²⁸

The effects of nanoparticle size on the catalytic rate of 4NP reduction has been studied by Lia *et al.* and an increase in reaction rate was realised for a decrease in nanoparticle size.³⁹ The amount of gold nanoparticles per catalytic reaction was kept constant and the expected result was a correlation between the catalytic rate and the total surface area of the catalyst. The expectation is an increase in total surface area with an increase in the nanoparticle size, for a constant nanoparticle concentration, and hence increases in catalytic activity. The opposite trend was observed as the catalytic activity increased with a decrease in nanoparticle size despite the decrease in total surface area with decreasing nanoparticle size, a topic well discussed in reviews by Somorjai *et al.*⁴⁰⁻⁴¹ When considering the results obtained for the RuDENs in this study, the catalytic rate shows an increase for the smaller G4-RuDEN nanoparticles over that of the larger G6-RuDEN nanoparticles. It is important to remember that these are surface normalised rate constants and they provide a first glance interpretation of the nanoparticle size effect.

In this case, the nanoparticle size effect is in agreement with that of the above-mentioned study reiterating that total surface area is not the only determining factor for catalytic activity when comparing nanoparticles of different sizes. The G5-RuDEN catalyst was of intermediate size for the three RuDEN catalysts. Contrary to the expected trend, there was not a decrease in the surface normalised rate constant going from G4-RuDEN to G5-RuDEN but a marked increase. The magnitude in size difference going from G4-RuDEN to G5-RuDEN is minimal compared to the size difference from G4-RuDEN to G6-RuDEN. The former are therefore in a more similar size regime when compared to G6-RuDEN. Given this observation, the results suggest that G5-RuDENs are of an optimal size. To gain further insights into these systems, we evaluated the RuDEN catalysts with experimental design aimed at the eventual utilisation of a Langmuir-Hinshelwood kinetic model.

3.3.1.2 Calculation of Langmuir-Hinshelwood parameters

A few considerations need to be taken into account before understanding the catalytic reduction of 4NP on the catalyst surface and analysing the system using the Langmuir-Hinshelwood model.

In the case of the preparation of nanoparticles, sodium borohydride is an important reducing agent and serves as an electron source. The surface of metal nanoparticles becomes charged by injection of electrons from the borohydride ions to the nanoparticle surface,^{37, 42} a process that is observed by a shift in the surface plasmon band for the particular metal.⁴³⁻⁴⁴ The presence of the plasmon band is, however, dependant on the size of the nanoparticle⁴⁵ and the particles in this investigation are less than 3 nm in diameter associated with an absence of this plasmon band.⁴⁶ The process of borohydride ion adsorption on nanoparticle surfaces has been investigated. Studies show that adsorption of the borohydride ion on the metal nanoparticle surface is a fast and reversible process with the rate determining step in the hydrolysis being the cleavage of the O-H bond in the water molecule.⁴⁷ Because both reactants adsorb to the nanoparticle surface for the reaction to occur, the interaction at the surface of the nanoparticle can be expressed in terms of Langmuir isotherms.

The kinetic data obtained for the reduction of 4NP using the various ruthenium DENs will be discussed in light of the Langmuir-Hinshelwood kinetic model. In the case of the borohydride adsorption, this is a fast and reversible process with a surface hydrogen being transferred to the nanoparticle surface upon adsorption. Subsequently, a 4NP molecule adsorbs on the nanoparticle surface and, like the adsorption of borohydride, this process is fast and reversible. The rate-determining step is the reaction between the adsorbed 4NP molecule and surface hydrogen species to form 4AP. The 4AP then dissociates and the catalytic site can be further occupied by reactants. As a result, the rate of 4NP reduction is dependent on the nanoparticle surface coverage by 4NP and BH_4^- (eq 4):

$$\frac{d[4NP]}{dt} = -kS\theta_{4NP}\theta_{BH_4} \quad (4)$$

where k is the actual rate constant and θ_{4NP} and θ_{BH_4} are the surface coverage values on the nanoparticle surface for 4NP and BH_4^- respectively. The surface coverage values are further defined by equations 5 and 6:

$$\theta_{4NP} = \frac{(K_{4NP}[4NP])^n}{1 + (K_{4NP}[4NP])^n + (K_{BH_4}[BH_4])^m} \quad (5)$$

$$\theta_{BH_4} = \frac{(K_{BH_4}[BH_4])^m}{1 + (K_{4NP}[4NP])^n + (K_{BH_4}[BH_4])^m} \quad (6)$$

As discussed by Wunder *et al.*³⁰, the kinetic data can be modelled on the Langmuir-Freundlich isotherm where the equation for k_{app} , derived from a substitution of equations 4, 5 and 6 into equation 2, is:

$$k_{app} = \frac{kS \cdot K_{4NP}^n [4NP]^{n-1} (K_{BH_4}[BH_4])^m}{(1 + (K_{4NP}[4NP])^n + (K_{BH_4}[BH_4])^m)^2} \quad (7)$$

where k is the actual rate constant (on the surface), S is the total surface area of the catalyst, K_{4NP} is the adsorption constant for 4NP on the catalysts surface, $[4NP]$ is the concentration of the 4NP, K_{BH_4} is the adsorption constant of sodium borohydride on the catalyst surface, $[BH_4]$ is the concentration of BH_4^- and n and m are Langmuir-Freundlich constants describing the heterogeneity of the catalyst surface.

The parameter boundary values were kept constant throughout each individual system to investigate whether the model would converge within the calculated apparent rate constant parameter boundaries. The parameter value boundaries are quite restricted and any changes cause a marked deviation of the experimental data from the model. Wunder *et al.* noted a similar observation for the kinetic evaluation of metal nanoparticles immobilised in polyelectrolyte brushes.³⁰ The calculated parameter values are listed in Table 3.2.

Table 3.2. Langmuir Freundlich rate constants and adsorption constants obtained for RuDENs.

Catalyst	k [mol.m ⁻² .s ⁻¹] (x 10 ⁻⁵)	K_{4NP} [L.mol ⁻¹]	K_{BH_4} [L.mol ⁻¹]	n	m
G4-RuDEN	7.3 ± 1.40	90 ± 6	3.6 ± 1.1	0.37 ± 0.11	0.85 ± 0.08
G5-RuDEN	9.5 ± 2.74	87 ± 4	5.4 ± 1.1	0.56 ± 0.11	0.57 ± 0.15
G6-RuDEN	5.6 ± 0.72	94 ± 4	1.1 ± 0.1	0.54 ± 0.03	0.62 ± 0.05

The parameter values give a quantitative explanation for the behaviour of the apparent rate constants with the subsequent changes in concentrations of BH_4^- and 4NP. Figure 3.3

illustrates the fitting of the various catalytic data to the Langmuir-Hinshelwood equation 4. The increase in 4NP concentration caused a decrease in the apparent rate constant as the surface of the nanoparticle becomes saturated with 4NP molecules.

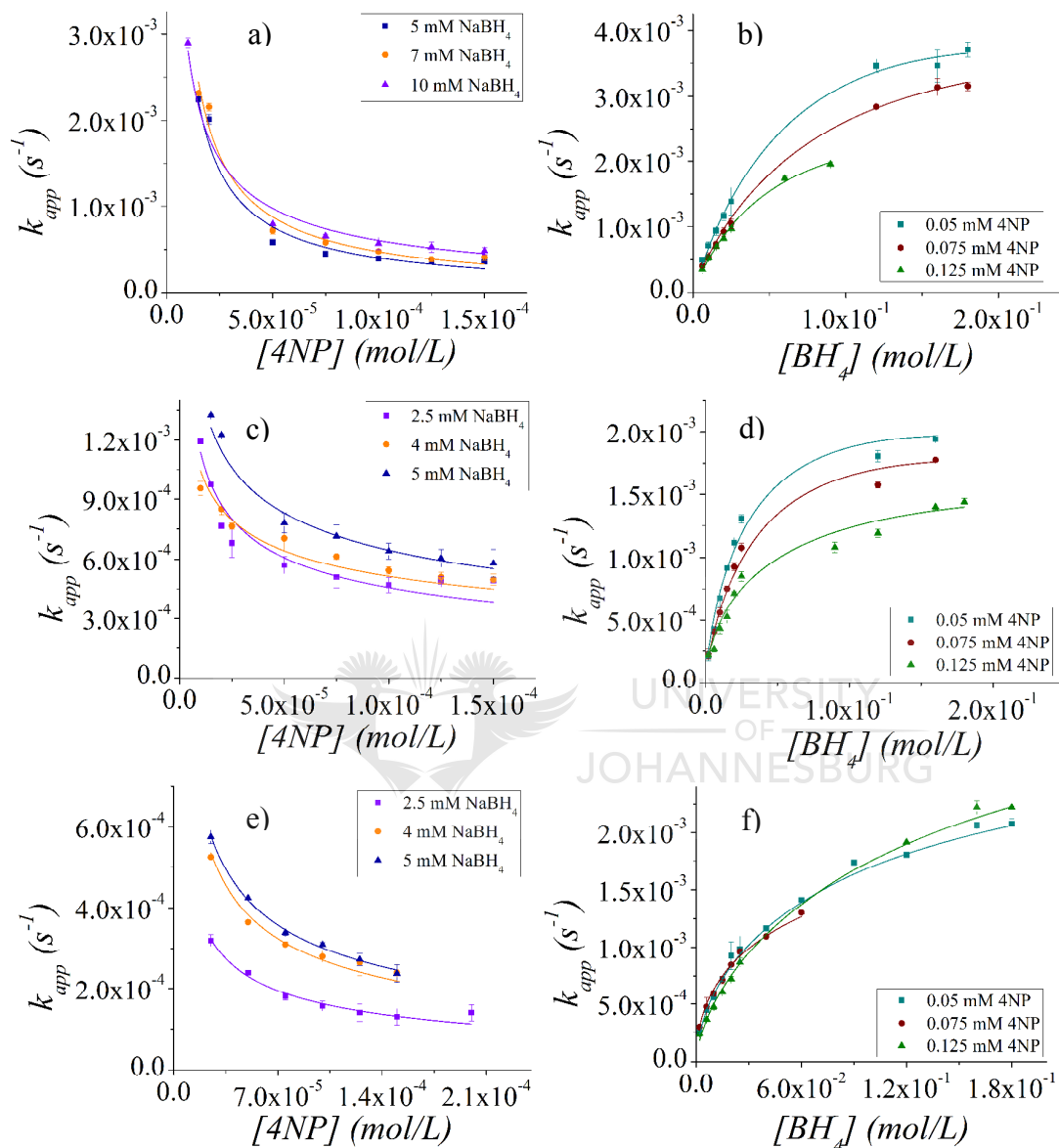


Figure 3.3. Figures a, c and e detail the dependence of k_{app} on the changes in 4NP concentration according to the Langmuir-Hinshelwood mechanism for G4-RuDEN (surface area 0.1256 m².L⁻¹), G5-RuDEN (surface area 0.0865 m².L⁻¹) and G6-RuDEN (surface area 0.2187 m².L⁻¹) respectively. Figures b, d and e detail the dependence of k_{app} on the changes in BH₄⁻ concentration according to the Langmuir-Hinshelwood mechanism for G4-RuDEN (surface area 0.1256 m².L⁻¹), G5-RuDEN (surface area 0.0865 m².L⁻¹) and G6-RuDEN (surface area 0.2187 m².L⁻¹) respectively. T = 298 K.

This leads to a significant decrease in the reaction of BH_4^- with the surface of the nanoparticle and consequently a decrease in the rate of electron transfer to the nanoparticle surface. The nonlinear behaviour of the apparent rate constant values with increase in BH_4^- and 4NP concentration suggests competitive adsorption of substrate and reactant on the nanoparticle surface. An optimal concentration of both BH_4^- and 4NP exists where a maximum catalytic rate is observed.

The quality of the data was assessed by calculating plots of $k_{app}[4NP]$ versus $\theta_{4NP}\theta_{\text{BH}_4}$. This was derived from a simple rearrangement of the Langmuir-Hinshelwood equation (7) with substitution of the surface coverage values θ_{4NP} (5) and θ_{BH_4} (6) to give equation (8a) and subsequently the relation (8b).

$$k_{app}[4NP] = kS \theta_{4NP}\theta_{\text{BH}_4} \quad (8a)$$

$$kS = \frac{k_{app}[4NP]}{\theta_{4NP}\theta_{\text{BH}_4}} \quad (8b)$$

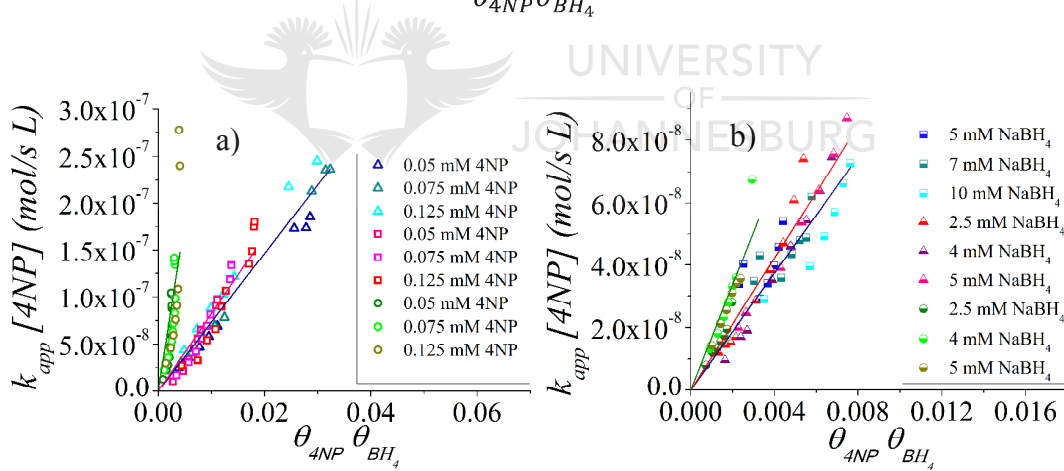


Figure 3.4. Plot of the product of apparent rate constant k_{app} and 4NP concentration [4NP] versus the product of the surface coverage for 4NP and BH_4^- , $\theta_{4NP}\theta_{\text{BH}_4}$. The solid line is the product of the rate constant k and surface area S . The squares, triangles and circles represent G4-RuDEN (surface area $0.1256 \text{ m}^2.\text{L}^{-1}$), G5-RuDEN (surface area $0.0865 \text{ m}^2.\text{L}^{-1}$) and G6-RuDEN (surface area $0.2187 \text{ m}^2.\text{L}^{-1}$) respectively. a) Illustration of the above mentioned data for constant 4NP concentration. b) Illustration of the above mentioned data for constant BH_4^- concentration.

Figure 3.4(a) illustrates the data obtained for varying BH_4^- concentrations and Figure 3.4(b) the data obtained for varying 4NP concentrations. The slope of the straight line represents the product of the kinetic constant, k , and the surface area, S , of the nanoparticle. These values are in agreement with the values calculated from the experimental values of k and S , considering the error associated with the calculation of both θ_{4NP} and $\theta_{\text{BH}_4^-}$. Given the validity of the present fit, the Langmuir-Hinshelwood model sufficiently models the behaviour of this catalytic reaction for RuDENs.

The results in Table 3.2 correlate with the findings for the surface normalised rate constants determined earlier for the effects of surface area on the rate constant. Analyses of the adsorption constants help clarify the observed behaviour. The kinetic constants, k , follow the same trend as the surface normalised rate constants, k_i where the highest rate constant was realised for G5-RuDEN and the lowest for G6-RuDEN. The 4NP adsorption constants obtained for the different catalysts show minimal differences in values. When considering the values obtained for the 4NP adsorption constants, these are 25 times, 16 times and 85 times larger than the BH_4^- adsorption constants for G4-RuDEN, G5-RuDEN and G6-RuDEN respectively.

An intermediate kinetic constant value was observed when evaluating G4-RuDEN. When comparing the nanoparticle size extremes for this set of catalysts, it is clear that there is an overall decrease in catalytic rate when only considering G4-RuDEN and G6-RuDEN. Given that this trend is not followed going from G4-RuDEN to G5-RuDEN, the results imply that G5-RuDEN represents an optimal sized nanoparticle for the catalytic reduction of 4NP. Nevertheless, the observed trend reflects through the parameters, K_{4NP} and $K_{\text{BH}_4^-}$, relative to each other where the increase in $K_{\text{BH}_4^-}$ associated with a disproportional decrease in K_{4NP} displays a higher kinetic constant, k .

The model provided assumes all catalytic sites to be active. However, the calculation of heterogeneity exponents (Freundlich isotherms) related to the adsorption/desorption of 4NP and BH_4^- implies heterogeneity of the adsorption sites. This correlation of heterogeneity to studies in reaction kinetics at a nanoparticle surface was discussed by Zhou *et al.*⁴⁸ In this study, the heterogeneity was rationalised by a spontaneous and catalysis-induced surface restructuring. The heterogeneity values, n , for each of the catalysts are $n = 0.37$, $n = 0.56$ and

$n = 0.54$ for G4-RuDEN, G5-RuDEN and G6-RuDEN respectively. This implies an increased heterogeneity from a perfectly Gaussian distribution of catalytically active sites defined by a n -value of one. The heterogeneity values for each system points to the surface not being uniform but the difference in these values does not seem as significant for comparing the RuDEN catalytic systems, except when comparing G5-RuDEN and G6-RuDEN to G4-RuDEN where G4-RuDEN has a significantly lower n -value.

The increase in catalytic rate with decrease in size might be rationalised by the larger Fermi level shift when high electron injecting species are present such as the presence of BH_4^- ions in the 4NP reduction reaction.⁴⁹ This effect is certainly more pronounced for smaller nanoparticles such as those in the current study. The increase in catalytic rate with a decrease in nanoparticle size from G6-RuDEN to G4-RuDEN for this study agrees with similar trends observed for smaller nanoparticles with a higher fraction of low coordination sites than larger particles with a larger fraction of high-coordination surface sites.⁵⁰ Previous reports indicate that larger nanoparticles have a lower surface heterogeneity with surfaces terminated by large terraces of identical surface atoms. The increase in heterogeneity with decrease in nanoparticle size is met with a significant change in the statistical distribution of surface atom types⁵¹ and concomitant increase in surface roughness.⁵² A higher fraction of coordinatively unsaturated surface atoms therefore exists for smaller nanoparticles. This increase in surface roughness helps increase the chemisorption of both 4NP and BH_4^- where the effect is more evident in the latter when considering the K_{BH_4} values obtained.

3.3.2 Calculation of thermodynamic parameters

Table 3.3 presents the calculated thermodynamic data for each of the catalysts used in this study. The temperature dependant studies were conducted for 4NP and BH_4^- concentrations of 0.05 mM and 5 mM respectively. Various groups have reported the activation energy for 4NP reduction albeit as catalysed by different metals.^{23, 34-35, 53-54} The activation energy was calculated for the apparent rate constant and therefore contains a dependency on the adsorption constants for BH_4^- and 4NP.

Table 3.3. Thermodynamic parameters E_a , ΔH and ΔS for the various RuDEN catalysts.

Catalyst	E_a (kJ.mol ⁻¹)	ΔH (kJ.mol ⁻¹)	ΔS (J.mol ⁻¹ .K ⁻¹)
G4-RuDEN	16.45 ± 0.73	14.08 ± 0.61	-256.55 ± 1.82
G5-RuDEN	23.35 ± 0.11	13.72 ± 0.37	-262.76 ± 0.54
G6-RuDEN	28.74 ± 1.60	26.89 ± 1.86	-219.90 ± 5.28

To account for these adsorption constants, further experiments are required but for the sake of comparison between the different RuDENs, this evaluation is sufficient. No literature precedence has been found to account for the thermodynamic parameter values of ruthenium nanoparticles in the evaluation of 4NP reduction in the presence of BH_4^- . The thermodynamic ΔH and ΔS parameters displayed in Table 3 will therefore be used mostly to discuss the nature of the reaction and the activation energy will be compared to literature values to ascertain whether RuDEN activation energies are within the expected range.

Table 3.4. Activation energy values for different nanoparticle catalyst systems evaluated in the reduction of 4NP.

Nanoparticle catalyst	E_a (kJ/mol)	Reference
Silver	41	36
Silver/Calcium Alginate	13.8	55
Gold/Calcium Alginate	20.5	55
Gold/Polyelectrolyte brush	43	56
CTAB stabilised gold rods	38	27
Pt nanocubes	14	57
Pt nanocubes/polystyrene microspheres	12	57
Citrate stabilized gold nanoparticles	21	26
Partially hollow gold nanoboxes	55	23
Hollow gold nanoboxes	44	23
Gold nanocages	28	23

The activation energies of various other nanoparticle systems evaluated in the reduction of 4NP are listed in Table 3.4. It is clear from the range of these values that the investigated system has activation energies well within the expected values when compared to obtained values for RuDENs depicted in Table 3.3. In the case of the activation energies observed for

the RuDEN catalysts, there is a decrease in the activation energy with a decrease in the particle size. This correlates with the expected trend of increase in the rate of the reaction with decrease in the particle size as mentioned earlier and concomitant increase in surface roughness. In each case, the reaction is endothermic as reflected in the positive ΔH -values 14.08 kJ.mol⁻¹, 13.72 kJ.mol⁻¹ and 26.89 kJ.mol⁻¹ for G4-RuDEN, G5-RuDEN and G6-RuDEN respectively. The entropy values obtained for each of the catalyst evaluations are all negative which agree with the endothermic nature of the reaction and suggesting energy input needed for the reaction to continue.

3.4 Conclusion

In this study, we have demonstrated that the Langmuir-Hinshelwood model, which assumes the adsorption of both reactants of the surface of the catalyst, is applicable to the study of 4NP reduction by RuDENs in the presence of BH₄⁻. The model allows for the calculation of three constants related to each system, the kinetic constant that describes the surface reactivity of the adsorbed species and the two thermodynamic adsorption constants K_{4NP} , for 4NP, and K_{BH_4} , for BH₄⁻. The correlation between size and catalytic rate was demonstrated where smaller nanoparticles display a higher catalytic rate. For the investigated catalysts there appears to be an optimum nanoparticle size for the catalytic reaction.

3.5 References

- [1] D. Astruc, *Nanoparticles and Catalysis*, WILEY-VCH, Weinheim, **2008**.
- [2] D. Astruc, F. Lu and J. R. Aranzaes, *Angew. Chem. Int. Ed.* **2005**, *44*, 7852.
- [3] P. Migowski and J. Dupont, *Chem. Eur. J.* **2007**, *13*, 32.
- [4] *Nanoparticles: From Theory to Application, 2nd, Completely Revised and Updated Edition* (Ed.: G. Schmid), Wiley-VCH, Weinheim **2010**, p. 217.
- [5] S. Mourdikoudis and L. M. Liz-Marzán, *Chem. Mater.* **2013**, *25*, 1465.
- [6] Y. Niu and R. M. Crooks, *C. R. Chimie* **2003**, *6*, 1049.
- [7] L. D. Pachón and G. Rothenberg, *Appl. Organometal. Chem.* **2008**, *22*, 288.
- [8] V. S. Myers, M. G. Weir, E. V. Carino, D. F. Yancey, S. Pande and R. M. Crooks, *Chem. Sci.* **2011**, *2*, 1632.
- [9] R. M. Crooks, M. Zhao, L. Sun, V. Chechik and L. K. Yeung, *Acc. Chem. Res.* **2001**, *34*, 181.

- [10] A. W. Bosman, H. M. Janssen and E. W. Meijer, *Chem. Rev.* **1999**, *99*, 1665.
- [11] J. Huang, T. Jiang, B. Han, W. Wu, Z. Liu, Z. Xie and J. Zhang, *Catal. Lett.* **2005**, *103*, 59.
- [12] E. T. Silveira, A. P. Umpierre, L. M. Rossi, G. Machado, J. Morais, G. V. Soares, I. J. R. Baumvol, S. R. Teixeira, P. F. P. Fichtner and J. Dupont, *Chem. Eur. J.* **2004**, *10*, 3734.
- [13] M. Zahmakıran, Y. Tonbulz and S. Özkar, *Chem. Commun.* **2010**, *46*, 4788.
- [14] L. M. Rossi and G. Machado, *J. Mol. Catal. A: Chem.* **2009**, *298*, 69.
- [15] J. Ning, J. Xu, J. Liu and F. Lu, *Catal. Lett.* **2006**, *109*, 175.
- [16] A. Stolle, T. Gallert, C. Schmöger and B. Ondruschka, *RSC Adv.* **2013**, *3*, 2112.
- [17] P. Lara, K. Philippot and B. Chaudret, *ChemCatChem* **2013**, *5*, 28.
- [18] G. Lafaye, C. T. Williams and M. D. Amiridis, *Catal. Lett.* **2004**, 96.
- [19] G. Lafaye, A. Siani, P. Mare and C. T. Williams, *J. Phys. Chem. B* **2006**, *110*, 7725.
- [20] K. A. Marvin, N. N. Thadani, C. A. Atkinson, E. L. Keller and K. J. Stevenson, *Chem. Commun.* **2012**, 48.
- [21] D. F. Yancey, L. Zhang, R. M. Crooks and G. Henkelman, *Chem. Sci.* **2012**, *3*, 1033.
- [22] R. Iyyamperumal, L. Zhang, G. Henkelman and R. M. Crooks, *J. Am. Chem. Soc.* **2013**, *135*, 5521.
- [23] J. Zeng, Q. Zhang, J. Chen and Y. Xia, *Nano Lett.* **2010**, *10*, 30.
- [24] S. Saha, A. Pal, S. Kundu, S. Basu and T. Pal, *Langmuir* **2010**, 26.
- [25] N. Pradhan, A. Pal and T. Pal, *Colloid Surf. A* **2002**, *196*, 247.
- [26] S. Panigrahi, S. Basu, S. Praharaj, S. Pande, S. Jana, A. Pal, S. K. Gosh and T. J. Pal, *J. Phys. Chem. C* **2007**, *111*, 4596.
- [27] Y. Khalavka, J. Becker and C. Sönnichsen, *J. Am. Chem. Soc.* **2009**, *131*, 1871.
- [28] K. Esumi, R. Isono and T. Yoshimura, *Langmuir* **2004**, *20*, 237.
- [29] H. Zhang, X. Li and G. Chen, *Journal of Materials Chemistry* **2009**, 19.
- [30] S. Wunder, F. Polzer, Y. Lu, Y. Mei and M. Ballauff, *J. Phys. Chem. C* **2010**, *114*, 8814.
- [31] N. C. Antonels and R. Meijboom, *Langmuir* **2013**, *29*, 13433.
- [32] 2.0.8.14953 ed., TGK Scientific Limited, **2010**.
- [33] OriginLab Corporation, One Roundhouse Plaza Northampton, **2010**.
- [34] Y. Mei, Y. Lu, F. Polzer and M. Ballauff, *Chem. Mater.* **2007**, *19*, 1062.
- [35] Y. Mei, G. Sharma, Y. Lu and M. Ballauff, *Langmuir* **2005**, *21*, 12229.
- [36] N. Pradhan, A. Pal and T. Pal, *Colloid Surf. A* **2002**, *196*, 247.

- [37] S. Carregal-Romero, J. Pérez-Juste, P. Hervés, L. M. Liz-Marzán and P. Mulvaney, *Langmuir* **2010**, *26*, 1271.
- [38] A. Bielejewska, A. Bylina, K. Duszczak, M. Fiałkowski and R. Hołyst, *Anal. Chem.* **2010**, *82*, 5463.
- [39] S. Kundu, K. Wang and H. Liang, *J. Phys. Chem. C* **2009**, *113*, 5157.
- [40] N. Musselwhite and G. A. Somorjai, in *Top. Catal.*
- [41] K. An and G. A. Somorjai, *ChemCatChem* **2012**, *4*, 1512.
- [42] A. Henglein and J. Lilie, *J. Am. Chem. Soc.* **1981**, *103*, 1059.
- [43] T. Ung, L. M. Liz-Marzán and P. Mulvaney, *J. Phys. Chem. B* **1999**, *103*, 6770.
- [44] R. Sardar, A. M. Funston, P. Mulvaney and R. W. Murray, *Langmuir* **2009**, *25*, 13840.
- [45] A. Moores and F. Goettmann, *New J. Chem.* **2006**, *30*, 1121.
- [46] J. C. Scaiano, J. C. Netto-Ferreira, E. Alarcon, P. Billone, C. J. B. Alejo, C.-O. L. Crites, M. Decan, C. Fasciani, M. González-Béjar, G. Hallett-Tapley, M. Grenier, K. L. McGilvray, N. L. Pacioni, A. Pardoe, L. René-Boisneuf, R. Schwartz-Narbonne, M. J. Silvero, K. G. Stamplecoskie and T.-L. Wee, *Pure Appl. Chem.* **2011**, *83*, 913.
- [47] G. Guella, B. Patton and A. Miotello, *J. Phys. Chem. C* **2007**, *111*, 18744.
- [48] X. Zhou, W. Xu, G. Liu, D. Panda and P. Chen, *J. Am. Chem. Soc.* **2010**, *132*, 138.
- [49] A. Henglein, *J. Phys. Chem.* **1993**, *97*, 5457.
- [50] H. Härle, U. Metka, H.-R. Volpp and J. Wolfrum, *Phys. Chem. Chem. Phys.* **1999**, *1*, 5059.
- [51] R. V. Hardeveld and F. Hartog, *Surf. Sci.* **1969**, *15*, 189-230.
- [52] H. Song, R. M. Rioux, J. D. Hoefelmeyer, R. Komor, K. Niesz, M. Grass, P. Yang and G. A. Somorjai, *J. Am. Chem. Soc.* **2006**, *128*, 3027.
- [53] M. A. Mahmoud, B. Snyder and M. El-Sayed, *J. Phys. Chem. Lett.* **2010**, *1*, 28.
- [54] Y. Lu, Y. Mei, R. Walker, M. Ballauff and M. Dreschler, *Polymer* **2006**, *47*.
- [55] S. Saha, A. Pal, S. Kundu, S. Basu and T. Pal, *Langmuir* **2010**, *26*, 2885.
- [56] M. Schrunner, F. Polzer, Y. Mei, Y. Lu, B. Haupt, M. Ballauff, A. Gödel, M. Drechsler, J. Preussner and U. Glatzel, *Macromol. Chem. Phys.* **2007**, *208*, 1542.
- [57] M. A. Mahmoud, B. Snyder and M. El-sayed, *J. Phys. Chem. Lett.* **2010**, *1*, 28.

Chapter 4 – Catalytic hydrogenation of toluene and the influence of various ionic liquids as catalyst coatings

4.1 Introduction

The catalytic hydrogenation of aromatic compounds is an interesting topic in science and has led to the development of various innovative catalytic systems. The hydrogenation of arenes is of industrial importance, an example being the hydrogenation of benzene to cyclohexane and subsequent oxidation to adipic acid and caprolactam that are important precursors in the production of nylon-6 and nylon-66.¹⁻² Hydrogenation is not only utilised in catalytic studies but has importance in industrial processes such as the removal of carcinogenic aromatic compounds from diesel fuels and the synthesis of cyclohexane,³ a widely used solvent. The hydrogenation of monocyclic arenes and their derivatives are of industrial importance and sometimes the desired product is the partially hydrogenated intermediate. Various synthetic routes are utilised for the production of cyclohexene for instance, cyclohexane halide dehydrohalogenation, cyclohexanol dehydration and cyclohexane dehydrogenation.⁴⁻⁶ These are quite involved chemical processes. From an economic standpoint, simpler methods for the production of partially hydrogenated arenes is of great interest.⁷⁻⁹ The selective hydrogenation of benzene to cyclohexene was achieved using finely divided ruthenium in an aqueous media with the incorporation of additives.^{8, 10-15} In most cases, the selectivity towards cyclohexene increased to just below 40%. Expectedly, cyclohexene selectivity decreased with further reaction time, and hence conversion, given that these were batch reactions and eventual hydrogenation of the cyclohexene occurs to form cyclohexane.

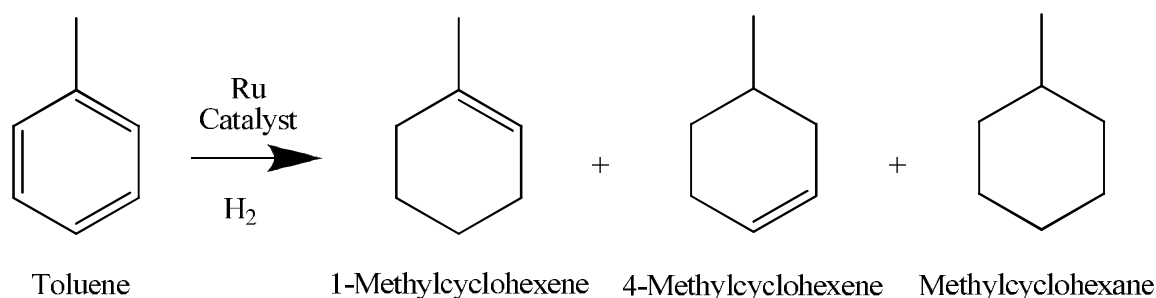
A more sophisticated method of enhancing the selectivity towards the partially hydrogenated arenes is the use of ionic liquids as additives. Known to stabilise nanoparticles, ionic liquids have also been used as solvents in the catalytic hydrogenation of arenes.^{2, 9, 16} In certain studies the enhanced selectivity towards the partially hydrogenated cycloalkene products in the presence of the ionic liquid was not highlighted. It may seem that the only purpose the ionic liquid serves is to stabilise the particle and ensure recyclability, since full hydrogenation of arenes can be obtained using conventional catalysts without ionic liquid or any other additives.¹⁶ Despite the heterogeneous nature of the previously mentioned finely divided

ruthenium with incorporated additives and improved selectivity towards cyclohexene, the utilisation of ruthenium nanoparticles in ionic liquids for the hydrogenation of benzene has shown appreciable selectivity to cyclohexene.^{2, 17} When comparing reactions conducted in ionic liquid with those in the absence of ionic liquid, reactions in the latter occur considerably faster.¹⁷ This difference is typically observed in multiphase reactions conducted in ionic liquids and is a result of the reaction being a mass-transfer controlled process.¹⁸ There is therefore a need for a catalytic system that allows for high selectivity to the partially hydrogenated intermediates while maintaining a high catalytic activity.

One way to minimise the mass-transfer control is to deposit the ionic liquid over a high surface area material to form a thin film and thus minimise the diffusion barrier observed for bulk ionic liquids. This concept of supported ionic liquid phase (SILP) catalysts has been successfully utilised in many catalytic reactions including hydrogenation reactions.¹⁹⁻²⁰ An investigation into the effects of different ionic liquids on the hydrogenation of citral using the same Pd catalyst saw a change in the selectivity profile for the different ionic liquids.²¹ Given the potential to change the activity and selectivity profile of a catalyst by introducing an ionic liquid in small quantities, Kernchen *et al.* proceeded to develop a similar catalytic system called the solid catalyst with ionic liquid layer (SCILL) catalyst.²² Borrowing from the concept of SILP catalysts, one feature that separates these two catalytic systems is that for SILP systems, it is the heterogenisation of a homogenous catalyst by dissolution in a suitable ionic liquid and deposition on a solid support material while SCILL catalysts consist of a heterogeneous catalyst coated with a suitable ionic liquid.

Essentially, the presence of the ionic liquid can affect the activity and selectivity of the catalyst by changing the intrinsic properties of the catalyst, therefore acting as a potential chemical modifier of the catalyst itself that is encouraged by chemical interaction of the ionic liquid with the catalytic surface.²² On the other hand, the ionic liquid could change the effective concentration of the substrates and various intermediates based on their solubilities in the different ionic liquids. In this case, for instance, if the desired products were the arene hydrogenation intermediates - namely the partially hydrogenated cycloalkenes - the ionic liquid should have a lower solubility for the latter. This would encourage separation of the partially hydrogenated intermediate to the organic phase and away from the ionic liquid coated catalyst surface, where further hydrogenation to the fully hydrogenated product could occur.²²

This chapter focuses on the evaluation of silica-supported RuDEN catalysts in the hydrogenation of toluene (Scheme 4.1).



Scheme 4.1. Scheme for the hydrogenation of toluene illustrating the partially hydrogenated products 1-methylcyclohexene and 4-methylcyclohexene and the fully hydrogenated product methylcyclohexane.

A silica-supported RuDEN catalyst will then be utilised as a SCILL catalyst by coating it with an ionic liquid. The effect of the presence of the ionic liquids on the activity and selectivity of the catalyst will be evaluated.

4.2 Experimental



The substrate and standards, toluene, n-decane, methylcyclohexane, 1-methylcyclohexene and 4-methylcyclohexene were purchased from Sigma-Aldrich and used as received.

4.2.1 Catalytic hydrogenation of toluene in a 100 cm³ autoclave.

Toluene hydrogenation experiments were performed in a Parr stainless steel autoclave with a volume of 100 cm³ fitted with a teflon cup, operated in batch mode and stirred at 1200 rpm. Depending on the reaction, the reaction conditions were set at 75 °C, 90 °C and 110 °C and a H₂ pressure of 10 bar. The catalyst (0.08-0.1 wt% Ru, 0.2-0.3 g, 1.84 μmol Ru) was transferred to the autoclave. The autoclave was charged with cyclohexane (30 cm³) and toluene (0.34 cm³, 0.2947 g, 3198.9 μmol) with n-decane as the internal standard (0.34 cm³). The reactor was purged thrice at ambient temperature with H₂ gas, depressurised and heated to 90 °C and allowed to stir at this temperature for 1 hour to allow catalyst activation. The desired temperature, either 75, 90 or 110 °C, was set and the reactor pressurised to a H₂

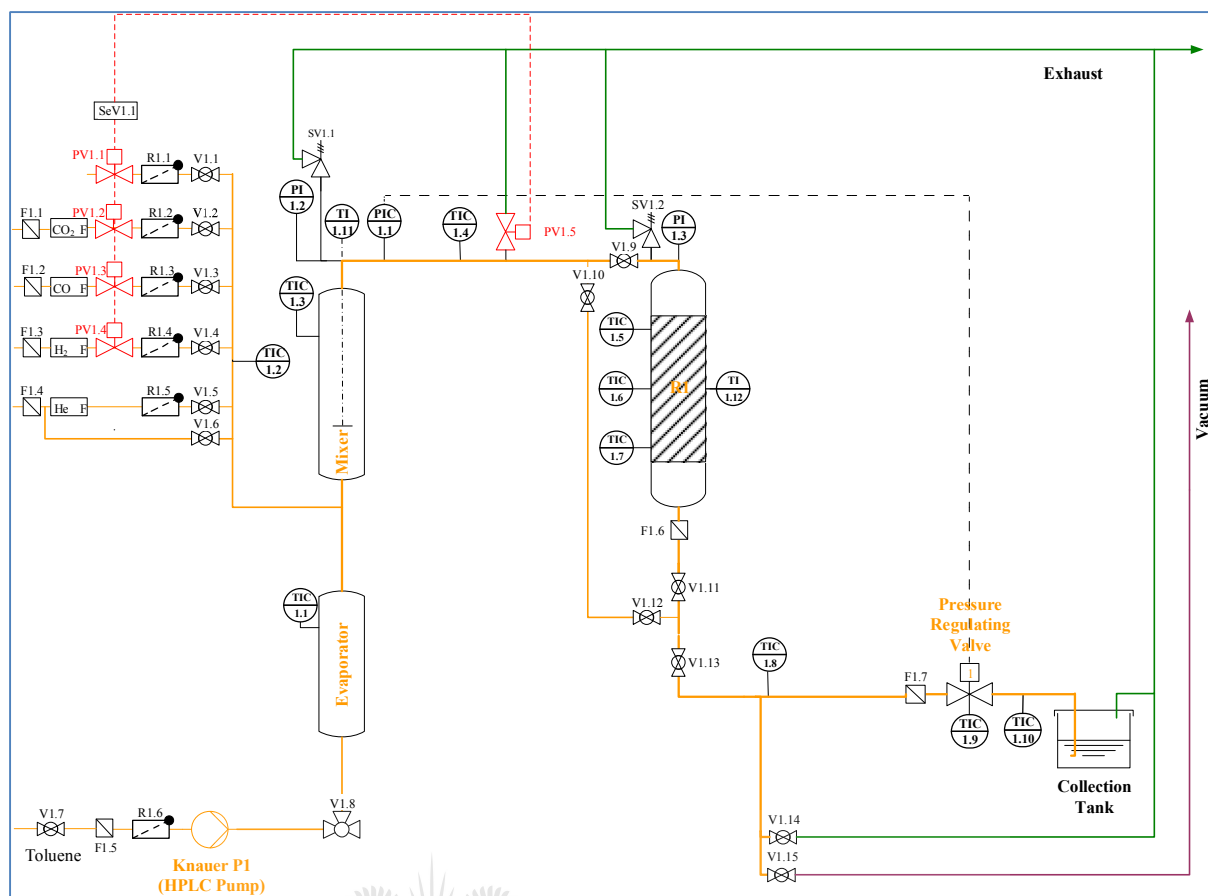
pressure of 10 bar to commence reaction. Samples of the reaction mixture were periodically taken and analysed by gas chromatography on a Shimadzu GC-2010 equipped with a 30 m Restek Rtx®-5 capillary column.

4.2.2 *Catalytic hydrogenation of toluene in a 300 cm³ autoclave.*

Toluene hydrogenation experiments were performed in a Parr stainless steel autoclave with a volume of 300 cm³ operated in batch mode and stirred at 1200 rpm. Depending on the reaction, the reaction conditions were set at 50 °C, 75 °C and 110 °C and a H₂ pressure of 10 bar or 30 bar. The catalyst (0.12-0.15 wt% Ru, 0.3-0.5 g, 7.00 μmol Ru) was transferred to the autoclave. The autoclave was then charged with cyclohexane (99 cm³) and toluene (1 cm³, 0.87 g, 9442 μmol) with n-decane as the internal standard (1 cm³). The reactor was purged thrice at ambient temperature with H₂ gas, depressurised and heated to 90 °C and stirred at this temperature for 1 hour to allow catalyst activation. The desired temperature, either 50, 75 or 110 °C was set and the reactor pressurised to a H₂ pressure of 10 bar or 30 bar to commence reaction. Samples of the reaction mixture were periodically taken and analysed by gas chromatography on a Varian 3900 GC equipped with a 50 m HP-PONA capillary column.

4.2.3 *Continuous flow catalytic hydrogenation of toluene.*

The catalytic reactions were conducted using a continuous flow rig as illustrated in Scheme 4.2. Toluene was taken from the reservoir bottle as a liquid and transported to an evaporator using a Knauer HPLC pump to control the molar flow. Both the hydrogen and helium gas were controlled by mass-flow controllers (5850 S series, Brooks Instruments). The gases were preheated and pumped along with the gaseous toluene into a mixing chamber, at isothermal conditions, filled with glass beads to ensure proper mixing and even heat distribution. The gas mixture could either enter the reactor or leave via a bypass. The reactor was positioned vertically with the gas flow from top to bottom and consisted of a stainless steel tube (10 mm diameter, 220 mm length) equipped with a bronze sinter plate for catalyst placement. A back pressure regulator valve (Samson) helped maintain the required reaction pressure and outlet gas flow. The outlet gaseous mixture was cooled with the assistance of cooling coils (TIC 1.10, Scheme 4.2) and collected in a Schott bottle.



Scheme 4.2. Schematic block diagram of the continuous flow rig utilised in the hydrogenation of toluene.

For the catalytic reactions, the tubular reactor loaded with the SCILL catalyst was fixed onto the rig and purged with flowing He gas. The reactor was then purged with H₂ gas and the catalyst left in a static H₂ gas atmosphere. The reaction temperature was raised to 110 °C and the catalyst allowed to activate for 1 hour. The desired temperature and flow rate was set as detailed later for the various reactions with the vaporised toluene and gas feed was then pumped over the catalyst bed. Samples of the reaction mixture were periodically taken by removing the Schott collection bottle and collecting the liquid sample in GC vials. The samples, with n-decane as internal standard, were analysed by gas chromatography on a Varian 3900 GC equipped with a 50 m HP-PONA capillary column.

4.3 Results and discussion

4.3.1 *The catalytic evaluation of the silica 60 supported RuDENS, RuSil60.*

Prior to evaluating the various ionic liquid coated catalysts, a series of optimisation reactions were conducted to find suitable reaction conditions. Initially the reactions were conducted using catalysts prepared from DENs that were dialysed to purify the nanoparticle solution. This purification step is especially important given the presence of sodium borohydride and excess chloride from the ruthenium trichloride hydrate precursor could potentially poison the catalyst surface. The immobilised nanoparticle catalysts showed either total inhibition of the reaction or inconsistent activity when prepared this way.

These observations indicated that the initial reaction conditions of 10 bar and 110 °C were most likely not ideal for toluene hydrogenation. An increase in the temperature to 120 °C did not improve the activity. Upon exhausting possible reasons for the reaction being inhibited, the only conclusion was that a catalyst poison was inhibiting the catalyst and that despite the extent of purification by dialysis, there must be traces of chloride. Nakumara *et al.* conducted an investigation into the effects of residual chloride on the hydrogenation activity of ruthenium catalysts.²³ Their findings depict that even trace amounts of residual chloride remaining after washing the catalyst with hot deionised water, significantly inhibited the catalyst. The catalysts were therefore washed with aqueous ammonia to remove residual chloride. This treatment was utilised for the series of silica supported RuDEN nanoparticles prior to the catalytic evaluation.

The RuSil60 catalysts were evaluated according to the catalytic activity and selectivity obtained for the hydrogenation of toluene. The reactions were conducted in a 100 cm³ stainless steel batch autoclave. The activity profiles of the catalysts are illustrated in Figure 4.1 for the conversion of toluene with time at different temperatures and an initial hydrogen pressure of 10 bar.

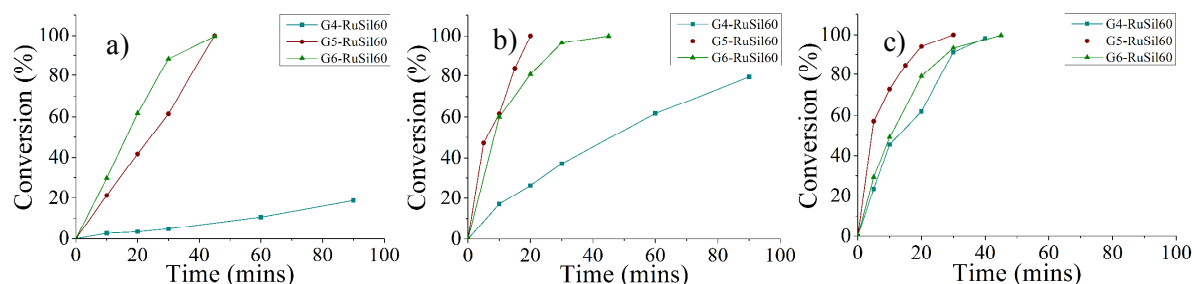


Figure 4.1. Graphs illustrating the toluene conversion profiles obtained using G4-RuSil60, G5-RuSil60 and G6-RuSil60 as catalysts at a 10 bar hydrogen pressure and at the temperatures: a) 75 °C b) 90 °C and c) 110 °C, with a 10 bar H₂ pressure, 3.19 mmol of toluene, 0.00184 mmol Ru and 30 cm³ of cyclohexane.

The reactions showed conversion of toluene for most of the reaction conditions and catalysts utilised with good conversion of toluene observed for both the G5-RuDEN and G6-RuDEN catalysts at the temperatures investigated. However, G4-RuDEN showed a considerably lower conversion compared to the former two catalysts. Reactions were complete within 40 minutes or less in the case of G5-RuDEN and G6-RuDEN and for G4-RuDEN, reactions were stopped before 100 minutes, as these reactions were mainly focused on identifying the most active catalysts that would be utilised later as SCILL catalysts with the use of various ionic liquids.

Evaluation based solely on the time taken to reach full conversion of the substrate does not provide a good quantitative measure of the performance of the catalyst with regard to its activity. The turnover frequency, however, provides a means of quantifying the activity of the various catalysts amongst each other. Figure 4.2 illustrates the turnover frequencies (TOF) expressed as the mole amount of toluene converted per mol of Ru per hour for the various catalysts at a conversion of >98% for the various reaction conditions. The TOF-values obtained for G4-RuSil60 depicts a typical increase with temperature. This is expected as the catalytic rate increases with an increase in the energy input. The TOF-values obtained when evaluating G5-RuSil60 and G6-RuSil60, however, do not show the expected trend with increase in temperature when compared to G4-RuSil60. There is an increase in TOF upon an increase in temperature from 75 °C to 90 °C although in the case of G6-RuSil60, this increase is less significant than that observed for G5-RuSil60. Upon further increase in temperature to 110 °C, the TOF-values for G5-RuSil60 and G6-RuSil60 both decrease. The decrease in TOF-value for an increase in temperature from 90 °C to 110 °C, for the catalysts G5-RuSil60 and G6-RuSil60, was not observed for G4-RuSil60.

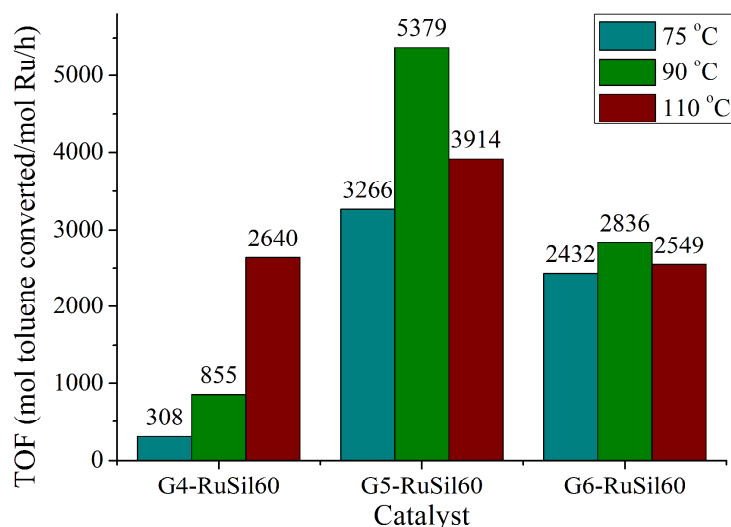


Figure 4.2. Turnover frequencies observed for the conversion of toluene utilising G4-RuSil60, G5-RuSil60 and G6-RuSil60 for temperatures 75 °C, 90 °C and 110 °C at a 10 bar H₂ pressure with 3.19 mmol of toluene, 0.00184 mmol Ru and 30 cm³ of cyclohexane.

When considering the size of the supported particle prior to the catalytic run, the G4-RuSil60 catalyst shows the largest average particle size of the three catalysts while the G5-RuSil60 and G6-RuSil60 catalysts have similar particle sizes to each other but smaller particle sizes than G4-RuSil60. The observed correlation between particle size and catalytic activity indicates that particles smaller than 2.5 nm result in an increase in catalytic performance. In this case, the Ru nanoparticle size smaller than 2.5 nm allows for the increased catalytic activity observed for G5-RuSil60 and G6-RuSil60.

When considering the TOF-values for G5-RuSil60 and G6-RuSil60, the activity of G5-RuSil60 is significantly higher at each temperature. In the previous comparison, particle size was the determining factor for the observed trend in catalytic activity. However, when comparing the G5-RuSil60 to G6-RuSil60 catalyst, their average Ru particle size is nearly identical. What this indicates is that lower generation dendrimers provide less stabilisation during the immobilisation procedure onto the amorphous silica 60 support and that a significant amount of sintering occurs even when avoiding the high temperature conventionally utilised during calcination. This was especially evident for G4-RuSil60. In part, this can be attributed to the nature of the support which, when compared to other supports such as alumina, has a lower overall surface area and would decrease the dispersity of the nanoparticles. Nevertheless, the support was chosen for its large pore size necessary to accommodate a layer of ionic liquid without filling the pores. The nature of the stabilising

agent, in this case the dendrimer, may have a significant impact on the activity of the nanoparticle and not just from a stabilising viewpoint. The increased activity of G5-RuSil60 in comparison to that of G6-RuSil60, given that both average Ru particle sizes on the support are similar, can be ascribed to the lower steric bulk of the G5-PAMAM-OH dendrimer in comparison to the G6-PAMAM-OH dendrimer. This observation is expected, given that in non-polar solvents, the dendritic structure is more compressed. One could argue that the dendrimer decomposes considerably at the temperature utilised, however, this will only be true for temperatures above the decomposition temperature of the dendrimer and in solvents that would facilitate the decomposition. However, given the timescale of the reaction the conditions utilised, a higher temperature would be required and any decomposition that occurs is minimal. Therefore, the most likely reason for this decrease in TOF with increase in temperature would be an increase in compacting and denaturing of this complex macromolecule around the nanoparticle.

Table 4.1. Comparison of the TOF for the RuSil60 catalyst compared to other supported Ru nanoparticles as catalyst in toluene hydrogenation

Entry	Catalyst	TOF ^a (mol toluene converted/mol Ru/h)	Reference
1	G4-RuSil60 ^a	855	this work
2	G5-RuSil60 ^a	5379	this work
3	G6-RuSil60 ^a	2836	this work
4	Ru-PVP-silica ^b	667	24
5	Ru-hectorite ^c	3550	25
6	Ru-MWCNT ^d	7	26
7	Ru-PVP ^e	550	27

^a T = 90 °C, P_{H₂} = 10 bar, ^b T = 110 °C, P_{H₂} = 4 bar, ^c T = 50 °C, P_{H₂} = 50 bar

^d T = 50 °C, P_{H₂} = 40 bar, ^e T = 120 °C, P_{H₂} = 20 bar

Table 4.1 depicts the TOF-values for the RuSil60 catalysts as well as literature examples of supported Ru catalysts utilised in the hydrogenation of toluene. When considering the results obtained using the RuSil system, it is clear that the performance, when compared to other systems, is good. Given this high activity, RuSil60 catalysts are ideal for further evaluation as SCILL catalysts given that the activity of the catalyst can decrease significantly upon use of ionic liquid additives.

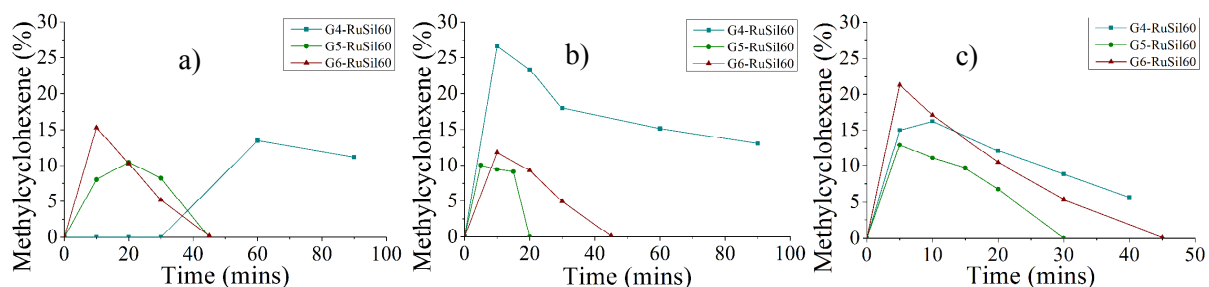


Figure 4.3. Selectivity to cyclohexenes observed during the evaluation of each catalyst for the hydrogenation of toluene at: a) 75 °C b) 90 °C c) 110 °C with a 10 bar H₂ pressure, 3.19 mmol of toluene, 0.00184 mmol Ru and 30 cm³ of cyclohexane.

The selectivity towards the partially hydrogenated methylcyclohexenes, was evaluated for each catalyst at the various temperatures as illustrated in Figure 4.3. The eventual product selectivity, when conducting the hydrogenation in batch mode, is towards the fully hydrogenated product, methylcyclohexane, despite the formation of methylcyclohexene. This is observed since even methylcyclohexene is eventually hydrogenated to methylcyclohexane. The selectivity profile therefore follows a somewhat parabolic trend for the formation of the partially hydrogenated alkenes, where the activity of the catalyst can be correlated to selectivity observed.

As discussed previously, G5-RuSil60 has the highest catalytic activity of the three RuSil60 catalysts and therefore has the lowest percentage of the partially hydrogenated methylcyclohexene products at any time, as observed in Figure 4.3. Given that this set of reactions were designed to optimise the reaction conditions, the best catalyst of the three RuSil60 catalysts for further studies involving the Ru-SCILL catalysts would be the G5-RuSil60. Instead, G6-RuSil60 was chosen to offset a balance between activity and stability where during the preparation of the RuSil60 catalysts, the G6-RuDENs best maintained its average size upon immobilisation on silica 60.

4.3.2 *Evaluation of the Ru-SCILL catalysts, based on RuSil60, in the hydrogenation of toluene and the influence of various ionic liquids on activity and selectivity.*

Ionic liquids are conventionally applied in a biphasic system, where the catalyst is dispersed in the ionic liquid. Activity is normally attenuated by the formation of a bilayer and in the case of hydrogenation, the poor solubility of hydrogen in the bulk of the ionic liquid when

compared to other solvents. To decrease the diffusion limitation of gaseous reactants, the bulk ionic liquid can be dispersed across a suitable solid support producing a thin ionic liquid film in the nanometer regime. With this rationale in mind, a series of ionic liquid coated catalysts with different amounts of ionic liquid were prepared to investigate the effects of the type of ionic liquid and the amount on the selectivity of the hydrogenation reaction. Additionally, the nominal thickness of the ionic liquid layer was varied to investigate the effects of the amount of ionic liquid. The catalysts were evaluated in batch mode reactions to monitor whether there is any change in the activity or selectivity for the various hydrogenates that are produced. The hydrogenation of toluene was investigated as a model reaction to evaluate the various catalysts.

The use of ionic liquids as a coating for the RuSil60 catalysts alters the properties of this heterogeneous catalyst. It is therefore necessary to identify which changes in the physical characteristics occur upon coating the catalyst to help understand the effects of the ionic liquid. The changes in the physical characteristics such as surface area, pore volume and pore diameter of the RuSil60 catalysts were investigated upon coating with the ionic liquid. The physical characteristics of the coated and uncoated catalysts are listed in Table 4.2. The uncoated catalyst, G6-RuSil60, was prepared according to the method described in chapter 2 for a metal loading of 0.08-0.10 wt% Ru as confirmed by ICP-OES. The BET analysis of the uncoated catalyst indicates a surface area (S_{BET}) of 462.1 m².g⁻¹, an average pore volume (V_p) of 0.82 cm³.g⁻¹ and an average pore diameter (D_p) of 56.2 Å. The 10% and 20% percentage ionic liquid values referred to for each of the SCILL catalysts, describe the percentage pore filling of the catalyst and correspond to an ionic liquid loading, α -value of 0.1 and 0.2 respectively.

Considering the data in Table 4.2, the change in surface area and pore volume is quite significant when comparing the uncoated catalyst to the coated catalyst. There is minimal difference in average pore diameter between the 10% and 20% G6-RuSCILL catalysts. More significantly, changes were observed for the surface area when comparing the 10% G6-RuSCILL catalysts to the 20% G6-RuSCILL catalysts. This change in the physical characteristics upon coating with an ionic liquid is consistent with literature and confirms the presence of the ionic liquid on the solid catalyst surface for the G6-RuSCILL catalysts.²²

Table 4.2. Surface area, average pore volume and average pore diameter for the uncoated and coated G6-RuSil60 catalysts.

Catalyst	Surface area, S_{BET} (m ² .g ⁻¹) ^a	Total pore volume, V_P (cm ³ .g ⁻¹) ^b	Average pore diameter, D_p (Å) ^b
Uncoated G6-RuSil60	462.1	0.82	56.2
10% [BMIM][BF ₄] G6-RuSCILL	286.5	0.64	63.6
10% [BMIM][PF ₆] G6-RuSCILL	314.5	0.64	58.6
10% [BMIM][NTf ₂] G6-RuSCILL	308.3	0.57	53.8
20% [BMIM][BF ₄] G6-RuSCILL	258.0	0.56	62.4
20% [BMIM][PF ₆] G6-RuSCILL	232.7	0.54	67.7
20% [BMIM][NTf ₂] G6-RuSCILL	259.2	0.51	56.2

^a Determined by BET analysis, ^b Determined by BJH analysis.

Another important characteristic that SCILL catalysts should have is the longevity of the ionic liquid coating. When designing a SCILL catalyst, the ionic liquid chosen should have good interaction with the support and catalyst and not have a high solubility in the reaction media. Post-run BET analysis was conducted to confirm whether the ionic liquid does remain on the catalyst and support after reaction.

Table 4.3 details the BET data obtained for the G6-RuSCILL catalysts with an ionic liquid loading, $\alpha = 0.2$, prior to and upon completion of the reaction. When comparing the surface areas before and after reaction to that of the uncoated catalyst, the values are considerably lower than the uncoated catalyst and the same holds for the average pore volume. Comparison of the BET results for only the pre- and post-run G6-RuSCILL catalyst indicates that there was no significant ionic liquid leaching as the surface area and average pore volume values are similar. The chosen ionic liquids are therefore suitable for use in the preparation of the Ru-SCILL catalysts for the hydrogenation of toluene, provided a H₂ pressure of 10 bar and temperature of 90 °C be kept.

The effect of the ionic liquid on the activity and selectivity of the reaction was investigated for the ionic liquids [BMIM][PF₆], [BMIM][BF₄] and [BMIM][NTf₂] for different degrees of pore filling with each ionic liquid. The reactions were allowed to continue for a period of 24

hours during which none of the reaction conditions allowed for the quantitative conversion of toluene. The overall rate of reaction decreased when compared to the uncoated catalysts that showed a quantitative conversion of toluene over a period of 40-60 minutes for G5-RuSil60 and G6-RuSil60. The presence of the ionic liquid therefore affects the coordination of the substrate and reactant molecules to the catalyst surface.

Table 4.3. Surface area, average pore volume and average pore diameter for the uncoated and pre- and post-run coated G6 catalysts with an ionic liquid loading α of 0.2.

Catalyst	Surface area, S_{BET} ($\text{m}^2 \cdot \text{g}^{-1}$) ^a	Total pore volume, V_p ($\text{cm}^3 \cdot \text{g}^{-1}$) ^b	Average pore diameter, D_p (\AA) ^b
Uncoated G6-RuSil60	462.1	0.82	56.2
Pre-catalytic run			
20% [BMIM][BF ₄] G6-RuSCILL	258.0	0.56	62.4
20% [BMIM][PF ₆] G6-RuSCILL	232.7	0.54	67.7
20% [BMIM][NTf ₂] G6-RuSCILL	259.2	0.51	56.2
Post-catalytic run			
20% [BMIM][BF ₄] G6-RuSCILL	275.5	0.58	60.1
20% [BMIM][PF ₆] G6-RuSCILL	203.4	0.56	78.5
20% [BMIM][NTf ₂] G6-RuSCILL	267.5	0.56	59.4

^a Determined by BET analysis, ^b Determined by BJH analysis.

The catalytic activities of the SCILL catalysts were expected to decrease with an increase in α -value. This is observed for an overall increase in the loading of ionic liquid using [BMIM][PF₆] and [BMIM][BF₄] as observed for Figures 4.4 (b) and 4.4 (c). This decrease in activity is, however, not observed when increasing the α -value for [BMIM][NTf₂]. Instead, there is an increase in the overall conversion with increase in the amount of [BMIM][NTf₂] quantitatively described by approximately a 50% conversion at 1440 minutes, as observed in Figure 4.4(c). This overall trend in percentage conversion was observed for G5-RuSCILL at 1440 minutes as well, further confirming the inherent positive effect of the increase in [BMIM][NTf₂] on the conversion of toluene for Ru-SCILL catalysts. The utilisation of ruthenium nanoparticles in an ionic liquid in typical arene hydrogenation reactions comprises a multiphase reaction.

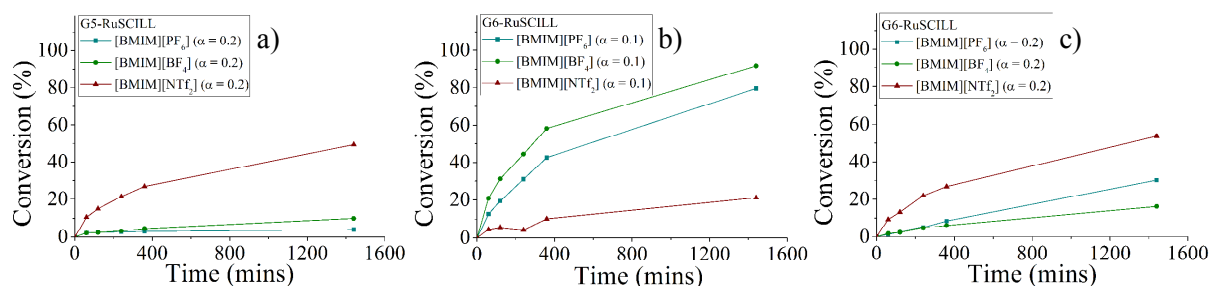


Figure 4.4. Graphs illustrating the toluene conversion profiles obtained using a) G5-RuSCILL with 20% pore filling of ionic liquid, b) G6-RuSCILL with 10% pore filling of ionic liquid and c) G6-RuSCILL with 20% pore filling of ionic liquid at a 10 bar H₂ pressure, a temperature of 90°C and with 3.19 mmol of toluene, 0.00184 mmol Ru and 30 cm³ of cyclohexane.

Unlike the hydrogenations conducted with SCILL catalysts, the interfacial area between the substrate containing organic phase and the catalyst containing ionic liquid phase is considerably smaller in the biphasic system. Despite this difference, studies investigating the preparation of ruthenium nanoparticles in different ionic liquids and their evaluation as catalysts in arene hydrogenation reactions provide some insight into the effect of the ionic liquid. Prechtl *et al.* prepared a series of ruthenium nanoparticles stabilised by the ionic liquids [BMIM][BF₄] and [BMIM][NTf₂] amongst others.¹⁶ The catalysts were evaluated for the hydrogenation of various arenes including toluene. Typically, reactions were conducted at 75 °C and a H₂ pressure of 4 bar and an 18 hour end of run analysis conducted for the products formed. The conversions of toluene obtained when evaluating the [BMIM][BF₄] and [BMIM][NTf₂] stabilised ruthenium colloid suspensions, were 40% and 85% respectively. This behaviour describes a system where the ionic liquid is defined as a bulk phase whereas for SCILL catalysts, the ionic liquid is a thin film covering the catalyst surface, dramatically reducing possible mass transfer limitations of the substrates and reactants. When comparing the overall trend in activity for the [BMIM][BF₄] and [BMIM][NTf₂] coated G6-RuSCILL catalysts with an α -value of 0.1, there is a significantly lower conversion of toluene after 1440 minutes for the latter. This is contrary to the previously discussed trend observed by Prechtl *et al.* for these two ionic liquids.¹⁶ Upon increasing the ionic liquid loading to an α -value of 0.2, an overall decrease in the percentage conversion was observed in all cases, except for the G6-RuSCILL catalyst coated with [BMIM][NTf₂] that showed an overall higher percentage conversion.

This suggests that even though both these are SCILL catalysts with thin ionic liquid coatings, the promotional effects of the [BMIM][NTf₂] ionic liquid is more evident for increased amounts of this ionic liquid. The trend observed for biphasic catalytic systems, corroborates the trend observed for the G6-RuSCILL catalysts for the ionic liquids [BMIM][BF₄] and [BMIM][NTf₂]. Similarly, this inversion in trend is observed when comparing the results obtained for the [BMIM][BF₄] and [BMIM][PF₆] G6-RuSCILL catalysts with increasing ionic liquid loading from an α -value of 0.1 to 0.2.

This same trend was observed by Rossi *et al.* for the activity of Ru colloids prepared from RuO₂ and stabilised by either [BMIM][BF₄] or [BMIM][PF₆] and their activity in arene hydrogenation at 75 °C and a H₂ pressure of 4 atm.² In this case, comparative results were obtained when using benzene as a substrate where a 96% conversion of benzene was observed after 13 hours for [BMIM][PF₆] Ru colloids and a 46% conversion after 20 hours when evaluating [BMIM][BF₄] Ru colloids. Silveria *et al.* observed the same trend for the hydrogenation of benzene when utilising Ru colloids stabilised with [BMIM][BF₄] and [BMIM][PF₆] using the Ru precursor, [Ru(cod)(cot)].¹⁷ When considering all these results, the difference in activity is most pronounced when comparing [BMIM][NTf₂] to that of [BMIM][BF₄] or [BMIM][PF₆] for an α -value of 0.1. For a higher α -value of 0.2, however, [BMIM][NTf₂] would be the suitable ionic liquid.

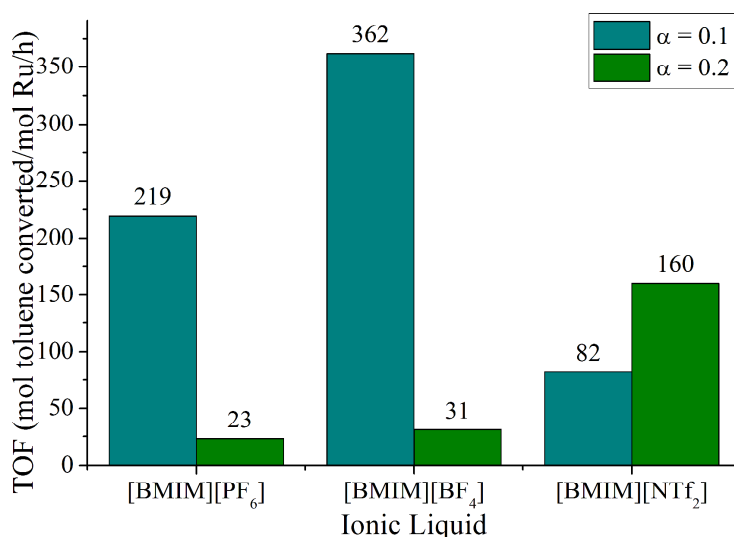


Figure 4.5. Turnover frequencies observed for the conversion of toluene at 60 minutes when evaluating G6-RuSCILL for the ionic liquids [BMIM][PF₆], [BMIM][BF₄] and [BMIM][NTf₂] for an $\alpha = 0.1$ and $\alpha = 0.2$ at a 10 bar H₂ pressure, a temperature of 90°C and with 3.19 mmol of toluene, 0.00184 mmol Ru and 30 cm³ of cyclohexane.

To better illustrate the influence of ionic liquid loading on the catalytic activity of the G6-RuSil60 catalyst, the TOF-values were calculated 60 minutes into the reaction for a pore filling of $\alpha = 0.1$ and $\alpha = 0.2$ as illustrated in Figure 4.5. The decrease in catalytic activity with increase in ionic liquid loading for [BMIM][PF₆] and [BMIM][BF₄] further reinforces the results illustrated in Figure 4.4 (b) and Figure 4.4 (c). The opposite trend is observed for [BMIM][NTf₂] that shows an increase in TOF upon increase in ionic liquid loading from $\alpha = 0.1$ to $\alpha = 0.2$. Interestingly, when considering the overall activity of the RuSCILL catalysts for an ionic liquid loading of $\alpha = 0.1$, the RuSCILL catalysts with [BMIM][PF₆] and [BMIM][BF₄] show a higher activity over that of [BMIM][NTf₂].

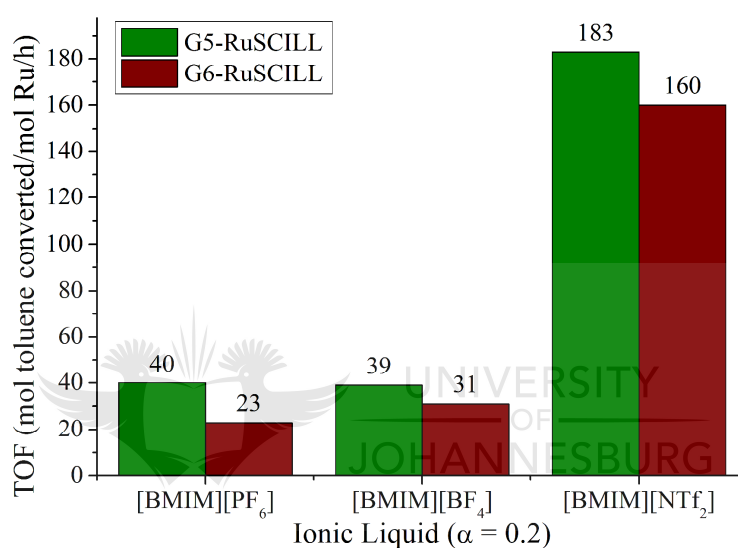


Figure 4.6. Turnover frequencies observed for the conversion of toluene at 60 minutes when evaluating the catalysts, G5-RuSCILL and G6-RuSCILL for the ionic liquids [BMIM][PF₆], [BMIM][BF₄] and [BMIM][NTf₂] with an $\alpha = 0.2$. Reactions were conducted at a 10 bar H₂ pressure, a temperature of 90°C and with 3.19 mmol of toluene, 0.00184 mmol Ru and 30 cm³ of cyclohexane.

The TOF values calculated for the evaluation of G5-RuSCILL are illustrated in Figure 4.6 for $\alpha = 0.2$ alongside those observed when evaluating the various G6-RuSCILL catalysts. The observed trends in TOF for the different ionic liquids, where [BMIM][PF₆] and [BMIM][BF₄] coated RuSCILL catalysts show lower TOF values than those with [BMIM][NTf₂], is observed for the G5-RuSCILL catalysts as well. This serves to further confirm the observed trend in catalytic activity for the different ionic liquid coated G6-RuSCILL catalysts.

The use of ionic liquid as a coating for supported ruthenium catalysts in a SCILL catalyst system was shown to have a significant impact on the activity of the catalyst. In some cases, the increased amount of ionic liquid resulted in the increased activity of the catalyst as was the case for [BMIM][NTf₂] coated catalysts. In other instances, a lower ionic liquid loading where the α -value is 0.1, gave better activity as was the case for either [BMIM][PF₆] or [BMIM][BF₄] coated RuSCILL catalysts. Of greater importance, is the selectivity profile observed when evaluating each of these RuSCILL catalysts with selectivity towards the partially hydrogenated product being sought after.

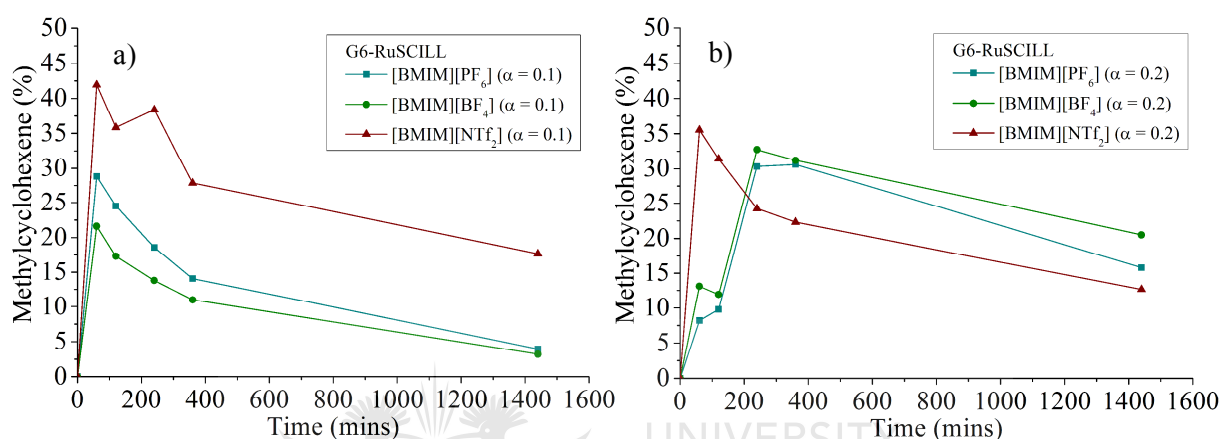


Figure 4.7. Illustration for the selectivity to cyclohexenes observed during the evaluation of each catalyst for the hydrogenation of toluene utilising G6-RuSCILL with the ionic liquids [BMIM][PF₆], [BMIM][BF₄] and [BMIM][NTf₂] for a) $\alpha = 0.1$ and b) $\alpha = 0.2$ at a 10 bar H₂ pressure, a temperature of 90°C and with 3.19 mmol of toluene, 0.00184 mmol Ru and 30 cm³ of cyclohexane.

The RuSCILL catalysts were therefore evaluated for their selectivity towards the partially hydrogenated methylcyclohexenes. Figure 4.7 illustrates the selectivity towards the partially hydrogenated methylcyclohexenes with time for the G6-RuSCILL catalysts with an ionic liquid loading of $\alpha = 0.1$ and $\alpha = 0.2$. The selectivity profile shows a similar trend as observed for the evaluation of the uncoated catalysts where there is an increase for methylcyclohexenes and steady decrease as they are further hydrogenated to methylcyclohexane.

The methylcyclohexene selectivity profile for the evaluation of G5-RuSCILL was compared to the earlier mentioned selectivity profile for G6-RuSCILL to help corroborate results obtained for the G6-RuSCILL catalyst as illustrated in Figure 4.8. The selectivity profile observed for G5-RuSCILL using [BMIM][PF₆] and [BMIM][BF₄] shown in Figure 4.8(a)

does not show the same trend as that observed when using G6-RuSCILL with the same ionic liquid coating. Considering the results obtained when utilising [BMIM][NTf₂], the selectivity profile observed for both catalysts are similar to G5-RuSCILL coated in [BMIM][NTf₂] showing a slightly lower selectivity towards the methylcyclohexenes, an observation that may be correlated to the inherently higher catalytic activity of G5-RuSCILL over that of G6-RuSCILL.

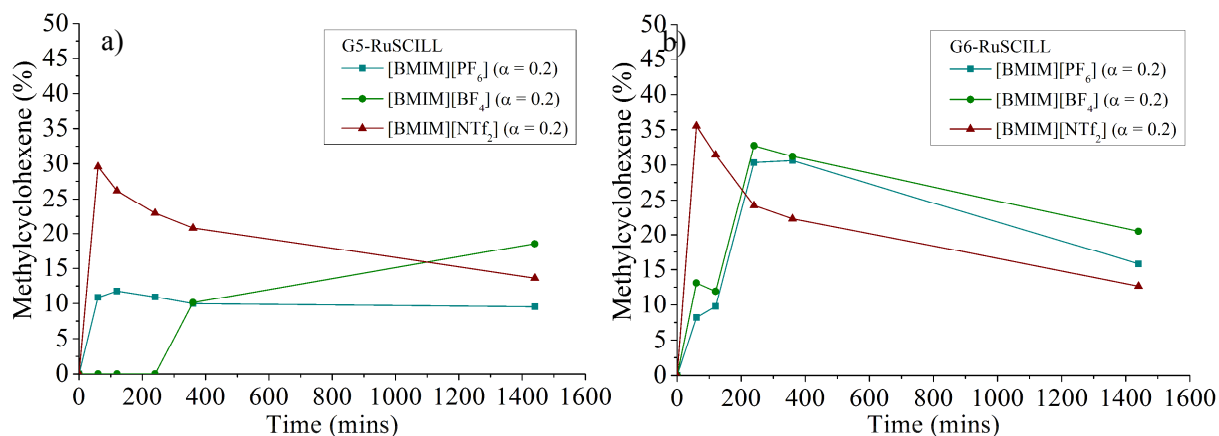


Figure 4.8. Illustration for the selectivity to cyclohexenes observed during the evaluation of each catalyst for the hydrogenation of toluene utilising a) G5-RuSCILL and b) G6-RuSCILL with the ionic liquids [BMIM][PF₆], [BMIM][BF₄] and [BMIM][NTf₂] for an $\alpha = 0.2$ at a 10 bar H₂ pressure, a temperature of 90 °C and with 3.19 mmol of toluene, 0.00184 mmol Ru and 30 cm³ of cyclohexane.

Previous studies have focused on inclusion of additives to the catalyst itself or the catalytic reaction mixture as a means to control the selectivity towards partially hydrogenated products in the hydrogenation of arenes. Typically, these additives adsorb to the active sites on the ruthenium nanoparticles that are required for the full hydrogenation of the arene. Hartog *et al.* observed this selectivity towards the cyclohexenes when hydrogenating benzene in the presence of an alcohol.²⁸ Improvement in this selectivity up to a cyclohexene selectivity of 30% was observed when conducting the hydrogenation of benzene in an aqueous solution of zinc salts. Consequently, the activity of the catalyst decreases significantly where the decrease in activity and increase in selectivity was ascribed to the excessive absorption of water on the active sites of the ruthenium catalyst.²⁹ In each of these cases the additive, whether it is the presence of the alcohol or water, acts as a modifier on the catalytic surface. Essentially, the surface active site configuration is changed due to the coordination of the additives.

The same behaviour occurs for the ionic liquids utilised in this study, where there is interaction between the respective ionic liquids and the surface active sites of the ruthenium nanoparticle. These interactions have been investigated *in situ* for the deposition of ionic liquids on platinum and palladium metal surfaces using physical vapour deposition (PVD) techniques.³⁰⁻³¹ The interactions were shown to be specific to certain particle sites for the displacement of CO by the ionic liquid and were different for the different metals.

Given that there is interaction between the nanoparticle surface and the ionic liquid and that it is known that additives such as water affect selectivity due to adsorption on sites that facilitate full hydrogenation of the arene, the overall performance of the catalyst is not only determined by the overall solubility of substrate and reactant in the ionic liquid. The catalyst performance is therefore dependant on the ability of the ionic liquid to act as a catalyst surface modifier.

To highlight the positive effect of the type and amount of ionic liquid on the selectivity towards methylcyclohexenes, a summary of the maximum methylcyclohexene selectivity is presented in Table 4.4 with the corresponding time, TOF and percentage conversion. In each case, the high selectivity towards methylcyclohexenes of 41.9% and 35.5% was observed when using [BMIM][NTf₂] as the ionic liquid for an α -value of 0.1 and 0.2 as shown in entries 3 and 6 respectively. Overall, the results suggest that each ionic liquid merits use as a suitable additive for the increased selectivity towards methylcyclohexenes. The appropriate balance between activity and selectivity will therefore determine which ionic liquid is utilised. For instance, compared to [BMIM][NTf₂] the lower selectivity towards methylcyclohexenes observed when using the ionic liquids [BMIM][BF₄] and [BMIM][PF₆] are 28.8% and 21.6% respectively. The observed activities are, however, significantly higher for these ionic liquids with a TOF of 219 and 361, as observed in Table 4.4 for entries 1 and 2 respectively. More importantly, these results are obtained in a batch reaction setup and to gain any insights into the possible performance of these catalysts in a continuous flow process, initial activity and selectivity of the catalyst is more significant as this correlates better with the reduced residence time of the substrate and reactant over the catalyst.

Table 4.4. Maximum selectivity towards methylcyclohexenes observed for different SCILL catalysts at various times and conversions.^a

Entry	Catalyst	Time (mins)	Conversion (%)	TOF ^b	Selectivity (%)
1	10% [BMIM][BF ₄] G6-RuSCILL	60	12.6	219	28.8
2	10% [BMIM][PF ₆] G6-RuSCILL	60	20.8	361	21.6
3	10% [BMIM][NTf ₂] G6-RuSCILL	60	4.7	82	41.9
4	20% [BMIM][BF ₄] G6-RuSCILL	360	8.4	24	30.6
5	20% [BMIM][PF ₆] G6-RuSCILL	240	4.6	20	32.7
6	20% [BMIM][NTf ₂] G6-RuSCILL	60	9.2	160	35.5

^a T = 90 °C and P_{H₂} = 10 bar^b mmol toluene converted/mmol Ru/hour

4.3.3 *The catalytic evaluation of the silica 100 supported RuDENs, RuSil100.*

The evaluation of the RuSil60 catalysts proved that supported RuDEN catalysts are suitable for the hydrogenation of toluene. The coating of the RuSil60 catalysts had a significant impact on the catalytic performance and in some cases led to an enhancement in the selectivity towards the partially hydrogenated product. The support material was then changed as the eventual objective of the use of SCILL catalysts is to evaluate their feasibility as catalysts in a continuous flow hydrogenation reaction. Preliminary evaluation was conducted to screen these catalysts by adopting the methodology used for the preparation of the RuSil60 catalysts. Important to note is the change in equipment used for the evaluation. The autoclave used in this study was a 300 cm³ stainless steel autoclave equipped with a gas impeller stirrer. Unlike the RuSil60 catalysts, only the G5-RuSil100 and G6-RuSil100 catalysts were evaluated in light of the better performance of the G5-RuSil60 and G6-RuSil60 catalysts over that of G4-RuSil60. The time resolved effects of changes in temperature on the conversion of toluene is illustrated in Figure 4.9 for the temperatures 50 °C, 75 °C and 100 °C. The temperature change from 50 °C to 75 °C does not show as significant a change in the conversion as seen when increasing the temperature to 110 °C.

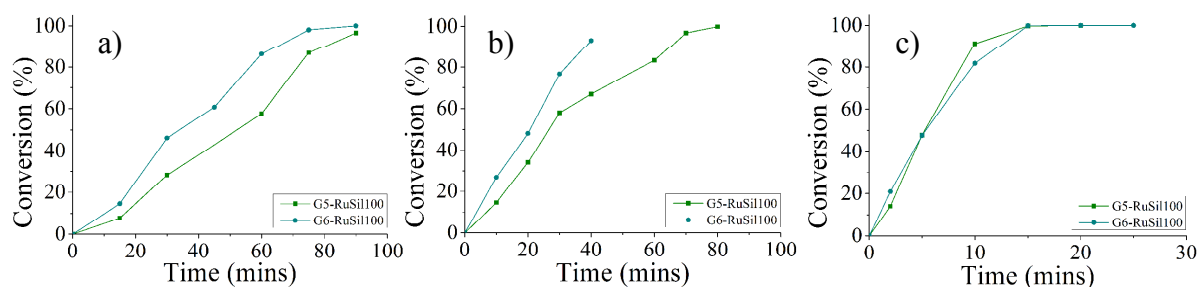


Figure 4.9. Graphs illustrating the toluene conversion profiles obtained using G5-RuSil100 and G6-RuSil100 as catalysts at a 10 bar hydrogen pressure and at the temperatures: a) 50 °C b) 75 °C and c) 110 °C, with 9.44 mmol of toluene, 0.007 mmol Ru and 99 cm³ of cyclohexane.

The reaction time decreases from an average of 90 minutes for a near quantitative conversion, in the case of reactions conducted at 50 °C and 75 °C, to less than 30 minutes when conducted at 110 °C. Similarly, when considering the results illustrated in Figure 4.10, there is an increase in conversion with increase in the temperature. The increase in conversion is, however, more proportional to the temperature since, unlike the reactions conducted at 10 bar H₂ pressure, there is an increase in the conversion upon increasing the temperature from 50 °C to 75 °C. A comparison of the results illustrated in Figure 4.9 and Figure 4.10 gives insight into the effects of H₂ pressure on the catalytic reaction. The change in H₂ pressure from 10 bar to 30 bar has minimal influence on reactions conducted at 50 °C. Reactions conducted at higher temperatures show a significant decrease in the time taken for near quantitative conversion. This is especially applicable to reactions conducted at 75 °C where an approximate 30 minute decrease in time was observed, to obtain near quantitative conversion, when evaluating the G6-RuSil100 catalyst.

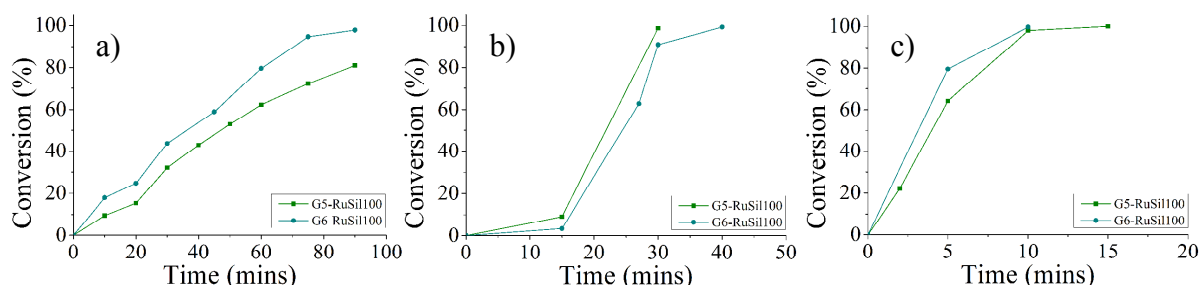


Figure 4.10. Graphs illustrating the toluene conversion profiles obtained using G5-RuSil100 and G6-RuSil100 as catalysts at a 30 bar hydrogen pressure and at the temperatures: a) 50 °C b) 75 °C and c) 110 °C, with 9.44 mmol of toluene, 0.007 mmol Ru and 99 cm³ of cyclohexane.

To gain better insight into the activity of each catalyst, the turnover frequency (TOF) was determined for each of the reaction conditions using the G5-RuSil100 and G6-RuSil100 catalysts. The turnover frequencies were calculated for each catalyst at a conversion of more than 95%. Figure 4.11 illustrates the various TOF-values obtained when evaluating the G5-RuSil100 and G6-RuSil100 catalysts at different temperatures and at a H₂ pressure of 10 bar and 30 bar. There is an expected increase in the TOF-value with an increase in temperature due to a decrease in mass transport limitations. The trend was observed for an increase in the pressure as well but was more evident at the temperatures above 50 °C.

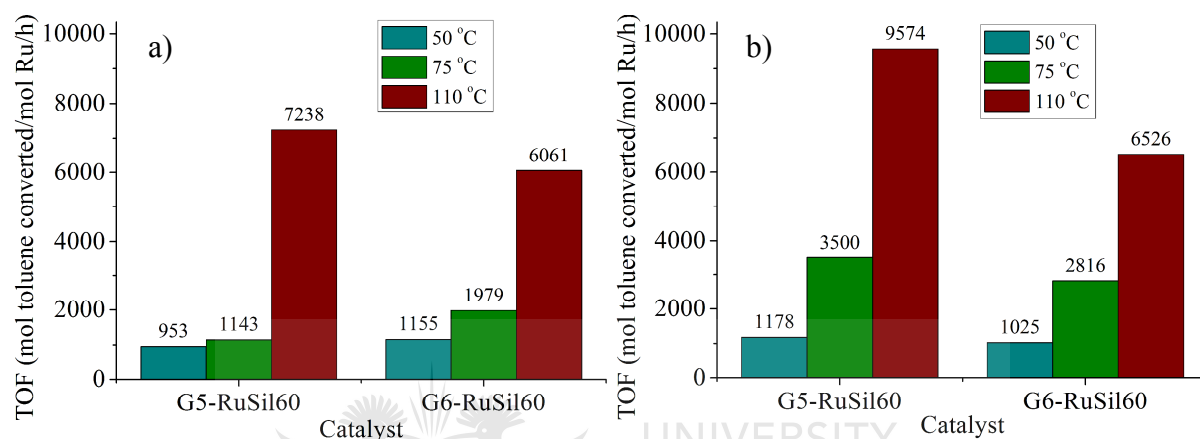


Figure 4.11. Turnover frequencies observed for the conversion of toluene at >95 % conversion utilising G5-RuSil100 and G6-RuSil100 for temperatures 50 °C, 75 °C and 110 °C at a H₂ pressure of a) 10 bar and b) 30 bar with 9.44 mmol of toluene, 0.007 mmol Ru and 99 cm³ of cyclohexane.

The time resolved selectivity profile for each of the catalytic reactions conducted using the RuSil100 catalysts is illustrated in Figure 4.12. Similar to the results obtained when evaluating the RuSil60 catalysts, there is an initial increase in the amount of methylcyclohexene and then eventually a decrease as all unsaturated hydrocarbons are hydrogenated. This is inherent to the nature of the batch reaction since the substrates and partially hydrogenated products are in a closed system saturated with H₂ gas, ideal for hydrogenation to occur. The trend in catalytic performance of the two RuSil100 catalysts for the lower temperatures of 50 °C and 75 °C changed upon increasing the pressure from 10 bar H₂ to 30 bar H₂. The catalytic activity was therefore higher when evaluating the G5-RuSil100 catalyst compared to the G6-RuSil60 catalyst for catalytic evaluations at 30 bar unlike the opposite trend seen at a 10 bar pressure. Given that the later evaluation of the effect of the ionic liquid as a coating will be investigated at a H₂ pressure of 10 bar, G6-RuSil100 was

chosen for preparing the RuSCILL catalysts. Additionally, the preservation of nanoparticle size observed during the immobilisation procedure, discussed in Chapter 2, further supports the use of G6-RuSil100. The improved stability observed when using G6-PAMAM-OH in the preparation of G6-RuDEN for immobilisation on silica 100 therefore, qualified the G6-RuSil100 as a catalyst for the preparation of RuSCILL for further evaluation.

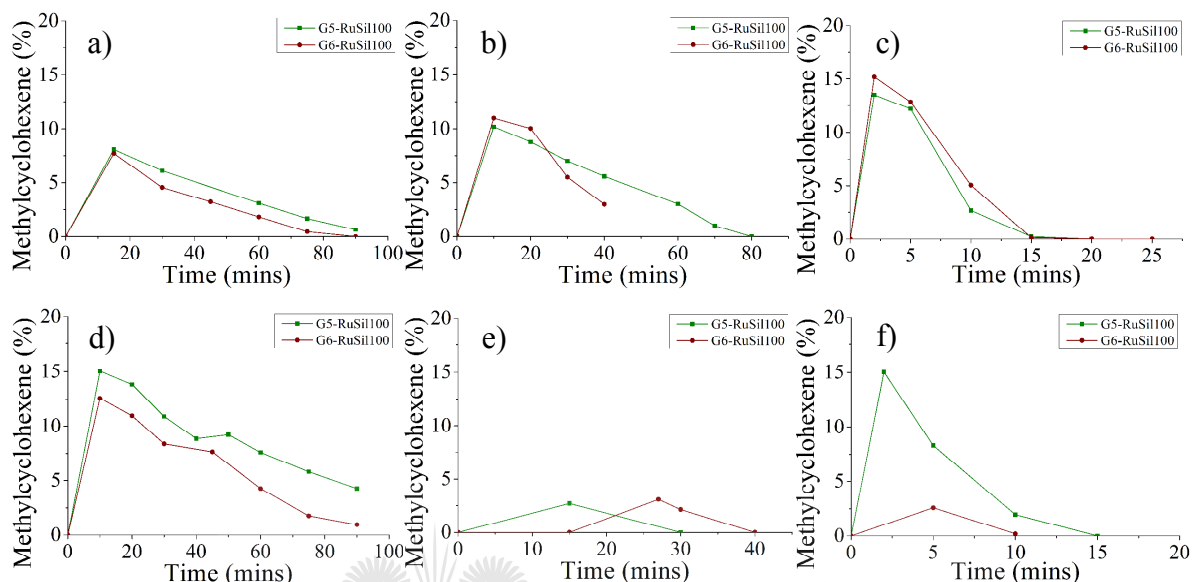


Figure 4.12. Illustration for the selectivity to cyclohexenes observed during the evaluation of each catalyst for the hydrogenation of toluene at a H₂ pressure of 10 bar and temperature of: a) 50 °C, b) 75 °C and c) 110 °C and a H₂ pressure of 30 bar and a temperature of: d) 50 °C, e) 75 °C and f) 110 °C with 9.44 mmol of toluene, 0.007 mmol Ru and 99 cm³ of cyclohexane.

4.3.4 Evaluation of the RuSil100-based RuSCILL catalysts in the hydrogenation of toluene and the influence of various ionic liquids on activity and selectivity.

Given the activity observed for the G6-RuSil100 catalyst, a series of preliminary evaluations for the effect of the presence of select ionic liquids on the catalytic performance was conducted. This was done to identify a catalyst to be evaluated in later preliminary continuous flow hydrogenation reactions. The ionic liquids used in the batch reactions were [BMIM][NTf₂], 1-octyl-3-methylimidazolium bis(trifluoromethylsulfonyl)imide, [OMIM][NTf₂], and 1-butyl-3-methylimidazolium octylsulfate, [BMIM][OcS]. Figure 4.13 illustrates the conversion and selectivity profile for the evaluation of the different ionic liquids utilised as catalyst coatings. There is an expected decrease in the conversion in some cases

when the ionic liquid coating is present as observed for Figure 4.13(a). This is true for the use of [BMIM][OcS] and [BMIM][NTf₂] with approximately a 100 minute induction period observed for the former. This was, however, not observed when evaluating [OMIM][NTf₂] as a catalyst coating with the reaction completing within 40 minutes. This could suggest better solubility of the substrate and products in the ionic liquid.

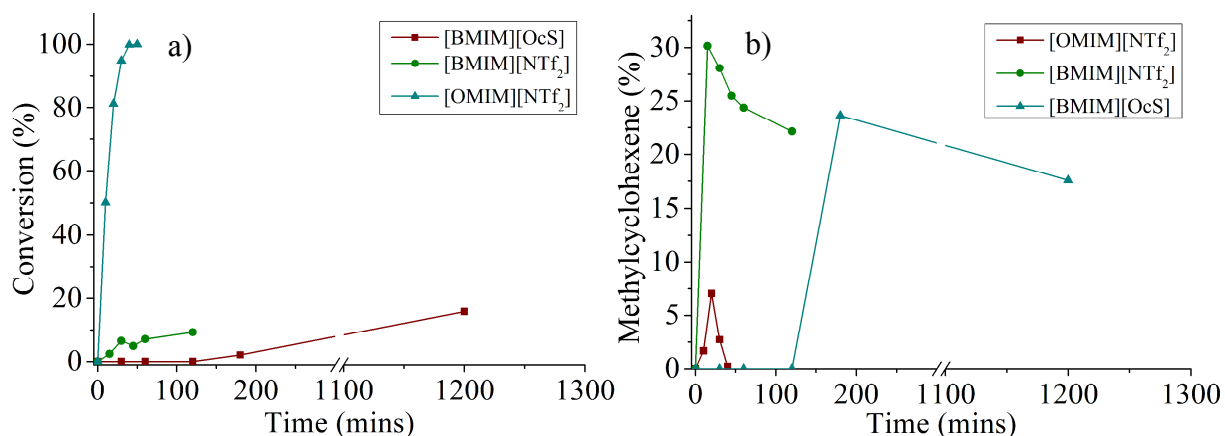


Figure 4.13. Figures illustrating the catalytic performance observed when evaluating the G6-RuSil100-based RuSCILL catalysts for the ionic liquids [OMIM][NTf₂], [BMIM][NTf₂] and [BMIM][OcS]. The graphs illustrate the: a) time-resolved conversion and b) the time-resolved methylcyclohexene selectivity using 9.44 mmol of toluene, 0.007 mmol Ru and 99 cm³ of cyclohexane at a H₂ pressure of 10 bar.

The selectivity profiles for the coated catalysts show an increase in the alkene selectivity over that of the uncoated catalyst as seen in Figure 4.13(b). The solubility of the substrates play an important role in the selectivity and this can be seen for [OMIM][NTf₂] that shows the lowest selectivity for the alkene intermediates amongst the other coated catalysts. It is possible that there is increased solubility of the substrate in this ionic liquid allowing better diffusion of the substrate to the catalyst surface given the solubility of aryl compounds increase with the increase in alkyl chain length of the imidazolium cation.³² In the case of the [BMIM][NTf₂] and [BMIM][OcS] coated catalyst, both show a higher selectivity for the alkene intermediate but this is accompanied with a decrease in catalytic activity. An induction period was observed for the catalyst coated with [BMIM][OcS] despite an incorporated activation time prior to the reaction. This is most likely due to the decreased solubility of the substrate in the ionic liquid and higher coordination strength of the ionic liquid to the nanoparticle surface. The nature of the interaction of the ionic liquid [OMIM][NTF₂] with the substrates and products does, however, require further study to fully substantiate the theory of solubility

effects. The RuSCILL catalyst with [OMIM][NTf₂] as a coating was therefore chosen for evaluation in the continuous flow hydrogenation given the decreased inhibition of the hydrogenation reaction observed.

4.3.5 *Continuous flow hydrogenation of toluene utilising RuSil100 and RuSCILL catalysts.*

The successful evaluation of the RuSil100 catalysts in the batch reactions indicated the potential of these catalysts to be used in the continuous flow gas phase hydrogenation of toluene. The use of Ru-SCILL catalysts are especially suited to gas phase continuous flow reactions where any leaching of the ionic liquid is minimised due to the difference in phase. The RuSil catalyst was evaluated in the gas phase hydrogenation of toluene prior to the evaluation of the RuSCILL catalysts to establish whether the catalyst showed appreciable activity in the absence of an ionic liquid. The RuSIL catalyst was activated prior to the reaction by exposing the catalyst to a static atmosphere of hydrogen at 1 bar and 90 °C. The gas phase hydrogenation was then conducted by introducing the toluene gas feed with a hydrogen partial pressure, P_{H_2} , of 2.7 bar and a total pressure, P_{total} , of 6 bar at 110 °C.

Figure 4.14 illustrates the results obtained for the percentage conversion of toluene and selectivity towards the partially hydrogenated products with time. There is a near quantitative conversion of toluene when utilising the uncoated RuSil catalyst at a temperature of 110 °C as shown for the red filled squares in Figure 4.14. The reactor was then cooled to 90 °C and the reaction allowed to continue. Similar to the activity of the catalyst at 110 °C, there was a near quantitative conversion of toluene for the same P_{H_2} and P_{total} at 90 °C. The reaction showed no selectivity towards the partially hydrogenated methylcyclohexenes with methylcyclohexane as the only product formed during the hydrogenation, as observed for the unfilled squares in Figure 4.14. Given the good activity of the RuSil catalyst in the gas phase hydrogenation of toluene, a series of catalysts coated in [OMIM][NTf₂] were prepared for an α -value of 0.1, 0.2 and 0.3 to investigate the effect of the amount of ionic liquid on the catalytic activity and selectivity towards the methylcyclohexenes. The ionic liquid [OMIM][NTf₂] was chosen for its greater miscibility with the substrate toluene, with hopes that this would help increase the activity given the decrease in activity of RuSil catalysts upon coating with an ionic liquid.

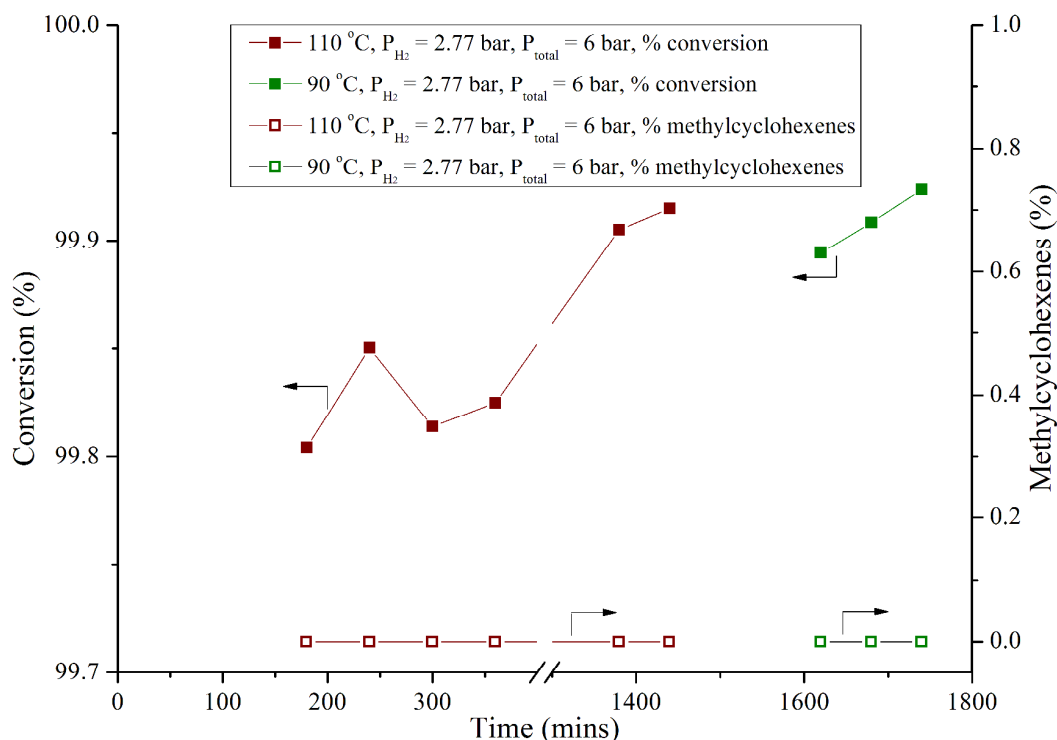


Figure 4.14. Continuous flow hydrogenation of toluene results for the % conversion and selectivity towards methylcyclohexenes with time when evaluating the uncoated G6-RuSil100 catalyst for $n_{\text{Ru}} = 0.0223$ mmol. Reaction parameters at the temperatures, a) 90 °C, H_2 flow rate = 16.65 $\text{ml}\cdot\text{min}^{-1}$, toluene flow rate = 2.59 $\text{ml}\cdot\text{min}^{-1}$, residence time = 6.82 sec b) 110 °C, H_2 flow rate = 16.54 $\text{ml}\cdot\text{min}^{-1}$, toluene flow rate = 2.73 $\text{ml}\cdot\text{min}^{-1}$, residence time = 6.83 sec.

Figure 4.15 illustrates the results obtained when evaluating the RuSCILL catalyst, with a pore filling of 10% which corresponds to an α -value of 0.1, utilising the ionic liquid [OMIM][NTf₂], in the gas phase continuous flow hydrogenation of toluene. The conversion of toluene increased from approximately 23% to 34% and then decreased to 12% at a time of 1140 minutes. A marginal increase in the selectivity towards the methylcyclohexenes of 0.6% was observed when compared to the selectivity observed when evaluating the uncoated catalyst, RuSil. Given the low selectivity to the methylcyclohexenes for an α of 0.1, the ionic liquid loading on the RuSil catalyst was increased to 0.2, corresponding to a 20% pore filling of the catalyst by the ionic liquid.

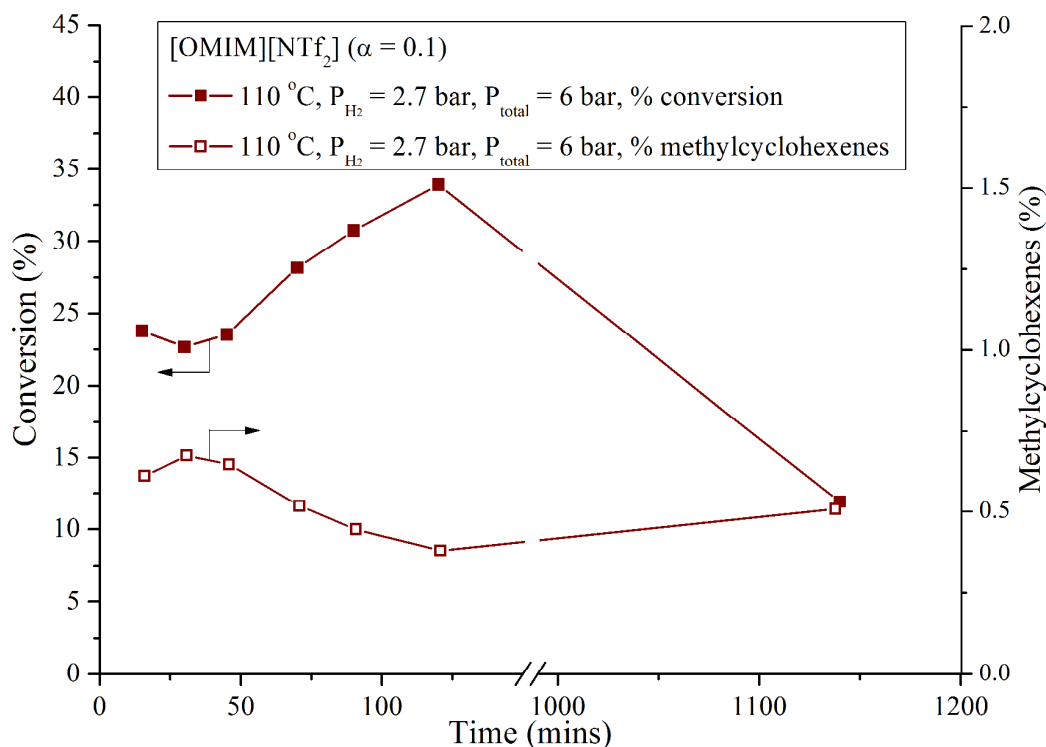


Figure 4.15. Continuous flow hydrogenation of toluene results for the % conversion and selectivity towards methylcyclohexenes with time when evaluating the coated RuSCILL catalyst with an ionic liquid loading of 0.1 and [OMIM][NTf₂] as ionic liquid. The reaction parameters utilised are 110 °C, H₂ flow rate = 16.54 ml.min⁻¹, toluene flow rate = 2.73 ml.min⁻¹, residence time = 7.70 sec with a n_{Ru} = 0.0193 mmol.

Figure 4.16 illustrates the conversion of toluene and selectivity to methylcyclohexenes over time when evaluating the RuSCILL catalyst with an [OMIM][NTf₂] ionic liquid loading, α , of 0.2. There is a large decrease in the overall conversion of toluene when compared to the RuSCILL catalyst with an α -value of 0.1. The selectivity towards the methylcyclohexenes increases to a maximum of 5.7% with an increase in the amount of ionic liquid to an α -value of 0.2. The ionic liquid loading was further increased for the RuSCILL catalyst with [OMIM][NTf₂] from an α -value of 0.2 to 0.3 to investigate whether a further increase in selectivity towards methylcyclohexenes would be observed.

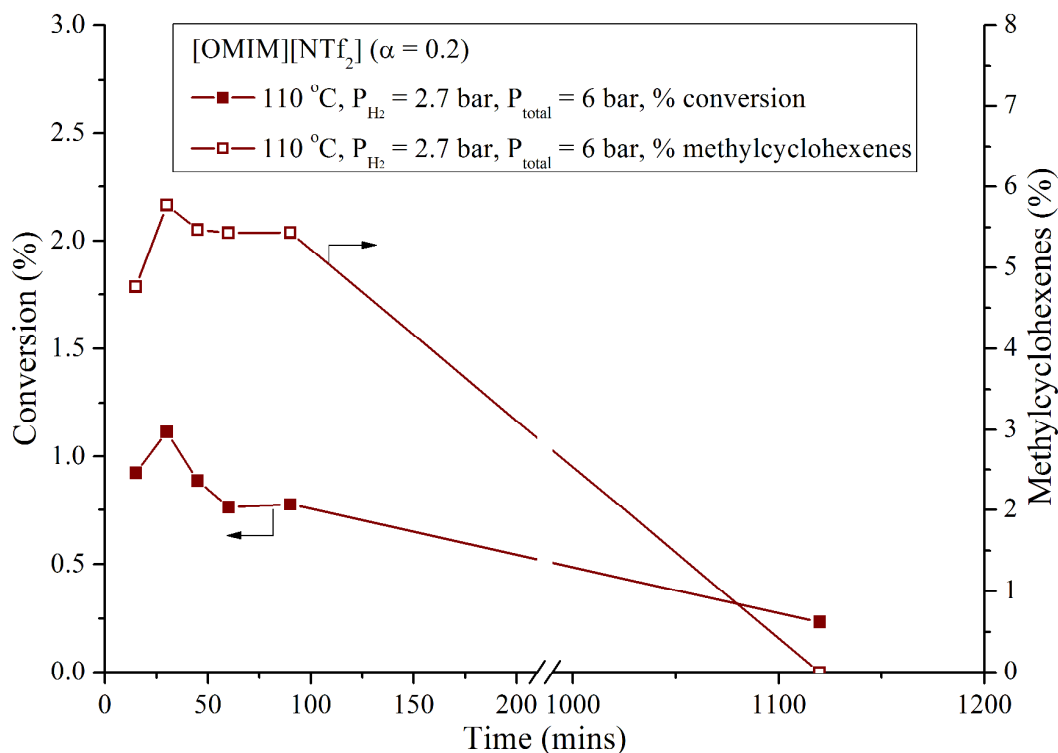


Figure 4.16. Continuous flow hydrogenation of toluene results for the % conversion and selectivity towards methylcyclohexenes with time when evaluating the coated RuSCILL catalyst with an ionic liquid loading of 0.2 and [OMIM][NTf₂] as ionic liquid. The reaction parameters utilised are 110 °C, P_{H₂} flow rate = 16.54 ml.min⁻¹, toluene flow rate = 2.73 ml.min⁻¹, residence time = 8.56 sec with a n_{Ru} = 0.0193 mmol.

Figure 4.17 illustrates the conversion of toluene and selectivity towards methylcyclohexenes with time when evaluating the [OMIM][NTf₂] coated RuSCILL catalyst with an ionic liquid loading, α -value, of 0.3. The conversion of toluene is comparable to that observed in Figure 4.11 for the catalyst with an α -value of 0.2. The reaction was conducted at 110 °C with an initial hydrogen partial pressure, P_{H₂}, of 2.7 bar and then later increased to a P_{H₂} of 4.6 bar for a P_{total} of 6 bar and 10 bar respectively. The increase in hydrogen pressure led to a slight increase in the percentage conversion. This increase in conversion of toluene is linked to an increase in concentration of hydrogen present for the hydrogenation.

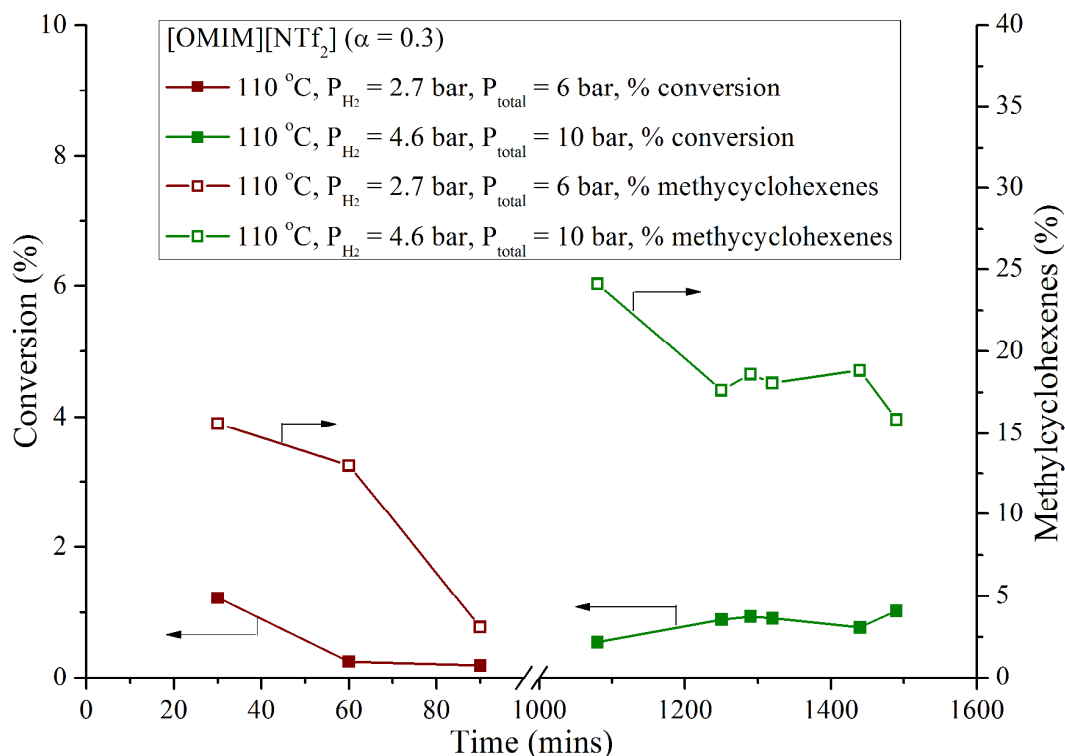


Figure 4.17. Continuous flow hydrogenation of toluene results for the % conversion and selectivity towards methylcyclohexenes with time when evaluating the coated RuSCILL catalyst with an ionic liquid loading of 0.3 and [OMIM][NTf₂] as ionic liquid and a $n_{Ru} = 0.0129$ mmol. Reaction parameters with a temperature of 110 °C at the pressures, a) $P_{total} = 6$ bar, H_2 flow rate = 16.54 ml.min⁻¹, toluene flow rate = 2.73 ml.min⁻¹, residence time = 6.29 sec b) $P_{total} = 10$ bar, H_2 flow rate = 9.92 ml.min⁻¹, toluene flow rate = 1.64 ml.min⁻¹, residence time = 10.48 sec.

The expectation is that with an increase in the ionic liquid loading there would be a concomitant decrease in the catalytic activity as observed for the increase in ionic liquid loading, progressing from the uncoated RuSil catalysts to the RuSCILL catalysts with an α -value of 0.1 and 0.2. The change in percentage conversion from an α -value of 0.2 to 0.3 is, however, less significant. More interestingly, there is a significant increase in the selectivity towards the partially hydrogenated methylcyclohexenes.

4.4 Conclusion

The dendrimer encapsulated nanoparticles supported on silica serve as good catalysts for the hydrogenation of toluene. The use of ionic liquids as coatings is an elegant method of affecting the selectivity profile of the RuSil catalysts for methylcyclohexenes in the

hydrogenation of toluene. Increased selectivity towards methylcyclohexenes was observed for each of the ionic liquids investigated, compared to the uncoated catalyst and the data suggests that there is an optimal ionic liquid loading for each ionic liquid. Despite this, the ionic liquid that showed a good balance between activity and methylcyclohexene selectivity is [BMIM][NTf₂]. Preliminary evaluations of a RuSCILL catalyst coated in [OMIM][NTf₂], which has a higher solubility for the substrate, proved the potential of this type of catalyst in gas phase continuous flow processes. The use of ionic liquids as coatings for solid supported catalysts, in SCILL systems, is relatively unexplored. Given the scope for producing ionic liquids with various properties, it is simply a matter of screening ionic liquids according to their interaction with the catalyst and reaction mixtures. This method of modifying the catalyst and changing the catalytic system dynamics where solubility of substrates and products is concerned provides a simple solution to the conventional methods previously discussed for producing partially hydrogenated products.

4.5 References

- [1] K. Weissermel and H.-J. Arpe, *Industrial Organic Chemistry*, VCH, New York, **1993**.
- [2] L. M. Rossi and G. Machado, *J. Mol. Catal. A: Chem.* **2009**, *298*, 69.
- [3] A. Corma, A. Martínez and V. Martínez-Soria, *J. Catal.* **1997**, *169*, 480.
- [4] S. C. Hu and Y. W. Chen, *J. Chem. Technol. Biotechnol.* **2001**, *76*, 954.
- [5] V. Mazzieri, F. Coloma-Pascual, A. Arcoya, P. L'Argentiere and N. S. Figoli, *Appl. Surf. Sci.* **2003**, *210*, 222-230.
- [6] A. G. Shastri, J. Schwank and S. Galvagno, *J. Catal.* **1986**, *100*, 446.
- [7] C. Milone, G. Neri, A. Donato and M. G. Musolino, *J. Catal.* **1996**, *159*, 253.
- [8] L. Ronchin and L. Toniolo, *Catal. Today* **2001**, *66*, 363.
- [9] E. T. Silveira, A. P. Umpierre, L. M. Rossi, G. Machado, J. Morais, G. V. Soares, I. L. R. Baumvol, S. R. Teixeira, P. F. P. Fichtner and J. Dupont, *Chem. Eur. J.* **2004**, *10*, 3734.
- [10] S.-C. Hu and Y.-W. Chen, *Ind. Eng. Chem. Res.* **1997**, *36*, 5153.
- [11] S.-C. Hu and Y.-W. Chen, *Ind. Eng. Chem. Res.* **2001**, *40*, 6099.
- [12] S.-C. Hu and Y.-W. Chen, *Ind. Eng. Chem. Res.* **2001**, *40*, 3127.

- [13] Z. Liu, W.-L. Dai, B. Liu and J.-F. Deng, *J. Catal.* **1999**, *187*, 253.
- [14] L. Ronchin and L. Toniolo, *Appl. Catal. A: Gen* **2001**, *208*, 77.
- [15] S. Xie, M. Qiao, H. Li, W. Wang and J.-F. Deng, *Appl. Catal. A: Gen* **1999**, *176*, 129.
- [16] M. H. G. Precht, M. Scariot, J. D. Scholten, G. Machado, S. R. Teixeira and J. Dupont, *Inorg. Chem.* **2008**, *47*, 8995.
- [17] E. T. Silveira, A. P. Umpierre, L. M. Rossi, G. Machado, J. Morais, G. V. Soares, I. J. R. Baumvol, S. R. Teixeira, P. F. P. Fichtner and J. Dupont, *Chem. Eur. J.* **2004**, *10*, 3734.
- [18] S. S. Divekar, B. M. Bhanage, R. M. Deshpande, R. V. Gholap and R. V. Chaudhari, *J. Mol. Catal.* **1994**, *91*, L1.
- [19] C. P. Mehnert, E. J. Mozeleski and R. A. Cook, *Chem. Commun.* **2002**, 3010.
- [20] M. Haumann and A. Riisager, *Chem. Rev.* **2008**, *108*, 1474.
- [21] J.-P. Mikkola, P. Virtanen, H. Karhu, T. Salmi and D. Y. Murzin, *Green Chem.* **2006**, *8*, 197.
- [22] U. Kernchen, B. Etzold, W. Korth and A. Jess, *Chem. Eng. Technol.* **2007**, *30*, 985.
- [23] T. Nakamura, M.-a. Ohshima, H. Kurokawa and H. Miura, *Chem. Lett.* **2010**, *36*, 62.
- [24] X. Zhou, T. Wu, B. Hu, T. Jiang and B. Han, *J. Mol. Catal. A: Chem.* **2009**, *306*, 143.
- [25] G. Süss-Fink, B. Mollwitz, B. Therrien, M. Dadrás, G. Laurenczy, A. Meister and G. Meister, *J. Cluster Sci.* **2007**, *18*, 87.
- [26] M. Jahjah, Y. Kihn, E. Teuma and M. Gómez, *J. Mol. Catal. A: Chem.* **2010**, *332*, 106.
- [27] M. Fang, N. Machalaba and R. A. Sánchez-Delgado, *Dalton Trans.* **2011**, *40*, 10621.
- [28] F. Haretog and P. Zwietering, *J. Catal.* **1963**, *2*, 79.
- [29] J. Ning, J. Xu, J. Liu and F. Lu, *Catal. Lett.* **2006**, *109*, 175.
- [30] M. Sobota, M. Happel, M. Amende, N. Paape, P. Wasserscheid, M. Laurin and J. Libuda, *Adv. Mater.* **2011**, *23*, 2617.
- [31] H.-P. Steinrück, J. Libuda, P. Wasserscheid, T. Cremer, C. Kolbeck, M. Laurin, F. Maier, M. Sobota, P. S. Schulz and M. Stark, *Adv. Mater.* **2011**, *23*, 2571.
- [32] P. J. Dyson, D. J. Ellis, W. Henderson and G. Laurenczy, *Adv. Synth. Catal.* **2003**, *345*, 216.

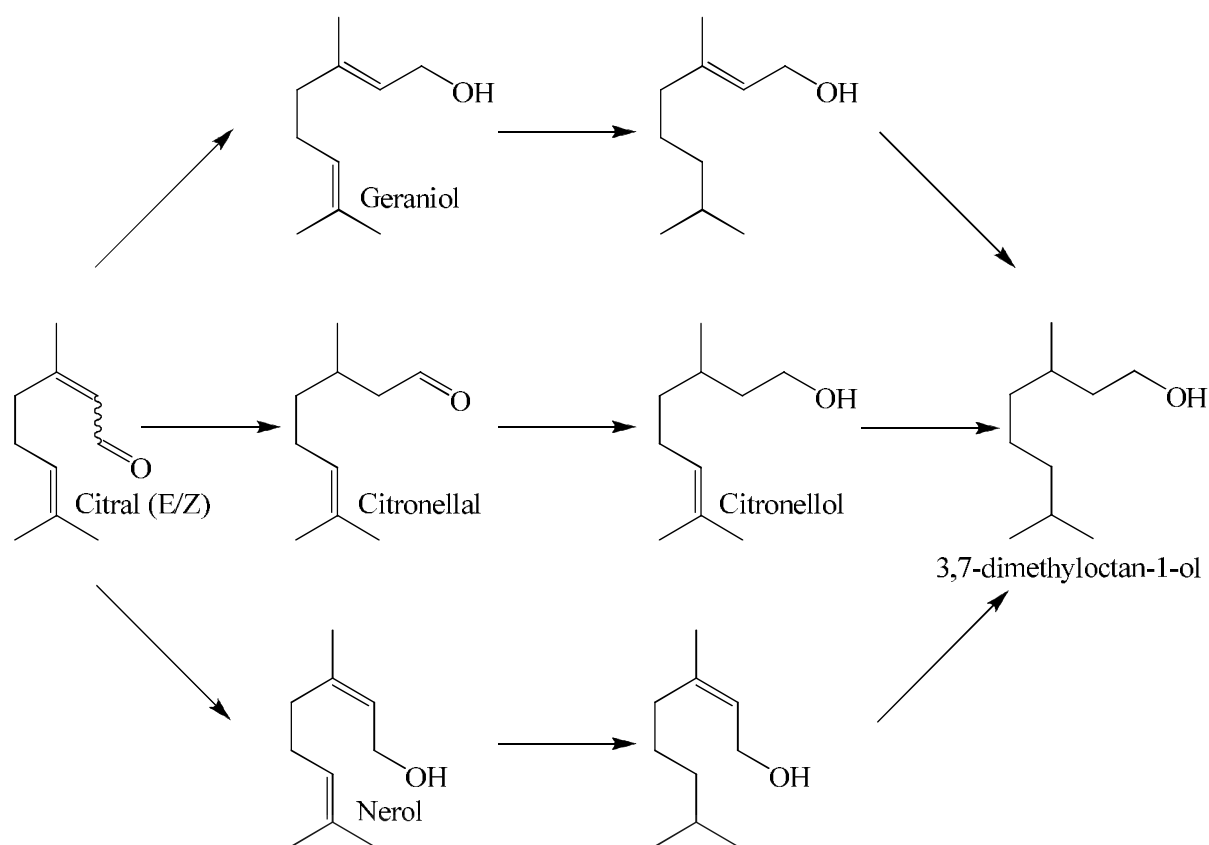
Chapter 5 - Hydrogenation of α,β -unsaturates.

5.1 Introduction

Studies into the activity and selectivity of catalysts are especially important when evaluating a new catalytic system. One model reaction that helps evaluate the potential catalytic application of heterogeneous catalysts is the chemoselective hydrogenation of α,β -unsaturated compounds. Terpenes are a class of compounds commonly used in the production of flavours, pharmaceuticals and fragrances with a large variety of these compounds being classified as α,β -unsaturated compounds. These compounds are usually extracted from the essential oils of plants using methods such as fractional distillation. Terpenoids like geraniol and its isomer nerol are commonly used in fragrances to contribute to a rose and citrus aroma respectively.¹ These can be synthetically derived from the selective hydrogenation of the α,β -unsaturated compound, citral, depending on whether hydrogenation occurs on the C=C bonds or the C=O bond.

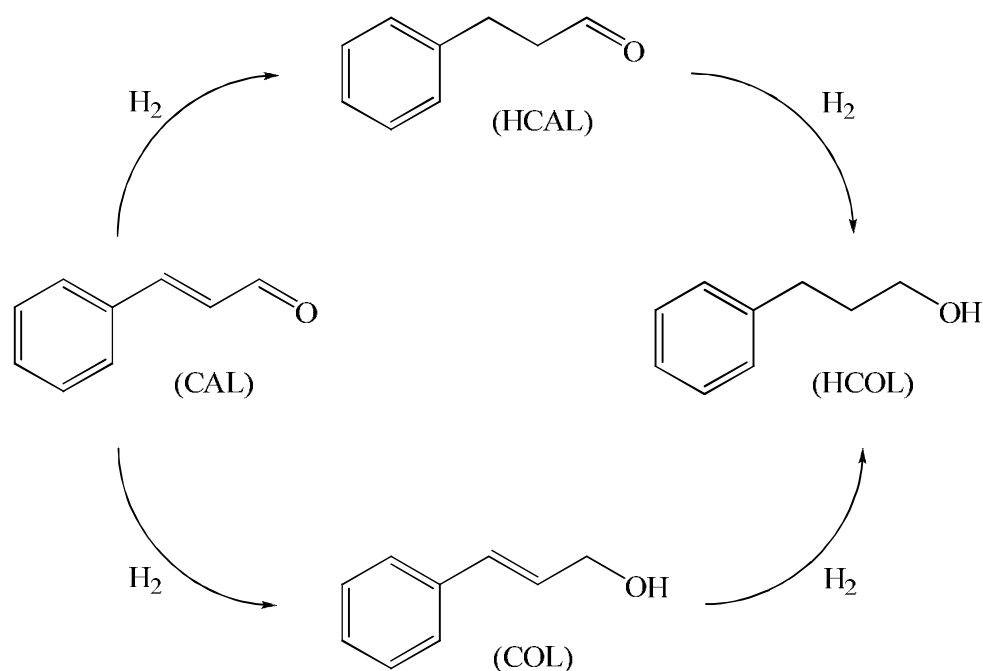
Investigations into the chemoselective hydrogenation of α,β -unsaturated compounds date as far back as the mid-1920s. The importance of unsaturated alcohols as an intermediate in the preparation of pharmaceuticals and fine chemicals has kept the chemoselective hydrogenation of α,β -unsaturated compounds a “hot topic”. In practice, the chemoselective hydrogenation proves challenging as the hydrogenation of the C=C bond is thermodynamically favoured over that of C=O by approximately a 35 kJ/mol difference.² Additionally, for kinetic reasons, C=C bond reactivity is higher than that of the C=O bond for hydrogenation. As a result, numerous theoretical studies have been conducted and comprehensive reviews published addressing this subject.³⁻⁶

The selectivity towards hydrogenation of the C=C bond and C=O bond is usually metal specific. In the case of citral hydrogenation, when considering supported Ru catalysts, the hydrogenation reaction produces citronellal, geraniol, nerol and citronellol as shown in Scheme 5.1.⁷⁻¹³



Scheme 5.1. Scheme for the hydrogenation of citral.

In the case of cinnamaldehyde, the inclusion of an aromatic ring in the α,β -unsaturated compound causes additional complexity with regards to the steric hindrance of the benzene ring, an effect dependant on the particle size.¹⁴ Typically, three main products can form from the hydrogenation of cinnamaldehyde (CAL) namely hydrocinnamaldehyde (HCAL), cinnamyl alcohol (COL), and hydrocinnamyl alcohol (HCOL), as illustrated in Scheme 5.2. Additionally, the selectivity can be influenced by the support and the solvent used.⁵ Low selectivity towards COL of 13% was observed at a 20% conversion when evaluating a Ru/SiO₂ catalyst using 2-propanol as solvent at a temperature of 60 °C and a hydrogen pressure of 10 bar.¹⁵ This selectivity increased to 40% COL with the use of Ru/Al₂O₃, highlighting the influence of the support in the preparation of the catalyst.¹⁵ In the case of Ru immobilised on carbon nanofiber (CNF), a 48% COL selectivity was observed at a 60% CAL conversion using 2-propanol as a solvent at 110 °C and 45 bar H₂ pressure.¹⁶ Modification of these Ru catalysts by other metals such as iron,¹⁷ copper,¹⁸ cerium¹⁹ or tin^{9, 20-21} can change the selectivity of the reactions to favour the hydrogenation of the C=O bond.



Scheme 5.2. Scheme for the hydrogenation of CAL.

Ionic liquids are low melting salts that usually remain molten at ambient temperature or temperatures below 100 °C.²² They are characterised by their low vapour pressure and usefulness as solvent amongst others. With the increase in their applications in catalysis, novel concepts for metal complex immobilisation have been developed such as supported ionic liquid phase catalysts (SILP).²³ These catalytic systems consist of the catalyst, solubilised in the ionic liquid and dispersed on a solid support material. This decreases the diffusional barrier usually present for the ionic liquid in bulk phase by dispersing the ionic liquid over a large surface area support and creating an ionic liquid layer with a thickness in the nanometer regime. The SILP catalysts were found to catalyse hydrogenation²⁴ reactions and the hydroformylation^{23, 25-26} of alkenes. Similarly, ionic liquids could be used as a coating for a supported metal catalyst and is referred to as a solid catalyst with ionic liquid layer (SCILL). One of the first SCILL catalysts was a silica supported nickel SCILL catalyst.²² The ionic liquid coating enhanced selectivity towards cyclooctene in the hydrogenation of cyclooctadiene.

Citral hydrogenation in the presence of an ionic liquid was realised by using supported nickel-tin¹ and palladium^{1, 27} catalysts. The activity of the catalyst was considerably decreased because of the low hydrogen solubility in the ionic liquid. The issue of low hydrogen solubility can be addressed by utilising the ionic liquid and the supported catalyst according to

the SCILL concept earlier described. Claus *et al.* conducted one of the first studies into the evaluation of supported Ru SCILL catalysts in citral hydrogenation.²⁸ The Ru/Al₂O₃ was modified with an ionic liquid layer based on either ionic liquids with [PF₆]⁻ or [NTf₂]⁻ as the anion to prepare SCILL catalyst. The catalysts showed an increased selectivity towards the alcohols, geraniol and nerol. This study was further extended with specific focus on the use of the [NTf₂]⁻ based ionic liquids, 1-butyl-3-methylimidazolium bis(trifluoromethylsulfonyl)imide, [BMIM][NTf₂], and 1-hexyl-3-methylimidazolium bis(trifluoromethylsulfonyl)imide, [HMIM][NTf₂], and change in the amount of ionic liquid used.²⁹ The results support their initial study with observed selectivity towards geraniol and nerol. Increase in the amount of [BMIM][NTf₂] used had little effect on the selectivity but decreased the overall conversion. This can be ascribed to the increase in diffusional barrier with increase in the amount of ionic liquid. Nevertheless, the presence of the ionic liquid does influence the selectivity profile towards hydrogenation of the C=O bond.

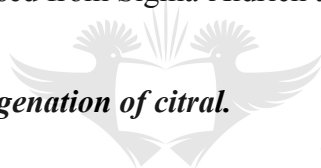
In the case of CAL hydrogenation, Pd based heterogeneous catalysts have been given most attention. Virtanen *et al.* evaluated a Pd supported ionic liquid catalyst (SILCA).³⁰ The catalyst consists of Pd nanoparticles in ionic liquid dispersed on a carbon cloth. The ionic liquids, *N*-butyl-4-methylpyridinium tetrafluoroborate, [NB4MPy][BF₄], and 1-butyl-3-methylimidazolium hexafluorophosphate, [BMIM][PF₆], were used and a lower conversion was observed for the latter. The selectivity was towards HCAL with the higher activity observed when using [NB4MPy][BF₄]. This observation was attributed to a possible increased solubility of H₂ for [NB4MPy][BF₄] compared to [BMIM][PF₆]. This study was further extended to include an investigation into the kinetics of the reaction.³¹ Similarly, Yokoyama *et al.* prepared a series of ionic liquid modified silica gels and with Pd nanoparticles dispersed in the grafted ionic liquid layer.³² The ionic liquids were *N*-3-(3-tri-ethoxysilylpropyl)-3-methylimidazolium based, [(TESP)MIm], with the anions, [Cl]⁻, [NO₃]⁻, [BF₄]⁻ and [PF₆]⁻. In each case, the selectivity was towards HCAL with turnover frequencies (TOF) of more than 22200 h⁻¹ in some cases.³² It is clear that there are many factors governing the activity and selectivity of the catalyst when utilised in the hydrogenation of α,β -unsaturated compounds. However, given the substantial amount of research conducted, the substrates citral and CAL are suitable compounds to benchmark the potential of the catalyst in the hydrogenation of α,β -unsaturated compounds.

This study focuses on the evaluation of Ru dendrimer encapsulated nanoparticles (DEN) supported on silica 60 as potential catalysts for the hydrogenation of citral and CAL. The dendrimer templated methodology of nanoparticle synthesis was chosen to ensure a narrow size distribution for the Ru nanoparticles prepared as detailed in chapter 2. The supported RuDEN catalysts were not calcined prior to use, to help maintain the stabilising effect of the dendrimer and thus help prevent sintering of the nanoparticles. The effect of an ionic liquid layer on the activity and selectivity of the uncoated catalyst was then evaluated for the ionic liquids, 1-butyl-3-methylimidazolium tetrafluoroborate, [BMIM][BF₄], [BMIM][PF₆], [BMIM][NTf₂], 1-ethyl-3-methylimidazolium ethylsulphate, [EMIM][EtS] and 1-ethyl-3-methylimidazolium octylsulphate, [EMIM][OcS].

5.2 Experimental

The substrates, standards and internal standard, citral, citronellal, citronellol, geraniol, nerol, cinnamaldehyde, hydrocinnamaldehyde, cinnamyl alcohol, hydrocinnamyl alcohol and n-decane were purchased from Sigma-Aldrich and used as received.

5.2.1 *Hydrogenation of citral.*



UNIVERSITY
OF
JOHANNESBURG

The hydrogenation of citral was performed in a Parr stainless steel autoclave with a volume of 100 cm³ fitted with a teflon cup, operated in batch mode and stirred at 1200 rpm. Depending on the reaction, the reaction conditions were set at 90 °C, 110 °C and 130 °C and a H₂ pressure of 10 bar and 30 bar. The catalyst (0.08-0.1 wt% Ru, 0.2-0.3 g, 1.84 μmol Ru) was transferred to the autoclave. The autoclave was charged with cyclohexane (30 cm³) and citral (0.156 cm³, 0.1393 g, 921.6 μmol) with n-decane as the internal standard (0.156 cm³). The reactor was purged thrice at ambient temperature with H₂ gas, depressurised and heated to 90 °C and allowed to stir at this temperature for 1 hour to allow catalyst activation. The desired temperature either 90, 110 or 130 °C was set and the reactor pressurised to a H₂ pressure of 10 bar or 30 bar to commence reaction. Samples of the reaction mixture were taken every 30 mins over a 240 min period and analysed by gas chromatography on a Shimadzu GC-2010 Plus equipped with a 30 m Restek Rtx-5 capillary column.

5.2.2 *Hydrogenation of cinnamaldehyde.*

The hydrogenation of cinnamaldehyde was performed in a Parr stainless steel autoclave with a volume of 100 cm³ fitted with a teflon cup, operated in batch mode and stirred at 1200 rpm. Depending on the reaction, the reaction conditions were set at 90 °C, 110 °C and 130 °C and a H₂ pressure of 10 bar, 30 bar and 40 bar. The catalyst (0.08-0.1 wt% Ru, 0.2-0.3 g, 1.84 μmol Ru) was transferred to the autoclave. The autoclave was charged with cyclohexane (30 cm³) and citral (0.116 cm³, 0.1218 g, 921.6 μmol) with n-decane as the internal standard (0.156 cm³). The reactor was purged thrice at ambient temperature with H₂ gas, depressurised and heated to 90 °C and allowed to stir at this temperature for 1 hour to allow catalyst activation. The desired temperature either 90, 110 or 130 °C was set and the reactor pressurised to a H₂ pressure of 10 bar, 30 bar or 40 bar to commence reaction. Samples of the reaction mixture were taken every 30 mins over a 240 min period and analysed by gas chromatography on a Shimadzu GC-2010 equipped with a 30 m Restek Rtx®-5 capillary column.

5.3 Results and discussion

5.3.1 *Evaluation of RuSil60 catalysts in the hydrogenation of citral.*

The series of RuSil60 catalysts, G4-RuSil60, G5-RuSil60 and G6-RuSil60 were evaluated in the hydrogenation of citral, with the intention of identifying a suitable catalyst for investigating the effect of ionic liquid coatings on those of the RuSil60 catalysts. Brief investigations into the effects of temperature and pressure on the activity of the catalyst were conducted using cyclohexane as the solvent. The effect of pressure on the conversion of citral was studied for a hydrogen pressure of 10 bar and 30 bar at a temperature of 90 °C and the reaction sampled at 120 and 240 minutes using the G4-RuSil60 catalyst. The conversion of citral at these conditions is illustrated in Figure 5.1. When comparing the results for citral conversion obtained at 10 bar and 30 bar, there is a 5-6% increase upon increasing the pressure from 10 bar. The increase in conversion of citral is therefore minimal for the threefold increase in hydrogen pressure. Despite the minimal increase, a hydrogen pressure of 30 bar was chosen to conduct further reactions. It must be noted that the increase in conversion of citral between 120 and 240 minutes is quite low suggesting that most of the conversion occurred during the initial stages of the reaction. The reaction methodology was revised to account for this and a 30-minute sampling interval adopted. The selectivity

observed in each reaction was towards citronellal exclusively. The results suggest that for the current reaction conditions, the hydrogenation of the C=C double bond is favoured.

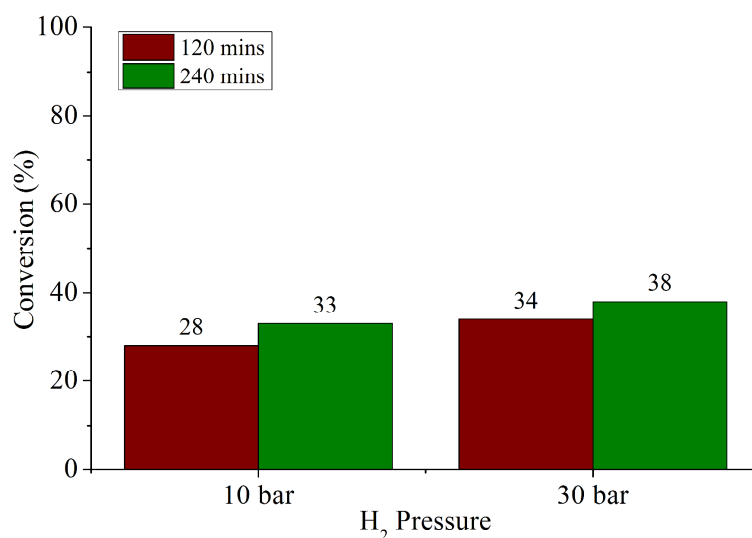


Figure 5.1. Pressure dependant conversion of citral at 120 minutes and 240 minutes for a H₂ pressure of 10 bar and 30 bar using the G4-RuSil60 catalyst.

The reaction conditions were then changed to investigate the effect of temperature on the activity and selectivity of the citral hydrogenation reaction. Figure 5.2 illustrates the time-resolved conversion of citral using the different RuSil60 catalysts and in the case of Figure 5.2(b), the end of run conversions of citral for the RuSil60 catalysts at different temperatures.

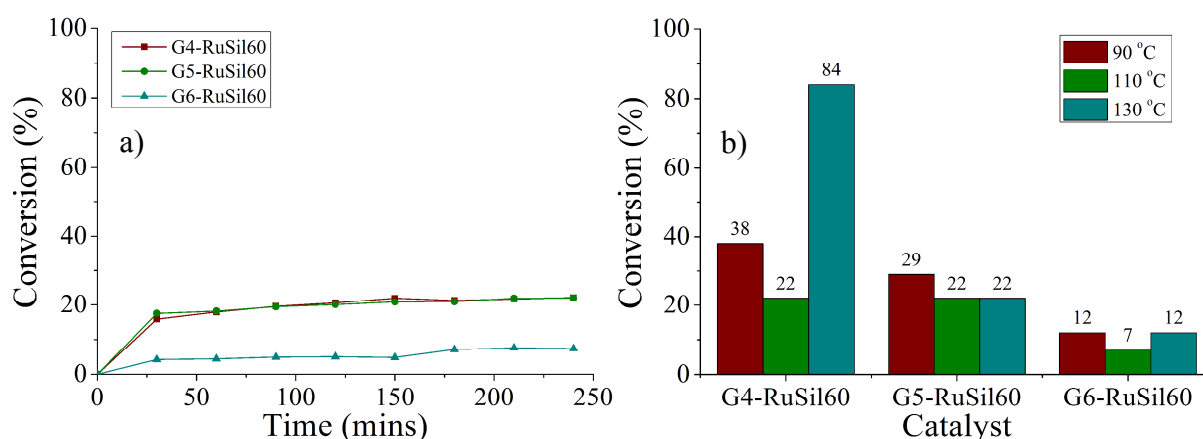


Figure 5.2. Conversion of citral using the various RuSil60 catalysts and at various temperatures illustrated by the, a) time-resolved conversion of citral at 110 °C and b) end of run conversion of citral at 90 °C, 110 °C and 130 °C.

The previous discussion on the effect of H₂ pressure on the conversion of citral, alluded to a possible larger initial conversion of citral when considering the minimal increase in conversion from 120 minutes to 240 minutes. Figure 5.2(a) illustrates this conversion trend where there is a high initial conversion of citral and levelling-off of the citral conversion during the course of the reaction. The reaction was therefore not allowed to exceed a 240-minute limit, as there is inhibition of the reaction after the higher initial activity. Important to note is that the catalyst is not deactivated as this would terminate the conversion and not just cause a decrease in the conversion rate. The effect of temperature on the end of run conversion of citral using the various RuSil60 catalysts is illustrated in Figure 5.2(b). The highest conversion was observed for the G4-RuSil60 catalyst for reactions conducted at 90 °C. This decrease in the conversion can be explained by the possible increase in steric hindrance with increase in dendrimer generation that inhibits adsorption of citral. When considering the effect of temperature increase on the conversion of citral for each of the RuSil60 catalysts, there is no evident correlation. The conversion of citral observed when evaluating G4-RuSil60 decreases with an increase in temperature from 90 °C to 110 °C and then increases upon increasing the temperature to 130 °C.

The decrease in conversion with increase in temperature can be explained by an increase in the inhibitory decarbonylation reaction.^{13, 33-35} This results in an increase in the amount of carbon monoxide which competitively adsorbs to active sites on the nanoparticle surface. The overall kinetic behaviour resulting from the decay in catalytic activity was seen for all citral hydrogenation reactions concerning the evaluation of RuSil60. Increase in temperature to 130 °C, leads to an increase in the conversion of citral in the case of G4-RuSil60 and G6-RuSil60. This increase in conversion is not observed upon increase of temperature to 130 °C when evaluating the G5-RuSil60 catalyst. The increase in conversion of citral upon increase in temperature to 130 °C is due to the increase in formation of unwanted side products as will be attended to in the discussion on selectivity. Given that the dendritic structure was not removed in preparation of the RuSil60 catalysts, increase in temperature shows little effect on the catalytic activity when evaluating the more sterically hindered G5-RuSil60 and G6-RuSil60.

As discussed earlier, the increase in temperature to 130 °C favours conversion of citral to isopulegol. Figure 5.3 illustrates the selectivity profile observed when evaluating the G6-RuSil60 catalyst at 110 °C and 130 °C and the G4-RuSil60 and G5-RuSil60 catalysts at 130 °C. The selectivity observed for all other reactions was exclusively for citronellal. When

considering the selectivity results obtained as detailed in Figure 5.3, there is a clear indication that the increased conversion of citral is a result of the increased formation of the side product isopulegol, formed by the cyclisation of citronellal.^{13, 35}

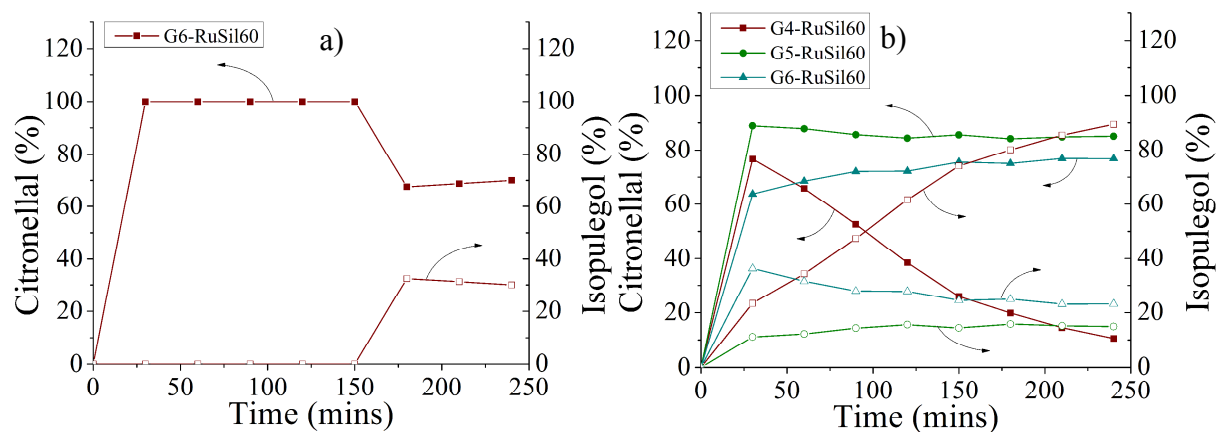


Figure 5.3. Selectivity observed for the citral hydrogenation reaction using the RuSil60 catalysts at a) 110 °C while evaluating G6-RuSil60 and b) 130 °C when evaluating G4-RuSil60, G5-RuSil60 and G6-RuSil60.

This causes an overall decrease in the percentage selectivity for citronellal. The overall percentage of citronellal in the reaction mixture does not change significantly when utilising G5-RuSil60 and G6-RuSil60, which indicates that formation of citronellal is rapid enough to compensate for the intrinsic rate of formation of isopulegol for the given reaction conditions. This is indicated by the levelling-off of the selectivity profiles for the evaluation of G5-RuSil60 and G6-RuSil60. The selectivity profile observed when evaluating G4-RuSil60 as a catalyst at 130 °C displays a dramatic increase in the selectivity towards isopulegol with time and this is met with a decrease in the selectivity towards citronellal. In this case, the formation of isopulegol is rapid enough to exceed formation of citronellal. The result suggests that the dendrimer stabiliser decomposes considerably at 130 °C. This results in a more exposed nanoparticle surface, allowing for an increase in the conversion of citral albeit with the formation of isopulegol.

5.3.2 Evaluation of RuSCILL catalysts in the hydrogenation of citral.

The results obtained for the RuSil60 catalysts indicate that the reaction is sensitive to the decarbonylation process that occurs during the hydrogenation of citral. This inhibitory effect is greatly due to the occupation of active sites by carbon monoxide that adsorbs on the

catalyst surface. The use of ionic liquid as a catalyst coating can influence the product selectivity observed when evaluating different catalysts. With this in mind, the results obtained when evaluating a series of RuSCILL catalysts with different ionic liquids is presented with focus on the effect of the ionic liquid on the catalyst activity and selectivity. The reactions were allowed to progress over a 240-minute period at 90 °C and a hydrogen pressure of 30 bar with sampling every 30 minutes. The temperature was chosen to help minimise any decomposition of the ionic liquid coating which can occur during reaction and further modify the nanoparticle surface.³⁶ Figure 5.4 illustrates the conversion of citral when using the various RuSCILL catalysts with the different ionic liquids.

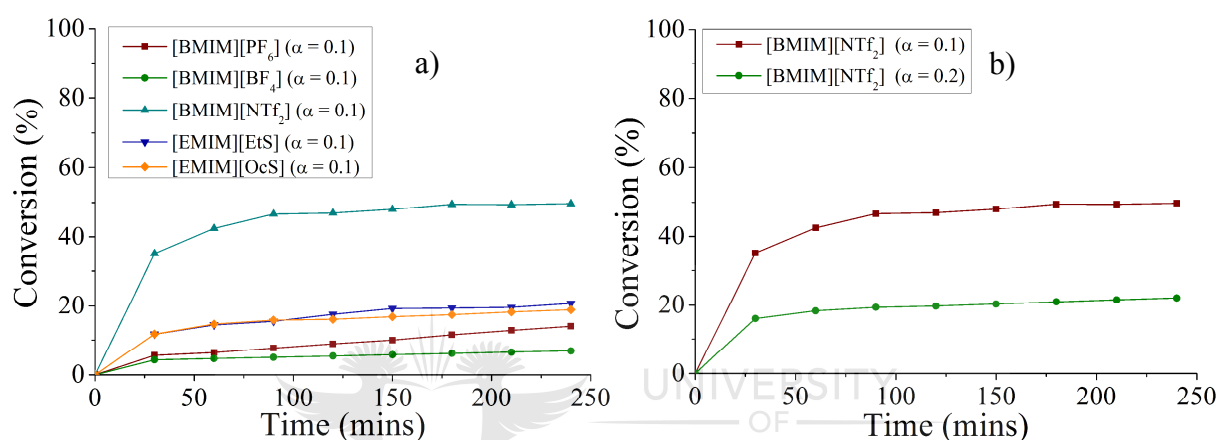


Figure 5.4. Conversion of citral using the various RuSCILL catalysts and at various temperatures. a) Time-resolved conversion of citral at 90 °C for various RuSCILL catalysts with an α -value of 0.1 and b) Time-resolved conversion of citral at 90 °C for various RuSCILL catalysts with the ionic liquid [BMIM][NTf₂] as coating for α -values of 0.1 and 0.2.

The end of run results for each of the evaluated RuSCILL catalysts and the G5-RuSil60 catalyst is presented in Table 5.1. When comparing the results of the RuSCILL catalysts to that of the RuSil60 catalyst, both increases and decreases in the conversion of citral were observed upon coating with the various ionic liquids. A decrease in the conversion was observed compared to the uncoated catalyst when using the ionic liquids [EMIM][EtS], [EMIM][OcS] and [BMIM][PF₆], [BMIM][BF₄] as coatings with an α -value of 0.1. The most significant decrease in activity was observed when using the [BMIM][PF₆] and [BMIM][BF₄] ionic liquid catalyst coatings as seen for entries 4 and 5 in Table 5.1.

In the case of [BMIM][PF₆], there is a 15% decrease in conversion, whereas a more evident 22% decrease in conversion was observed using [BMIM][BF₄] as the ionic liquid coating when compared to the uncoated catalyst.

Table 5.1. Citral hydrogenation results with G5-RuSil60 and RuSCILL catalysts in cyclohexane using various ionic liquids as coatings at a temperature of 90 °C and a H₂ pressure of 30 bar. Results shown are for end of run (240 mins).

Entry	Ionic liquid	α	Citral Conversion (%)	Citronellal (%)
1	None ^a	-	29	100
2	[BMIM][NTf ₂]	0.1	50	100
3	[BMIM][NTf ₂]	0.2	22	100
4	[BMIM][PF ₆]	0.1	14	100
5	[BMIM][BF ₄]	0.1	7	100
6	[EMIM][EtS]	0.1	21	100
7	[EMIM][OcS]	0.1	19	100

^a Uncoated G5-RuSil60 catalyst

When comparing entries 1 and 2, a significant increase in the conversion of citral to 50% was observed when using the ionic liquid [BMIM][NTf₂] as a catalyst coating with an α -value of 0.1 when compared to the uncoated catalyst, G5-RuSil60. This increase in conversion observed when using [BMIM][NTf₂] as an ionic liquid coating, suggests that the presence of this ionic liquid minimises the effect of decarbonylation. The increase in activity is most likely competitive displacement of CO by the ionic liquid. The [NTf₂]⁻ ionic liquids are known to displace CO, a property that was exploited in the study of ligand effects in a model SCILL system.³⁶ The ionic liquid was said to show strong ligand-like interactions with the surface of the nanoparticle. This would suggest that the ionic liquid has a negative effect on the activity of the nanoparticle given the strong interaction, possibly leading to an overwhelming competitive inhibition of adsorption of the substrate during reaction. This possible inhibition by a [BMIM][NTf₂] ionic liquid layer over a Pd/SiO₂ catalyst is, however, minimal in the hydrogenation of citral as observed by Claus *et al.*²⁹ The adsorption of H₂ to the catalyst surface is dependent on the partial pressure of the gas, especially when evaluating a SCILL catalyst. The ionic liquid therefore serves as a diffusional barrier, for a threshold partial pressure, inhibiting adsorption of CO, given the considerably lower partial pressure of CO when compared to H₂. In this sense, the ionic liquid has a two-fold purpose, providing a diffusional barrier for the CO gas, a poison, and additionally displacing any CO gas that coordinates to the nanoparticle surface. Despite the advantages, the inhibitory effects of CO was not completely overcome despite the increase in citral conversion observed over the uncoated catalyst. Given the promotional effect of [BMIM][NTf₂] on the catalytic activity of

the G5-RuSil60 catalyst for an α -value of 0.1, a RuSCILL catalyst with an increased ionic liquid layer thickness for an α -value of 0.2 using [BMIM][NTf₂] as ionic liquid was prepared and evaluated. The increase in ionic liquid coating to an α -value of 0.2, caused a significant decrease in the conversion of citral when compared to the [BMIM][NTf₂] coated catalyst in entry 2 and the uncoated catalyst in entry 1. The decrease in conversion of citral with an increase in the amount of [BMIM][NTf₂] most certainly is ascribed to the increase in ionic liquid layer thickness that causes some diffusion limitation for the substrate and reactants.

5.3.3 Evaluation of RuSil60 catalysts in the hydrogenation of cinnamaldehyde.

The RuSil60 catalysts were evaluated in the hydrogenation of CAL. Similar to citral, CAL has an α,β -unsaturated moiety, although bonded to an aromatic ring. This increases the complexity for selectivity during conversion as the hydrogenation can potentially occur on the C=C bond, the C=O bond of the aldehyde or the aromatic ring. Despite this, the hydrogenation of the aromatic ring carbon double bonds becomes progressively more difficult with more substituted aromatic ring systems.³⁷ Therefore, hydrogenation is likely to occur on the α,β -unsaturated moiety.

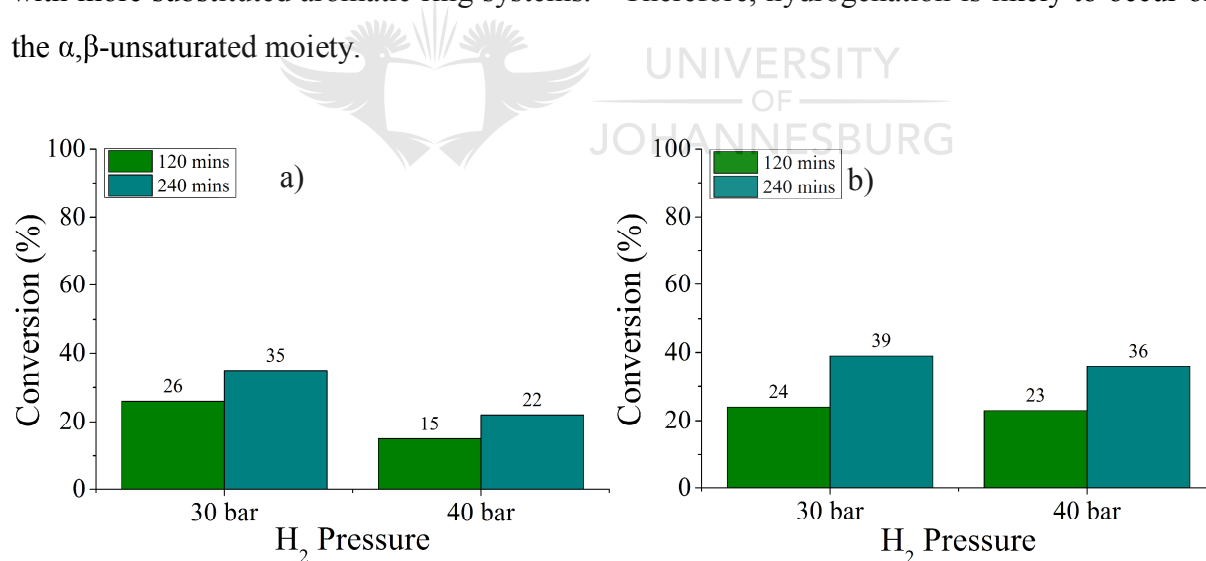


Figure 5.5. Pressure dependant conversion of CAL at 120 minutes and 240 minutes for a H₂ pressure of 30 bar and 40 bar at a temperature of a) 110 °C and b) 130 °C using the G6-RuSil60 catalyst.

The effect of pressure on the hydrogenation of CAL was investigated using the G6-RuSil60 catalyst as illustrated in Figure 5.5. Reactions conducted at a 10 bar H₂ pressure showed no activity. When considering the results illustrated in Figure 5.5(a), a decrease in the conversion of CAL was observed for an increase in hydrogen pressure from 30 bar to 40 bar at 110 °C.

The same behaviour was observed when conducting the pressure variation study at 130 °C, albeit the decrease in conversion with increase in pressure was not as pronounced as illustrated in Figure 5.5(b), where end of run conversion was only 3% lower for the pressure increase. The increase in pressure therefore seemed to have an inhibitory effect on the catalytic activity. The result suggests a possible competitive adsorption of hydrogen versus CAL on the catalyst surface for the pressure higher than 30 bar when using the G6-RuSil60 catalyst. This claim will, however, require further studies to substantiate and thus for the purposes of studying other reaction parameter effects, the H₂ pressure was kept at 30 bar.

The effect of reaction temperature on the activity and selectivity of the different RuSil60 catalysts was investigated for the temperatures 90 °C, 110 °C and 130 °C. Figure 5.6 illustrates the time resolved conversion of CAL at 90 °C and the end of run conversion of CAL when evaluating the various RuSil60 catalysts. A high initial conversion of CAL was observed when evaluating the G5-RuSil60 catalyst as illustrated in Figure 5.6(a). This conversion rate decreases somewhat after the first 30 minutes of reaction. This trend is similar to that observed for citral hydrogenation except that the inhibition is less pronounced for the hydrogenation of CAL.

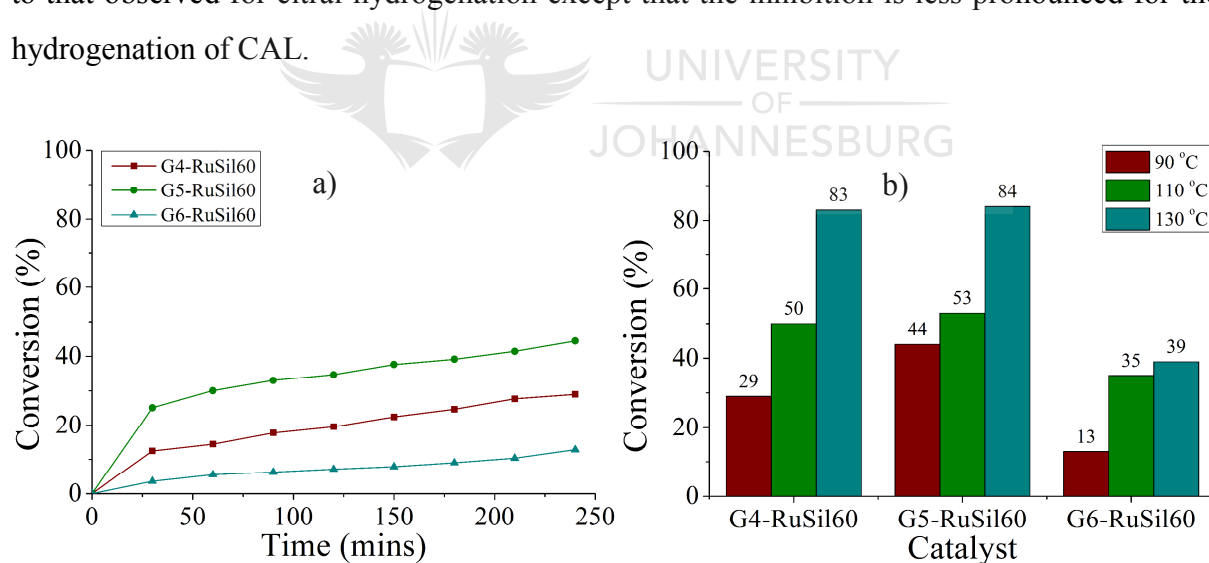


Figure 5.6. Conversion of CAL using the various RuSil60 catalysts and at various temperatures and a H₂ pressure of 30 bar. a) Time-resolved conversion of CAL at 90 °C and b) End of run conversion of citral at 90 °C, 110 °C and 130 °C.

Similarly, this behaviour was observed when evaluating the G4-RuSil60 catalyst; however, this trend was not as evident when evaluating the G6-RuSil60 catalyst. The catalytic rate increased with an increase in temperature as illustrated in Figure 5.6(b). Overall, the lowest activity was observed for the G6-RuSil60 catalyst. This is most likely because of the

increased steric crowding by the higher generation dendrimer, which restricts diffusion of the substrate to the nanoparticle surface similar to the results obtained when evaluating the hydrogenation of citral. The end of run conversions observed when evaluating the G4-RuSil60 and G5-RuSil60 catalysts are similar when conducting the reaction at 110 °C and 130 °C. When considering the end of run conversion for reactions conducted at 90 °C, G5-RuSil60 shows the highest conversion of CAL. To gain better insight into the performance of the catalyst, the catalytic activity was evaluated with regard to the selectivity for the various catalytic products.

Figure 5.7 illustrates the time-resolved selectivity profile for each of the RuSil60 catalysts at 90 °C. In each case, the selectivity is towards HCAL with a steady decrease with time when evaluating the G4-RuSil60 catalyst and less significant decrease with time when evaluating the G5-RuSil60 and G6-RuSil60 catalysts. Table 5.2 presents the end of run data obtained for the RuSil60 catalysts at the various temperatures. The selectivity was towards HCAL in each case, showing selectivity for the hydrogenation of the C=C double bond. Reactions conducted at 110 °C and 130 °C, when evaluating G4-RuSil60 and G5-RuSil60, show an increase in the selectivity towards HCOL, a product of the full hydrogenation of CAL.

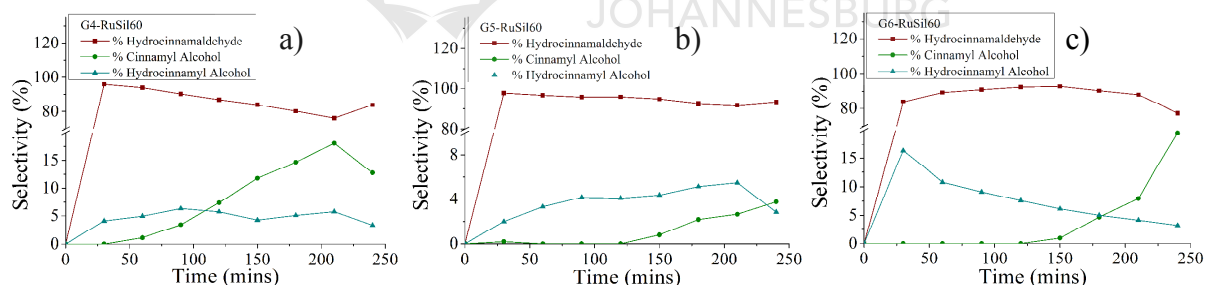


Figure 5.7. Selectivity observed for the CAL hydrogenation reaction at 90 °C and a 30 bar H₂ pressure for the RuSil60 catalysts : a) G4-RuSil60, b) G5-RuSil60 and c) G6-RuSil60.

An increase in the selectivity towards HCAL was observed when evaluating the G6-RuSil60 catalyst coupled with a lower conversion of CAL when compared to G6-RuSil60 and G5-RuSil60. The selectivity towards HCAL was highest, especially at higher temperature, when compared to the other RuSil60 catalysts. Studies into factors affecting the selectivities observed in the hydrogenation of α,β -unsaturated compounds reveal that basic promoters such as sodium hydroxide increase selectivity towards the saturated aldehyde.³⁸

Table 5.2. CAL hydrogenation results with RuSil60 catalysts in cyclohexane using various ionic liquids as coatings at a H₂ pressure of 30 bar. Results shown are for end of run.

Entry	Catalyst	Temperature (°C)	Conversion ^a (%)	Product selectivity (%)		
				HCAL	COL	HCOL
1	G4-RuSil60	90	29	84	13	3
2	G4-RuSil60	110	50	68	24	8
3	G4-RuSil60	130	83	57	19	24
4	G5-RuSil60	90	44	93	4	3
5	G5-RuSil60	110	53	71	18	11
6	G5-RuSil60	130	84	62	12	26
7	G6-RuSil60	90	13	77	20	3
8	G6-RuSil60	110	35	99	-	1
9	G6-RuSil60	130	39	93	6	1

^a End of run conversion at 240 mins.

Essentially, the G6-PAMAM-OH dendrimer that stabilises the Ru nanoparticles for G6-RuSil60 catalyst has the highest amount of tertiary amines. This increased basicity by the tertiary amines over that inherent to the G4-RuSil60 and G5-RuSil60 catalysts, could effectively increase selectivity towards the saturated aldehyde, HCAL. However, further studies are required to substantiate this reasoning. In each case, the full hydrogenation product derives from the further hydrogenation of either HCAL or COL.

5.3.4 Evaluation of RuSCILL catalysts in the hydrogenation of CAL.

The RuSCILL catalysts were evaluated for the various ionic liquids [BMIM][NTf₂], [BMIM][PF₆], [BMIM][BF₄], [EMIM][EtS] and [EMIM][OcS] for an α -value of 0.1 using the G5-RuSil60 catalyst with reaction conditions of 30 bar H₂ and a temperature of 90 °C. The time resolved conversion of CAL is illustrated in Figure 5.8 for the various RuSCILL catalysts.

The initial conversion (30 minutes) is high and with the catalytic rate somewhat lower for the remainder of the reaction. Similar to the hydrogenation of citral, the decarbonylation is likely present during the hydrogenation of CAL.

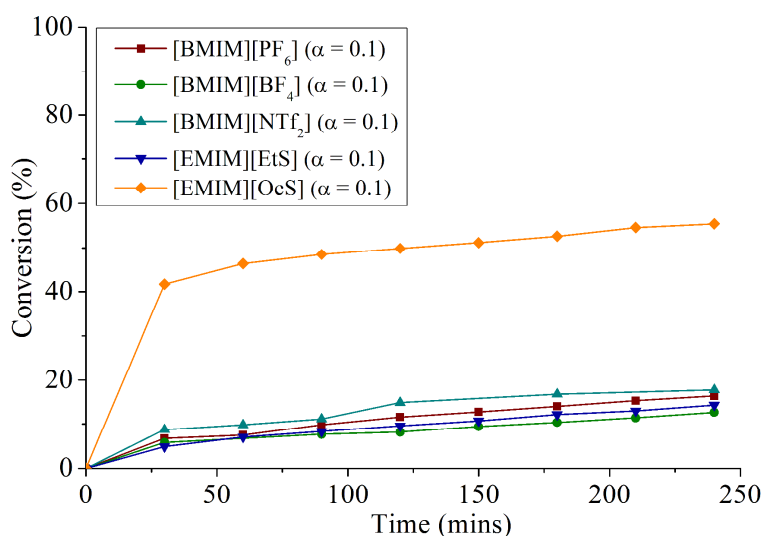


Figure 5.8. Time-resolved conversion of CAL using the various RuSCILL catalysts with an α -value of 0.1 and at 90 °C and 30 bar H₂.

Table 5.3 presents the end of run data collected at 240 minutes when evaluating the G5-RuSil60 and RuSCILL catalysts in the hydrogenation of CAL. The results for entries 2-6 indicate a significant increase in the activity of the catalyst when using the ionic liquid, [EMIM][Ocs]. In the case of the remaining ionic liquids used as coatings, there was hardly any difference in conversion. When comparing the results obtained when using [EMIM][Ocs] as ionic liquid coating to that of the uncoated catalyst, an increase in conversion was observed. The [EMIM][Ocs] therefore has a positive effect on the catalyst properties. The remaining ionic liquids caused a significant decrease in the activity when used as a coating for the G5-RuSil60 catalyst. The lack in variation of the conversion results when considering the [BMIM]⁺ ionic liquids for entries 2-4 suggest that the anions, namely [NTf₂]⁻, [PF₆]⁻ and [BF₄]⁻, are not as significant in increasing the performance of the catalyst. The use of [EMIM][EtS] with its shorter cation chain length compared to the [BMIM]⁺ ionic liquids showed no significant change in catalytic activity. However, comparison of the results obtained when using [EMIM][EtS] and [EMIM][Ocs] reveals that the possible enhancement in catalytic activity is due to the presence of the longer alkyl side chain for the [Ocs]⁻. This could suggest a possible interaction of the anion with the catalyst surface that modifies the catalytic surface and to some degree prevents adsorption of the CAL for reaction to occur.

Table 5.3. CAL hydrogenation results with G5-RuSil60 and RuSCILL catalysts in cyclohexane using various ionic liquids as coatings. Results shown are for end of run (240 mins).

Entry	Ionic liquid	Conversion (%)	Product selectivity (%)		
			HCAL	COL	HCOL
1	None ^a	44	93	4	3
2	[BMIM][NTf ₂]	18	100	-	-
3	[BMIM][PF ₆]	16	100	-	-
4	[BMIM][BF ₄]	13	100	-	-
5	[EMIM][EtS]	14	100	-	-
6	[EMIM][OcS]	55	100	-	-

^a G5-RuSil60 catalyst

Given the complexity of the effect of ionic liquids on catalytic activity, further studies are required to ascertain the effects of the anion on the catalytic activity where the ionic liquids with long chain anions should be evaluated.

5.4 Conclusion

In the present study a series of silica supported RuDENs were synthesised and evaluated in the chemoselective hydrogenation of the α,β -unsaturated compounds, citral and cinnamaldehyde. The effects of changes in reaction parameters were investigated and a strong dependence on temperature was observed when considering the selectivity. Unfortunately, higher temperatures favour the formation of side products such as isopulegol in the case of the citral hydrogenations. When comparing the yield of each reaction, the data suggests a dependence on the nature of the stabiliser on the activity. It is, however, difficult to compare the activity conclusively given the poisoning by CO or the high to exclusive selectivity towards C=C bond hydrogenation at conditions used to evaluate both Ru-Sil60 and RuSCILL catalysts. The decarbonylation pathway for the hydrogenation reactions has a detrimental effect on the activity of the catalyst and inhibition was observed after an initial higher catalytic activity in all cases. The use of ionic liquids as catalyst coatings had a positive effect on the catalytic activity in some instances, a reason certainly ascribed to the displacement of the adsorbed CO poison on the catalyst surface formed during decarbonylation. This increase

in activity with addition of an ionic liquid coating was not observed for all the ionic liquids and might be related to the coordination strength of the ionic liquid on the nanoparticle surface. The presence of the ionic liquid did, however, influence selectivity towards hydrogenation of the C=C bond in each case. Further studies are required to better understand the details surrounding the effects of ionic liquids on the activity and selectivity of the catalyst.

5.5 References

- [1] M. Steffan, M. Lucas, A. Brandner, M. Wollny, N. Oldenburg and P. Claus, *Chem. Eng. Technol.* **2007**, *30*, 481.
- [2] C. Mohr and P. Claus, *Sci. Prog.* **2001**, *84*, 311.
- [3] P. Claus, *Top. Catal.* **1998**, *5*, 51.
- [4] P. Gallezot and D. Richard, *Catal. Rev. Sci. Eng.* **1998**, *40*, 81.
- [5] P. Mäki-Arvela, J. Hájek, T. Salmi and D. Y. Murzin, *Appl. Catal. A: Gen* **2005**, *292*, 1.
- [6] V. Ponec, *Appl. Catal. A* **1997**, *149*, 27.
- [7] J. Álvarez-Rodríguez, A. Guerrero-Ruiz, I. Rodríguez-Ramos and A. Arcoya-Martín, *Catal. Today* **2005**, *107-108*, 302.
- [8] B. Bachiller-Baeza, A. Guerrero-Ruiz, P. Wang and I. Rodríguez-Ramos, *J. Catal.* **2001**, *204*, 450.
- [9] S. Galvagno, C. Milone, A. Donato, G. Neri and R. Pietropaolo, *Catal. Lett.* **1993**, *18*, 349.
- [10] D. Manikandan, D. Divakar and T. Sivakumar, *Catal. Lett.* **2008**, *123*.
- [11] L. Mercadante, G. Neri, C. Milone, A. Donato and S. Galvagno, *J. Mol. Catal. A: Chem* **1996**, *105*, 93.
- [12] G. Neri, L. Mercadante, A. Donato, A. M. Visco and S. Galvagno, *Catal. Lett.* **1994**, *29*, 379.
- [13] U. K. Singh and M. A. Vannice, *J. Catal.* **2001**, *199*, 73.
- [14] X. Ni, B. Zhang, C. Li, M. Pang, D. Su, C. T. Williams and C. Liang, *Catal. Commun.* **2012**, *24*, 65.
- [15] M. Lashdaf, A. O. I. Krause, M. Lindblad, M. Tiitta and T. Venäläinen, *Appl. Catal. A* **2003**, *241*, 65.
- [16] M. L. Toebes, F. F. Prinsloo, J. H. Bitter, A. J. v. Dillen and K. P. d. Jong, **2003**.

- [17] B. Bachiller-Baeza, A. Guerrero-Ruiz, P. Wang and I. Rodríguez-Ramos, *J. Catal.* **2001**, *204*, 450.
- [18] J. Álvarez-Rodríguez, A. Guerrero-Ruiz, I. Rodríguez-Ramos and A. Arcoya, *Micropor. Mesopor. Mater.* **2008**, *110*, 186.
- [19] B. Bachiller-Baeza, I. Rodríguez-Ramos and A. Guerrero-Ruiz, *Appl. Catal. A* **2001**, *205*, 227.
- [20] S. Galvagno, C. Milone, A. Donato, G. Neri and R. Pietropaolo, *Catal. Lett.* **1993**, *17*, 55.
- [21] A. M. Silva, O. A. A. Santos, M. J. Mendes, E. Jordão and M. A. Fraga, *Appl. Catal. A* **2003**, *241*, 155.
- [22] U. Kernchen, B. Etzold, W. Korth and A. Jess, *Chem. Eng. Technol.* **2007**, *30*, 985.
- [23] M. Haumann and A. Riisager, *Chem. Rev.* **2008**, *108*, 1474.
- [24] C. P. Mehnert, E. J. Mozeleski and R. A. Cook, *Chem. Commun.* **2002**, 3010.
- [25] C. P. Mehnert, R. A. Cook, N. C. Dispenziere and M. Afeworki, *J. Am. Chem. Soc.* **2002**, *124*, 12932.
- [26] A. Riisager, R. Fehrmann, S. Flicker, R. v. Hal, M. Haumann and P. Wasserscheid, *Angew. Chem. Int. Ed.* **2005**, *44*, 815.
- [27] K. Anderson, P. Goodrich, C. Hardacre and D. W. Rooney, *Green Chem.* **2003**, *5*, 448.
- [28] J. Arras, M. Steffan and P. Claus, in *1st SynTOP Smart Synthesis and Technologies for Organic Processes*, VDI-Berichte 2039, VDI-Verlag GmbH, Postdam, Germany, **2008**, pp. 109-114.
- [29] J. Arras, M. Steffan, Y. Shayeghi, D. Ruppert and P. Claus, *Green Chem.* **2009**, *11*, 716.
- [30] P. Virtanen, H. Karhu, K. Kordas and J.-P. Mikkola, *Chem. Eng. Sci.* **2007**, *62*, 3660.
- [31] P. Virtanen, T. Salmi and J.-P. Mikkola, *Ind. Eng. Chem. Res.* **2009**, *48*, 10335.
- [32] Y. Kume, K. Qiao, D. Tomida and C. Yokoyama, *Catal. Commun.* **2008**, *9*, 369.
- [33] M. Burgener, R. Wirz, T. Mallat and A. Baiker, *J. Catal.* **2004**, *228*, 152.
- [34] P. Mäki-Arvela, N. Kumar, K. Eränen, T. Salmi and D. Y. Murzin, *Chem. Eng. J.* **2006**, *122*, 127.
- [35] J. Álvarez-Rodríguez, I. Rodríguez-Ramos, A. Guerrero-Ruiz, E. Gallegos-Suarez and A. Arcoya, *Chem. Eng. J.* **2012**, *204-206*, 169.
- [36] M. Sobota, M. Happel, M. Amende, N. Paape, P. Wasserscheid, M. Laurin and J. Libuda, *Adv. Mater.* **2011**, *23*, 2617.

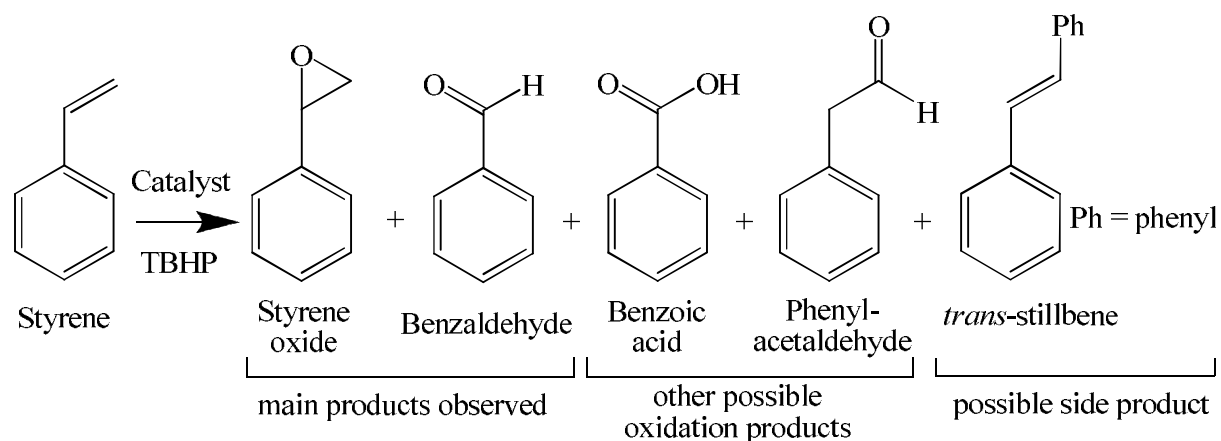
- [37] M. H. G. Pechtl, M. Scariot, J. D. Scholten, G. Machado, S. R. Teixeira and J. Dupont, *Inorg. Chem.* **2008**, *47*, 8995.
- [38] V. Satagopan and S. B. Chandalia, *J. Chem. Technol. Biotechnol.* **1994**, *59*, 257.



Chapter 6 – The oxidation of styrene using RuDENs and silica-supported RuDENs as catalysts with *t*-butyl hydroperoxide as oxidant and the effect of ionic liquids as additives.

6.1 Introduction

The selective liquid phase oxidation of hydrocarbons is a broad area of research. Most catalytic systems utilised in industry comprise the use of mixed metal oxides or ordered mesoporous materials as catalysts. The performance of such catalysts in commercial applications and the general trends observed in their utilisation is the subject of recent literature.¹⁻³ The epoxidation of alkenes can be catalysed by using supported metal nanoparticles, with gold catalysts having received significant attention over the past years.⁴ Research into the epoxidation of styrene is of great scientific importance as this reaction is often used as a probe into the activity of catalysts in the epoxidation of terminal alkenes.⁵⁻⁷ Styrene oxide is an important intermediate in the formation of various other fine chemicals and even pharmaceuticals. The conventional method of styrene oxide production uses styrene as a starting material and oxidation occurs in the presence of a suitable oxidising agent, usually a peracid. The use of peracids, however, has the disadvantage that these oxidizing agents are corrosive, hazardous to handle and may lead to the formation of undesired side products. As an alternative, safer oxidising agents, such as the peroxides TBHP and H₂O₂ can be used as oxidants in the oxidation of styrene with the possible products illustrated in Scheme 6.1.



Scheme 6.1. Illustration of the styrene oxidation by TBHP.

The organic peroxide TBHP is one of the most commonly used peroxides and serves as a better oxidant for alkene oxidations. The conventional catalysts utilised in styrene oxidation can include the use of gold and silver nanoparticles and highly active molybdenum-cobalt catalysts. The use of supported dendrimer templated gold nanoparticles supported on titania has been studied.⁸

Ruthenium metal nanoparticles are a versatile redox catalyst and in the case of oxidation reactions, are usually utilised in the oxidation of alcohols.⁴ These can include various activated alcohols such as benzylic and allylic alcohols and unactivated alcohols such as saturated alcohols. White *et al.* prepared RuO₂ nanoparticles with a mean diameter of 1.3 nm on a zeolite support using a hydrothermal method.⁹ The catalyst exhibited a high conversion in the aerobic oxidation of alcohols under mild reaction conditions with turnover numbers (TON) of 5-15. Mizuno *et al.* evaluated the alumina supported Ru catalysts, Ru/Al₂O₃, in the solvent-free oxidation of alcohols.¹⁰ The study demonstrated the versatility of the catalyst to oxidize alcohols, which can possess sulphur atoms, nitrogen atoms or carbon-carbon double bonds. Additionally, it could be recycled several times without loss in activity and without any leaching. The applicability of commercially available Ru catalysts was demonstrated by evaluating the commercial Ru/C catalyst in the oxidation of alcohols.¹¹ The heterogeneous Ru/C catalyst catalysed the oxidation of primary and secondary benzyl alcohols to their corresponding carbonyl compounds at temperatures ranging from 50-90 °C. Importantly, the general applicability of the commercial Ru/C catalysts was demonstrated by further oxidation reactions utilising allylic and aliphatic alcohols. Despite the progress in the use of Ru nanoparticles in the oxidation of alcohols, there are few literature reports as observed in a recent review.⁴ This versatility of Ru nanoparticles in catalysis and especially oxidation should be extended to other oxidation reactions such as the epoxidation of alkenes.

Given this potential avenue of investigation into the versatility of ruthenium as an oxidation catalyst, there are considerations to be taken when choosing a ruthenium nanoparticle catalyst. Transition metal nanoparticles with a narrow or uniform size distribution are desired with aims at correlating any changes in catalyst activity with the physical characteristics to some degree. Various methods exist for the preparation of nanoparticles, including the use of ionic liquids,¹² polymers,¹³ low molecular weight¹⁴ and macromolecular organic ligands¹⁵ as stabilisers all of which are categorised by their ability to stabilise nanoparticles. Dendrimers are classified as a macromolecular organic ligand and are used as stabilisers in the preparation

of dendrimer templated nanoparticles. The commercially available PAMAM dendrimer proves a versatile dendrimer template due to the presence of stabilising internal tertiary amines found within the dendritic architecture. While PAMAM dendrimers prove to be good stabilisers, of greater importance is the minimal passivation of the catalytic surface by the tertiary amines, making these DENs ideal for catalytic evaluation.¹⁵⁻¹⁷ Few studies exist detailing the use of RuDENs in catalytic reactions and to the best of our knowledge; none exist so far detailing the use of RuDENs as catalysts for the epoxidation of alkenes. An important aspect in the epoxidation of alkenes is the optimisation of selectivity towards the epoxide.

Ionic liquids are salts with melting points below 100 °C. They have attracted attention in catalytic reactions and can affect the selectivity profiles of certain reactions.¹² Concerning the oxidation of styrene, relatively few studies exist utilising the ionic liquid as a solvent or additive to investigate their effect on the selectivity of the reaction. The effect of catalytic amounts of the ionic liquids [BMIM][BF₄] and [BMIM][PF₆] (*ca.* 2.5 wt% of substrate) on the oxidation of styrene by H₂O₂ in the presence of palladium chloride as a catalyst was investigated.¹⁸ Subsequently, a mixture of [BMIM][BF₄] and water was used as reaction media to conduct the Wacker oxidation using a Pd/Cu catalyst under oxygen atmosphere.¹⁹ Han *et al.* evaluated a series of Ni²⁺-containing ionic liquids immobilized on silica in the oxidation of styrene using H₂O₂ as an oxidant but the selectivity was primarily towards benzaldehyde.²⁰ Chiappe *et al.* conducted a somewhat comprehensive screening of ionic liquids as solvents for the oxidation of the styrene using PdCl₂ as the catalyst precursor and H₂O₂ as the oxidant.²¹ Various hydrophilic and hydrophobic ionic liquids were utilised where the former favoured the oxidation products and the latter, the formation of dimerization side product and the phenylmethylketone product. They reasoned that the formation of Pd(0) in the hydrophobic ionic liquid was the cause for the side products.

Given the relatively unexplored utilisation of Ru nanoparticles in the oxidation reactions, especially when compared to metals such as gold, investigations were conducted into evaluation of RuDENs as catalysts in the oxidation of alkenes. The RuDEN catalysts were prepared utilising the G4-PAMAM-OH, G5-PAMAM-OH and G6-PAMAM-OH dendrimers as templates for various dendrimer:metal ion ratios. The resulting RuDENs were supported on silica 60 with aims of heterogenising the system. The RuDENs solutions and silica supported RuDEN catalysts, described in an earlier chapter, were evaluated as oxidation catalysts in the

epoxidation of styrene as a model for their activity towards the oxidation of terminal alkenes. Thereafter, the effects of the ionic liquids [BMIM][PF₆], [BMIM][BF₄], [BMIM][NTf₂], [EMIM][EtS] and [EMIM][OCS] as an additive was investigated for the various systems for various masses of the ionic liquid added to the reaction.

6.2 Experimental

The substrates, standards and internal standard, styrene, styrene oxide, benzaldehyde, benzoic acid, phenylacetaldehyde, *cis*-stilbene, *trans*-stilbene and *n*-decane were purchased from Sigma-Aldrich and used as received. The solvents ethanol, acetonitrile, tetrahydrofuran and N,N-dimethylformamide were purchased from Sigma-Aldrich and used as received.

6.2.1 Catalytic oxidation of styrene

All catalytic oxidations of styrene were conducted under aerobic conditions in a 10 cm³ round bottom flask equipped with a magnetic stirrer and heated in a silicon oil bath. A typical RuDEN catalytic evaluation reaction was conducted by adding the appropriate amount of RuDEN solution (0.25–2.50 μmol Ru) into the round bottom flask charged with solvent (4-5 cm³), styrene (1.0-2.5 mmol) and TBHP (2.0-7.5 mmol) up to a total volume of 6 cm³. A typical RuSil60 catalytic evaluation reaction was prepared by transferring the appropriate amount of RuSil60 catalyst (20-50 mg RuSil60, 0.2-2.0 μmol Ru) into the round bottom flask charged with solvent (5.0-5.2 cm³), styrene (2 mmol) and TBHP (4 mmol). The oil bath was heated prior to reaction and the reactions heated under reflux with stirring. The reaction was sampled prior to reaction, every 2 hours for the first 6 hours and then at 24 hours and diluted with ethanol containing *n*-decane as an internal standard. The catalytic products were analysed by gas chromatography (Shimadzu GC 2010) equipped with a Restek Rtx®-5 column and flame ionisation detector. In the case of the RuSil60 evaluations, the samples were filtered through a nylon filter prior to analysis.

6.3 Results and Discussions

The RuDEN catalysts were evaluated in the oxidation of styrene with the use of TBHP as an oxidant. A series of optimisation experiments were conducted prior to the comparison of the different catalysts. These comprised investigations into the effects of overall reactant and

substrate concentration, oxidant loading, different catalyst loadings, different temperatures, varying the solvents used for the reaction and catalyst choice. Thereafter, the effect of ionic liquid as additives on the activity and selectivity of the reaction was investigated.

6.3.1 Evaluation of RuDEN catalysts.

6.3.1.1 The effects of overall concentration of catalyst, substrate and oxidant on catalytic activity.

Optimisation reactions were conducted to find the optimal concentration of substrate and reactants in solution using a molar ratio of mol Ru in catalyst:substrate:oxidant of 1:1000:2000. The catalyst utilised for this part of the study was G6-RuDEN. The effective concentrations of the reaction mixtures are listed in Table 6.1 to illustrate the effect of varying the overall concentration of the substrate and reactants on the catalytic activity of the catalyst.

Table 6.1. Catalytic conversion and yield observed for various overall concentrations of catalyst, styrene and TBHP, maintaining a molar ratio of catalyst:substrate:oxidant of 1:1000:2000.

Entry	Ru (mM)	Styrene (mM)	TBHP (mM)	Styrene conversion (%)	Benzaldehyde (%)	Styrene oxide (%)
1	0.17	167	333	15	3	12
2	0.25	250	500	22	4	19
3	0.33	333	667	45	15	29
4	0.42	417	833	60	24	35

^a Reaction volume of 6 cm³, T = 85 °C, t = 1440 mins

The reactions were conducted at 85 °C in DMF for 1440 minutes with sampling every 120 minutes for the first 360 minutes and thereafter at 1440 minutes. In the case of the data presented in Table 6.1, only end of run analysis was considered to identify the reaction conditions that would provide the highest overall oxidation of styrene. Entries 1-4 show an increase in the conversion of styrene when increasing the overall concentration of catalyst, styrene and oxidant. The results suggest a change in the mass transfer characteristics of the reaction system when changing the concentration. This phenomenon manifests in an increase in reaction rate with an increase in the concentration of the reactants therefore minimising

mass transfer limitation. Given the high conversion of styrene as shown for entry 4, the proceeding reactions investigating the effects of catalyst concentration, solvent effects and the effect of ionic liquids as additives was investigated using this amount of substrate and oxidant.

6.3.1.2 Effects of oxidant loading.

The effect of TBHP on the conversion of styrene and selectivity towards styrene oxide was investigated in order to determine the optimal styrene:TBHP ratio. The role of TBHP in the oxidation of styrene is primarily to serve as an oxygen source in the formation of the epoxidation product, styrene oxide. The oxidant may further partake in the conversion of styrene oxide to benzaldehyde or further decompose during the reaction to the inactive *t*-butanol. The amount of TBHP in any reaction is therefore crucial, given these possible pathways for its consumption. It is therefore, necessary to find a ratio of styrene:TBHP that will ensure a significant conversion of styrene and maintain a high selectivity towards styrene oxide. The conversion of styrene was investigated for the ratios of 1:1, 1:2, 1:2.5 and 1:3 for styrene:TBHP as illustrated in Figure 6.1.

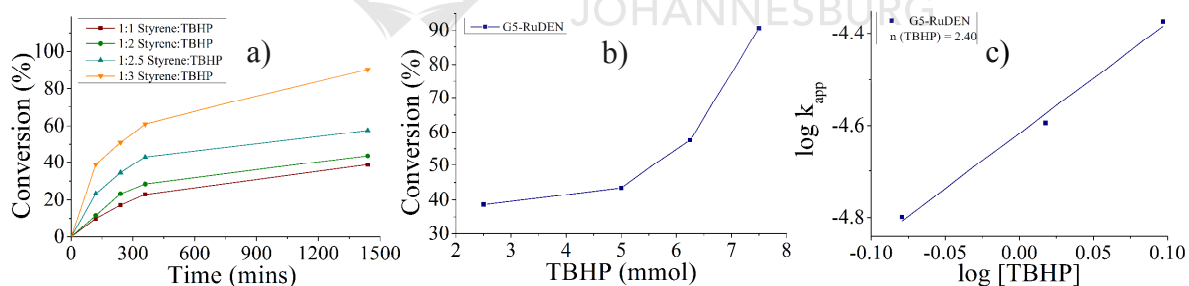


Figure 6.1. Conversion of styrene, utilising G5-RuDEN as a catalyst, for the various molar ratios of styrene:TBHP of 1:1, 1:2, 1:2.5 and 1:3 for a) the time resolved conversion of styrene, b) the dependence of styrene conversion on the amount of TBHP and c) double-log plots of the dependence of the rate on the concentration of TBHP. Reactions were conducted using 0.0025 mmol Ru, 2.5 mmol styrene and at a temperature of 85 °C.

An expected increase in the conversion of styrene was observed for the increase in TBHP concentration. The conversion increases exponentially with an increase in the amount of TBHP, especially with a styrene:TBHP ratio of 1:2 and above as illustrated in Figure 6.1(b). To gain more insight into the correlation between the conversion of styrene and the TBHP

concentration, the double-log dependency of the apparent rate constant on the concentration was plotted as illustrated in Figure 6.1(c). The reaction order with respect to TBHP concentration was estimated from the slope of this double-log graph. The reaction order has a fractional value of 2.40, which indicates that the mechanistic role of TBHP in the reaction is intricate relative to the reaction rate.

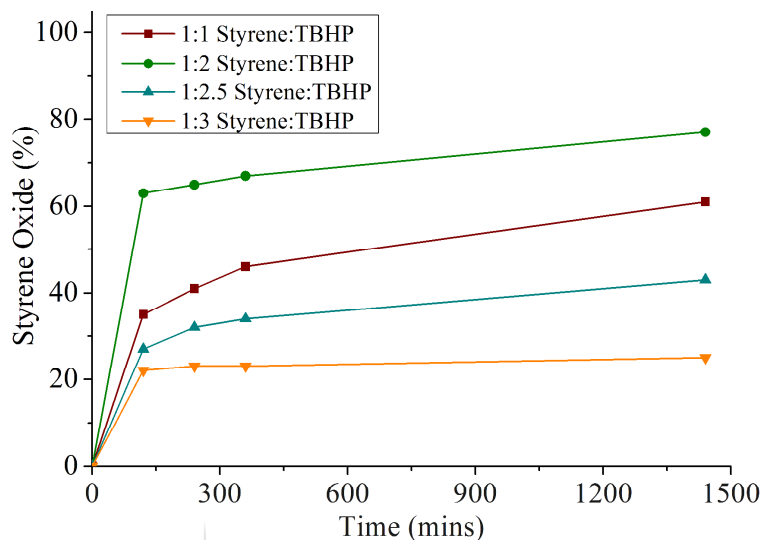


Figure 6.2. The time resolved styrene oxide selectivity observed, while utilising G5-RuDEN as a catalyst, for various molar ratios of styrene:TBHP of 1:1, 1:2, 1:2.5 and 1:3. Reactions were conducted using 0.0025 mmol Ru, 2.5 mmol styrene and at a temperature of 85 °C.

In this case, a styrene:TBHP ratio of 1:3 would seem ideal given the high conversion of above 90%, but consideration should be given to the styrene oxide selectivity as well. The selectivity towards styrene oxide was calculated as a compositional percentage of styrene oxide in the total amount of product formed for the various ratios of styrene:TBHP as illustrated in Figure 6.2. The selectivity towards styrene oxide increases with an increase in the styrene:TBHP ratio of 1:1 to 1:2 which is expected as there is a larger amount of oxidant available for the conversion of styrene to styrene oxide. This increase in selectivity towards styrene oxide is, however, not maintained upon increasing the styrene:TBHP ratio above 1:2. Instead, a further increase in styrene:TBHP ratio results in a dramatic decrease in selectivity towards styrene oxide from 77% to 43% and further to 25% when increasing the styrene:TBHP ratio from 1:2 to 1:2.5 and then to 1:3 respectively. This decrease in the selectivity towards styrene oxide correlates with the formation of side products namely, *trans*-stilbene upon increasing the amount of TBHP in the reaction. Given the highest selectivity towards styrene oxide observed

when using the styrene:TBHP ratio of 1:2, this ratio was maintained throughout the subsequent reactions.

6.3.1.3 Effects of catalyst loadings.

The effect of catalyst loading was investigated utilising the G5-RuDEN catalyst. The reaction was conducted at a temperature of 85 °C, DMF as the solvent and a 0.42 mM, 417 mM and 833 mM concentration of Ru, styrene and TBHP respectively. Figure 6.3(a) illustrates the conversion of styrene over a 1440 minute period for various amounts of the RuDEN catalyst. A percentage conversion for styrene of 25% and less was observed for catalyst amounts varying from a 0.01 mol% Ru to 0.05 mol% Ru. Upon increase in the catalyst loading, to 0.07 mol% Ru and 0.1 mol% Ru there is a further increase in the percentage conversion to between 30-40%. A dramatic increase in the conversion of styrene was seen for an increase in catalyst loading to 0.2 mol%. This trend of increase in percentage conversion of styrene with increase in mol% of Ru is clearly illustrated in Figure 6.3(b). There is a linear increase in the percentage conversion of styrene with an increase in mol% Ru. The graph was not drawn through the origin as a small degree of autoxidation occurs at these reaction conditions in the presence of the oxidant and absence of the catalyst. The conversion of styrene in the absence of catalyst and presence of TBHP is approximately 7% after 1440 minutes. The double-log plot for the dependency of the rate of the reaction on the concentration of Ru is illustrated in Figure 6.3(c).

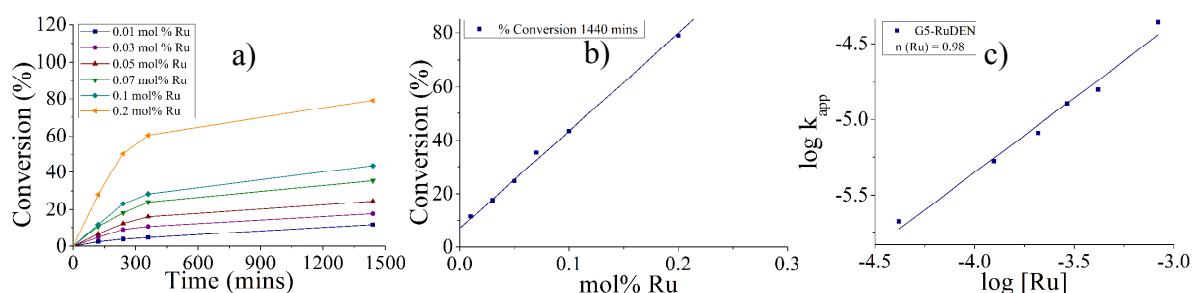


Figure 6.3. Conversion of styrene, utilising G5-RuDEN as a catalyst, for various molar percentages of ruthenium depicted by the, a) time resolved conversion of styrene for different mol% of Ru, b) percentage conversion of styrene with increase in mol% Ru and c) double-log plot of the dependence of the rate on the concentration of Ru at a time of 1440 mins. Reactions were conducted using 2.5 mmol styrene and 5 mmol TBHP at a temperature of 85 °C.

The slope gives an estimation of the order of the reaction relative to the catalyst concentration for the given reaction conditions.²² The calculated value for the order of the reaction referred to as the n-value is close to unity with a value of 0.98. This indicates a direct proportionality between the rate of the reaction and the concentration of Ru in the catalytic reaction and agrees well with the linear increase in conversion of styrene with an increase in the catalyst concentration as illustrated in Figure 6.3(b). The turnover frequencies (TOF) were calculated at a 10% styrene conversion, as depicted in Figure 6.4, to gain insight into the activity of the catalysts as shown in Figure 6.4. The TOF values increased from 51 to 76 upon increasing the mol% Ru from 0.01% to 0.07% respectively. Thereafter, there was a decrease in the TOF upon increasing the catalyst loading to 0.1 mol% Ru. Further increase in the catalyst loading to 0.2 mol % Ru caused an increase in the TOF-value to 64 (mol styrene converted/mol Ru/h). The decrease in TOF-value upon increase in the catalyst loading is unexpected since catalytic activity should increase with an increase in catalyst loading. This expected trend was observed when considering the results depicted in Figure 6.3 where the higher catalyst loading exhibited an overall increase in the end of run styrene conversion. Strangely, the expected increase in TOF with increase in catalyst loading was observed once again for the increase in mol% Ru from 0.1 mol% to 0.2 mol% albeit the values are still lower than that observed at 0.07 mol%.

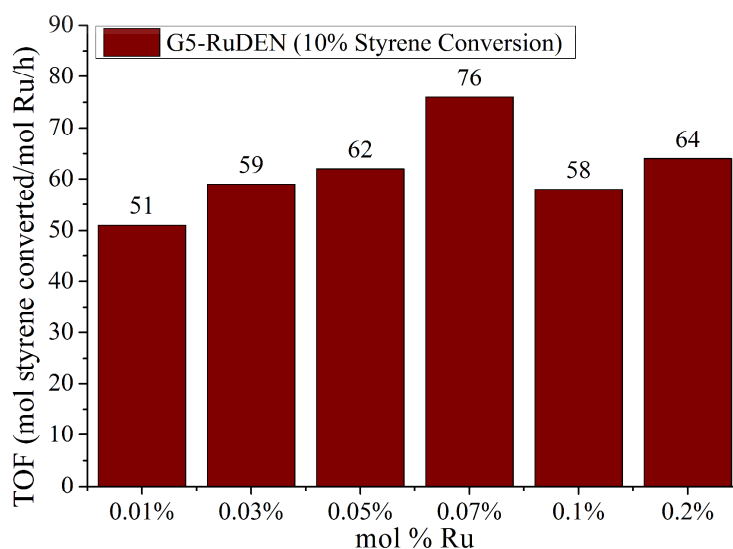


Figure 6.4. Turnover frequencies observed for a 10% conversion of styrene utilising G5-RuDEN as a catalyst. Reactions were conducted using 2.5 mmol styrene and 5 mmol TBHP at a temperature of 85 °C.

The only means of maintaining the overall increase in TOF for the reactions with a catalyst loading of 0.1 mol% and 0.2 mol% is to have an increase in their conversion at 10% conversion of styrene. This requirement when compared to the results obtained for the reaction suggests a possible alternate reaction pathway for the oxidant.

Figure 6.5 illustrates the time resolved selectivity towards styrene oxide observed when evaluating the G5-RuDEN for various catalyst loadings. A greater selectivity towards styrene oxide ranging between 60-80% was observed when utilising a metal catalyst loading of 0.01-0.10 mol% Ru. The lowest selectivity towards styrene oxide was observed when utilising a catalyst loading of 0.2 mol% Ru. The results suggest that an increase in conversion leads to a decrease in the selectivity towards styrene oxide.

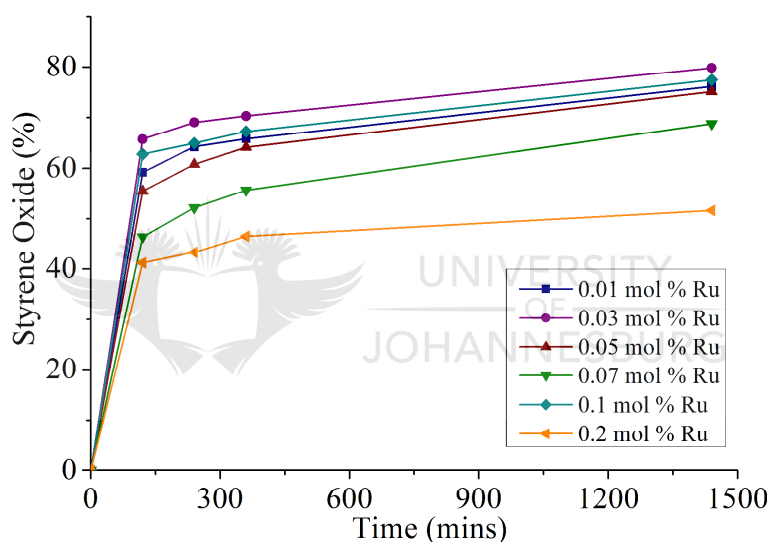


Figure 6.5. The time resolved styrene oxide selectivity observed for different catalyst loadings utilising the G5-RuDEN catalyst. Reactions were conducted using 2.5 mmol styrene and 5 mmol TBHP at a temperature of 85 °C.

To help understand this observation better, one need to consider the possible reaction pathways of TBHP as an oxidant. The epoxidation of styrene is made possible by TBHP as an oxygen source with the by-product of spent TBHP being *t*-butanol. Styrene oxide is, however, not the only product of the oxidation reaction and the formation of benzaldehyde is observed as well. The formation of benzaldehyde may result from the subsequent attack of styrene oxide by TBHP. The inverse correlation between the amount of styrene converted and the selectivity towards styrene oxide suggests that increase in the concentration of styrene oxide leads to an increase in benzaldehyde formed. The formation of benzaldehyde seems to be

dependent on the overall concentration of styrene oxide present where increase in epoxidation increases the overall concentration of styrene oxide and promotes benzaldehyde formation. Given the additional consumption of TBHP with the formation of benzaldehyde, an accelerated decrease in the concentration of TBHP occurs and in light of the previously discussed concentration effects, could lead to a decrease in the rate of conversion of styrene. This rationale is reflected in the overall decrease in conversion rate with time as evident in figure 6.3(a). This observed decrease in the epoxidation of styrene was, however, most evident upon increasing the metal catalyst loading to 0.2 mol% Ru. This further reinforces the use of a 0.1 mol% Ru catalyst loading for optimal intrinsic styrene oxide selectivity.

6.3.1.4 Temperature effects.

The effects of temperature on the catalytic activity and selectivity of the G6-RuDEN catalysed oxidation of styrene with the use of TBHP was studied. The reactions were conducted at 50 °C, 70 °C and 85 °C. Figure 6.6 illustrates the oxidation of styrene with time for the various temperatures utilised. Similar to the other styrene conversion graphs, there is a rapid conversion of styrene over the first 6 hours but this rate of conversion decreases as the reaction proceeds.

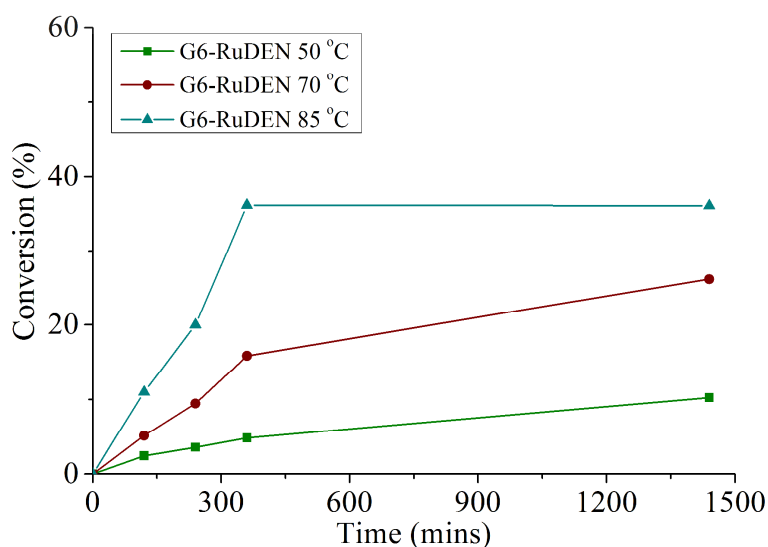


Figure 6.6. Conversion of styrene observed when conducting the experiment at 50 °C, 70 °C and 85 °C while utilising the G6-RuDEN catalyst. Reactions were conducted using 2.5 mmol styrene and 5 mmol TBHP and in DMF as solvent.

An expected increase in conversion of styrene was observed for an increase in the reaction temperature from 50 °C to 85 °C. Considering the results obtained, an average increase of 8% styrene conversion was observed for a 10 °C increase in temperature. The selectivity profile for the styrene oxidation products was determined at the various temperatures utilised as illustrated in Figure 6.7. The selectivity towards styrene oxide increased with an increase in conversion for the first 120 minutes of the reaction and thereafter remained almost constant. The increase in temperature promotes the formation of styrene oxide when increasing the reaction temperature from 50 °C to 70 °C. When considering the earlier correlation between the total conversion and the decrease in selectivity observed towards styrene oxide, it was reasoned that increased rate could cause an increase in the conversion of styrene oxide towards benzaldehyde. This process could be either oxidant mediated or a case of decomposition of styrene oxide by the catalyst. Additionally reasoning could be that any factor that increases the rate of the reaction could increase the rate of formation of benzaldehyde. In this case, however, the increase in temperature from 70 °C to 85 °C, did not cause a significant change in the styrene oxide conversion and hence the temperature does not necessarily promote a decrease in the selectivity towards styrene oxide. The reaction temperature of 85 °C is therefore ideal, as styrene conversion is highest of the three temperatures.

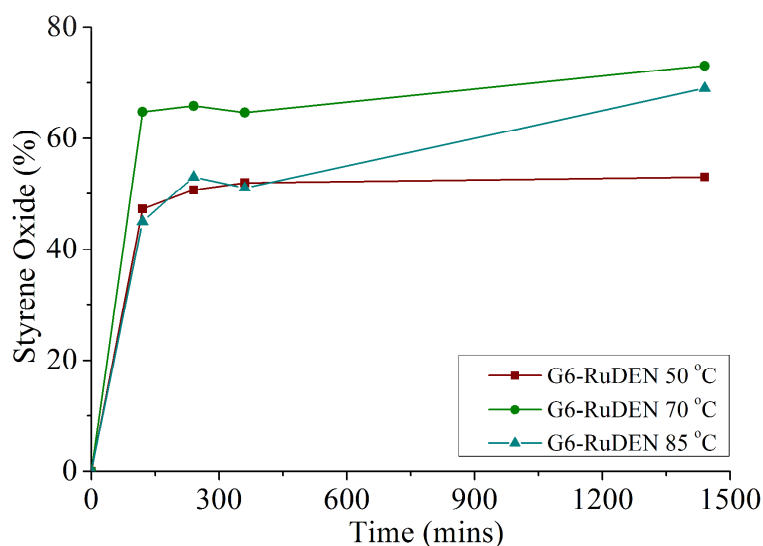


Figure 6.7. Styrene oxide selectivity observed with time when conducting the experiment at 50 °C, 70 °C and 85 °C while utilising the G6-RuDEN catalyst. Reactions were conducted using 2.5 mmol styrene and 5 mmol TBHP and in DMF as solvent.

6.3.1.5 Solvent effects.

The effect of the type of solvent on the catalytic activity and selectivity for the styrene oxidation reaction was investigated for the solvents, N,N-dimethylformamide (DMF), acetonitrile, ethanol, cyclohexane and tetrahydrofuran. Figure 6.8 illustrates the conversion of styrene with time when using the various solvents. The solvent that showed the highest amount of conversion after a 1440 minute period was acetonitrile. Similar conversions of styrene were observed when using ethanol and cyclohexane for a conversion of approximately 60% at 1440 minutes. The use of DMF as a solvent was accompanied with a styrene conversion of about 40%. The lowest conversion of styrene was observed when using tetrahydrofuran as a solvent. The use of cyclohexane as a solvent resulted in the formation of a biphasic reaction. In the case of acetonitrile and tetrahydrofuran, the reaction mixture went turbid upon adding the aqueous RuDEN catalyst stock solution. It is important to note that for all the solvents except DMF, instability of the RuDENs was observed as the formation of a precipitate. The solvent efficiency when correlated with the various organic solvents observes the following trend tetrahydrofuran \ll DMF $<$ cyclohexane $<$ ethanol $<$ acetonitrile.

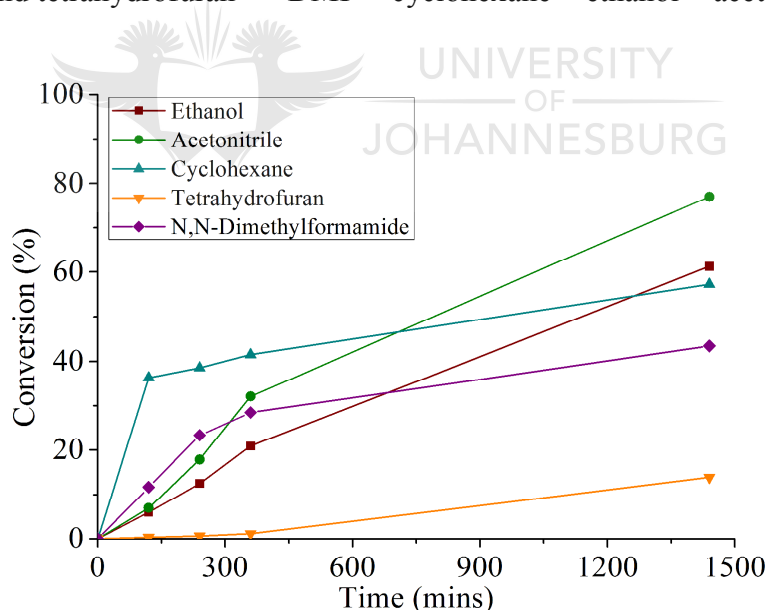


Figure 6.8. Conversion of styrene observed over 1440 minutes when using the solvents, ethanol, acetonitrile, N,N-dimethylformamide, tetrahydrofuran and cyclohexane while utilising the G5-RuDEN catalyst. Reactions were conducted using 2.5 mmol styrene and 5 mmol TBHP at a temperature of 85 °C.

Table 6.2 details the dielectric constants and oxygen solubility for selected solvents together with the end of run styrene conversion and styrene oxide yield. The dielectric constant is a

relative measure of the solvent polarity. The trend in activities observed when using the different solvents does not seem to correlate with the trend in dielectric constants where a higher dielectric constant would be associated with a higher solvent polarity and higher activity of the catalyst. This suggests that the polarity of the solvent is not the only factor associated with the overall activity for styrene oxidation when using the RuDEN catalyst. If reasoned on terms of polarity, DMF and acetonitrile should show similar styrene conversion values at 1440 minutes. Amongst the polar solvents, a lower conversion was observed when using DMF. Given that DMF efficiently solvated the RuDENs, this could suggest an increase in coordination of the solvent to the particle surface when compared to the other coordinating solvents, where the formation of a precipitate was observed. Additionally, the presence of the stabilising dendrimer could show superior miscibility with the amide containing DMF given that the PAMAM-OH dendrimer contains the same functionality. This further encourages interaction of DMF with the RuDEN surface. These inhibitory competitive coordination effects are less significant in the case of ethanol and acetonitrile that show a higher conversion.

Table 6.2. The solvent properties and their effects on the RuDEN catalysed oxidation of styrene with TBHP as the oxidant.

Entry	Solvent	ϵ/ϵ_0^{23}	O ₂ solubility (mol%) ²⁴	Styrene conversion ^a (%)	Styrene oxide selectivity ^a (%)	Benzaldehyde selectivity (%)
1	Acetonitrile	38	0.041	77	60	40
2	DMF	37	-	43	77	23
3	Ethanol	25	-	61	34	66
4	Tetrahydrofuran	8	-	14	8	92
5	Cyclohexane	2	0.125	57	7	93

^a Values for % styrene conversion and % styrene oxide taken at 1440 min. Ru (0.0025 mmol), styrene (2.5 mmol), TBHP (5 mmol), 85 °C.

The presence of oxygen in the reaction system favours the oxidation of styrene to an extent. These reactions were all conducted under aerobic conditions and therefore it is important to rationalise the activity of the catalyst as a function of the varying solubility of oxygen in these solvents. This is mostly applicable to the non-polar cyclohexane which, given the previous

rationale, should have shown the lowest activity. In this case, the styrene conversion observed when using cyclohexane as a solvent could be attributed to the increased solubility of oxygen in the solvent. The lowest conversion was observed when using tetrahydrofuran as solvent. The low activity observed when conducting the reaction in THF, is possibly caused by the coordinating ability of the solvent. In principle, the same rationale applies as for DMF.

The selectivity profile observed when using the different solvents correlates with polarity as well. It seems that the more polar solvents favour the formation of styrene oxide, which implies a more conservative oxidation pathway – an observation consistent with the non-radical mechanism.⁵ The presence of a polar solvent is thought to inhibit the formation of oxygen radicals for these aerobic reactions, especially given that the solubility of oxygen in the polar solvents is considerably lower than that in non-polar solvents.⁵ This helps explain why the styrene oxide selectivities in the less polar tetrahydrofuran and non-polar cyclohexane are considerably lower than those observed when using the polar solvents.

6.3.1.6 *The effects of catalyst choice*

Three different RuDENs were prepared for the evaluation of RuDEN catalysts in the styrene oxidation reaction. A catalyst concentration of 0.1 mol% Ru was used in each of the reactions based on the total Ru concentration of the RuDEN catalyst stock solutions calculated from ICP-OES results. The conversion of styrene was monitored over a 1440 minute period while using the various RuDEN catalysts. The conversion results are illustrated in Figure 6.9 for the various RuDEN catalysts evaluated. The total conversion of styrene after a 1440 minute period ranges from 36% to 51% for the various catalysts evaluated. Amongst the three catalysts, G4-RuDEN gave the highest end of run conversion of styrene with a percentage conversion of 51%. The percentage styrene conversion follows the trend G6-RuDEN < G5-RuDEN < G4-RuDEN for the RuDEN catalysts investigated.

Further insight into the catalytic performance of the RuDENs is given by calculating the TOF-values as illustrated in Figure 6.10. The TOF-values were calculated at a 20% styrene conversion and reflect the initial activity of the catalyst before a dramatic decrease in the activity is observed. The TOF values reflect the overall trend discussed for the conversion of styrene where the activity for G4-RuDEN is highest and that of G5-RuDEN and G6-RuDEN being similar.

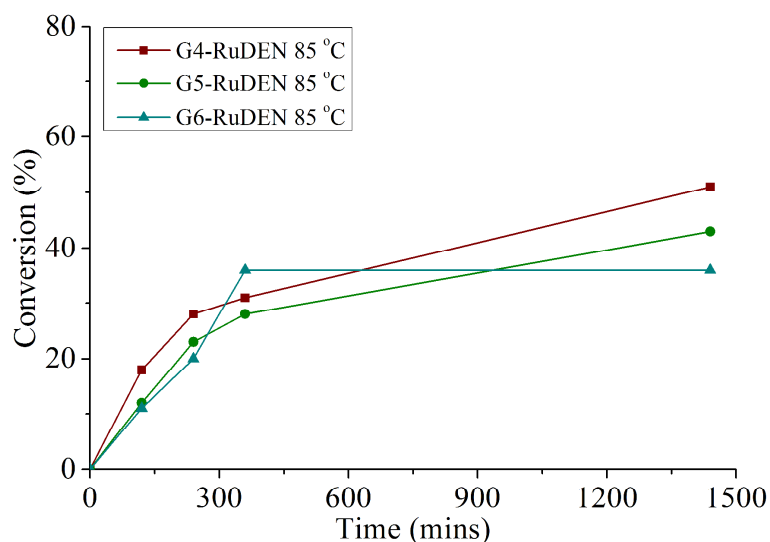


Figure 6.9. Conversion of styrene observed when evaluating the G4-RuDEN, G5-RuDEN and G6-RuDEN catalysts at a 0.1 mol% Ru catalyst loading. Reactions were conducted at 85 °C using 2.5 mmol styrene and 5 mmol TBHP and in DMF as solvent.

One aspect to consider when comparing these systems is that the catalyst loading is the same for each reaction and based on the total metal and not only the surface atom concentration. Considering the amount of total surface atoms, smaller nanoparticles like that of G4-RuDEN have a higher ratio of surface atoms to the total amount of atoms when compared to the larger nanoparticles seen for the G5-RuDEN and G6-RuDEN system.

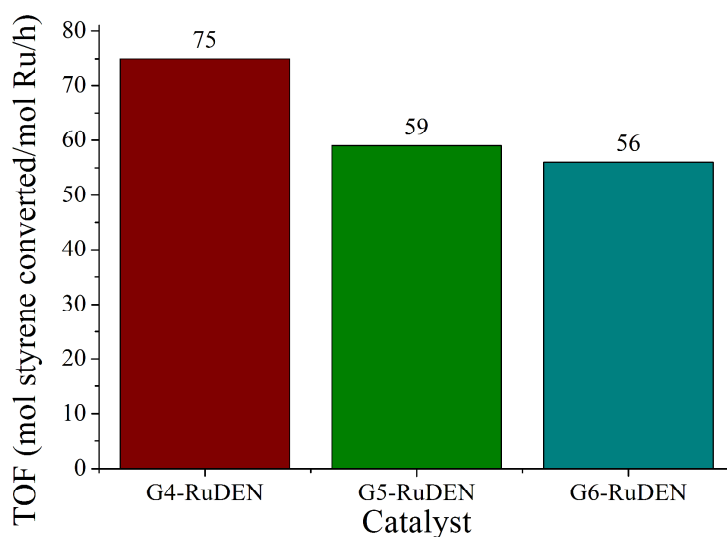


Figure 6.10. Turnover frequencies observed for a 20% conversion of styrene while utilising catalysts G4-RuDEN, G5-RuDEN and G6-RuDEN. Reactions were conducted using 0.0025 mmol Ru, 2.5 mmol styrene and 5 mmol TBHP at a temperature of 85 °C.

The higher activity observed for G4-RuDEN would be ideal when choosing a catalyst for further catalytic studies but consideration has to be given to the selectivity towards styrene oxide. Therefore, it is important to consider all the evaluation data concerning both the activity and selectivity to find a suitable balance between these performance criteria. Table 6.3 details the TOF, % products formed and the styrene oxide selectivity observed for the RuDEN catalysts. The increased reactivity of G4-RuDEN corresponds to a 50% selectivity towards styrene oxide. In comparison to the results obtained for G5-RuDEN and G6-RuDEN, there is a significant decrease in the selectivity towards styrene oxide but an increase in the activity of the catalyst. Additionally, this increase in activity observed when using G4-RuDEN is accompanied by the formation of side products as shown in Table 6.3 for the % other products formed. In this case, G4-RuDEN is not ideal for further evaluations as selectivity towards styrene oxide is lowest amongst the catalysts evaluated and the formation of side products is encouraged.

Table 6.3. Catalytic conversion, TOF-values, % products formed and % styrene oxide selectivity observed for various RuDEN catalysts G4-RuDEN, G5-RuDEN and G6-RuDEN.^a

Entry	Catalyst	TOF ^b	Styrene Oxide ^c (%)	Benzaldehyde ^c (%)	Other ^c (%)	Styrene oxide selectivity (%)
1	G4-RuDEN	75	25	17	8	50
2	G5-RuDEN	59	34	10	-	77
3	G6-RuDEN	56	24	10	-	70

^a Reactions were conducted using 0.0025 mmol Ru, 2.5 mmol styrene and 5 mmol TBHP at a temperature of 85 °C ^b TOF in mmol styrene converted/mmol_{Ru}/hour at 20 % styrene conversion ^c Total percentage of each product formed from styrene ^d Percentage of styrene oxide relative to all products formed.

There is not much difference in the activity of the G5-RuDEN and G6-RuDEN catalysts when considering the TOF values obtained in each case. The selectivity towards styrene oxide observed when using G5-RuDEN is, however, significantly higher than that observed when using G6-RuDEN. The G5-RuDEN catalyst was therefore chosen as the RuDEN catalyst for further catalytic evaluation.

6.3.1.7 Effects of ionic liquids and amounts of ionic liquids used.

The effects of various ionic liquids on the catalytic activity of G5-RuDEN were investigated. The ionic liquids [BMIM][PF₆], [BMIM][BF₄], [BMIM][NTf₂] and [EMIM][Ocs] were evaluated for the various amounts of ionic liquid, 0.1 g, 0.3 g and 0.5 g. The reactions were conducted using a 0.1 mol % Ru catalyst loading with 2.5 mmol styrene and 5 mmol TBHP at a temperature of 85 °C and in DMF as a solvent. Figure 6.11 illustrates the conversion of styrene with time for the various types and amounts of ionic liquid as additive in the reaction. Similar to the reactions without ionic liquid, there is a high initial rate of styrene conversion, which eventually tapers off as the reaction proceeds. This is usually seen after the first four hours of the reaction for all the reactions except that where 0.1 g of [EMIM][Ocs] is used.

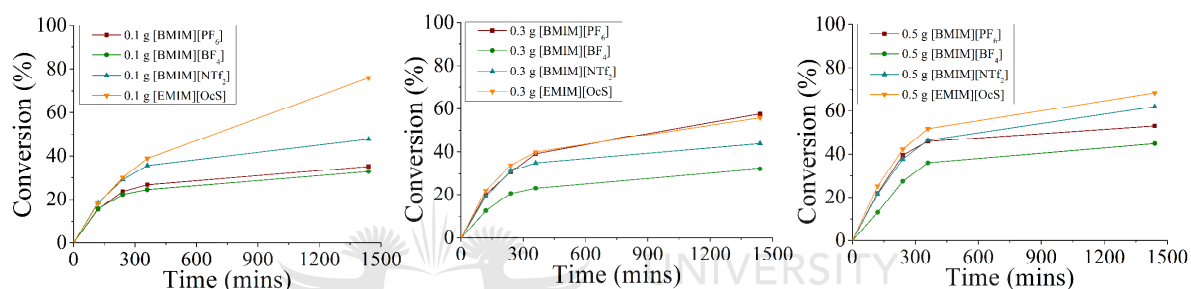


Figure 6.11. Conversion of styrene for various amounts of the ionic liquids [BMIM][PF₆], [BMIM][BF₄], [BMIM][NTf₂] and [EMIM][Ocs] a) 0.1 g of ionic liquid b) 0.3 g of ionic liquid and c) 0.5 g of ionic liquid while utilising the G5-RuDEN catalyst. Reactions were conducted using 2.5 mmol styrene and 5 mmol TBHP at a temperature of 85 °C and in DMF as a solvent.

In this case, the reaction continues after four hours at a much higher rate than any of the other ionic liquid dosed reactions and eventually reaches a styrene conversion of 76%. The increase in styrene conversion going from an ionic liquid loading of 0.3 g to 0.5 g is, however, minimal and to gain more insight into the actual effect of the ionic liquid, they should be compared individually for the type of ionic liquid and the effect of increasing the amount. This data is presented in Table 6.4 for the ionic liquid free system and the ionic liquid loaded systems.

The effect of the presence of ionic liquid on the styrene conversion after a 1440 minute period is shown for each of the reactions with the ionic liquid as an additive (entries 2-13) and in the

absence of ionic liquid (entry 1). The ionic liquids [BMIM][PF₆], [BMIM][BF₄] and [BMIM][NTf₂] show no significant effect in increasing the conversion of styrene when compared to the reaction conducted in the absence of ionic liquid for ionic liquid loadings of 0.1 g and 0.3 g. In some cases, the presence of the ionic liquid has a negative effect on the catalytic activity as shown for entries 2, 3 and 8. There is, however, an optimal ionic liquid loading for two of the three ionic liquids that affect a significant increase in conversion. In the case of [BMIM][NTf₂], an increase in conversion to 62% is seen for a 0.5 g (entry 7) amount of ionic liquid. For [BMIM][PF₆], an increase in conversion to 58% and 53% from 35% when using 0.1 g, is observed for 0.3 g and 0.5 g (entries 9-10) of the ionic liquid respectively. The use of [EMIM][OcS] as ionic liquid had a positive influence on the activity of the catalyst for all loadings of the ionic liquid as shown for entries 10-12 in Table 6.4.

Table 6.4. The effect of the various ionic liquids and amounts of ionic liquid on the % styrene conversion and the % styrene oxide selectivity.^a

Entry	Ionic liquid	Ionic liquid amount (g)	Styrene conversion (%)	Styrene oxide selectivity (%)
1	None	-	44	77
2	[BMIM][BF ₄]	0.1	33	78
3	[BMIM][BF ₄]	0.3	32	77
4	[BMIM][BF ₄]	0.5	45	71
5	[BMIM][NTf ₂]	0.1	48	58
6	[BMIM][NTf ₂]	0.3	44	48
7	[BMIM][NTf ₂]	0.5	62	51
8	[BMIM][PF ₆]	0.1	35	64
9	[BMIM][PF ₆]	0.3	58	50
10	[BMIM][PF ₆]	0.5	53	60
11	[EMIM][OcS]	0.1	76	51
12	[EMIM][OcS]	0.3	56	52
13	[EMIM][OcS]	0.5	68	42

^a Values for % styrene conversion and % styrene oxide taken at 1440 min. Ru (0.0025 mmol), styrene (2.5 mmol), TBHP (5 mmol), 85 °C.

In comparison to the other ionic liquids, this increase was most pronounced when using an ionic liquid amount of 0.1 g. The styrene conversion increased to 76% (entry 11) from the

reference 44% (entry 1) styrene conversion observed for the ionic liquid free reaction. The effect of the presence of ionic liquid on selectivity towards styrene oxide was investigated for the reactions loaded with the different ionic liquids. A significant decrease in the selectivity towards styrene oxide was observed with the use of the ionic liquids [BMIM][PF₆], [BMIM][NTf₂] and [EMIM][Ocs] (entries 5-13). When considering the results previously discussed for trends in the activity, a decrease in the catalytic activity correlated with an increase in the styrene oxide selectivity for the reactions conducted at 85 °C. This was, however, not observed when using any of the ionic liquids except [BMIM][BF₄]. The results obtained for the evaluation of [BMIM][BF₄] therefore closely resembles results obtained for the use of the catalysts without ionic liquid especially when considering the result observed when using a 0.5 g amount of the ionic liquid.

6.3.2 Evaluation of RuSil60S catalysts

The RuDEN catalysts previously evaluated for the epoxidation of styrene comprised a system where the particles were not supported on a solid support material. The preparation of RuSil60S catalysts previously described were evaluated for the epoxidation of styrene with the use of TBHP as an oxidant. Optimisation reactions were conducted initially to identify the ideal conditions for conducting this reaction with the given catalyst.

6.3.2.1 Effects of catalyst loadings

The effect of the catalyst loading on the conversion and selectivity observed for the G6-RuSil60S catalyst was investigated. Figure 6.12 illustrates the styrene conversion profile for the different catalyst loadings and the overall trend seen for the different end of run conversions. The linear increase in the conversion of styrene deviates from the usual conversion trend observed with the RuDENs, where there is a rapid initial conversion of the substrate and then decrease in the rate of the conversion as seen in Figure 6.12(a). This can be ascribed to a solvent effect as shown earlier when evaluating the RuDEN catalyst and investigating solvent effect. In that case, when comparing the polar solvents DMF and THF, the former shows a rapid initial reaction rate whereas the latter observed an overall linear conversion trend. When considering the overall conversion of styrene, there is an expected increase in the end of run conversion of styrene with an increase in the catalyst loading.

Unlike the trend observed for the evaluation of the RuDEN catalyst, the trend in catalyst loading deviates from the linear trend earlier observed. This suggests disproportionality in the changes of reaction rate for an increase in the catalyst loading and possibly the presence of mechanisms other than the epoxidation of styrene. Given the complexity of the mechanism for the epoxidation of styrene in the presence of TBHP and the inherent intricacy of the heterogeneous reaction, the reaction order was not calculated as done for the RuDEN catalysts.

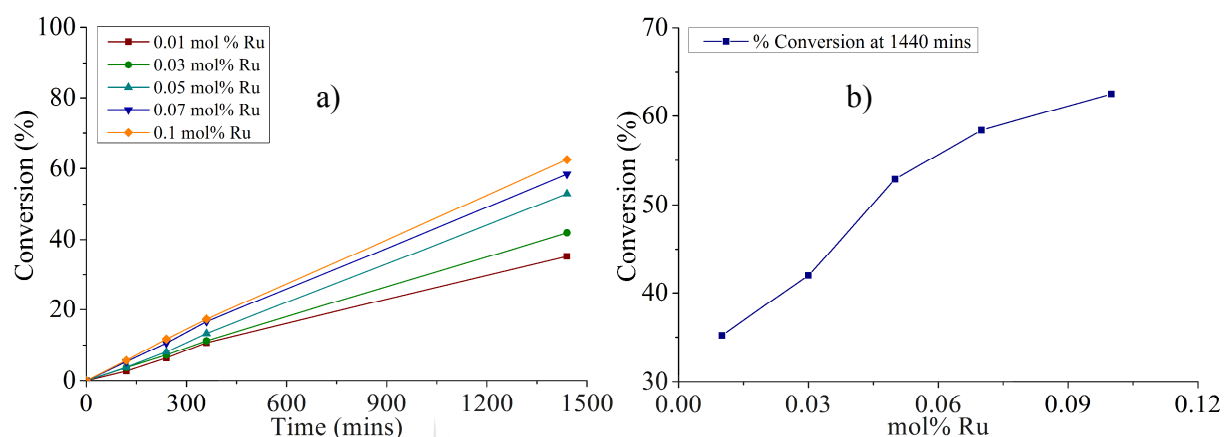


Figure 6.12. Conversion of styrene for various molar percentages of ruthenium using the G6-RuSil60S catalysts a) Time resolved conversion of styrene for different mol percentages of Ru and b) Percentage conversion of styrene at a time of 1440 mins for different mol percentages of Ru. Reactions were conducted using acetonitrile as a solvent, 2 mmol styrene and 4 mmol TBHP at a temperature of 85 °C.

This observation is further reinforced when considering the TOF-values obtained for the various mol% Ru loadings as illustrated in Figure 6.13. There is an exponential decrease in the TOF-value as the mol% Ru increases despite the opposite trend observed for the end of run styrene conversion (Fig. 6.12a).

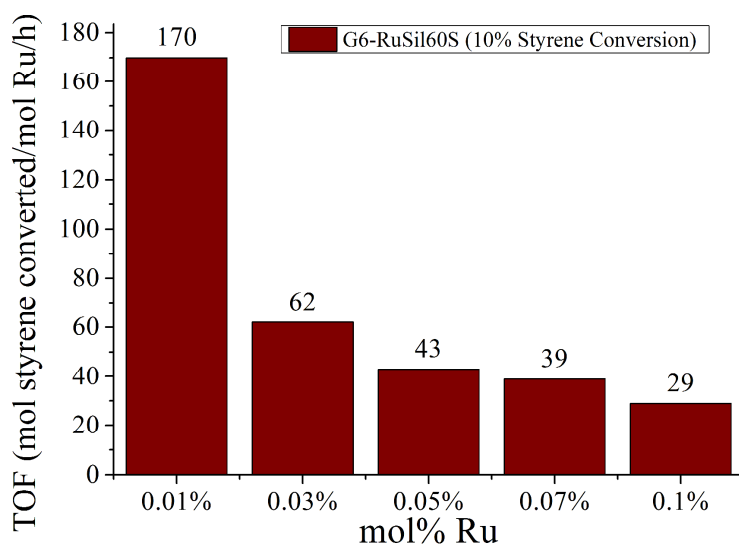


Figure 6.13. Turnover frequencies observed for a 10% conversion of styrene utilising G6-RuSil60S as a catalyst. Reactions were conducted using acetonitrile as a solvent, 2 mmol styrene and 4 mmol TBHP at a temperature of 85 °C.

The selectivity towards styrene oxide was determined for the course of the reaction as illustrated in Figure 6.14. The selectivity towards styrene oxide does not change significantly and even for the minute changes does not show any correlation with a change in the catalyst loading. Despite the minimal change in the selectivity with change in catalyst loading, a high selectivity towards styrene oxide was maintained for all catalyst loadings.

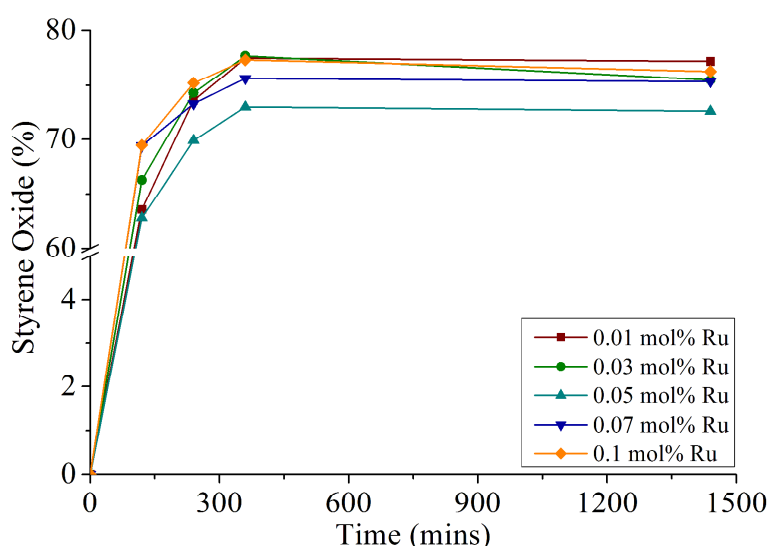


Figure 6.14. The time resolved styrene oxide selectivity observed for different catalyst loadings when evaluating the G5-RuSil60S catalysts. Reactions were conducted using acetonitrile as a solvent, 2 mmol styrene and 4 mmol TBHP at a temperature of 85 °C.

6.3.2.2 *Solvent effects*

The effect of solvent choice on the epoxidation of styrene was investigated when evaluating the G6-RuSil60S catalyst. Unlike the RuDEN catalysts evaluated, these catalysts are characteristically more heterogeneous and show more phase compatibility with the solvents, whereas the aqueous RuDEN catalysts formed biphasic systems with non-polar solvents like cyclohexane. This is especially important for the precipitation of particles, which was observed for all solvents except DMF when evaluating the RuDENs. The conversion of styrene with time is illustrated in Figure 6.15 for the various solvents utilised in this study. The highest end of run conversion was observed when using ethanol as a solvent. Similar conversions were observed when utilising cyclohexane and acetonitrile. The lowest end of run conversion was observed when utilising DMF as a solvent.

It seems that for the heterogeneous RuSil60S catalyst, the coordinating solvent, DMF, has a negative effect on the catalytic activity when compared to results obtained when using RuDEN as catalysts. This observed decrease in the catalytic activity could be due to an increased interaction of the solvent with the catalyst, an interaction that could be facilitated by interaction with surface silanols of the support. This interaction of the solvent with the support could bring the solvent into closer proximity with the supported Ru nanoparticle and hence facilitates interaction with the nanoparticle. The more reactive radical mechanism pathway, as earlier referred to for the evaluation of the RuDEN catalysts, facilitates the high conversion of styrene observed for the non-polar solvent cyclohexane. The increase in conversion for a non-polar solvent is observed when using cyclohexane as a solvent for the styrene epoxidation for the G6-RuSil60S catalyst. The higher conversion observed when utilising ethanol can be ascribed either to the higher polarity of the solvent which facilitates a non-radical pathway or to the weaker coordinating ability of the solvent when compared to coordinating solvents like DMF and acetonitrile. To gain further insight into the different styrene conversion profiles observed when using the different solvents, consideration is given to the selectivity towards styrene oxide.

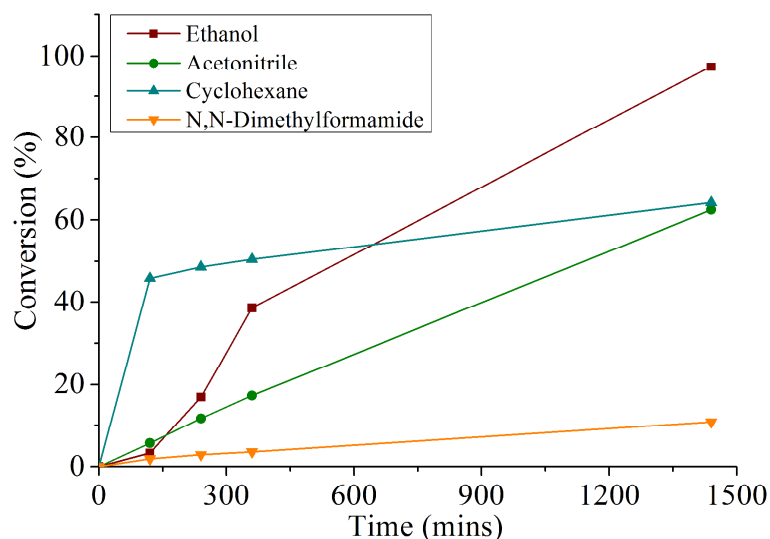


Figure 6.15. Conversion of styrene observed over 1440 minutes utilising the G6-RuSil60S catalyst and using the solvents, ethanol, acetonitrile, N,N-dimethylformamide, tetrahydrofuran and cyclohexane. Reactions were conducted using 0.002 mmol Ru, 2 mmol styrene and 4 mmol TBHP at a temperature of 85 °C.

The time-resolved selectivity towards styrene oxide observed when utilising the different solvents, is illustrated in Figure 6.16. The styrene oxide selectivity observed when using the polar solvents acetonitrile and DMF, increases up to an end of run value of 76%. This is expected for the polar solvents, which favour the more conservative epoxidation mechanism that occurs at the nanoparticle surface, and to a lesser extent, the radical mechanism observed when using non-polar solvents. In the case of ethanol and cyclohexane, there is a dramatic decrease in the selectivity towards styrene oxide when compared to the results observed when using acetonitrile and DMF. This suggests that the radical mechanism is favoured when using these solvents as the formation of products other than styrene oxide are observed and hence styrene oxide selectivity decreases.

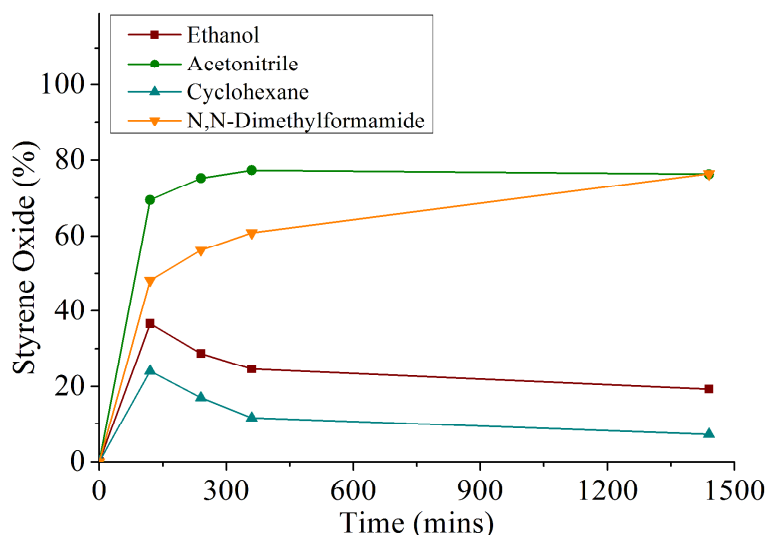


Figure 6.16. Styrene oxide selectivity observed over 1440 minutes utilising the G6-RuSil60S catalyst when using the solvents, ethanol, acetonitrile, N,N-dimethylformamide, tetrahydrofuran and cyclohexane. Reactions were conducted using 0.002 mmol Ru, 2 mmol styrene and 4 mmol TBHP at a temperature of 85 °C.

When comparing the results obtained for ethanol and cyclohexane, there is, however, an increase in the selectivity towards styrene oxide, which reiterates the effect of polarity and solvent type on the reaction mechanism favoured as discussed in chapter 6.3.1.5. The high selectivity towards styrene oxide and good activity towards the conversion of styrene observed when utilising acetonitrile makes this the ideal solvent for evaluating the RuSil60S catalysts.

6.3.2.3 *The effects of catalyst choice*

The series of RuSil60S catalysts were evaluated in the oxidation of styrene to investigate any differences in the performance of the various supported RuDEN particles. The metal loading, was kept at 0.1 mol% Ru for all the catalytic reactions investigating the effect of catalyst choice. Figure 6.17(a) illustrates the conversion of styrene with time when evaluating the various RuSil60S catalysts. The overall end of run styrene conversion ranged from 64-92% for the different RuSil60S catalysts. The percentage styrene conversion follows the trend G6-RuSil60S < G5-RuSil60S < G4-RuSil60S for the RuSil60S catalysts evaluated. This activity profile trend for the different RuSil60S catalysts is reinforced by the TOF values illustrated in Figure 6.17(b) where the TOF value is highest for G4-RuSil60S and lowest for G5-RuSil60S. When considering the activity of the different catalysts, it would seem that the most efficient

catalyst is G4-RuSil60S. The overall performance of the catalyst, however, depends on the selectivity towards the styrene oxide while maintaining a balance with the catalytic activity.

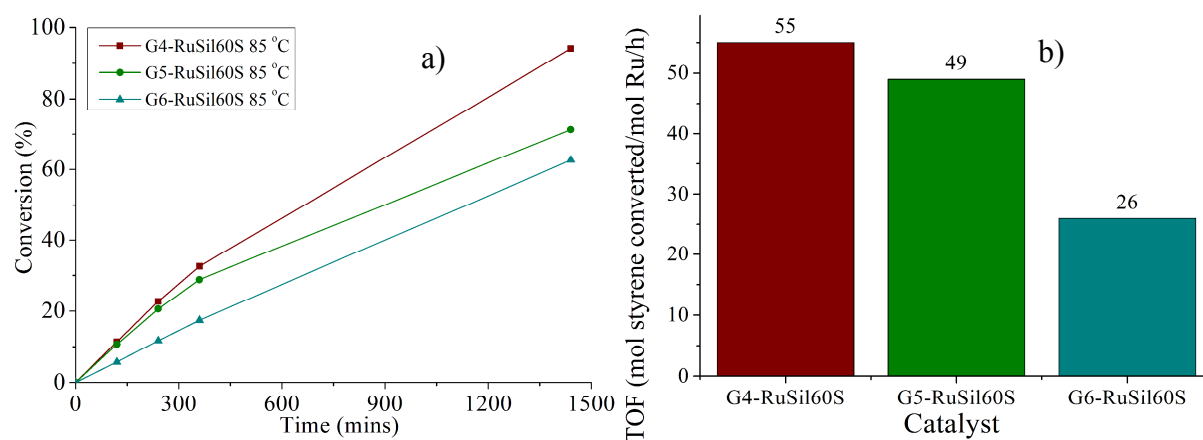


Figure 6.17. Conversion of styrene observed when conducting the experiment using G4-RuSil60S, G5-RuSil60S and G6-RuSil60S at a 0.1 mol % Ru catalyst loading. Reactions were conducted using 0.002 mmol Ru, at 85 °C with acetonitrile as solvent, 2 mmol styrene and 4 mmol TBHP.

The time resolved selectivity towards styrene oxide is illustrated in Figure 6.18, and for all the catalysts; the selectivity is maintained throughout the course of the reaction. When comparing the selectivity obtained for the different catalysts, the highest end of run styrene oxide selectivity was obtained when using G6-RuSil60S as a catalyst.

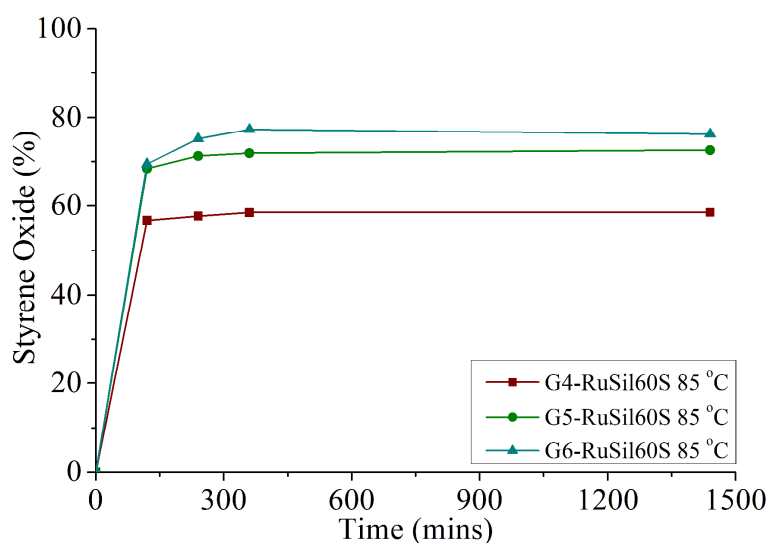


Figure 6.18. Styrene oxide selectivity observed with time when utilising the catalysts G4-RuSil60S, G5-RuSil60S and G6-RuSil60S as a catalyst. Reactions were conducted using 0.002 mmol Ru, 2 mmol styrene and 4 mmol TBHP at a temperature of 85 °C.

The selectivity towards styrene oxide is slightly lower when utilising G5-RuSil60S and the lowest selectivity was observed when utilising G4-RuSil60S as a catalyst. This trend shows an inverse correlation to the activity of the RuSil60S catalysts. It seems that for the reaction conditions utilised, catalysts that are more active observe lower styrene oxide selectivity. This could suggest decomposition of styrene oxide to other oxygenate species by virtue of the increase in catalytic activity for G5-RuSil60S and G4-RuSil60S when compared to G6-RuSil60S.

6.3.2.4 Effects of ionic liquids and amounts of ionic liquids used

The effects of an ionic liquid as an additive on the activity of the RuDEN catalysts was discussed earlier and in certain cases, an improvement in the catalytic activity was observed. This was most evident when using the [EMIM][OcS] ionic liquid as an additive when utilising the G5-RuDEN catalyst. When considering the overall conversion behaviour for each reaction, they all follow a more linear time resolved conversion trend than the logarithmic behaviour observed when evaluating the RuDEN catalyst in DMF as a solvent. This suggests that the solvent effect, that acetonitrile causes, is still present. The presence of ionic liquid and the amount used does, however, affect the catalytic activity to some degree as illustrated in Figure 6.19 and is more evident when using a 0.3 g amount of ionic liquid than a 0.1 g amount of ionic liquid.

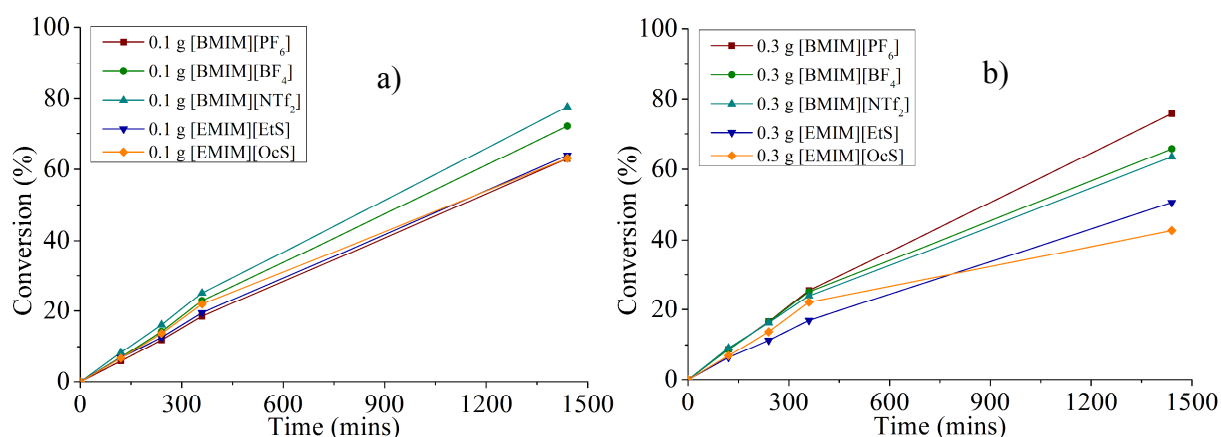


Figure 6.19. Conversion of styrene for various amounts of the ionic liquids [BMIM][PF₆], [BMIM][BF₄], [BMIM][NTf₂] and [EMIM][OcS] as additive for the ionic liquid mass, a) 0.1 g of ionic liquid and b) 0.3 g of ionic liquid while utilising the G6-RuSil60S catalyst. Reactions were conducted using 0.002 mmol Ru, 2 mmol styrene and 4 mmol TBHP at a temperature of 85 °C and in DMF as a solvent.

The time resolved styrene oxide selectivity profile observed when using the ionic liquid as additive is illustrated in Figure 6.20. The selectivity to styrene oxide shows an initial increase as the reaction progresses when evaluating all the ionic liquids. However, over the period of 360-1440 minutes, a decrease in selectivity was observed when evaluating [EMIM][OeS]. In this case, the use of the ionic liquid [EMIM][OeS] has a negative effect on the styrene oxide selectivity beyond 360 minutes of reaction time.

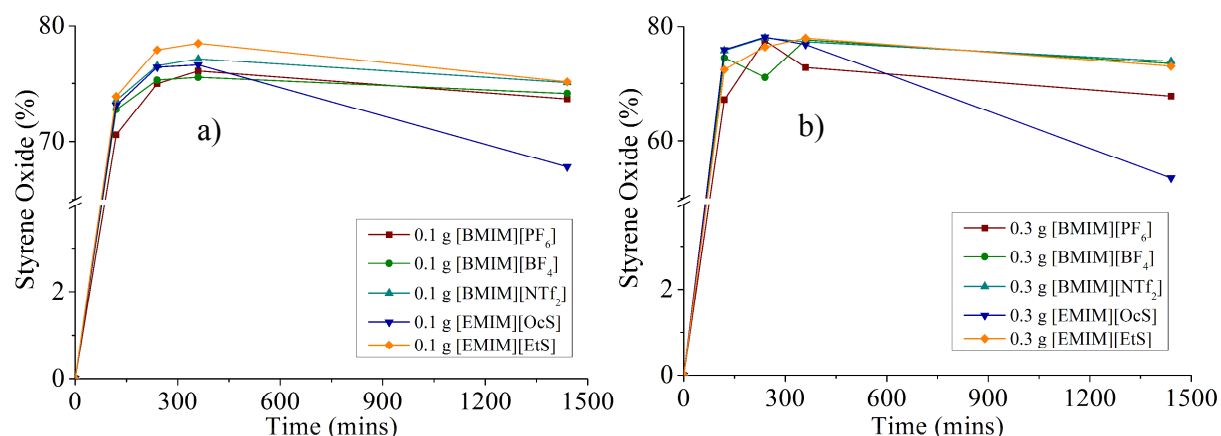


Figure 6.20. Styrene oxide selectivity observed for various amounts of the ionic liquids [BMIM][PF₆], [BMIM][BF₄], [BMIM][NTf₂] and [EMIM][OeS] as additive for the ionic liquid mass, a) 0.1 g of ionic liquid and b) 0.3 g of ionic liquid while utilising the G6-RuSil60S catalyst. Reactions were conducted using, 0.002 mmol Ru, 2 mmol styrene and 4 mmol TBHP at a temperature of 85 °C.

To gain better insight into the specific changes in the activity when using the different ionic liquid additives, consideration is given to all the end of run evaluation data as depicted in Table 6.5. The conversion of styrene shows an increase from 63% for the G6-RuSil60S catalyst to 72% and 78% with minimal change in the styrene oxide selectivity when using the ionic liquids [BMIM][BF₄] and [BMIM][NTf₂] respectively.

Table 6.5. The effect of the various ionic liquids and amounts of ionic liquid on the % styrene conversion and the % styrene oxide selectivity.^a

Entry	Ionic liquid	Ionic liquid amount (g)	Styrene conversion (%)	Styrene oxide selectivity (%)
1	None ^b	-	63	76
2	[BMIM][BF ₄]	0.1	72	74
3	[BMIM][BF ₄]	0.3	66	73
4	[BMIM][NTf ₂]	0.1	78	75
5	[BMIM][NTf ₂]	0.3	64	74
6	[BMIM][PF ₆]	0.1	63	74
7	[BMIM][PF ₆]	0.3	76	68
8	[EMIM][EtS]	0.1	64	75
9	[EMIM][EtS]	0.3	51	73
10	[EMIM][OcS]	0.1	63	68
11	[EMIM][OcS]	0.3	43	54

^a Values for % styrene conversion and % styrene oxide taken at 1440 min. Ru (0.002 mmol), styrene (2 mmol), TBHP (4 mmol), 85 °C. ^b No ionic liquid present only G6-RuSil60S catalyst.

6.4 Conclusion

The RuDEN and RuSil60S catalysts were evaluated as catalysts in the oxidation of styrene using TBHP as the oxidant. The reactions were optimised according to the parameters, oxidant loading, catalyst loading, temperature and solvent. An increase in catalytic rate was observed for an increase catalyst concentration up to a degree and in the case of increasing the TBHP, this was observed as well. The temperature studies conducted for the RuDEN catalysts demonstrated an increase in catalytic rate with increase in the temperature and this was kept for evaluating the RuSil60S catalysts. The choice of solvent has an impact on the catalytic activity where polar solvents generally give good activity, however, if the solvent is coordinating, the activity decreases when compared to less-coordinating solvents. Solvent choice, however, was based on the compatibility of the solvent with the catalytic system and stabilisation of the nanoparticles. The choice and amount of ionic liquid can affect the activity and selectivity of the catalyst and based on the results of this study, requires optimisation of these two parameters for each ionic liquid. However, this proves that there is scope for the

study of various other ionic liquids as additives in oxidation reactions with peroxides as oxidants. This study proves the potential of RuDENs and RuSils as catalysts in the oxidation of styrene in the presence of an oxidant. As supported catalysts they show good activity in the oxidation of styrene and with further studies can be evaluated in reactions using molecular oxygen as the oxidant source. The activity and selectivity profiles of these catalysts can also be tuned by the use of ionic liquids which, with optimal utilisation, may potentially replace the need for a solvent.

6.5 References

- [1] J.-M. Brégeault, *Dalton Trans.* **2003**, 3289.
- [2] T. Punniyamurthy, S. Velusamy and J. Iqbal, *Chem. Rev.* **2005**, *105*, 2329.
- [3] F. Rosowski, S. Storck and J. Zühlke, *Oxyfunctionalization of Alkyl Aromatics. Handbook of Heterogeneous Catalysis*, Wiley-VCH Verlag GmbH & Co. KGaA, **2008**, pp. 3425–3433.
- [4] N. Dimitratos, J. A. Lopez-Sanchez and G. J. Hutchings, *Chem. Sci.* **2012**, *3*, 20.
- [5] P. Lignier, S. Mangematin, F. Morfin, J.-L. Rousset and V. Caps, *Catal. Today* **2008**, *138*, 50.
- [6] N. S. Patil, B. S. Uphade, P. Jana, S. K. Bharagava and V. R. Choudhary, *J. Catal.* **2004**, *223*, 236.
- [7] M. Turner, V. B. Golovko, O. P. H. Vaughan, P. Abdulkin, A. Berenguer-Murcia, M. S. Tikhov, B. F. G. Johnson and R. M. Lambert, *Nature* **2008**, *454*, 981.
- [8] M. Nemanashi and R. Meijboom, *Catal. Lett.* **2013**, *143*, 324.
- [9] B.-Z. Zhan, M. A. White, T.-K. Sham, J. A. Pincock, R. J. Doucet, K. V. R. Rao, K. N. Robertson and T. S. Cameron, *J. Am. Chem. Soc.* **2003**, *125*, 2195.
- [10] K. Yamaguchi and N. Mizuno, *Angew. Chem. Int. Ed.* **2002**, *41*, 4538.
- [11] S. Mori, M. Takubo, K. Makida, T. Yanase, S. Aoyagi, T. Maegawa, Y. Monguchi and H. Sajiki, *Chem. Commun.* **2009**, 5159.
- [12] P. Migowski and J. Dupont, *Chem. Eur. J.* **2007**, *13*, 32.
- [13] G. Schmid, *Nanoparticles: From Theory to Application, 2nd, Completely Revised and Updated Edition* (Ed.: G. Schmid), Wiley-VCH, Weinheim **2010**, p. 217.
- [14] S. Mourdikoudis and L. M. Liz-Marzán, *Chem. Mater.* **2013**, *25*, 1465.
- [15] Y. Niu and R. M. Crooks, *C. R. Chimie* **2003**, 1049.

- [16] V. S. Myers, M. G. Weir, E. V. Carino, D. F. Yancey, S. Pande and R. M. Crooks, *Chem. Sci.* **2011**, *2*, 1632.
- [17] R. M. Crooks, M. Zhao, L. Sun, V. Chechik and L. K. Yeung, *Acc. Chem. Res.* **2001**, *34*, 181.
- [18] V. V. Namboodiri, R. S. Varma, E. Sahle-Demessie and U. R. Pillai, *Green Chem.* **2002**, *4*, 170.
- [19] I. A. Ansari, S. Joyasawal, M. K. Gupta, J. S. Yadav and R. Gree, *Tetrahedron Lett.* **2005**, *46*, 7507.
- [20] G. Liu, M. Hou, J. Song, Z. Zhang, T. Wu and B. Han, *J. Mol. Catal. A: Chem.* **2010**, *316*, 90.
- [21] C. Chiappe, A. Sanzone and P. J. Dyson, *Green Chem.* **2011**, *13*, 1437.
- [22] I. Chorkendorff and J. W. Niemantsverdriet, *Concepts of Modern Catalysis and Kinetics* (Eds.: I. Chorkendorff, J. W. Niemantsverdriet), WILEY-VCH Verlag GmbH & Co. KGaA, Weinheim, **2003**, p. 27.
- [23] C. Reichardt, *Solvents and Solvent Effects in Organic Chemistry*, 3 ed., Wiley-VCH Verlag GmbH & Co., Weinheim, **2003**, p. 471.
- [24] S. J. Ashcroft and M. B. Isa, *J. Chem. Eng. Data* **1997**, *42*, 1244.



Chapter 7 – Conclusion and recommendations

7.1 Conclusion

Size controlled ruthenium nanoparticles were prepared using PAMAM-OH dendrimers as templates. This was achieved by preparing DENs with a dendrimer:ruthenium molar ratio of 1:40, 1:80 and 1:160 using the G4-PAMAM-OH, G5-PAMAM-OH and G6-PAMAM-OH dendrimer respectively. The preparation of the RuDENs were monitored using UV/Vis spectrophotometry and FTIR spectroscopy. The size of the RuDENs was determined using HRTEM and ranged from 1.2-2.2 nm depending on the dendrimer and dendrimer:metal ratio utilised. The nanoparticles show no visible agglomeration when kept stirring under inert atmosphere.

The extraction of the RuDEN nanoparticles was attempted using ionic liquids and alkylamines as extractants. The extractions were monitored using UV/Vis spectrophotometry. Although the ionic liquids demonstrated some potential for the extraction of ruthenium nanoparticles from the dendrimer, the alkylamines proved more efficient for this purpose. Amongst the alkylamines, octylamine demonstrated greater efficiency in ruthenium nanoparticle extraction from all the RuDEN catalysts. This was most evident for the G5-RuDEN and G6-RuDEN catalysts since extraction using oleylamine became impeded due to steric reasons. Further insight into the use of octylamine as extractant was obtained by HRTEM analysis of the ruthenium particle size prior to extraction. An increase in ruthenium nanoparticle size was observed when extracting nanoparticles from the G4-RuDEN and G5-RuDEN catalysts. A decrease in particles size was observed when extracting ruthenium nanoparticles from the G6-RuDEN catalyst. This observation led to the conclusion that the extraction from the lower generation G4-PAMAM-OH and G5-PAMAM-OH dendrimers was more facile. The extraction of particles from the G6-PAMAM-OH dendrimer was size selective and despite the larger particle size observed for G6-RuDENs, ruthenium nanoparticles of an average 1.5 nm diameter were extracted. This is indicative of the steric stabilisation of the larger ruthenium nanoparticles within the G6-PAMAM-OH microenvironment. Further study is however required to increase the efficiency of the extraction since only partial extraction was possible.

The RuDENSs were successfully immobilised on amorphous silica 60 and silica 100 support material. Sintering of the nanoparticles was observed in most cases as confirmed by HRTEM results. The increase in particle size was highest when using silica 60 compared to silica 100. This observation is attributed to the increased pore size of the silica 100 which facilitates migration of the RuDENSs and hence increases interaction of the RuDENSs with the inner surface area of the support. This helps increase dispersity and minimise interaction between the immobilised RuDENSs during catalyst preparation. The change in particle size upon immobilisation was more evident for the G4-RuDEN and G5-RuDEN catalysts. The increased generation therefore has a more stabilising effect on the nanoparticle during the immobilisation process. Although other characterisation methods such as PXRD, SEM and H₂ chemisorption were attempted, they were of little use. The absence of conclusive results from PXRD and SEM measurements does, however, confirm that the nanoparticles are quite small and below the detection limit. The methodology utilised for the preparation of the RuSil catalysts minimised decomposition of the dendrimer template as confirmed by TGA results. A series of ionic liquid coated catalysts referred to as RuSCILL catalysts were prepared using the ionic liquids [BMIM][PF₆], [BMIM][BF₄], [BMIM][NTf₂], [EMIM][EtS] and [EMIM][OcS]. The presence of the ionic liquid was confirmed using TGA measurements.

The RuDENSs were then evaluated as catalysts in the reduction of 4-nitrophenol in the presence of sodium borohydride. The kinetic data obtained from the reactions was modelled according to the Langmuir-Hinshelwood model. The model assumes the adsorption of both substrate and reactant on the catalyst surface before reaction occurs. The study demonstrated the usefulness of this model in the study of the reduction of 4-nitrophenol by RuDENSs in the presence of BH₄⁻. Three constants related to each system were calculated. These include the kinetic constant, k , that describes the reaction of the surface adsorbed species and the thermodynamic adsorption constants, K_{4NP} , for 4NP, and K_{BH_4} , for BH₄⁻. A correlation between size and activity was observed with smaller nanoparticles displaying a higher catalytic rate. Amongst the RuDEN catalysts investigated, G5-RuDEN displayed the highest activity indicating an optimal nanoparticle size for the catalytic reaction.

The RuSil catalysts serve as good catalysts in the hydrogenation of toluene even in the presence of the dendrimer. The catalytic activity was evaluated for each of the RuSil60 and RuSil100 catalysts. For each of the RuSil catalysts, the G5-RuSil catalyst displayed the highest activity.

The selectivity for all of the batch mode reactions was towards the fully hydrogenated product methycyclohexane. The catalysts were coated in a series of ionic liquids to give RuSCILL catalysts. An increase in selectivity towards the methycyclohexenes was observed for each of the ionic liquid coatings. The ionic liquid that gave the best results where both activity and selectivity is concerned was [BMIM][NTf₂]. To gain insight into extending the application of this system, preliminary studies were conducted to investigate the feasibility of these catalysts in continuous flow processes. The activity of the RuSil and a RuSCILL catalyst coated in [OMIM][NTf₂] was evaluated where this ionic liquid has a higher solubility for the substrate. Both catalytic systems were active, proving their potential as catalysts in gas phase continuous flow processes. Additionally, increased selectivity towards the methycyclohexenes was observed when evaluating the RuSCILL catalyst for the gas phase hydrogenation of toluene.

The RuSil60 and RuSCILL catalysts were evaluated in the chemoselective hydrogenation of the α,β -unsaturated compounds, citral and cinnamaldehyde. Reaction temperature had a strong influence on the catalytic selectivity where an increase in temperature led to an increase in the formation of side products such as isopulegol in the case of the citral hydrogenation. The inhibition of catalyst activity was observed during the evaluation of the RuSil60 catalysts and is ascribed to the decarbonylation pathway that occurs. This process results in the formation of CO which acts as a poison on the catalyst surface and slowly inhibit the reaction and occurs for both hydrogenation reactions. An increase in the activity of the catalyst was observed when utilising [BMIM][NTf₂] and [EMIM][Ocs] as a catalyst coating for the hydrogenation of citral and cinnamaldehyde respectively. The increase in activity observed when utilising the ionic liquid was ascribed to displacement of the adsorbed CO poison on the catalyst surface formed during decarbonylation. Additionally, the presence of the ionic liquid favoured the selective hydrogenation of the C=C double bond for all the ionic liquids evaluated as coatings.

Lastly, the evaluation of RuDENs and RuSil catalysts in the oxidation of styrene with TBHP as oxidant was conducted. Various reaction parameters such as oxidant loading, catalyst loading, temperature and solvent choice were investigated. Increase in activity was observed with an increase in oxidant loading and increase in temperature. This increase was only evident up to an extent when increasing the catalyst loading. The choice of solvent plays a significant role in the catalytic activity where more coordinating solvents can lead to a decrease in the catalytic activity. The motivation was to find a solvent that was compatible with the catalyst. In this case, the stabilising effect of DMF on the RuDENs was advantageous despite a slight

decrease in activity. The solvent most compatible with the RuSil catalysts was acetonitrile. The ionic liquids were soluble in both solvents which facilitated their utilisation as additives in the oxidation reactions. The choice of ionic liquid requires optimisation of the amount used to ensure the desired selectivity while maintaining good catalytic activity. With regards to improved activity, the ionic liquids [EMIM][OcS] and [BMIM][NTf₂] were ideal when evaluating the RuDEN and RuSil catalysts respectively. The changes in selectivity specifically towards styrene oxide was not as distinct amongst the ionic liquids, when compared to reactions conducted in the absence of ionic liquid.

7.2 Recommendations

There are very few studies concerning the use of RuDENs as catalysts. The studies highlighting mainly their preparation and immobilisation. This work serves to demonstrate the applications of RuDENs and the silica supported RuDENs referred to as RuSil60 catalysts. Any further studies could investigate:

- The search for more efficient methods of extracting Ru nanoparticles from the dendrimer template with the aim of recycling the dendrimer.
- The effects of the size of dendrimer on the catalytic activity which can be achieved by preparing RuNPs of the same size in each of the dendrimer generations.
- The influence of different support materials as solid supports, such as mesoporous silicas, and the effect on the selectivity of the reactions.
- Studies into the application of the RuDEN catalyst in oxidation reactions using molecular oxygen as an oxidant which can include established literature applications in the oxidation of alcohols.
- The further application of the RuSil catalysts in continuous flow reactions.
- The use of other ionic liquids and separating possible effects of the anion and cation of the catalytic performance.

The presence of an ionic liquid on the catalyst surface can affect the catalytic performance. There is therefore, more scope for studies into understanding the exact mechanism of this control by the ionic liquid. The RuDEN catalysts have however proved to be versatile catalysts and warrant further study based on the recommendations provided.